Theoretical and Experimental Advances in the Development of Isochoric Cryopreservation Techniques

By

Matthew Powell-Palm

A thesis submitted in partial satisfaction of the
requirements for the degree of
Doctor of Philosophy

in

Engineering- Mechanical Engineering

in the

Graduate Division

of the

University of California, Berkeley

Committee in charge:

Professor Boris Rubinsky, Chair
Professor Chris Dames
Professor Kevin Healy

Summer 2020

Theoretical and Experimental Advances in the Development of Isochoric Cryopreservation Techniques

By

Matthew Powell-Palm

Abstract

Theoretical and Experimental Advances in the Development of
Isochoric Cryopreservation Techniques

By

Matthew Powell-Palm

Doctor of Philosophy in Engineering- Mechanical Engineering

University of California, Berkeley

Professor Boris Rubinsky, Chair

The realization of on-demand organ and tissue availability could yield a benefit to global health comparable to the curing of cancer, unleashing the full potential of modern transplantation science without its current geographic, socioeconomic, and technical limitations. However, a seemingly simple scientific problem has thus far restricted this reality: our inability to preserve organs outside the body for extended periods of time.

Generally, in order to arrest the metabolism of an *ex vivo* biologic and prevent it from expiring, one must reduce its temperature to well below the freezing point of water (its principal material component). However, the formation of ice within complex vascularized systems proves catastrophic, and thus a wonderfully fundamental puzzle emerges: How can we prevent water from freezing, when equilibrium thermodynamics demand that it should freeze? Over the past 70 years, efforts to address this question have taken an overwhelmingly chemical approach. However, techniques driven by the use of cytotoxic non-physiological cryoprotectants to modulate freezing point has not yielded clinically-relevant advancements at the whole-organ scale to date, and thus a fundamentally different approach is needed.

This thesis presents theoretical and experimental explorations of an alternative, non-chemical approach to cryopreservation based on the rich and unexplored thermodynamic and kinetic behaviors of water and ice confined under isochoric (constant-volume) conditions. We herein develop fundamental analytical tools with which to probe isochoric phase equilibria and nucleation kinetics across volumes; reveal critical consequences of water confinement at the micro- and macroscales; experimentally demonstrate previously unrealized phase behaviors in isochoric systems in stable equilibrium, metastable equilibrium, and non-equilibrium scenarios; provide initial biological validation of isochoric cryopreservation with whole mammalian organs and tissues; and evince the additional value of isochoric freezing processes in the food industry. We develop several distinct isochoric techniques for varied preservation applications and generate baseline thermodynamic data for each, which, alongside the biological results reported herein, we hope will serve as a foundation from which the community may further advance the unique domain of isochoric freezing.

To Mom, Dad, Nate, Pookie, Becca, and Meghan— for holding down the fort while I'm away.

Acknowledgements

Looking retrospectively upon my time in Berkeley, I realize the impossibility of exiting your PhD the same person you entered as. Such enormous intellectual growth is required in so short a time that were your personal growth to lag too far behind, the emotional imbalance would have you bleeding out the ears. Thus, in bidding farewell to this transformative chapter of my life, I have many special people to thank for their contributions to my growth in all directions.

To my advisor, the inimitable Boris Rubinsky: On paper, we wound up together by chance—in practice, I reckon it was fate and a pinch of divine providence that landed me in 6124 Etcheverry Hall. There are too many things to thank you for: introducing me to the wonderful world of isochoric thermodynamics; assuring me that it's okay to abandon the beaten path in favor of the wilds; teaching me the ever-so-limited value of pomp and prestige; demonstrating the value of radical creativity; et cetera and et cetera, on into the night. However, above all, I want to thank you for your abiding kindness, care, and support. As I prepare to leave the PhD, I realize how exceedingly rare it is to have an advisor who you can truly and fully embrace as family, and who you can count on to remain in your corner through thick and thin. It's been a pleasure, a privilege, and a plain old good time—thank you.

To my many other course-correcting mentors throughout the years: Jon Malen, you shepherded me through my idiot undergrad days, showed me that a sense of humor indeed has a home in the sciences, and are I'm certain the only reason I was admitted to graduate school. I reckon the singular event most responsible for setting me on this scientific career path was that email you sent me junior year—"Hi Matt, I saw you and the chicken on a magazine. Nice." Chris Dames, you've provided a routinely shocking model of combined humility and prowess that I strive to emulate, and I'm grateful for your supportive presence throughout my time here. Kevin Healy, thanks for letting me prowl around your lab and distract your students these last few years. Randy Quam, Buck Buchanan, Kim Popham; you folks have supported me from the get-go, and I have high hopes for the coming generations of Montanan scientists with you all at the wheel.

To my closest scientific collaborators, without whom my deep and abiding love of thermodynamics would never have flourished: Gideon Ukpai, I am constantly thankful that you and I were tossed into this mess together, and that we've gotten to dream-team it for so long. It's been a joy in lab and in MoLo alike, and I look forward to a lifetime of freezing things together. Chenang Lyu, I'm grateful for the basketball, mooncakes, nap chair, hot pot, and every other quirky snippet of fun you drug into lab over the years, and for your enduring friendship and assistance. Wenhao Sun, you helped me to distill from the ethereal my broader scientific vision, and helped to convince me that there are big problems that even us little people can tackle. Drew Lilley, having someone equally young and green as I to fawn over the wonders of thermo with has both eased the isolation of specialized work and kept my perspectives fresh. Tony Consiglio, of everyone not in the Rubinsky Lab to camp out for a year at a Rubinsky Lab desk, you were the most stimulating by far.

To the grad-school gang I'll always hold near to my heart: Gideon, Drew, Tony, Jason, Eloïse, Colleen, and Fernando, you folks helped to keep me fat and happy, balanced and humble, and I

shiver at the idea of Berkeley without you. Allen, we're an old married couple at this point, but I'm increasingly grateful with each passing year that fate has kept our friendship so tightly woven.

Finally, to my parents and my siblings: The most difficult trial I've faced these last three years has been spending them 1,027.63 miles away from you guys. Mom and Dad, you've kept me honest and afloat my whole life, and blessed me with the uncorruptible sense of family that keeps me unafraid of falling. Nate, you've kept me driven, both to beat you to finding fame and fortune and to catch up with you on finding love and contentment. Pookie, you've been my most uflagging artistic companion these many years, and watching you grow into yourself (and your chin!) has been one of the great joys of my life. Becca, I'm less terrified of meandering into adulthood with you there to greet me, and uncling your children has lit up my heart like only dancing babies can. Meghan, I miss you, and you know you can always call me collect from St. Peter's landline. I love you guys.

To the innumerable other people I've met along the way, each of whom has uniquely shaped my journey in the way that only you can—thanks.

Table of Contents

List of Figure Descriptions

curves for varying absolute system volumes. The Gibbs Limit gives the system behavior at the limit of infinite system volume, and the Helmholtz Limit at the critical system volume at which the free energy curve begins to increase monotonically. C. Critical radius as a function of system volume for various temperatures, with critical system volumes marked. D. Phase diagram mapping the critical system volume as a function of temperature. In the kinetically dominated regime, all $\Delta\emptyset$ curves will be monotonically increasing, and thus no kinetic pathway to nucleation will exist.

2.4. Schematic of spherical bubble a rigidly confined liquid medium.

2.5. Transient excitation of a gas bubble in an ultrasonic pressure field. (a) Acoustic pressure signal of frequency 40 kHz and amplitude 1.5 bar as a function of cycle period, $\omega t/2\pi$. (b) Time evolution of relative bubble radius, R_b/R_0, for various values of relative confinement radius, R_c/R_0. Equilibrium bubble radius, $R_0 = 2.09\mu$m. (c) Pressure of water at bubble interface.

1.6. Peak collapse pressures experienced during cavitation in confined volumes. (a) Dependence of maximum cavitation pressure on degree of system confinement. For a system at a bulk temperature (0°C here) subjected to a given pressure field, three distinct regions of behavior can be identified as the degree of confinement varies. At system volumes approaching infinity (the isobaric limit), pressure will not vary with confinement, and will not differ from the pressures experienced in an unconfined system. Under increasing confinement, a transition zone emerges in which peak pressures decreases rapidly with decreasing system volume. Finally, at sufficiently small system volumes, cavity collapse will become kinetically prohibited and the bubble will stably oscillate, producing no significant changes in pressure. (b). Dependence of maximum cavitation pressure on degree of system confinement for varying degrees of bulk supercooling. (c) Dependence of maximum cavitation pressure on excitation frequency. (d) Dependence of maximum cavitation pressure on initial bubble radius at the isobaric limit of system confinement.

2.7. Dependence of transition zone on material properties. (a) Compressibility, K^{-1}. (b) Surface tension, σ.

2.8. Transient high-pressure solidification processes for systems of varying bulk temperatures sonicated at 30 kHz. (a) Phase diagram of water with isentropic compression curves for bulk system temperatures of 0, -5, -10, -15, -20 and -25°C, color coded according to the color bar at right. The water-ice liquidus line (solid black) shows the equilibrium boundary between the liquid water phase (above the line) and the ice phases Ih, III, V, VI, and VII (below the line), as labelled along the bottom of the plot. Isentropic compression curves (dashed lines) show the temperature-pressure thermodynamic path followed by water as it is isentropically compressed from a varying initial temperatures. As compression increases, the water will traverse through the equilibrium regions of several different ice phases. Both the liquidus line and the isentropic compression curves were calculated using the standard IAPWS multiparameter equations of state. (b) Magnitude of transient supercooling encountered during isentropic compression, e.g. the difference $\Delta T_{supercooling}$ between the liquidus curve and a given isentropic compression curve. Curves are truncated at the maximum pressure reached during cavity collapse for a given bulk temperature. (c) The same maximum transient supercooling as a function of confinement volume, adapted

according to the pressure-confinement volume relations provided in Figure 2. (d) Minimum ice VII induction time encountered during cavity collapse as a function of confinement volume, as calculated using classical nucleation theory. The dashed line represents the critical induction time threshold, defined by the average duration of a high-pressure collapse event (here 1 ns). Minimum ice VII induction times beneath this threshold will lead to formation of ice VII nuclei during cavity collapse, while induction times above the threshold will not.

2.9. Ice VII kinetic phase diagram. For a given ultrasonic excitation frequency and bulk temperature, there exists a critical confinement volume beneath which the induction time of ice VII is too great to induce nucleation within the approximately 1ns period during which cavity collapse causes quasi-isentropic compression. The dashed lines indicate the boundary that separates the confinement regimes in which nucleation of ice VII can (above a given line) and cannot (beneath a given line) occur.

3.1. Comparison of isobaric (T-P) and isochoric (T-V) thermodynamic conditions for water and ice. A. Isobaric systems maintain contact with a pressure reservoir (the atmosphere in the context of this work), and thus fluctuate constantly in density at the microscopic scale. At atmospheric pressure, water in an isobaric system will transform entirely to ice-1h at sub-zero centigrade temperatures. B. Isochoric systems are held at constant-volume, isolated from the atmosphere, and thus do not fluctuate in density. Water in an isochoric system will not freeze entirely at sub-zero centigrade temperatures, instead forming a two-phase water-ice equilibrium.

3.2. Disturbance experiments to evaluate supercooling stability. A. Schematic representation of each of the four disturbance experiments. Full experimental descriptions available in Methods. B. Timelapse photo series of an isobaric chamber following impact from a drop height of one foot. Ice nucleation proceeds quickly and can be easily visually detected. C. Timelapse photo series of an isochoric chamber following impact from a drop height of one foot. Supercooling remains stable and ice does not nucleate.

3.3. Nucleation frequency upon exposure to external disturbances for conventional isobaric, isobaric oil-sealed, and isochoric systems. A. Nucleation frequency for all systems as a function of disturbance type. Solid markers and lines represent 65 ml chambers, hollow markers and dotted lines represent 130 ml chambers. Lines between markers are plotted for visual assistance, and to not indicate a quantitative trend. B-E. Results for each disturbance type grouped by system type and volume. Statistically significant differences ($P < 0.05$) between system types at a given volume are marked by differing letters. Significant differences between volumes of a given system type are marked by an asterisk (*). Marked values provide the mean and error bars provide the standard deviation.

3.4. Comparison of the stability of the free water surface in vibrating systems under standard isobaric conditions and isobaric oil-sealed conditions. A. Standard isobaric conditions. The water-air interface is observed to be highly unstable, and extensive entrainment of air is evident in the water layer. B. Isobaric oil-sealed conditions. The oil-air interface is observed to be highly unstable, but the water-oil interface remains stable. Extensive entrainment of air is observed in the oil layer, but the water layer remains air-free.

3.5. Cap modification to allow effective air removal in sealing of isochoric chambers. *Left top:* Standard polypropylene cap, as used for assembly of isobaric chambers. *Left bottom:* inverted chamber after assembly with standard cap. Bulk pockets of air can be observed. *Right top:* Polyprolyene cap with press-fit aluminum plug, as used for assembly of isochoric chambers. As the cap is threaded onto the chamber, the plug displaces a small volume of water, which forces out any air remaining in the mouth of the chamber or trapped in the cap itself. This displaced liquid and air is able to escape past the threads as the cap is being tightened, until the final point of closure, at which the roof of the lid meets the lip of the chamber and forms a rigid seal. *Right bottom:* inverted chamber after assembly with modified cap. No air bubbles can be seen, and no bulk motion of the fluid can be observed during inversion.

3.6. Elements of isochoric system and experimental setup. a) Isochoric chamber with pressure transducer and thermocouple. b) Two Isochoric systems in the Planer controlled rate freezer before the start of an experiment.

3.7. Typical (a) cooling and (b) warming temperature history. Representative plots of temperature measured during immersion of isochoric chambers in liquid nitrogen for 15 min and warming in air at room temperature, respectively. The average cooling rate during immersion was 53.2 °C/min, and the average warming rate was 2.9 °C/min. (c)The pre-programmed temperature profile in the Planer controlled rate freezer for the slow cooling protocol. The freezing and warming rate between set temperatures was 20 °C/min.

3.8. Typical pressure measurements in the isochoric chamber for pure Unisol solution. The pressures achieved during cooling and during warming are almost the same, indicating that those measurements are during thermodynamic equilibrium. These experiments established the baseline for interpreting the effect of adding Propane-diol and Me_2SO. A) Cooling in steps from room temperature down to -160˚C and warming back to room temperature, and B) For rapid cooling in liquid nitrogen for 15 minutes followed by warming in air.

3.9. Typical pressure measurements in the isochoric chamber for Unisol mixed with propane-diol in various concentrations. Vitrification, denoted by no pressure increase, is observed in the 30% (w/v) Propane-diol (PD) solution during the rapid immersion in liquid nitrogen. Devitrification can be seen during the warming when the pressure is observed to increase. A) 10% (w/v) PD in Unisol cooled in steps from room temperature down to -160˚C and warmed back to room temperature. B) 10% (w/v) PD in Unisol rapidly cooled in liquid nitrogen for 15 minutes and warmed in air. C) 20% (w/v) PD in Unisol cooled in steps from room temperature down to -160˚C and warmed back to room temperature. D) 20% (w/v) PD in Unisol rapidly cooled in liquid nitrogen for 15 minutes and warmed in air. E) 30% (w/v) PD in Unisol cooled in steps from room temperature down to -160˚C and warmed back to room temperature. F) 30% (w/v) PD in Unisol rapidly cooled in liquid nitrogen for 15 minutes and warmed in air.

3.10. Typical pressure measurements in the isochoric chamber for Unisol mixed with Propane-diol (PD) in various concentrations. Vitrification, denoted by no pressure increase, can be seen in the 40% (w/v) PD solution during the rapid immersion in liquid Nitrogen. Devitrification can be seen during the warming when the pressure increases again. Vitrification, known to occur at 44% (w/v), can also be seen by no pressure change. A) 40% (w/v) PD in Unisol cooled in steps from

room temperature down to -160˚C and warmed back to room temperature. B) 40% (w/v) PD in Unisol rapidly cooled in liquid nitrogen for 15 minutes and warmed in air. C) 44% (w/v) PD in Unisol cooled in steps from room temperature down to -160˚C and warmed back to room temperature. D) 44% (w/v) PD in Unisol rapidly cooled in liquid nitrogen for 15 minutes and warmed in air.

3.11. Typical pressure measurements in the isochoric chamber for Unisol mixed with 30% (w/v) Me_2SO. A) Cooled in steps from room temperature down to -160˚C and warmed back to room temperature. B), C) & D) Rapidly cooled in liquid nitrogen for 15 minutes and warmed in air. No pressure increase in one of the three rapid cooling runs which suggests this concentration is on the limit for vitrification in isochoric conditions, which is much lower than the 49% (w/v) Me_2SO concentration observed at atmospheric pressure.

3.12. Typical pressure measurements in the isochoric chamber for Unisol mixed with Me_2SO in various concentrations. Vitrification, indicated by no change in pressure, can be seen in the 35% (w/v) Me_2SO solution during the rapid immersion in liquid Nitrogen. Vitrification, known to occur at 49% (w/v) Me_2SO, can also be seen by no pressure change. A) 35% (w/v) Me_2SO in Unisol cooled in steps from room temperature down to -160˚C and warmed back to room temperature. B) 35% (w/v) Me_2SO in Unisol rapidly cooled in liquid nitrogen for 15 minutes and warmed in air. C) 49% (w/v) Me_2SO in Unisol cooled in steps from room temperature down to -160˚C and warmed back to room temperature. D) 49% (w/v) Me_2SO in Unisol rapidly cooled in liquid nitrogen for 15 minutes and warmed in air.

3.13. Single-phase isochoric freezing. A. Schematic of an experimental isochoric chamber, loaded with a single homogeneous solution. Cross-sectional view depicts the two-phase liquid-solid equilibrium characteristic of isochoric freezing. B. Phase diagram of pure water. The equilibrium states of an isochoric system occupy the labeled liquidus curve between ice-1h and water between 0°C and the triple point of water, ice-1h, and ice III. C. Ice percentage vs. temperature for a generic series of solutions of varying solute concentration in an isochoric system. As the solute concentration increases, the freezing point of the solution will decrease and the ice percentage curve will shift deeper in temperature.

3.14. Multiphase isochoric freezing. A. Pressure-temperature diagram depicting the equilibrium states occupied by a system consisting of two distinct aqueous phases, one internal to and one external to the mass-impermeable boundary Γ. The system will follow three distinct paths as temperature decreases, presented conceptually in schematics B – D: On Path 1 (B), only the internal phase forms ice. This path is identical to the liquidus curve of the phase diagram of the internal phase. Path 2 (C) covers the temperature range between the temperature at which the internal phase has frozen completely and the pressure-adjusted freezing point of the external phase. On Path 3 (D), the external phase also forms ice. This phase represents a pressure-adjusted liquidus curve for the external phase.

3.15. Experimental results (markers) and theoretical predictions (curves) for a multiphase isochoric system employing an external phase of 2M glycerol and 0.9% physiological saline and an internal phase of pure water. Three internal phase volumes are presented: 12%, 24% 36% (presented left to right). A. Pressure data (measured directly). The theoretical internal phase liquidus line (blue)

is extended over the entire temperature range for easy reference to single-phase isochoric behavior. B. Ice percentage data (calculated from pressure data). C. Percent increase in concentration (calculated from pressure data).

3.16. Comparison of thermodynamic behaviors between single-phase isochoric and isobaric systems and a multiphase isochoric system. A. Comparison of the concentration increase experienced in a solution of 2M glycerol and 0.9% saline in an isobaric, single-phase isochoric, and multiphase isochoric system. B. Calculated freezing point curves for various solutions of interest to cryopreservation in a multiphase isochoric system, as a function of internal water phase volume. The freezing points of the solutions in a single-phase isochoric system can be found intersecting the y-axis (at 0% internal water volume).

4.1 Process and principles of isochoric preservation. (A) Schematic of isochoric preservation apparatus in exterior and cross-section views at various subfreezing temperatures. (B) Temperature-pressure relations in an isochoric system at subfreezing temperatures. (C) Comparison of NaCl concentration as a function of temperature during isochoric and atmospheric isobaric freezing of a NaCl solution, which at a pressure of 1 atm had a physiological concentration of 0.9% w/w.

4.2 Hematoxylin & eosin stains of tissue taken from the left ventricle of hearts preserved under a variety of conditions. Images captured at a 20x objective. (A) Fresh, healthy heart. (B) Heart preserved on ice at atmospheric pressure for one hour. Arrows identify points of interstitial edema. (C) Heart preserved at -4 °C (40.62 MPa) under isochoric conditions for one hour. Arrows identify points of interstitial edema. (D) Heart preserved at -6 °C (59.84 MPa) under isochoric conditions for one hour. Arrows identify example contraction bands. (E) Heart preserved at -8 °C (77.71 MPa) under isochoric conditions for one hour. Arrows identify example contraction bands.

4.3. Histological evaluation. (A) Overall injury scores considering integrity of myocyte structure, including regular arrangement of sarcomeres, interstitial edema, presence of contraction bands, and myocyte swelling. (B) Percent area occupied by interstitial edema in hearts preserved on ice in atmospheric conditions and at -4C (40.62 MPa) under isochoric conditions.

4.4. Pressure-time dependence of hearts based on functional evaluations. Healthy, rhythmically beating hearts are classified as optimal, hearts experiencing ventricular fibrillation or otherwise irregular beating are classified as sup-optimal, and hearts that failed to revive at all upon perfusion are classified as compromised.

4.5. Histological sections at 20x magnification from the left ventricular wall stained with Hematoxylin & Eosin. Hearts were classified as sub-optimal after exhibiting ventricular fibrillation upon perfusion after preservation under the following conditions: a. -2 ºC, 21 MPa, 6 hours. b. -4 ºC, 41MPa, 2 hours. c. -6 ºC, 59MPa, 1hour. Examples of contraction bands are marked by arrows, an example of disrupted sarcomeres is marked by the rectangular box, and an example of vacuolization is marked by the circle.

5.17. Transmission electron microscopy (TEM) (left) and field emission scanning electron microscopy (FE-SEM) (right) images of *S.* Typhimurium after (a) overnight growth (no treatment), (b) isobaric freezing at -15°C for 24 hours, or (c) isochoric freezing at -15°C (135MPA) for 24 hours. Bacteria subjected to isochoric freezing show cytoplasmic separation and bulk morphological deformation. Scale bars indicate 1 μm for TEM images and 2 μm for FE-SEM images.

5.18. Transmission electron microscopy (TEM) (left) and field emission scanning electron microscopy (FE-SEM) (right) images of *L. monocytogenes* after (a) overnight growth (no treatment), (b) isobaric freezing at -15°C for 24 hours, or (c) isochoric freezing at -15°C (135MPA) for 24 hours. Scale bars indicate 1 μm for TEM images and 2 μm for FE-SEM images.

5.19. Equilibrium states of isochoric systems at various temperatures and comparison to a standard isobaric system frozen at atmospheric pressure. a. Conceptual schematic. b. Phase diagram of water and ice, with the thermodynamic path followed during isochoric freezing indicated by the yellow arrows. c. Variation of the ice mass phase fraction with temperature for solutions of increasing solute concentration.

5.20. Ratio of the energy required to bring a system to equilibrium at subfreezing temperatures between 0 and -20C under isochoric and isobaric conditions (isochoric/isobaric) for different solutions, including: pure water, saline solution of concentration equivalent to fresh meat or fish, sucrose solution of concentration equivalent to cherries (14.5 brix), and sucrose solution of concentration equivalent to pomegranate (21.5 brix). a, Ratios considering two systems of identical size. b, Ratios considering an isochoric system sized such that the portion remaining unfrozen at a given temperature is equal to the total size of the isobaric system.

5.21. Isochoric Phase Change Model: A finite, one-dimensional, two-phase system is considered, bounded by an outer surface with an oscillating prescribed temperature and an insulated (symmetry) boundary. The time-dependent position of the phase change interface is marked by $S(t)$. The domain $0 < x < S(t)$ represents the solid (frozen) region, and the domain from $S(t) < x < B$ represents the liquid (unfrozen) region. The temperature at the interface is the phase change temperature of the system, which varies with interface position.

5.22. Internal temperature fluctuations experienced under isochoric (solid line) and isobaric (dashed line) conditions for various input parameters: a, Amplitude is varied. D = 0.1 m; w = 1/7200 s, T_D = -12C. b, Characteristic system length is varied; w = 1/7200 s, A = 4C, T_D = -12C. c, Frequency is varied; D = 0.1 m; A = 4C, T_D = -12C. *Note: all curves have been phase-shifted in time for ease of comparison.*

5.23. Ratios of the amplitude of temperature fluctuation experienced within identical systems under isochoric and isobaric conditions (isochoric/isobaric). a, Ratios for an applied amplitude of A = 4C and design temperature T_D = -12C, with varying frequency and characteristic length. b, Ratios for frequency w = 1/7200 s, with varying applied amplitude A, design temperature T_D,

and characteristic length. Note that curves for varying values of A at a given design temperature appear indistinguishable.

List of Table Descriptions

List of co-authors and collaborators

The following sections include work contributed to by the co-authors and collaborators listed here. In instances in which the work has been previously published, a citation is included in parentheses.

2.1. Wenhao Sun, Boris Rubinsky ([1])

2.2. Gideon Ukpai, Anthony Consiglio, Boris Rubinsky

3.1. Alexander Koh-Bell, Boris Rubinsky ([2])

3.2. Yanfang Zhang, Gideon Ukpai, Alexandra Grigoropoulos, Bradley Weegman, Michael Taylor, Boris Rubinsky ([3])

3.3. Justin Aruda, Boris Rubinsky ([4])

4.1. Lili Wan, Charles Lee, Anshal Gupta, Bradley Weegman, Mark Clemens, Boris Rubinsky ([5])

4.2. Lili Wan, Mark Clemens, Boris Rubinsky ([6])

4.3. Justin Aruda, Yanfang Zhang, Boris Rubinsky ([7])

5.1. Cristina Bilbao-Sainz, Amanda Sinrod, Lan Dao, Gary Takeoka, Tina Williams, Delilah Wood, Gideon Ukpai, Justin Aruda, David Bridges, Vivian Wu, Tara McHugh, Boris Rubinsky ([8])

5.2. Cristina Bilbao-Sainz, Amanda J.G. Sinrod, Lan Dao, Gary Takeoka, Tina Williams, Delilah Wood, Bor-Sen Chiou, David Bridges, Vivian Wu, Chenang Lyu, Tara McHugh, Boris Rubinsky

5.3. David Bridges, Cristina Bilbao-Sainz, Gideon Ukpai, Tina Williams, Deliah Wood, Amanda Sinrod, Tara McHugh, Vivian Wu, Boris Rubinsky

5.4. Boris Rubinsky ([9])

1. Introduction: Phase-Change Thermodynamics and the Dream of Full-Organ Cryopreservation

For as long as humanity has ruminated on the elements, it has harbored conflicting feelings about the cold. Many of the benchmark feats of human engineering throughout time immemorial—the mastery of fire, the discovery of electricity, so on and so forth—have been brought to bear against it, in the ongoing effort to manage our nature as warm-blooded creatures. Conversely, the remarkable ability to delay the expiration of food, vaccines, and other biologics via refrigeration and freezing has played an unmistakable role in the gradual improvement of global health. Thus, from instance to instance, field to field, our impressions of the relative benefits and behaviors of the cold are wonderfully varied.

As it pertains to human biology, the notion that exposure to extreme cold may prove beneficial (rather than damning) is quite young; methods of producing cryogenic temperatures were not developed until the late 18th century, and it was only the dawn of the 20th century that saw the first concerted scientific efforts to leverage the deep cold for medical benefit in the preservation of mammalian biological matter.

At the heart of these efforts sits metabolism, the sum total mechano-electro-chemical processes that comprise what we know as life. Like most energetic processes, metabolism is highly temperature dependent. As the internal temperature of living biological matter is reduced, its metabolism slows strongly, grinding to a near-halt at the temperatures of dry ice (-80°C) or liquid nitrogen (-196°C) and preventing natural biological aging or expiration. It is the simple fact of this temperature dependence that gave birth to the modern notion of cryopreservation, the goal of which is to delay or defeat the natural expiration of *ex vivo* biological constructs for medical purposes.

Stemming from *krúos,* the Ancient Greek word for frost, the grander field of "cryobiology" that we now know to encompass all manner of low-temperature medical efforts was born following the pivotal (and accidental!) discovery of the cryoprotective effects of glycerol in 1948[10], which ignited the now-70 year long quest for cryopreservation protocols that would enable long-term preservation of complex living biological constructs.

The grand challenge facing cryobiologists can be boiled (or perhaps frozen) down into a single simple conundrum: In order to suspend the metabolic activities of biological matter, it must be held at temperatures well below the freezing point of water, its principal chemical constituent. However, both intracellular and extracellular ice formation within complex tissues is damning[11–13], and thus a wonderfully fundamental problem emerges: How can we hold water at temperatures beneath its freezing point without allowing it to freeze?

Efforts to answer this question over the past seven decades have taken an overwhelmingly chemical approach, largely defined by the search for non-physiological cryoprotectant agents

(CPAs) that substantially depress the equilibrium freezing point of water whilst maintaining sufficiently non-cytotoxic, sufficiently diffusible at low temperatures, etc[14,15]. However, at the full-organ and tissue scale, this approach has yielded few meaningful advances since the 1980's, and thus fundamentally new approaches to the problem of cryopreservation are sought.

In this thesis, I will present theoretical and experimental advancements in the exploration of a new generation of non-CPA-driven cryopreservation protocols. Instead of manipulating the chemistry of a system to attain desired stable phase behavior, my work seeks to manipulate the broader thermodynamic context— escaping conventional temperature-pressure thermodynamic boundary conditions to induce new phase equilibria, alter nucleation kinetics, or stabilize metastable phases. In particular, I will explore the rich thermodynamic and kinetic behaviors of water and ice in systems confined under isochoric (constant-volume) conditions, examining both stable equilibrium, metastable, and non-equilibrium phase change scenarios, and provide initial experimental validation of the promise of isochoric preservation techniques for full-organ cryopreservation. I will also demonstrate the translatability of the isochoric freezing concepts developed herein to food preservation domain, and identify continuing research objectives and paths by which this work may be carried into the future.

1.1 Motivation: An organ and tissue preservation crisis

An average of twenty people die every day while waiting for an organ transplant in the United States. More than 114,000 patients currently sit on the transplant waiting list, and every ten minutes, another is added[16]. With only approximately 10% of the global need for organ transplantation currently being met, many will die there[16].

Organ and tissue transplantation represents one of the great medical achievements of the 20th century, and its widespread adoption has the potential to radically transform medicine as we know it. Currently however, the demand for transplantation across the globe overwhelms the supply. Factors contributing to this dilemma do include matters of law, policy, and economics, but the principle factor constraining widespread transplantation is much simpler: preservation.

Transplantable organs and tissues must originate from living donors and only have a few hours of viability once removed from the body. Current *ex vivo* survival time for lungs and hearts is limited to 4 to 6 hours[17]—barely long enough to perform the transplantation procedure itself, let alone perform a comprehensive donor-recipient matching or fly the organ coast-to-coast.

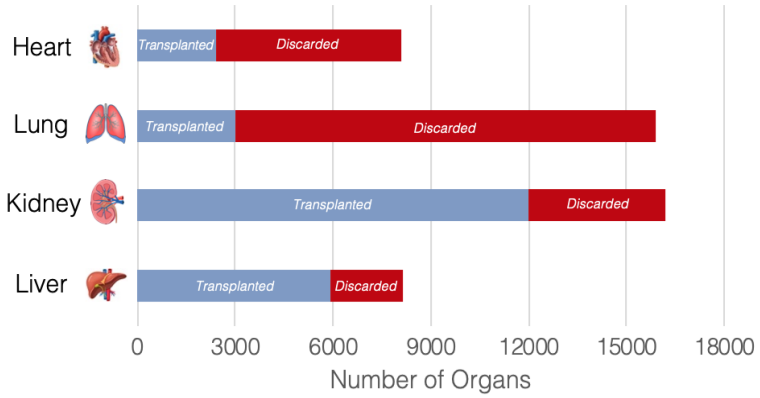

Figure 1.1. Utilization of organs obtained from organ donors in the US.

In principle, one organ donor can provide up to eight viable organs (and many additional tissues), but only three organs are transplanted on average[16,18]. Due to our extremely limited current ability to preserve and transport organs outside the body, each year thousands of abdominal organs are disposed of, while more than 70% of all thoracic and pulmonary organs (hearts and lungs) are not transplanted (Figure 1), equating to thousands of preventable deaths. Furthermore, transplant centers typically only have *one hour* to respond to a potential organ from a donor and decide whether to accept it or not[18]. This time constraint leads to a large number of rejected organs due to uncertainties in patient immunological compatibility and availability, further increasing organ waste.

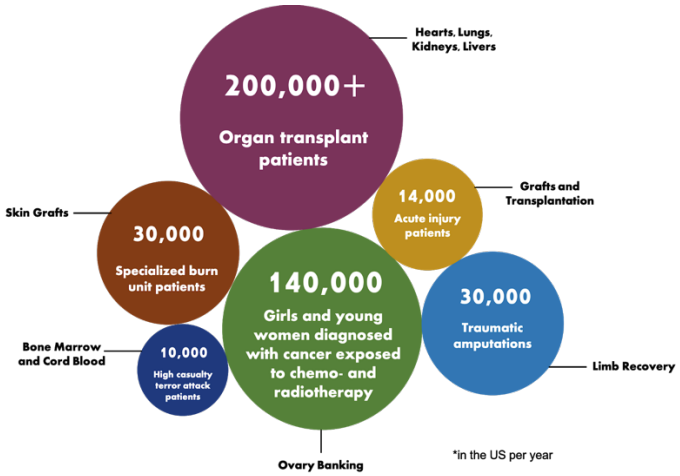

Figure 1.2. Number of patients in the U.S. would benefit from effective preservation of organs and tissues.

Organ and tissue preservation is a global public health issue. As shown in Figure 2, the breadth of patients requiring transplants is expansive – cancer patients, victims of terrorism and natural disasters, heart attack victims, and burn victims are just a few examples — and transcends continents and cultures. Access to life-saving medical care is a human right, but currently our most

powerful surgical techniques are hamstrung by our simple inability to preserve donor organs. At present, no effective full-organ preservation and transportation method exists to address these issues. Development of such a method could revolutionize the healthcare industry and democratize organ transplantation globally, and represents the grand challenge of the modern cryobiologist.

1.1.2 Current Clinical Organ and Tissue Preservation Techniques

The most common clinical preservations methods for preservation of organs and tissues involve rapid onsite cooling using an oxygenated cold-storage solution on ice to prevent hypoxic (oxygen deficiency) damage and reduce cellular metabolism. As stated, metabolism depends strongly on temperature; thus by cooling an organ *ex vivo*, the rate at which it naturally expires can be slowed, and the period for which it can be preserved depends directly on how low a storage temperature can be achieved. In today's healthcare landscape, only two methods, static cold storage (SCS) and hypothermic machine perfusion (HMP), are clinically approved for cold-storage of kidneys, while only SCS is approved for livers, lungs, pancreases, and hearts.

In current clinical contexts, static cold storage of organs is usually performed at 4°C and atmospheric pressure. While these conditions slow the deterioration of organ quality by reducing the temperature, current SCS is acutely limited in its range, because as temperature decreases below 4°C, the threat of freezing becomes imminent[19]. This limit on organ preservation temperature using SCS translates to only brief periods of preservability. As such the organ must be transported rapidly using helicopters, ground transport, or private commercial airplanes, which dramatically increases the total cost of the procedure. This short viability time furthermore demands that a surgical team be ready day-or-night at a moment's notice. These infrastructural limitations not only lead to waste of available organs, but also make the miracle of modern transplantation unavailable to many people[18], including those who cannot afford the up-to-one million dollar bill and those who live far from the country's largest city hospitals. Thus, even if an appropriate organ match is found for a patient in critical need, regional and financial limitations may prevent them from receiving transplant surgery. Unfortunately, this disproportionately negatively affects less privileged populations who do not live close to hospitals and cannot afford to move closer to one.

It has been estimated that, should we be able to eliminate these myriad infrastructural and technological supply constraints on donor organs, *more than 30% of all deaths in the United States could potentially be prevented*[16,18].

1.1.3 Emerging organ and tissue preservation techniques in the high-subzero temperature range

Traditionally, cryopreservation protocols have targeted the deep cryogen temperature regimes (-196°C to -80°C) at which cellular metabolism is near-totally arrested and years-long preservation is enabled. While this regime remains an ultimate target for the cryobiology community (see here an excellent review of modern efforts[20]) , it has been acknowledged in recent years that even short-term (on the scale of days or weeks) preservation of sensitive biologics such as complex tissues or organs could be transformational, enabling intercontinental transportation of these materials, unprecedented sharing of biological resources for both medicine and research between countries,

etc[16]. Thus the development of effective preservation techniques that operate in the high-sub-zero centigrade temperature range (-20°C to -3°C) are of paramount interest in the quest for near-term solutions to the organ and tissue preservation crisis. While comprehensive reviews of the high-subzero preservation literature are elsewhere[17,20,21], I will briefly discuss techniques of particular relevance to the modern cryobiologist.

In the past two decades, many new techniques have emerged which target the high sub-zero temperature range. Notable among these are equilibrium non-freezing (also known as "liquidus tracking") techniques in which cryoprotectant agents are administered gradually to the biologic and surrounding solution as cooling progresses, with the goal of maintaining the biologic above the freezing point of the solution at all times whilst minimizing diffusion limitations and osmotic shock issues[22–24], and equilibrium controlled or partial freezing techniques, inspired by the wood frog *Rana sylvatica*, which seek not prevent to ice formation within the biologic but to limit its damage and control its growth[21,25–27]. These techniques, while certainly marked by increased sophistication of execution, bear significant conceptual similarity to the classical techniques of the early and mid-20th century, and revolve around the core phenomenon of cryoprotectant freezing point depression. While demonstrating promise in some smaller tissue constructs, with fundamental diffusion and toxicity limitations linked to the infiltration of high-concentrations of cryoprotectants into complex biological structures, implicitly lack volumetric scalability, and have not been validated in full-organ systems. A third high-subzero technique however has been demonstrated on systems varying from red blood cells to full human livers, and accounts for a sharp majority of recent studies producing successful full-organ trials: thermodynamic supercooling.

When an aqueous solution remains liquid at temperatures below its equilibrium freezing point, it exists in a metastable "supercooled" state. In this state the thermodynamic driving forces that propel phase change are insufficiently strong to cause immediate spontaneous freezing, and a delicate pseudo-equilibrium is achieved. The capacity for supercooling of a given solution is a function of a wide-range of parameters, including volume, temperature, surface interactions with its container or surroundings, solutes, etc., and our current ability to rigorously predict supercooling efficacy in solutions containing various solutes and biological materials is limited. However, early experimental work applying supercooling to the preservation of various biologics has shown tremendous potential.

Huang et al. demonstrated a simple first-order procedure in which they capped vials of cellular suspensions with an oil phase (commercially available mineral and vegetable oils) in order to eliminate the air-water interface (which was determined to provide a prominent nucleation site for ice) and achieved supercooling of volumes relevant to cellular preservation (up to 100 ml) for up to 100 days at temperatures as deep as -20°C, reporting human red blood cell viabilities above 90% [28]. Applying supercooling in combination with sub-normothermic machine perfusion and relatively light concentrations of cryoprotectants 3-OMG and PEG, Berensden et al. developed a protocol enabling 4-day preservation of rat livers at -6°C, representing a tripling of the current clinically achievable preservation period[29]. While the net success of this preservation protocol cannot be extricated from the technologically-complex machine perfusion step, it is regardless a strong indicator of the potential of supercooling in preservation whole-organ or complex tissue applications. This combined supercooling/machine perfusion approach was also successfully

scaled to human livers[30] (with the addition of the cryoprotectant glycerol), demonstrating 27+ hour preservation at -4°C and validating the first successful doubling of the preservable period of a human organ in the modern age. Amir et al. further achieved a 5-fold increase in preservability of rat hearts using anti-freeze proteins derived from Arctic fish, which enable a unique state of stable supercooling at -1.3°C [31,32].

The chief and potentially grounding drawback of supercooling techniques is of course the lack of global thermodynamic stability[33]. All manner of mechanical or thermal perturbations to a metastable system can cause nucleation and growth of the stable (ice-1h) phase, leading to rapid and irreversible destruction of the tissue. It is this lack of stability which limits the depths of temperature reachable by supercooling, and perhaps more importantly in these early stages, limits the potential utility of supercooling techniques outside of an ultra-controlled laboratory environment. Looking towards the dream of transportable, non-geographically limited organ preservation, fundamental efforts to enhance the stability of supercooling techniques must be undertaken in order to realize this approach at the clinical or industrial scale. Rigorous effort to document the capacity for supercooling across the wide gamut of oft-employed preservation solutions and thermodynamic contexts could provide a roadmap enabling the development of high-efficacy, low-cost supercooling protocols.

1.2 Isochoric Freezing: A thermodynamic approach to a thermodynamic problem

Life on planet Earth has evolved under near-constant pressure conditions, and thus, motivated both by intuition and experimental ease, the overwhelming majority of all biological research has been conducted under these same conditions. This includes of course cryobiological research, which has nigh-invariably been conducted in isobaric (constant pressure) thermodynamic contexts, be they under atmospheric pressure or otherwise[34].

Given that two natural variables are required to specify the state of a given thermodynamic system, analysis of the thermodynamic problem of cryopreservation (e.g. the management of the phase transition of water) has traditionally been approached in terms of the natural variables temperature and pressure. This *T-P* framework is of course the most familiar to us for nearly all material applications— standard phase diagrams have *T-P* axes; we tabulate the thermophysical properties of matter at constant temperatures and pressures; we analyze the energetic behavior of materials using the Gibbs free energy *G(T,P),* etc. – and thus our most base intuitions about the behavior of the physical world are colored by this *T-P* lens.

Of particular relevance to cryobiology are our intuitions about the transition of water from its liquid form to its most common solid polymorph, ice-1h. The standard *T-P* phase diagram for water is provided in Figure 3.b. Ignoring kinetic effects (e.g. given an infinite amount of time), when we take water at constant atmospheric pressure and bring it from room temperature to some temperature below its atmospheric freezing point (273.15 K), we expect that it will freeze *completely*. This result is both consistent with our many quotidian observations of the freezing of water (imagine the filling and freezing of a tray of ice cubes), consistent with the phase diagram below, in which the two *T-P* points described each sit squarely in a single-phase region, and consistent with Gibbs' Phase Rule, one of the most fundamental tools guiding our understanding of phase existence or co-existence.

This core expectation about water's tendency to transition completely to ice is present throughout the past century of cryobiological research, consistent with the constant-temperature constant-pressure conditions under which said research has been conducted. These conditions however, are not a *requirement* of cryobiological research, but rather merely a *convenience*, and indeed if we shake the yoke of the *T-P* thermodynamic context, change the natural variables of the thermodynamic system in which water is compelled to freeze, our basest expectations about the phase behaviors of H_2O will change accordingly.

The notion of isochoric (constant-volume) cryopreservation was first conceived of by Boris Rubsinky in 2005[35], and is based on altering the thermodynamic context in which the freezing process occurs. Rubinsky et al. demonstrated that by physically confining water in a high-strength sealed container (depicted schematically in Fig. 3.a) with no air-infiltration and no exposure to the atmospheric pressure reservoir, the natural variables governing the thermodynamics of the confined system become temperature and *volume*, as opposed to temperature and pressure, and the phase change equilibria of the system shift radically.

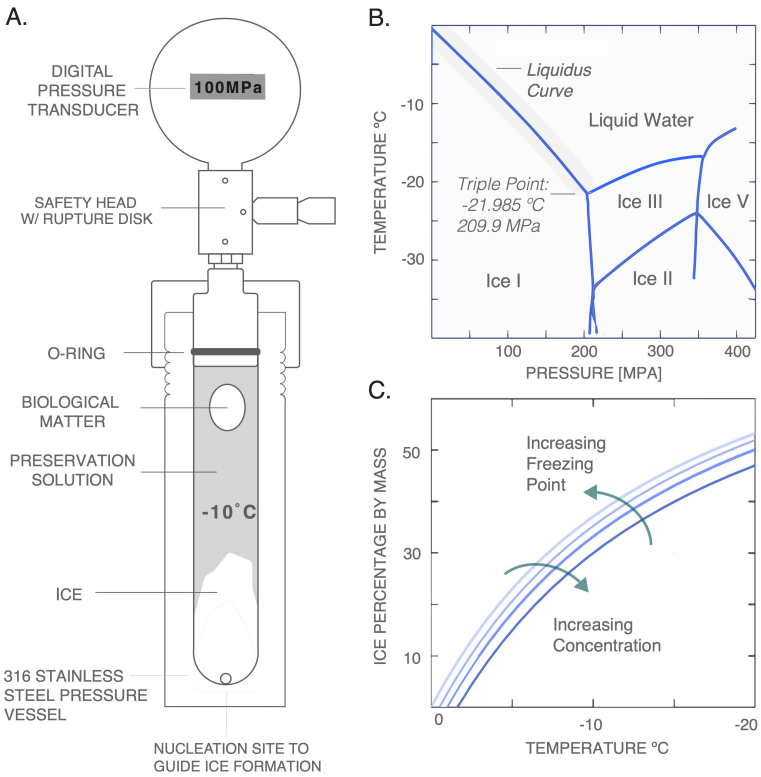

Figure 1.3. Isochoric freezing. **A**. Schematic of an experimental isochoric chamber, loaded with a single homogeneous solution. Cross-sectional view depicts the two-phase liquid-solid equilibrium characteristic of isochoric freezing. **B.** Phase diagram of pure water. The equilibrium states of an isochoric system occupy the labeled liquidus curve between ice-1h and liquid water between 0°C and the triple point of water, ice-1h, and ice III. **C.** Ice percentage vs. temperature for a generic series of solutions of varying solute concentration in an isochoric system, with the uppermost curve representing pure water. As the solute concentration increases, the freezing point of the solution will decrease and the ice percentage curve will shift deeper in temperature.

Given that ice-1h has a greater specific volume than liquid water (a relatively uncommon material feature), as the temperature is reduced and ice begins to form within the constrained system, its expansion causes an increase in pressure, consistent with Le Chatelier's principle, and this increase in pressure resists further expansion. By solving for mechanical equilibrium based on the compressibilities and thermal expansion of water and ice in an isochoric system, it can thus be demonstrated that between the atmospheric melting temperature (0°C) and the triple-point of water, ice-1h, and ice-III (-21.985°C) water and ice will maintain a *continuous* two-phase equilibrium (occupying thermodynamic states along the liquidus curve highlighted in Fig. 3.b), with approximately 46% (m/m) of the system remaining liquid at -20°C (Fig. 3.c).

In the context of cryopreservation, this stable and continuous two-phase equilibrium has significant and obvious implications—by performing cryopreservation within an isochoric system, the initial formation of ice will no longer lead to the inevitable freezing of the entire volume, as in an isobaric system. Instead, the growth of ice can be *restricted* and predictably controlled, and at any given subzero temperature above the triple point, biological matter may be stored in the portion that remains liquid without the threat of freezing. Furthermore, this significant change in phase behavior does not require chemical modulators or complex experimental efforts—it is enabled simply by constraining the macroscopic volume of the system, thus shifting its thermodynamic context from *T-P* space to *T-V* space.

Following the conception of the premise, a suite of early works clarified the base experimental operating principles of isochoric freezing, validating the pressure-temperature relationships observed in macroscale isochoric chambers comprised of high-strength metallic cylinders[36,37], clarifying the effects of unintended air infiltration[38], and hypothesizing effects that isochoric conditions may have on homogenous nucleus formation[39]. These initial studies culminated in the first validation of isochoric cryopreservation with live biological matter, in which the nematode *C. Elegans* was successfully revived after brief preservation at -6°C in an isochoric chamber, demonstrating the validity of the core cryopreservation hypothesis presented in Rubinsky's original 2005 work and setting the scene for the explorations presented in this thesis.

1.3 The Task of this Thesis

The goal of this thesis is two-fold. Firstly, it aims to explore the many rich thermodynamic and kinetic consequences of conducting phase transformations in macroscopically confined, constant-volume systems, and to meditate more generally on the value of escaping the *temperature-pressure* boundary conditions that have dominated the last 150 years of thermodynamic research and education. Secondly, it aims to envision and realize novel routes through which these alternative thermodynamic contexts may be applied to the grand challenge of preserving full organs and tissues outside the body, charting an alternative path forward which diverges from the overwhelmingly chemical approach that has defined cryobiology for the past eight decades.

The work will be subdivided into four central sections, each featuring varied investigations under a common theme. The first section will delve into the thermodynamics and kinetics of isochoric freezing at the fundamental theoretical scale, deriving new analytical tools which take system volume as a natural variable and allow nuanced probing of the effects of confinement at multiple scales on phase transition phenomena. The second section will present a series of applied experimental studies charting various previously unrealized thermodynamic phenomena observed

in isochoric systems, including stabilization of metastable supercooled water, enhanced vitrifiability of various aqueous solutions, and unique thermodynamic paths charted by isochoric systems featuring multiple chemical constituents. The third section will report a series of preliminary biological studies, which include the first validations of isochoric freezing in the cryopreservation of whole mammalian organs and tissues and indeed the first-ever demonstration of sub-zero centigrade heart preservation in the absence of chemical cryoprotectants. The fourth and final section will explore the concurrent potential of isochoric preservation in the food industry, featuring studies demonstrating high-efficacy long-term preservation of sensitive food constructs with high textural quality and nutritional retention, reporting significant inactivation of foodborne bacteria during isochoric freezing, and presenting heat transfer and thermodynamic analysis estimating that the incorporation of isochoric freezing could dramatically increase the energy efficiency of the global food cold chain.

The nature of this research ensures that the content included in the ensuing chapters will vary substantially in the fields from which it draws, incorporating elements of materials thermodynamics, heat transfer, fluid dynamics, biology, medicine, food science, etc. Thus, the author hopes that this document may serve as an apt starting point for any future researchers interested in navigating the largely-uncharted waters of isochoric cryopreservation, regardless of their specific backgrounds, and wishes the reader a stimulating journey through the chapters to come.

Chapter 2. Fundamental thermodynamic explorations of multiphase phenomena in confined isochoric systems

Classical thermodynamics is a self-consistent theoretical framework capable of describing equilibrium in terms of almost any conceivable physical variables, be they extensive or intensive, simple (pressure, volume) or more nuanced (epitaxy, stress-strain, electromagnetic fields, etc.). Thus it may be argued that the central challenge of classical thermodynamics is not to develop *a* formulation to describe the phase behavior of a given system, but to develop *the most appropriate* formulation based on what aspects and dependences of the system the formulator is attempting to probe.

In the case of the isochoric thermodynamics of water and ice, this distinction becomes very poignant—given our advanced understanding of the temperature-pressure relationship of water and ice, the compressibilities and expansion coefficients of each phase, etc., it is tempting to analyze isochoric freezing based on simple requirements of mechanical equilibrium between the phases, whilst applying some conservation of total volume. This approach will indeed generate first-order insight into the system—one can predict the phase fraction, the liquidus curve, etc.—but it fundamentally misses the broader implication of the *T*-*V* thermodynamic context: the *dependence* of system behavior on volume.

In this chapter, we will derive new theory to expose the unique effects of confinement at multiple scales on various phase change phenomena by incorporating volume (and abandoning pressure) as a natural variable of the thermodynamic system. We will derive a new *T*-*V* phase diagram for water and ice-1h based on the Helmholtz free energy surfaces, derive an isochoric theory of classical nucleation, reveal the existence of critical confinement volumes beneath which ice-1h is kinetically prohibited from forming, and explore the myriad effects of confinement on cavitation and cavitation-induced nucleation phenomena, using only the classical thermodynamic formalism.

2.1 Freezing water at constant volume and under confinement

Water is essential to nearly all biological, climatological, and industrial functions on planet Earth. Of enduring scientific interest are the various phase transitions undergone by water; both within the liquid state, and between its numerous condensed phases [40–45]. One phase transformation of emerging importance is the freezing of water in an undeformable, constant-volume container. This transformation has been identified in the bioengineering community as a compelling potential route to the ice-free cryopreservation of organs and tissues[46–49], is being investigated for low-temperature thermal phase-change energy storage[9], and may aid in describing fundamental atmospheric and climatological processes[50]. Recent molecular dynamics simulations and physical

observations have suggested that confinement of water in various meso- and nanoscale constrained-volume contexts can limit ice formation[50–58], and recent experimental work has also demonstrated that macroscopic confinement in isochoric (constant-volume) systems also restricts ice growth[59] and alters kinetic behavior[3,9]. Given this recent interest, a robust, multi-scale theoretical treatment of the thermodynamics and kinetics of freezing water in isochoric (constant-volume) systems is needed.

The phase transitions of water are generally described using natural variables of temperature T and pressure P, which correspond to the Gibbs thermodynamic potential $G(T,P)$. Consider the freezing of pure water in an undeformable container (that is, at constant volume). Water expands upon freezing to ice-1h, and should the container have a lower specific volume than that of ice-1h, the contents of the system will never be able to freeze entirely, resulting in a two-phase water-ice equilibrium. The standard T-P phase diagram for pure water includes only single-phase regions, so this anticipated two-phase equilibrium of water and ice under isochoric conditions cannot be quantified in a straightforward fashion from the traditional water phase diagram. By retaining pressure as a natural variable, one is forced to analyze this two-phase equilibrium as occurring between two distinct entities—the ice and the water—and one must solve for mechanical equilibrium by balancing the bulk moduli of the solid and liquid phases against the hydrostatic pressure that emerges as the ice forms and expands [59]. While the equilibrium states of the system can indeed be predicted using this approach, the mathematical formulation proves awkward, and must be continuously re-solved as temperature and pressure are altered.

While the Gibbs potential is appropriate under most physical contexts, it is only one of many possible Legendre transforms of the internal energy, $U(S,V)$, which has natural variables of entropy S and volume V. Should a situation arise in which the Gibbs free energy ceases to be convenient, it should be replaced in favor of a better-suited potential. For the case of freezing under isochoric conditions, a more elegant thermodynamic approach is to exchange pressure as a natural variable in favor of volume, thereby leveraging the Helmholtz thermodynamic potential for this analysis. In this description, the thermodynamic boundary conditions are reframed around the containing vessel, describing the entire two-phase water-ice system at once.

Herein we use the Helmholtz free energy to derive the equilibrium phase behaviors of water held in a constant-volume system at subzero temperatures. Our derivation yields the T-V phase diagram for water and ice, featuring a prominent two-phase equilibrium region, analogous to those found in binary eutectic phase diagrams. We also derive a classical nucleation theory for ice under isochoric conditions, which reveals fundamental differences between the kinetics of freezing under constant volume versus constant pressure. In isochoric systems, we reveal the existence of a critical absolute volume threshold (on the order of microns), under which nucleation of ice becomes kinetically prohibited. Our analyses here provide a classical foundation from which to analyze the thermodynamics and kinetics of freezing in isochoric systems; establishing context to interpret the phenomenology of water and ice under these important boundary conditions.

2.2.1 Developing a T-V Phase Diagram based on the Helmholtz Free Energy

Phase diagrams are constructed by a projection of the lowest free-energy phases onto axes of the natural thermodynamic variables. The choice of natural variables governs the geometry of the free-energy surfaces, and thereby the phase coexistence behavior in the resulting phase diagram.

In order for a homogeneous single-phase substance to be stable, its internal energy surface, U, must be positive-definite; $\partial^2 U/\partial X^2 > 0$, where X are the extensive thermodynamic variables $X = S$ *(entropy), V (volume), N (particle number), etc*. When it is not convenient to use an extensive natural variable, a new thermodynamic potential can be constructed with intensive natural variables, $Y = T$ *(temperature)*, P *(pressure)*, μ *(chemical potential)*, *etc*, by a Legendre transformation of the extensive variable with respect to its intensive conjugate, $U - (\partial U/\partial X)X = U - YX$ [60]. Following a Legendre transformation, the curvature of the free-energy surface becomes concave-down in the corresponding intensive thermodynamic variable(s) [61], or otherwise retains the concave-up curvature of U in the extensive variable(s) [62].

The Gibbs potential has intensive natural variables of temperature and pressure, and thus Gibbs free-energy surfaces are concave-down in both T and P. Projection of the lowest Gibbs free-energy phase onto the temperature and pressure axes recovers the standard T-P phase diagram, as shown for H_2O in Figure 2.1A, constructed using thermodynamic data from the International Association for the Properties of Water and Steam (IAPWS) [63,64]. For a single-component system like H_2O, phase coexistence is governed by the intersection of these concave-down free-energy surfaces, resulting in a 1-dimensional phase-coexistence line in the T-P plane.

In an isochoric system however, the natural variables should be temperature and volume, rather than pressure, which corresponds to the Helmholtz thermodynamic potential, F. We can construct $F(T,V)$ for water and ice-1h by a Legendre transform of Gibbs free energy data as:

$$F(T,V) = G(T,P(V)) - PV \qquad (2.1)$$

Because V is extensive and T is intensive, F is convex in volume ($\partial^2 F/\partial V^2 > 0$), and concave-down in temperature.

The convexity of the Helmholtz free-energy as a function of volume fundamentally changes the nature of phase coexistence in the T-V space. The lowest free-energy envelope now includes tangent lines between the convex $F_{water}(V)$ and $F_{ice}(V)$ curves, which signify a 2D two-phase equilibrium region, as opposed to a 1D phase-coexistence line. Gibbs called these tangent lines "Lines of Dissipated Energy" [65], along which a single-phase homogeneous substance can reduce its free-energy by forming a heterogeneous mixture of two phases. These tangent lines are analogous to those used in the convex hull construction of binary eutectic phase diagrams, which are constructed from the Gibbs free energy, $G(T,x)$[66]. The convex hull construction can be applied to both $G(x)$ and $F(V)$ because both composition (x) and volume (V) are extensive variables, and thus their free-energy surfaces are convex-up.

By projecting the lowest-energy convex hull formed by the F_{water} and F_{ice} surfaces in Fig. 2.1B, we construct the T-V phase diagram for water, shown in Fig. 2.1C. To the best of our knowledge, this phase diagram has not been reported previously in the literature. The T-V phase diagram of water features a two-phase equilibrium region, where the equilibrium phase fraction can be solved using the Lever rule, in the same manner employed for T-x binary eutectic phase diagrams[66]. For the reader's reference, the phase fraction as a function of temperature and system specific volume is shown in Figure 2.1D.

At a given temperature, the slope of these tangent lines, $(\partial F/\partial V)_T$, provides the pressure that the two-phase mixture exerts onto the constant-volume container. We mark these pressure isoclines on the T-V phase diagram in Figure 2.1C. Note that in the equilibrium two-phase region, the tangent lines connect the water and ice-1h free energy curves, implying that water and ice experience the same pressure, which is indeed a requirement for mechanical equilibrium.

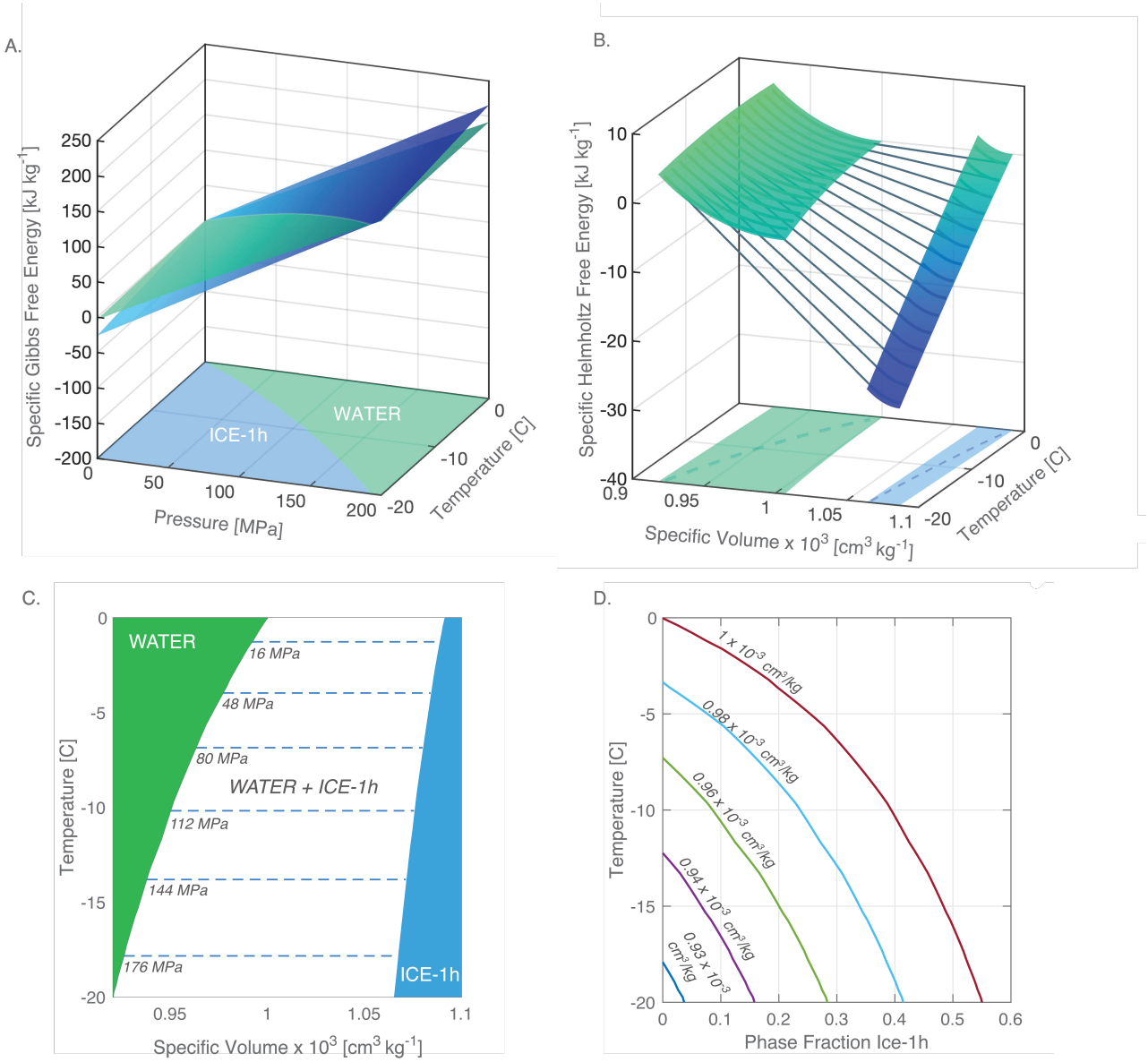

Figure 2.1. Thermodynamic landscapes of water and ice-1h under different thermodynamic boundary conditions. A. Gibbs free energy landscape of water and ice-1h in a system with natural variables temperature and pressure. The projection on the temperature-pressure plane gives the standard phase diagram for water. **B.** Helmholtz free energy landscape of water and ice-1h in a system with natural variables temperature and volume (plotted here in specific form for convenience). Common tangents between the phases define the range over which a two-phase mixture in equilibrium will produce the lowest system free energy. The slope of the common tangent gives the equilibrium pressure of the system. **C.** T-V (temperature-volume) phase diagram for water and ice-1h. **D.** Phase fraction of ice-1h as a function of temperature at various system specific volumes.

2.1.2 Physical motivations for an isochoric nucleation theory

The equilibrium *T-V* phase diagram produced in Fig. 1C is specific-volume dependent, as the phase-coexistence regions define thermodynamic equilibrium regardless of the amount of material present. We next show that the kinetics of nucleation in isochoric systems are additionally dependent on the absolute volume of the system container, and we leverage both dependencies to derive an isochoric theory of nucleation.

Consider the process of isochoric freezing, in which a closed, fixed-volume container filled with pure water is brought below 0°C to a metastable supercooled state (Fig. 2.2A). Before ice nucleates, the supercooled water will experience some pressure P_1, which is given by the slope of the tangent line $\partial F_{water}/\partial v$ at the specific volume of the container, as marked on Figure 2.2B. When ice-1h nucleates, the nascent nucleus will exert further pressure on the water and the container, and because the total system volume cannot change, the container will exert equal and opposite pressure back on both the water and the ice nucleus (Fig. 2.2C). This reduces the specific volume of ice and water, and increases their specific free energy according to the *F(v)* curves shown in Fig. 2.2B. We name the energy required for this pressurization of the system and densification of the initial liquid phase the "isochoric growth penalty", which can be interpreted as an energetic penalty that the solid phase must pay in order to grow within a system of constrained absolute and specific volume.

Intuitively, the magnitude of this penalty must vary with the absolute volume of the system; growth of a single ice nucleus confined in an ocean will cause no appreciable effect, but growth of the same nucleus in a nanoscale container may compress the remaining water significantly.

The pressure within the system is therefore a function of the relative phase fraction of ice that has grown. Because water and ice remain in constant mechanical equilibrium, the pressure experienced by both phases will be equal. Recalling that the pressure within a given phase at a given specific volume is described by the slope of the line tangent to its *F(v)* curve at that volume, this physical constraint can be illustrated by a "parallel tangent construction" as shown in Fig. 2B., whereby the specific volumes and energies of each phase for a given phase-fraction of ice are identified by the points on the *F(v)* curves for water and ice that yield parallel tangents between the phases.

The use of this parallel tangent construction to track continuity of pressure between phases is analogous to the tangent construction originally used by Gibbs to describe continuity of chemical potential between phases in binary systems at constant temperature and pressure[67]. During the growth of ice in an isochoric system (and the accompanying densification of both phases), the tangent lines will remain parallel while gradually increasing in slope until the two lines merge and form the common tangent, which marks the two-phase equilibrium state shown in Figure 1 and provides the equilibrium pressure $P_{equilibrium}$.

2.1.3 Mathematical formulation of the system

In the preceding section, it was established that in an isochoric system, the specific free energies of water and ice do not remain constant during the process of nucleation and growth, instead shifting dynamically along their respective $F(v)|_T$ curves according to the parallel tangent construction. In order to mathematically describe this behavior, an expression relating the specific volumes (and thus free energies) of the phases as a function of ice nucleus growth is needed.

Given a closed isochoric system, mass and volume must be conserved

$$m_{\text{system}} = m_{\text{ice}} + m_{\text{water}} \qquad (2.2)$$

$$V_{\text{system}} = V_{\text{ice}} + V_{\text{water}} \qquad (2.3)$$

which further implies conservation of specific volume. However, we note that the conservation of specific volume does not take the form $v_{\text{system}} = v_{\text{ice}} + v_{\text{water}}$ as might be expected, because the system specific volume is not itself an inherently conserved quantity; it is instead conserved as a simple mathematical consequence of the conservation of the system mass and volume, and is thus given by definition as:

$$v_{\text{system}} = \frac{V_{\text{system}}}{m_{\text{system}}} = \frac{V_{\text{ice}}+V_{\text{water}}}{m_{\text{ice}}+m_{\text{water}}} \qquad (2.4)$$

The requirement of equal pressure throughout the system provides the final constraint. Leveraging the parallel tangent logic, the pressures of ice and water during the non-equilibrium nucleation process can be tracked along the $F-v$ curves by their derivatives:

$$-\left(\frac{dF_{\text{water}}}{dv}\right)|_{v_{\text{water}}} = -\left(\frac{dF_{\text{ice}}}{dv}\right)|_{v_{\text{ice}}} \qquad (2.5)$$

In Appendix A1.1, we use these four constraints to determine the specific volumes of each phase as a function of nucleus volume $(v_{\text{water}}(V_{\text{ice}}), v_{\text{water}}(V_{\text{ice}}))$ along the reaction coordinate of the nucleation process. These specific volumes thereby give the specific free energy for both water and ice, $F_{\text{water}}(v_{\text{water}}(V_{\text{ice}})), F_{\text{ice}}(v_{\text{ice}}(V_{\text{ice}}))$ as a function of the ice nucleus volume, enabling derivation of the nucleation barrier.

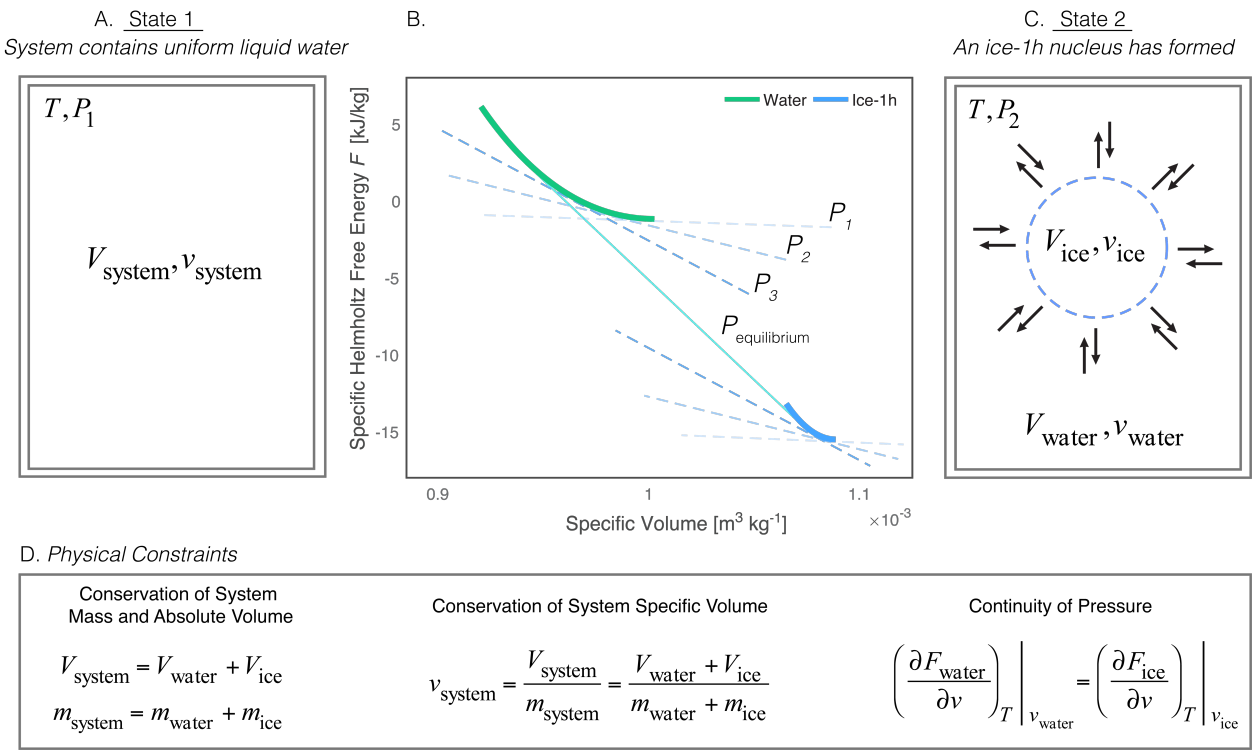

Figure 2.2. Conceptual formulation of the nucleation process in an isochoric system. A. The initial state of the system, in which the contents are entirely liquid. In this state, the absolute volume V and specific volume v of the system will equal that of the water phase by definition, as no ice is present. **B.** Parallel tangent construction. For an emergent ice nucleus of absolute volume V_{ice} in a system of absolute volume V_{system}, the specific volume and free energy of each phase can be found by identifying the points on each curve that will satisfy conservation of system mass, absolute volume, and specific volume, while producing tangent lines ($\partial F/\partial v$) that are parallel to one another, indicating continuity of pressure P throughout the system. At equilibrium, the tangent lines of the two phases will become colinear and the system will experience the equilibrium pressure $P_{equilibrium}$. **C.** A second state of the system, in which the finite mass and volume of the system are now split between water and ice phases possessing different absolute volumes (V_{ice} , V_{water}) and specific volumes (v_{ice} , v_{water}). The pressure within the system increases to $P_2 > P_1$ due to the expansion of the ice nucleus. **D.** Statement of the conservation relations governing the system.

2.1.4 Derivation of an isochoric nucleation barrier

We consider now two states that the isochoric system may occupy (Fig. 2.2A/C), subject to the established physical constraints (Fig. 2.2D). For clarity, we will describe the total free energy of the system with the variable $\emptyset$, and the specific Helmholtz free energies of each phase as F_{water} and F_{ice}. The subscripts 1 and 2 will be used to denote the values of parameters in States 1 and 2.

In State 1, the entire system is in the liquid phase, and its free energy is thus given by:

$$\emptyset_1 = F_{\mathrm{water}_1} m_{\mathrm{system}} \quad (2.6)$$

in which $F_{\mathrm{water}_1} = F_{\mathrm{water}}\left(v_{\mathrm{water}_1} = v_{\mathrm{system}}\right)$. In State 2, an ice-1h nucleus of absolute volume V_{ice} has formed, dividing the system into two phases with specific volumes $v_{\mathrm{water}}(V_{\mathrm{ice}})$ and $v_{\mathrm{ice}}(V_{\mathrm{ice}})$. Defining the ice phase fraction of the system as

$$f = \frac{m_{\mathrm{ice}}}{m_{\mathrm{system}}} = \frac{V_{\mathrm{ice}}\, v_{\mathrm{system}}}{v_{\mathrm{ice}}\, V_{\mathrm{system}}} \quad (2.7)$$

and incorporating a standard interfacial free energy term γ which scales with the surface area of the ice nucleus A_{ice}, the total free energy of State 2 is given by:

$$\emptyset_2 = \emptyset_1 + \Delta\emptyset = [\, F_{\mathrm{water}_2} \times (1-f) \;+\; F_{\mathrm{ice}_2} \times f \,] m_{\mathrm{system}} + \gamma A_{\mathrm{ice}} \quad (2.8)$$

in which $F_{\mathrm{water}_2} = F_{\mathrm{water}}\left(v_{\mathrm{water}_2} = v_{\mathrm{water}}(V_{\mathrm{ice}})\right)$ and $F_{\mathrm{ice}_2} = F_{\mathrm{ice}}\left(v_{\mathrm{ice}_2} = v_{\mathrm{ice}}(V_{\mathrm{ice}})\right)$. Rearranging these equations and grouping specific free energy terms by phase, the free energy change $\Delta\emptyset$ upon formation of a nucleus is given by:

$$\Delta\emptyset = \emptyset_2 - \emptyset_1 = \left[\, (F_{\mathrm{water}_2} - F_{\mathrm{water}_1}) + (F_{\mathrm{ice}_2} - F_{\mathrm{water}_2})\, f \,\right] m_{\mathrm{system}} + \gamma A_{\mathrm{ice}} \quad (2.9)$$

The two energy difference terms in eqn. (2.9) have distinct and meaningful physical significance. $(F_{\mathrm{water}_2} - F_{\mathrm{water}_1})$ describes the "isochoric growth penalty", or the energy required to pressurize the system and densify the water phase, which the emergent ice nucleus must provide in order to grow. This term will always be positive. $(F_{\mathrm{ice}_2} - F_{\mathrm{water}_2})$, which will always be negative, gives the bulk free energy difference between the phases at their present specific volumes, which is weighted by the phase fraction f in order to capture the two-phase nature of the equilibrium system.

The free energy change accompanying the formation of an ice nucleus in an isochoric system can thus be reduced to the following:

$$\Delta\emptyset = \left[\, \Delta F_{\mathrm{isochoric\,growth}} + \Delta F_{\mathrm{bulk}}\, f \,\right] m_{\mathrm{system}} + \gamma A_{\mathrm{ice}} \quad (2.10)$$

The interfacial and bulk free energy terms in eqn. (2.10) are roughly analogous to those found in classical nucleation theory; the former will scale with the surface area of the nucleus in the positive direction, the latter with its volume or mass in the negative. However, it is crucial to note that within the Gibbs formulation, the bulk free energy difference between water and ice is considered constant— whereas in an isochoric system, it varies as a function of the ice phase fraction, decreasing in magnitude as the ice grows in a reflection of the fact that the ultimate thermodynamic destination of the system is a state of two-phase water-ice equilibrium, not complete freezing.

The isochoric growth penalty term is unique to systems of constrained volume, and will be shown next to fundamentally alter the nucleation behavior.

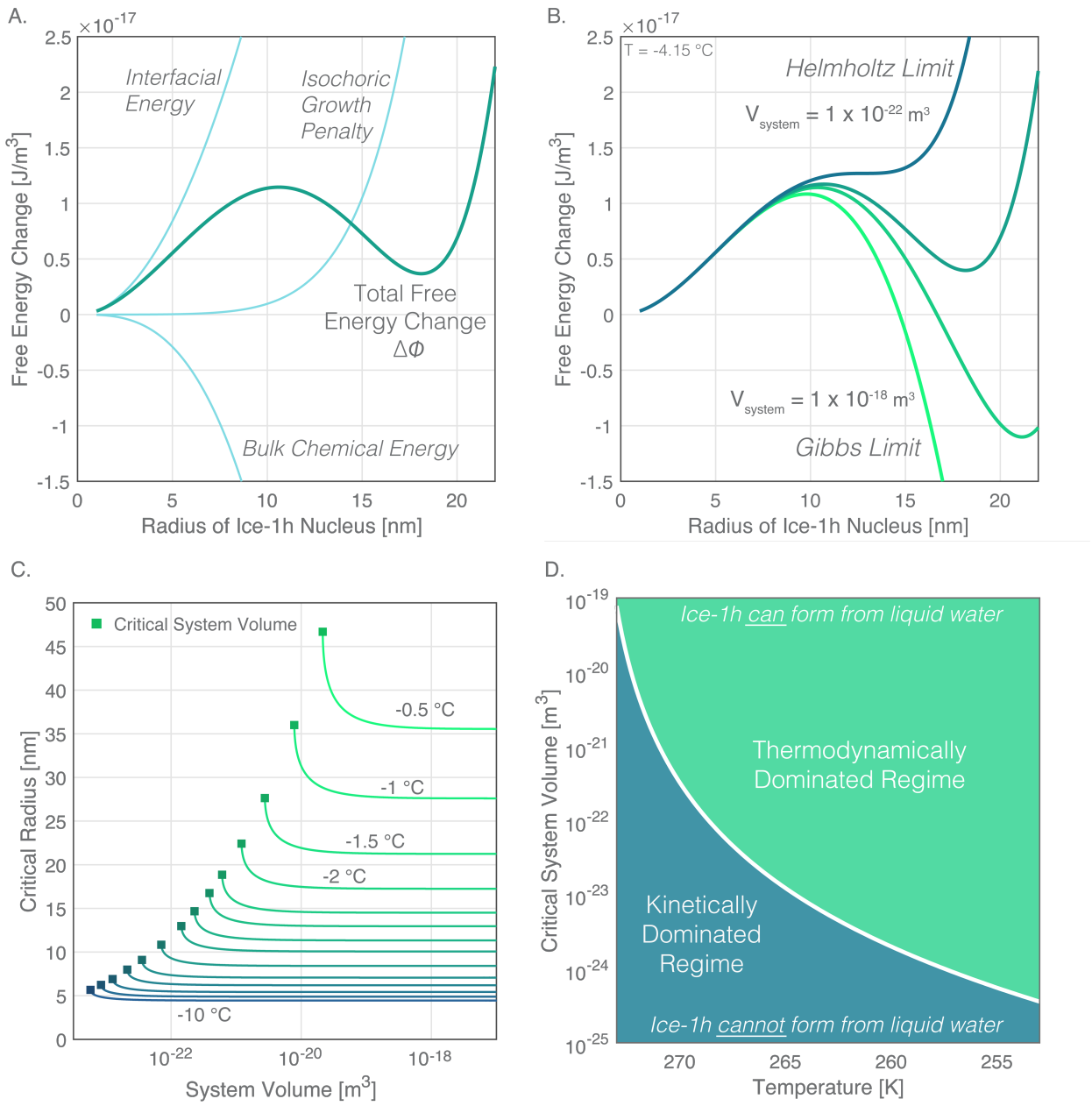

Figure 2.3. Nucleation kinetics in isochoric systems. A. Total free energy change ΔØ accompanying the formation of a spherical ice-1h nucleus as a function of radius. The interfacial, isochoric growth, and bulk free energy components contributing to the total are plotted independently. **B.** ΔØ curves for varying absolute system volumes. The Gibbs Limit gives the system behavior at the limit of infinite system volume, and the Helmholtz Limit at the critical system volume at which the free energy curve begins to increase monotonically. **C.** Critical radius as a function of system volume for various temperatures, with critical system volumes marked. **D.** Phase diagram mapping the critical system volume as a function of temperature. In the kinetically dominated regime, all ΔØ curves will be monotonically increasing, and thus no kinetic pathway to nucleation will exist.

2.1.5 Kinetic effects of isochoric confinement

In Figure 2.3A, we plot the total free energy change $\Delta\emptyset$ alongside the three separate energy contributions; the interfacial energy, the bulk energy, and the isochoric growth penalty. Our calculations for Figure 2.3A describe a single ice-1h nucleus of spherical geometry in a system of absolute volume $V_s \sim 2\ x\ 10^{-22}\ m^3$ at a temperature of $-4.15°C$, with an assumed interfacial free energy relation[68] of $\gamma = (28.0 + 0.25T)\ mJ\ m^{-2}$ (additional parameters available in Appendix A1.2). Figure 2.3B features additional $\Delta\emptyset$ curves for the same temperature but varying absolute system volumes V_s. These plots reveal a fundamental difference between ice formation at constant volume and ice formation at constant pressure: in the classical Gibbs formulation, the $\Delta G(radius)$ curve features *one* critical point, while in an isochoric system there are two critical points.

Classically, the critical point of the free energy curve is a maximum and defines the nucleation barrier, or the energetic barrier after which continued ice growth will lower the free energy of the system indefinitely until the entirety has changed phase. In the isochoric case however, ice growth is not indefinite—it must cease upon reaching the equilibrium phase fraction, in accordance with the *T-V* phase diagram (Fig. 2.1C/D). This limitation is captured kinetically by the isochoric growth term, and thus the $\Delta\emptyset$ curves can possess two critical points; the first a maximum at which the bulk driving force for phase transition overcomes the penalty of forming a new phase interface, and the second a minimum at which the isochoric growth energy overcomes the bulk driving force.

Importantly, because the isochoric growth term is a function of the absolute system volume (scaling as $V_{\text{ice}}/V_{\text{sys}}$), its contribution vanishes at the infinite volume limit, consistent with intuition. In this case, which we label the Gibbs Limit in Figure 2.3B, the $\Delta\emptyset$ free energy curve will be identical to that found using the classical Gibbs formulation, featuring only an initial maximum.

Conversely, as the system volume decreases the relative contribution of the isochoric growth term increases, both introducing the second critical point (corresponding to the phase fraction limitation) and increasing the critical radius of the nucleation barrier. This increase is captured in Fig. 2.3C, given as a function of absolute system volume for various sub-freezing temperatures. Note that at temperatures close to the freezing point, the effect of the volume constraint on isochoric nucleation can be significant even under relatively large system volumes—on the order of microns.

Our derivation further reveals the existence of a discrete absolute system volume, which we term the critical confinement volume, below which the second critical point will reach an energy equal to the first, erasing the inflection point between them and yielding a nucleus free energy curve that increases monotonically with radius. A representative free energy curve at this absolute volume threshold is labeled as the Helmholtz Limit in Fig. 2.3B. These critical confinement volumes are also marked on the critical radius curves in Fig. 2.3C, indicating the system volume at which the critical radius for nucleation would become infinite. These critical system volumes are then plotted independently against temperature in Fig. 3D, resulting in a "kinetic phase diagram" for freezing water under confined volumes. Our kinetic phase diagram reveals a unique implication for systems of constant volume: there exists a volumetric regime in which nucleation of ice-1h from the supercooled liquid state is kinetically impossible.

Notably, the existence of ice within this regime is not thermodynamically prohibited—comparing Fig. 2.3C with Fig. 2.1D it can be seen that these critical ice nucleus volumes are orders of magnitude smaller than the equilibrium phase fraction limit. These results indicate that ice could

theoretically *exist* at these system volumes (e.g. if an ice crystal was artificially seeded in the system and the volume was then constrained), but that supercooled water simply has no kinetic pathway to freezing in a sufficiently confined isochoric system.

2.1.6 The merits of a classical approach to confined thermodynamics

Many recent studies, based principally on molecular dynamics simulations or experimental observations, have suggested that confinement of water at small volumes limits ice formation [50–57]. This effect has been variously described as a depression of the equilibrium melting point, a purely probabilistic effect, a result of complex hydrogen or polar interactions, etc., and has been reported nigh-exclusively in systems with geometric constraints on the order of single nanometers[50,51,53,56]. Our results corroborate these previous findings of confinement-based freeze-inhibition, but also suggest that this behavior has more fundamental origins, and can in fact occur at characteristic length scales up to hundreds of nanometers (Fig. 2.3C/D). By making an appropriate choice of thermodynamic boundary conditions, in this case constant volume vs. constant pressure, we are able to infer this effect directly from high-level thermodynamic and kinetic analysis, without resorting to atomistic arguments. Furthermore, because volume itself is incorporated as a natural variable within our model, its applicability is not limited to a single system scale, and can instead be applied continuously from the nanoscale to the macroscale.

Other recent works have leveraged similarly unconventional classical thermodynamic boundary conditions to reveal previously inaccessible thermodynamic and kinetic information[69], using free-energy expressions that can include forms of thermodynamic work beyond temperature and pressure—including surface work (size, adsorption) [70,71], elastic work (epitaxy, stress-strain) [72,73], electromagnetic work (electrical polarization, magnetic polarization) [74,75], chemical work (such as compositional variation, precursor activity) [76,77], and more. These findings as a whole suggest that the Gibbs free energy alone is unable to capture the wide range of thermodynamic equilibria and kinetic behaviors encountered in materials systems in the diverse modern technological environment.

The kinetic analysis provided herein only describes the formation of the first ice-1h nucleus in an infinitely rigid container (e.g. a container of truly constant volume), and is subject to further simplifying assumptions, including the assumptions of spherical nuclei and that the first nucleus to form from supercooled water will be hexagonal and not cubic in structure[78]. A standard form of the temperature-dependent interfacial free energy is also assumed[68], though this relation may in fact vary in as-of-yet undetermined ways under the described isochoric conditions. Despite these simplifying assumptions, the conceptual insights revealed herein provide the foundations for a wide range of further study, and outline the limiting energetic behaviors of ice nuclei in isochoric systems. We anticipate that in systems that deviate from the conditions and assumptions described herein, ice nucleation kinetics will lie somewhere between the identified Gibbs and Helmholtz limits. For example, systems of nanoscale volume found in biological matter may experience a reduced isochoric growth penalty due to the finite rigidity of the container, but the excess energy required to grow in a constrained volume is still a physically pertinent feature. Conversely, within the thick-walled metallic containers employed in cryopreservation, the assumption of infinite rigidity is likely acceptable, but the macroscopic volumes are too large to appreciate the effect of a single ice nucleus. The continuity of pressure within the system remains however, forcing every growing nucleus to interact with every other via pressure, and thus some macroscopic effect on the kinetics may still be observed. This may have useful implications, such as enhanced or high-

stability supercooling due to heightened nucleation barriers, and ensemble-level analysis built from the single-nucleus isochoric nucleation theory should be studied in the future.

We further anticipate that additional analytical study of water under alternative thermodynamic boundary conditions (e.g. constant electric field, polarization density, etc.) may yield further profound results currently inaccessible under the constant-pressure Gibbs formulation. It should also be noted that the isochoric nucleation analysis developed herein is not exclusive to the water/ice-1h transition, but can also be applied to any other confined system in which a phase transformation results in a higher molar volume, such as in elemental Gallium.

2.2 Suppression of cavitation-induced nucleation in systems under isochoric confinement

Efforts to suppress the nucleation of solid phases in supercooled liquids are ubiquitous in fields ranging from metallurgy[79] to food science[80], and nucleation suppression has recently emerged as an essential route towards long-term organ and tissue preservation[28,30,81]. Nucleation is difficult to avoid in mobile or industrial contexts however[33], because acoustic agitations of any kind can cause the liquid phase to cavitate, which results in ultrarapid, high-pressure nucleation events[82,83]. In this section, we explore the effects of isochoric (constant-volume) confinement on the cavitation dynamics and nucleation kinetics of aqueous systems exposed to ultrasonication, one of most reliable sources of rapid nucleation[84]. We herein unify bubble dynamics, thermodynamics, and classical nucleation theory to demonstrate that confinement across multiple volume scales can dramatically decrease peak cavity collapse pressures and dampen cavitation-induced nucleation under a wide range of operating conditions. Furthermore, we demonstrate the existence of a critical confinement volume, on the order of 10^8 times larger than the cavitating bubble itself, beneath which cavitation-induced nucleation becomes entirely kinetically prohibited. Our results reveal fundamental insights into the effects of multi-scale confinement on kinetic phase change processes, and suggest that confinement could provide a compelling route towards high-stability supercooling.

Mechanical and acoustic stimuli of all manner have been known to induce ice nucleation from supercooled liquids for over a century[85], and the seminal works of Hickling[82,83] clarified this effect to be caused by the collapse of cavitating bubbles within the liquid. Collapse events occur over the span of nanoseconds, and can cause local pressure excursions on the order of several gigapascals in the surrounding medium. In low-thermal-diffusion media such as water, this dynamic compression is sufficiently rapid to be considered quasi-isentropic, and will thus drive the local water up in temperature along an isentrope as it pulses in pressure[82]. During this quasi-isentropic compression, the liquid water rapidly traverses the equilibrium domains of several high-pressure ice polymorphs, and the thermodynamic driving forces for nucleation skyrocket as the delta between the equilibrium temperature of the polymorph and the temperature along the isentrope increases. Ice VII clusters will form nigh-instantaneously during such dynamic compression processes[83,86,87], and it is assumed that these short-lived clusters then serve as ultra-potent nucleation sites for ice-1h upon return of the water to its initial temperature and pressure[82], producing the macroscopic result of rapid ice-1h formation associated with sonic agitation of supercooled water[84].

Given the extreme consistency of cavitation-induced nucleation, ultrasonicated systems (which aggressively cavitate) provide an excellent platform for the study of nucleation suppression. In our recent experimental work (discussed in the following chapter)[88], it was observed that macroscopic volumes of supercooled water (~100 mL) confined in an isochoric container were resistant to nucleation via ultrasonication as well as other mechano-acoustic stimuli, suggesting the absence or dampening of cavitation-induced nucleation processes. In the present work, we conduct a fundamental analysis of the effects of multiscale confinement on cavitation-induced ice nucleation, and in the process uncover fundamental limiting behaviors relevant to cavity collapse, nucleation, and the broader spectrum of kinetic processes under confinement.

2.2.1 Cavitation dynamics: A confined model

In formulating this analysis, we must first acknowledge that the nucleation phenomena of interest are mathematically linked to cavitation via quasi-isentropic compression, the magnitude of which is dependent upon the pressure excursions encountered during cavity collapse. Thus, we begin by analyzing the dependence of cavity collapse dynamics on confinement.

The derivations presented herein follow the approach implemented by Gilmore[89], modified for consideration of a finite domain. The problem considered herein describes cavitation dynamics under confinement in an isochoric container subjected to an ultrasonic pressure field, enabling study of collapse effects as a function of container size. The mathematical formulation is defined by a single spherical bubble located at the center of a rigid, spherical vessel, as shown in Fig. 2.4.

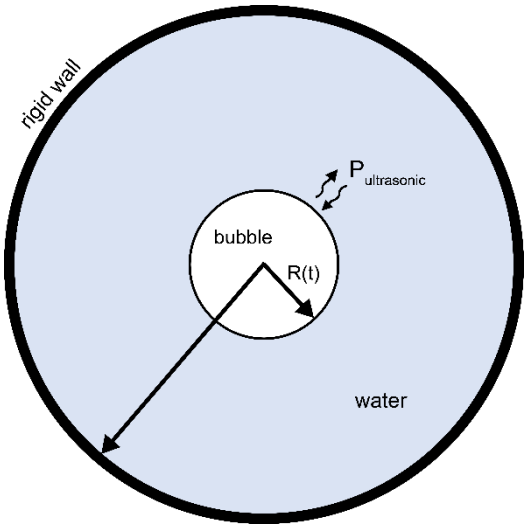

Figure 2.4: Schematic of spherical bubble in a rigidly confined liquid medium.

Radial, compressible flow is prescribed, and the gas inside the bubble is assumed to be spatially uniform. The effect of gravity and any initial temperature variations are neglected. Thus, the equations of motion describing the conservation of mass and momentum in the liquid are

$$\frac{1}{\rho}\frac{d\rho}{dt}+\frac{1}{r^2}\frac{\partial(r^2u)}{\partial r}=0 \tag{2.11}$$

$$\frac{\partial u}{\partial t}+u\frac{\partial u}{\partial r}+\frac{1}{\rho}\frac{\partial p}{\partial r}=0 \tag{2.12}$$

where ρ is the density, u is the velocity and p is the pressure. The viscosity enters the problem solely as a boundary condition, as will be seen later, since viscous effects are confined to a thin boundary layer at the bubble surface and have been found to have a negligible effect on bubble dynamics[89–91].

The momentum equation is integrated from the liquid-gas interface at the bubble wall, R_b, to the container wall or confinement radius, R_c:

$$\int_{R_b}^{R_c} \left[\frac{\partial u}{\partial t} + u\frac{\partial u}{\partial r} + \frac{1}{\rho}\frac{\partial p}{\partial r}\right] dr = \int_{R_b}^{R_c} \frac{\partial u}{\partial t} dr + \left[\frac{1}{2}u^2 + h\right]_{R_b}^{R_c} \tag{2.13}$$

where the enthalpy at constant entropy, h, is given as

$$h = \int_{p_0}^{p} \frac{dp}{\rho} \tag{2.14}$$

The remaining integral in Equation 3 can be written as

$$\int_{R_b}^{R_c} \frac{\partial u}{\partial t} dr = \int_{R}^{R} \frac{1}{r^2}\frac{\partial (r^2 u)}{\partial t} dr \tag{2.15}$$

and using the definitions

$$\frac{1}{r^2}\frac{\partial (r^2 u)}{\partial t} = \frac{\partial u}{\partial r} + \frac{2u}{r} = \Delta_l \tag{2.16}$$

$$\frac{Du}{Dt} = \frac{\partial u}{\partial t} + u\frac{\partial u}{\partial r} \tag{2.17}$$

it can be reformulated by partial integration to obtain:

$$\int_{R_b}^{R_c} \frac{\partial u}{\partial t} dr = \left[-r\frac{Du}{Dt} + ru\Delta_l - 2u^2\right]_{R_b}^{R_c} + \int_{R}^{R} r\frac{\partial \Delta_l}{\partial t} dr \tag{2.18}$$

The remaining integral in Equation 8 can be evaluated by recognizing that the quantity $r\Delta_l$ is invariant in the acoustic approximation and thus satisfies the relation:

$$\frac{D(r\Delta_l)}{Dt} = \frac{\partial (r\Delta_l)}{\partial t} + c\frac{\partial (r\Delta_l)}{\partial r} = 0 \tag{2.19}$$

where c is the speed of sound in the liquid. Utilizing this, the integrated momentum equation can be assembled to yield:

$$\left[-r\frac{Du}{Dt} + r\Delta_l(u - c) - \frac{3}{2}u^2 + h\right]_{R_b}^{R_c} = 0 \tag{2.20}$$

From the continuity equation we find

$$\Delta_l = -\frac{1}{\rho}\frac{D\rho}{Dt} = -\frac{1}{K}\frac{Dp}{dt} \tag{2.21}$$

In the barotropic approximation, pressure is only a function of density, $p = p(\rho)$, and is described by the relation

$$K = \rho c^2 = \rho \frac{dp}{d\rho} \tag{2.22}$$

where K is the liquid bulk modulus and c is the speed of sound. Herein, K and c are evaluated at equilibrium conditions. Substituting this into Equation 2.20, we get

$$\left[-r\frac{Du}{Dt} + \frac{rc}{K}\left(1 - \frac{u}{c}\right)\frac{Dp}{Dt} - \frac{3}{2}u^2 + h\right]_{R_b}^{R_c} = 0 \tag{2.23}$$

To obtain an equation describing the motion of the bubble interface, Equation 2.23 must be evaluated at the bubble wall and confinement wall. The boundary conditions satisfied by the liquid at the bubble wall, assuming no diffusion of gas through the interface, are

$$u(R_b, t) = \dot{R}_b \tag{2.24}$$

$$p(R_b, t) = P_g(t) - \frac{2\sigma}{R_b} - 4\mu\frac{\dot{R}_b}{R_b} + P_A \sin(\omega t) \tag{2.25}$$

where, R_b is the evolving bubble radius, σ is the surface tension of the gas-liquid interface, μ is the liquid viscosity, $P_g(t)$ is the pressure of the gas within the bubble, P_A is the amplitude and ω is the frequency of the imposed ultrasonic pressure disturbance. The over dot indicates d/dt.

Adopting a polytropic equation of state, the pressure within the bubble under adiabatic conditions is given by the relation

$$P_g(t) = \left(p_{l,0} + \frac{2\sigma}{R_{b,0}}\right)\left(\frac{R_{b,0}}{R_b}\right)^{3\gamma} \tag{2.26}$$

where γ is the ratio of specific heats, c_p/c_v. Since the container walls are assumed rigid, the liquid satisfies the condition

$$u(R_c, t) = 0. \tag{2.27}$$

It has been shown that large pressure variations due to bubble collapse during transient cavitation are only felt within a distance of few bubble radii from the bubble wall [82]. Thus, to a first-order approximation, it can be assumed that the density in the liquid varies uniformly due to the evolving bubble volume. Utilizing the relation from Equation 2.22, the pressure of the liquid at the container wall can written as

$$p(R_c, t) = K \ln\left(\frac{{R_c}^3 - {R_{b,0}}^3}{{R_c}^3 - {R_b}^3}\right) + p_{l,0} \tag{2.29}$$

where $R_{b,0}$ is the initial bubble radius and $p_{l,0}$ is the initial liquid pressure.

Following the approach implemented by Gilmore[89], the Kirkwood-Bethe approximation is adopted, which allows the integrated momentum equation from Equation 2.23 to be formulated as

$$\left[-r\left(1-\frac{u}{c}\right)\frac{du}{dt}-\frac{3}{2}\left(1-\frac{u}{3c}\right)u^2+\frac{rc}{K}\left(1-\frac{u}{c}\right)\frac{dp}{dt}+\left(1+\frac{u}{c}\right)h\right]_{R_b}^{R_c}=0 \tag{2.30}$$

The enthalpy, h, as defined in Equation 2.24 is evaluated in terms of pressure to yield

$$h=\int_{p_0}^{p}\frac{dp}{\rho}=\frac{K}{\rho_0}\left(1-\exp\left\{\frac{p_0-p}{K}\right\}\right). \tag{2.31}$$

By evaluating Equations 2.30 and 2.31 utilizing the boundary conditions, a second-order nonlinear ordinary differential equation is obtained describing the time evolution of the bubble radius:

$$\left(1-\frac{\dot{R}_b}{c}\right)R_b\ddot{R}_b+\frac{3}{2}\left(1-\frac{\dot{R}_b}{c}\right)\dot{R}_b^2+\frac{R_c c}{K}\frac{dP_c}{dt}-\frac{R_b c}{K}\frac{dP_b}{dt}\left(1-\frac{\dot{R}_b}{c}\right)+h_c-\left(1+\frac{\dot{R}_b}{c}\right)h_b=0 \tag{2.32}$$

This equation can be readily numerically integrated to find the bubble radius as a function of time, $R_b(t)$. It is easily observed that in the limit of infinite confinement radius, the model reverts to the traditional Gilmore equation describing bubble dynamics in an infinite (isobaric) medium.

In the analysis described herein, the physical properties (viscosity, surface tension, density, speed of sound and bulk modulus) are evaluated at equilibrium conditions using values from the IAPWS R6-95(2018) formulation[92].

2.2.2 Cavitation Dynamics: Effects of Confinement

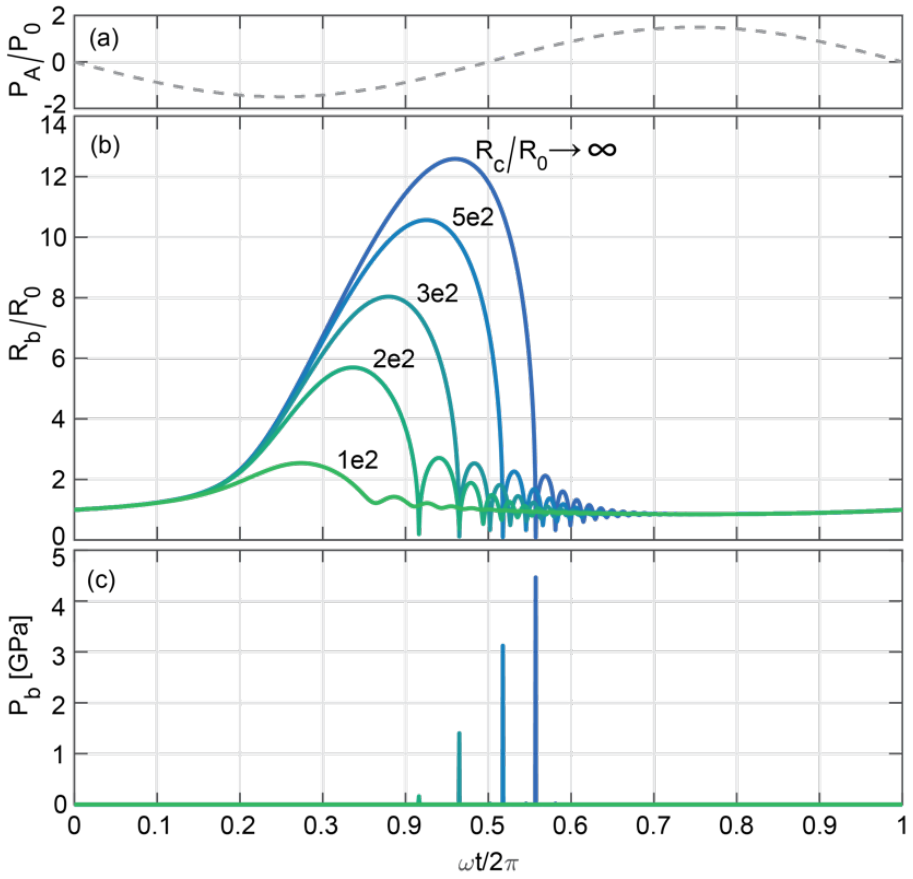

Figure 2.5: Transient excitation of a gas bubble in an ultrasonic pressure field. (a) Acoustic pressure signal of frequency 40 kHz and amplitude 1.5 bar as a function of cycle period, $\omega t/2\pi$. (b) Time evolution of relative bubble radius, R_b/R_0, for various values of relative confinement radius, R_c/R_0. Equilibrium bubble radius, $R_0 = 2.09\mu$m. (c) Pressure of water at bubble interface.

The resulting bubble growth and collapse dynamics are depicted in Figure 2.5 for varying confinement volumes. The bubble initially grows as tension is applied by the pressure field (shown in Fig. 2.5a), reaching a maximum size following the point of minimum applied pressure. As the cycle continues, the applied tension is released and the resulting force imbalance at the interface of the oversized bubble causes a violent collapse (Fig. 2.5b), during which the bubble radius may recoil to less than one tenth its equilibrium size. Given that the pressure within the bubble varies as $R_b{}^{-3\gamma}$ (in which γ is the ratio of specific heats for air), these collapse events result in brief periods (0.5 – 2 ns) of extreme pressure on the order of gigapascals, as shown in Fig. 2.5c.

The degree to which the system is confined (i.e. the ratio of the total confined system volume to the initial bubble volume) significantly alters bubble dynamics, acutely reducing the maximum bubble size reached and the peak pressure experienced during collapse (Fig. 2.5b/c). Physically speaking, this reduction is driven by the finite compressibility of the confined liquid phase; as the bubble grows, the reduction of the volume occupied by water must be accompanied by an increase in hydrostatic pressure, which retards further growth of the bubble.

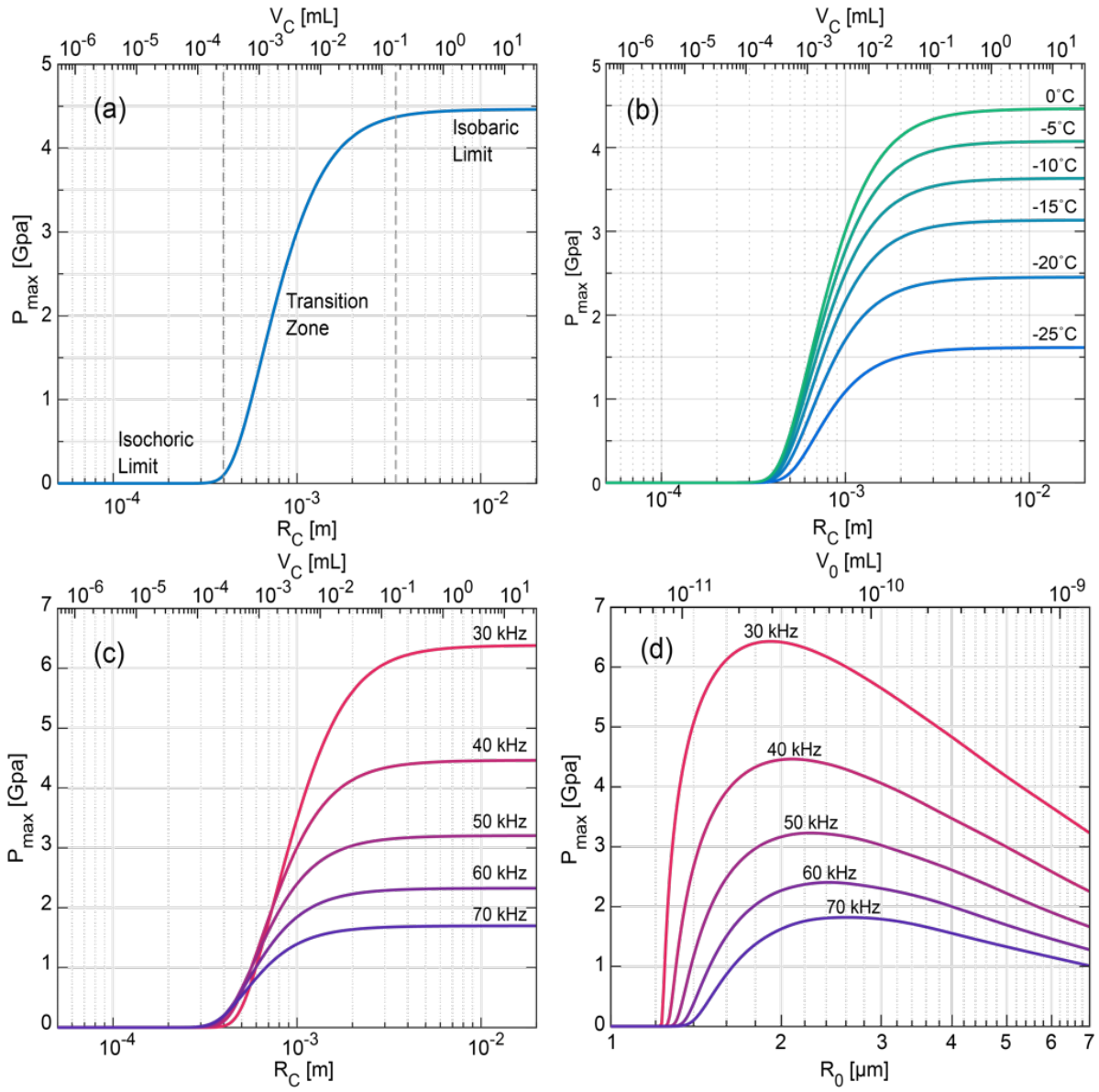

Figure 2.6: Peak collapse pressures experienced during cavitation in confined volumes. (a) Dependence of maximum cavitation pressure on degree of system confinement. For a system at a bulk temperature (0°C here) subjected to a given pressure field, three distinct regions of behavior can be identified as the degree of confinement varies. At system volumes approaching infinity (the isobaric limit), pressure will not vary with confinement, and will not differ from the pressures experienced in an unconfined system. Under increasing confinement, a transition zone emerges in which peak pressures decreases rapidly with decreasing system volume. Finally, at sufficiently small system volumes, cavity collapse will become kinetically prohibited and the bubble will stably oscillate, producing no significant changes in pressure. (b). Dependence of maximum cavitation pressure on degree of system confinement for varying degrees of bulk supercooling. (c) Dependence of maximum cavitation pressure on excitation frequency. (d) Dependence of maximum cavitation pressure on initial bubble radius at the isobaric limit of system confinement.

In Figure 2.6, the according effects of confinement on peak collapse pressure are demonstrated for varying system conditions, across which three distinct behavior regimes emerge (Fig. 2.6a). At the limit of infinite system volume, which is approached at system volumes on the order of 10^{11} times greater than the initial bubble volume, the bubble dynamics are unaffected by the container.

We term this volume scale the isobaric limit, as the results become equivalent to a system operating under unconfined isobaric conditions.

As the degree of confinement increases (i.e. the container volume decreases), the bubble dynamics enter a "transition zone", in which the bubble begins to feel the effect of confinement and the peak collapse pressures begin to decline.

Given that the peak collapse pressure is integrally related to the maximum radius reached by the bubble during the growth period, the origin and behavior of this transition zone can be probed by performing a static force balance on the bubble at its point of maximum growth. During the tension phase of the ultrasonic stimulation, the ultrasonic pressure and pressure within the bubble (Equations 15, 16) are balanced by the pressure due to the compression of the water volume (Equation 19). Taking the ultrasonic pressure to be equal to the driving pressure amplitude, the balance can be written as

$$K \ln\left(\frac{R_c^3 - R_{b,0}^3}{R_c^3 - R_{b,max}^3}\right) + p_{l,0} = \left(p_{l,0} + \frac{2\sigma}{R_{b,0}}\right)\left(\frac{R_{b,0}}{R_{b,max}}\right)^{3\gamma} + P_A \tag{2.33}$$

Shown in Figure 2.7 is the normalized maximum bubble radius produced from eqn. 2.33 as a function of confinement radius for a range of values of liquid compressibility, K^{-1}, and surface tension, σ. The degree of confinement at which the transition zone is centered is dominated by the compressibility (K^{-1}) of the liquid phase, while the width of the transition zone is largely dependent on the surface tension (σ). Although this static scaling analysis does not include the effect of viscosity or sonic velocity, detailed analysis utilizing the full bubble dynamics model shows that viscosity has a similar effect to surface tension, though to a weaker degree, and that sonic velocity has a similar effect to compressibility, which is expected given their direct relationship (Equation 12).

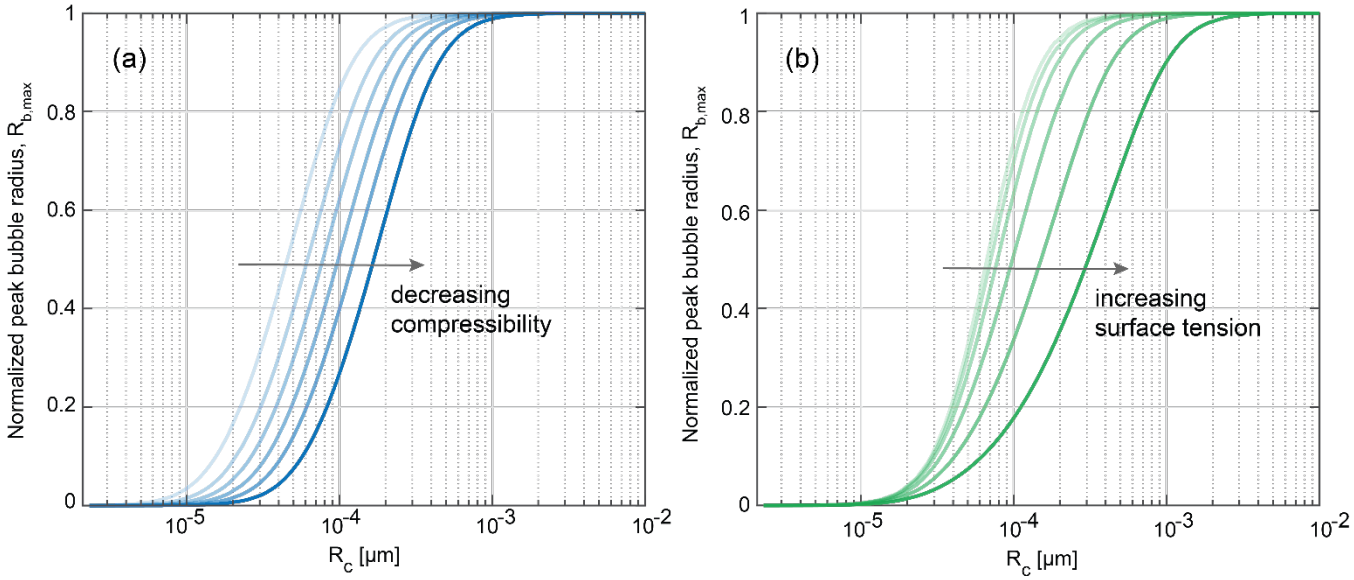

Figure 2.7: Dependence of transition zone on material properties. (a) Compressibility, K^{-1}. (b) Surface tension, σ.

This scaling relation (eqn. 2.33) describes the approximate dependence of the maximum bubble radius on confinement, which serves as an effective first-order proxy for the peak collapse pressure and allows for convenient approximation of the confinement scales at which an arbitrary liquid with bulk modulus K and surface tension σ will start to see an arrest of cavitation dynamics.

The third and final regime depicted in Fig. 2.6a, encountered at system volumes approximately 10^7 times larger than the initial bubble volume, demonstrates the existence of a critical confinement under which bubble collapse becomes entirely prohibited. Resistance from the rigid container prevents the bubble from reaching sufficient size to drive an unstable collapse event, and it instead merely oscillates stably in response to the applied pressure field (as shown in the bottommost profile in Fig. 2.5b). We term this volume range the isochoric limit, and at confinement volumes in this regime, the system will experience no significant excursions in pressure.

The three regimes identified in Fig. 2.6a remain consistent as operational parameters are varied, though the discrete peak pressures encountered may change significantly. In particular, reduction of the bulk system temperature significantly dampens collapse intensity (Fig. 2.6b), due principally to the large increase in the viscosity of water at subzero centigrade temperatures, and reduction of the excitation frequency (Fig. 2.6c) increases collapse intensity, due to an increased tensioning period in which the bubble is allowed to grow preceding collapse. The dependence of peak collapse pressure on the initial bubble size is also shown in Fig. 2.6d, acknowledging that in an experimental context, a bubble field will exist with a distribution of cavitating bubble sizes. Throughout the collapse analyses presented in this work, the initial bubble radius that yields the highest collapse pressure for a given frequency is employed, ensuring description of the most extreme possible response.

2.2.2 Transient Supercooling Analysis

With peak collapse pressures obtained as a function of confinement, we are now empowered to relate confinement to high-pressure transient ice nucleation by evaluating the thermodynamic path taken by the water surrounding the bubble during a collapse event. As originally suggested by Hickling[82], we model the compression of the local water as quasi-isentropic, assuming that thermal diffusion is negligible at the relevant nanosecond timescales. In Fig. 2.8a, compression isentropes for water evaluated from multiple bulk system temperatures are plotted overtop of the H_2O phase diagram, allowing calculation of the temperature difference $\Delta T_{supercooling}$ between the compressed metastable liquid phase and the relevant equilibrium phase of ice as a function of pressure. This temperature difference is plotted in Fig. 2.8b for various isentropes. As the water is quasi-isentropically compressed, depending on its bulk system temperature, it can pass through the equilibrium regions of up to five high pressure polymorphs of ice, with the most radical supercooling invariably occurring in the ice VII region.

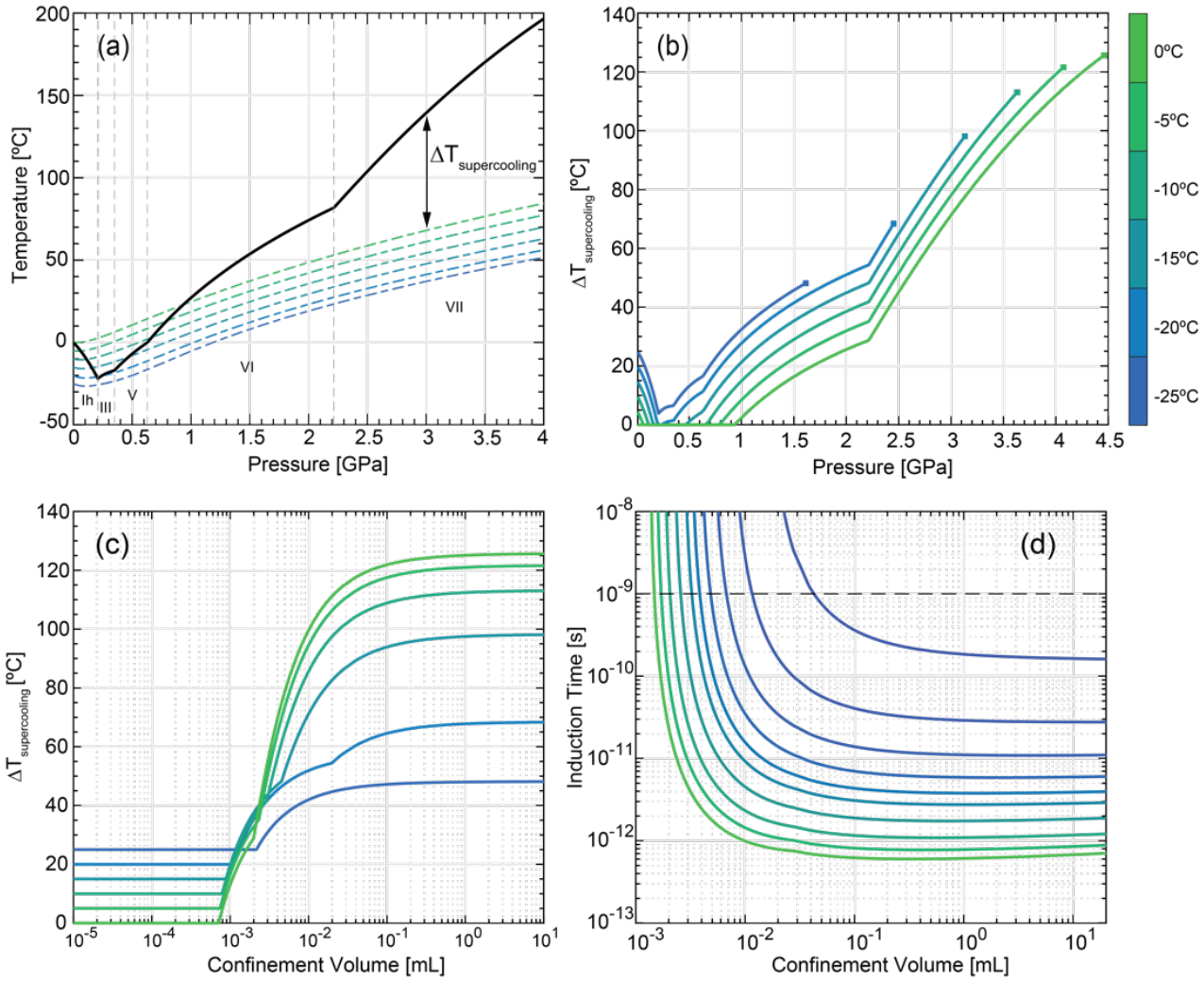

Figure 2.8: Transient high-pressure solidification processes for systems of varying bulk temperatures sonicated at 30 kHz. (a) Phase diagram of water with isentropic compression curves for bulk system temperatures of 0, -5, -10, -15, -20 and -25°C, color coded according to the color bar at right. The water-ice liquidus line (solid black) shows the equilibrium boundary between the liquid water phase (above the line) and the ice phases Ih, III, V, VI, and VII (below the line), as labelled along the bottom of the plot. Isentropic compression curves (dashed lines) show the temperature-pressure thermodynamic path followed by water as it is isentropically compressed from a varying initial temperatures. As compression increases, the water will traverse through the equilibrium regions of several different ice phases. Both the liquidus line and the isentropic compression curves were calculated using the standard IAPWS multiparameter equations of state[92,93]. (b) Magnitude of transient supercooling encountered during isentropic compression, e.g. the difference $\Delta T_{supercooling}$ between the liquidus curve and a given isentropic compression curve. Curves are truncated at the maximum pressure reached during cavity collapse for a given bulk temperature. (c) The same maximum transient supercooling as a function of confinement volume, adapted according to the pressure-confinement volume relations provided in Figure 2. (d) Minimum ice VII induction time encountered during cavity collapse as a function of confinement volume, as calculated using classical nucleation theory. The dashed line represents the critical induction time threshold, defined by the average duration of a high-pressure collapse event (here 1 ns). Minimum ice VII induction times beneath this threshold will lead to formation of ice VII nuclei during cavity collapse, while induction times above the threshold will not.

By now combining the confinement-pressure results of Fig. 2.6b with the pressure-supercooling results of Fig. 2.8b, the maximum transient supercooling encountered at a given confinement volume can be calculated (Fig. 2.8c), and the same confinement limits seen in the collapse pressure can be observed. At the isochoric limit, the maximum supercooling encountered in the system will simply be defined by the bulk system temperature, as no cavitation will occur. At the isobaric limit, significant cavity collapse pressures will drive $\Delta T_{supercooling}$ into the range

of hundreds of degrees, principally in the ice VII region of the phase diagram. These extreme degrees of supercooling were originally predicted to order-of-magnitude accuracy by Hickling[82], but have never been evaluated as a function of volume or confinement.

Reduction of the maximum transient supercooling can be observed at remarkably large confinement volumes, on the order of 10^9 times larger than the bubble itself, and increases acutely over the volume range corresponding to the transition zone. Across confinement volumes, the maximum supercooling encountered is also a strong function of the bulk system temperature, though counterintuitively, increasing bulk supercooling decreases later cavitation-induced supercooling, due to the significant dampening of bubble collapse dynamics that occurs with the increasing viscosity of water at low temperatures.

2.2.4 Cavitation-induced Nucleation: Effects of Confinement

We now incorporate the maximum transient supercooling results developed in Fig. 2.8c into classical nucleation theory (CNT) and examine the induction time required for the nucleation of a high-pressure solid phase as a function of confinement. To simplify this analysis, we make the crucial assumption that the only high-pressure polymorph of ice likely to form during the quasi-isentropic compression process is ice VII, though each isentrope will briefly pass through regions in which ice V or ice VI may be more thermodynamically stable. This assumption is based on previous experimental observations of ice nucleation during quasi-isentropic dynamic shock compression, in which metastable ice VII was found to form preferentially to stable ice VI due its lower interfacial free energy[94,95]. Furthermore, growth of ice VII has been observed at the same time scales as cavity collapse (~single nanoseconds)[87,95,96], and the relative degree of supercooling is highest in the ice VII region.

Using the Myint equation of state[97] to analyze the thermodynamic driving forces between compressed water and ice VII along each compression isentrope, CNT enables calculation of a transient induction time of the form

$$\tau = \frac{8k_B T}{\pi^2 \lambda D^*} \tag{2.34}$$

which was originally formulated by Kaschiev[98] and describes the time required for a cluster of ice VII particles to reach the critical size required for nucleation. In eqn. 2.34, $k_B T$ is the energy scaling factor, D^* is a frequency factor describing the rate of attachment of additional molecules to a critical cluster, and λ describes the curvature at the top of the energy barrier. The full mathematical description of the factors used in equation (2.34) is provided in Table 2.1. The mode of analysis and choice of parameter symbols follows Myint et al[96].

Table 2.2: Classical Nucleation Theory Formulae

Description	Equation
Induction time (i.e., time needed for a subcritical cluster to become a supercritical cluster and form a stable nucleus).	$\tau = \frac{8k_B T}{\pi^2 \lambda D^*}$

Description	Equation
Note: no arbitrary scaling factor has been applied in our work, as was done by Myint et. al[86]. This results in our calculations representing a conservative limit on the induction time of ice VII nucleation during cavity collapse (e.g. the fastest induction time possible).	
Frequency factor (i.e., attachment rate of molecules to critical clusters)	$D^* = \frac{4\pi {R^*}^2 \gamma}{V_{solid}}$
Curvature at the top of the energy barrier	$\lambda = 2\pi k_B T Z^2$
Growth rate	$\gamma = \left(\frac{k_B T}{m}\right)^{1/2} \frac{\Delta\mu}{k_B T}$
Zel'dovich factor (i.e., probability that a critical cluster will grow)	$Z = \left(\frac{\Delta G^*}{3\pi k_B T {n^*}^2}\right)^{1/2}$
Critical energy barrier to nucleation	$\Delta G^* = \frac{16\pi\sigma^3}{3\rho_{solid}^2 \Delta\mu^3}$
Critical cluster size	$n^* = \frac{32\pi\sigma^3}{3\rho_{solid}^2 \Delta\mu}$
Critical cluster radius	$R^* = \frac{2\sigma}{\rho_{solid}\Delta\mu}$
Difference in bulk chemical potential between the solid and liquid phases. Values are obtained form the equations of state provided by Myint et. al [97]	$\Delta\mu = \mu_{solid} - \mu_{liquid}$
Molecular volume	$V_{solid} = 1/\rho_{solid}$

For a given transient cavitation pressure, the interfacial free energy of ice VII was linearly interpolated between the two reference points indicated by Myint et. al[87], which are provided in Table 2.2 below.

Table 2.2: Interfacial free energies of ice VII

Pressure [GPa]	**Interfacial Free Energy σ [mJ/m^2]**
1.58	23.0
7	129

Armed with the maximum supercooling encountered at a given confinement volume (Fig. 2.8c) and the pressure-temperature paths followed during quasi-isentropic compression of the water, the fastest induction time possible at a given confinement volume can be calculated for various degrees of bulk supercooling (Fig. 2.8d). The isobaric and isochoric limiting behaviors are once again

observable: the induction time stabilizes to a constant minimum value at large system volumes, and it arcs toward infinity as the system volume decreases and the cavitation dynamics driving nucleation are extinguished.

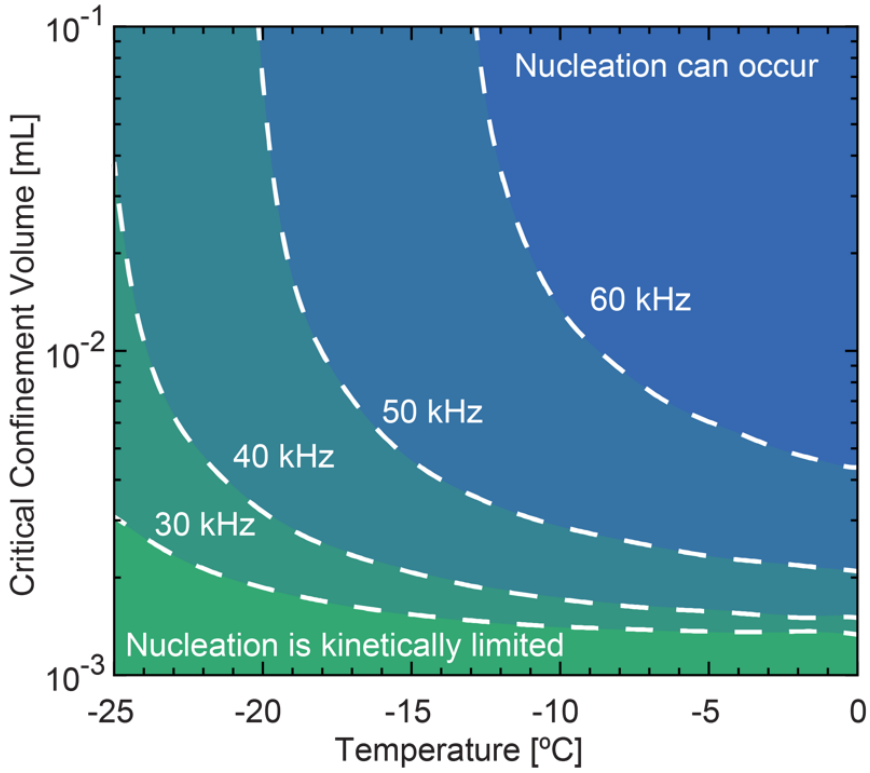

Figure 2.9: Ice VII kinetic phase diagram. For a given ultrasonic excitation frequency and bulk temperature, there exists a critical confinement volume beneath which the induction time of ice VII is too great to induce nucleation within the approximately 1ns period during which cavity collapse causes quasi-isentropic compression. The dashed lines indicate the boundary that separates the confinement regimes in which nucleation of ice VII can (above a given line) and cannot (beneath a given line) occur.

In order to estimate whether cavitation-induced ice VII nucleation will ultimately occur, we can now compare the induction time required for the formation of a stable nucleus to the period over which the pressure excursion due to cavity collapse occurs. Previous experimental work has observed ultra-rapid formation of metastable ice VII at dynamic pressures as low as 1.8 GPa[94]; we thus examined the period over which the collapse pressure remained greater than or equal to this pressure, finding across bulk system temperature and frequency conditions a value of approximately 0.5 – 1.5 ns. This period can be applied as a critical threshold for the induction time of a high-pressure solid phase, and is plotted as a dashed line on Fig. 2.8d. If the calculated induction time at a given confinement volume rests under this threshold, ice VII has a kinetic route to nucleation. If the induction time is above this threshold however (i.e. if it takes longer than ~1ns for a critical cluster of ice VII to form), the collapse pressure will dissipate before a stable nucleus can form, effectively kinetically prohibiting cavitation-induced nucleation.

The discrete confinement volumes at which the induction time curves plotted in Fig. 2.8d cross the collapse period threshold thus represent a critical phenomenon: the degree of confinement at which cavitation-induced nucleation becomes kinetically prohibited. This "critical confinement" volume can be plotted as a function of system parameters, herein the bulk temperature of the resting system and the driving frequency of the ultrasonication, to develop a kinetic phase diagram

establishing the temperature - confinement boundary under which cavitation-induced nucleation will not occur for a given driving frequency (Fig. 2.9).

2.2.5 Scale of confinement effects and extension to macroscopic systems

The single-bubble analysis performed herein reveals several important consequences of system confinement: it can dampen bubble collapse dynamics, reduce transient supercooling during cavitation, and ultimately restrict cavitation-induced nucleation. Furthermore, there exist calculable critical confinement volumes at which discrete kinetic behaviors (bubble collapse, nucleation of high-pressure polymorphs) can be prohibited entirely. Perhaps most surprising however is the volume scale at which these myriad confinement effects come into play: For a single cavitation bubble on the order of 10^{-11} mL in volume, across sonication frequencies and bulk system temperatures, bubble collapse and cavitation-induced nucleation become kinetically prohibited at minimum critical confinement volumes on the order of 10^{-4} mL and 10^{-3} mL, respectively.

These remarkably large single-bubble confinement volumes suggest that the observed confinement effects may also translate to bulk macroscopic systems, which produce large populations of simultaneously cavitating bubbles upon ultrasonication. For example, recent estimations of the number density of cavitating bubbles in water sonicated in the 20 – 200 kHz frequency range suggest that approximately 10^3 bubbles may cavitate per mL of liquid[99]. As a first-order approximation, if a hypothetical bulk system is ultrasonicated at 30 kHz and confined at 10 mL, the volume may be divided evenly by the number density of bubbles to arrive at an effective confinement volume per bubble of 10^{-2} mL, which is well within the transition zone for transient supercooling (Fig. 2.8c) and approaching the critical confinement threshold for cavitation-induced ice VII nucleation (Fig. 2.9).

It must be noted however that the critical confinement volumes calculated in this work describe only the most extreme possible cavitation scenario, in which the equilibrium size of the cavitating bubble corresponds to the peak displayed in Fig. 2.6d, which will yield the greatest possible collapse pressure and the highest pursuant likelihood of ice VII nucleation. Experimentally, a cavitating bubble field in a macroscopic system will include a wide distribution of larger and smaller bubbles[99], which will inevitably produce significantly smaller pressure excursions upon collapse and reduce the likelihood of nucleation. Nucleation-suppressing confinement effects may thus potentially be observed at much larger scales than those considered here, and indeed in our proof-of-concept experimental investigation of nucleation in supercooled confined systems[88] (discussed in the next chapter), suppression of nucleation was observed in macroscopically confined systems on the order of 100 mL that were supercooled to -3°C and ultrasonicated at 55 kHz. Although a full bubble field analysis is required to accurately extend the present model to experimentally relevant multi-bubble systems, the experimental findings described in[88] provide preliminary experimental confirmation of our proposed nucleation suppression mechanism, and future experimental efforts should not rule out confinement as a means of suppressing cavitation-induced effects at any scale.

The need for robust control of ice nucleation has become increasingly clear in light of recent successes in medical supercooling[30,81], which have yielded excellent biological results but have thus far not proven translatable outside a highly controlled laboratory environment[33]. Cavitation-induced nucleation of high-pressure polymorphs is the dominant mechanism by which supercooled systems are destabilized upon mechanical or acoustic perturbation (as occurs variously during

transportation and clinical use), and thus any supercooling approach intended for practical use must work to suppress this mechanism.

Our results herein suggest that isochoric confinement can significantly hinder cavitation-induced nucleation, and, taken in combination with other recent works investigating the limiting effects of isochoric confinement on other ice nucleation and growth mechanisms[88,100,101], suggest that confinement may provide a compelling route toward robust nucleation suppression in supercooled systems.

2.3. Looking Forward: New approaches to classical phase equilibria

The studies discussed in this chapter revolve around replacing an intensive natural variable (pressure) with its extensive conjugate (volume) in order to probe the phase equilibria and kinetic phenomena and encountered in experimental systems held at constant volume. This simple thermodynamic alteration analytically reveals critical phenomena not easily shown using the conventional Gibbs temperature-pressure formalism, and speaks to the more general need for an updated approach to classical thermodynamic studies.

Throughout both the research literature and educational literature, the dominance of the *T-P* thermodynamic context and the Gibbs potential is abundantly clear. However, as the interests of materials science increasingly move away from simple macroscale systems, the applicability of this potential grows thin, and the need for efficient approaches to deriving new phase equilibria and kinetic relations under *arbitrary* alternative thermodynamic conditions is clear.

In this ever-complicating materials discovery environment, the study of complex phase equilibria (including metastable equilibria, equilibria under magnetic and electric influences, etc.) has shifted significantly over the last several decades toward atomistic approaches such as molecular and dynamics and DFT. These approaches are computationally expensive however, and the results they yield are only as sound as the classical thermodynamic understanding that underlies them. Thus, the author argues that there is significant need for generalized *classical* approaches consistent with current materials challenges.

In specific, the fundamental relationships upon which we lean most heavily for our intuitions about phase transition must be updated and generalized for modern applications. Take for example Gibbs' Phase Rule, a cornerstone of undergraduate materials' science education. This rule is only fit to describe a simple system specified by two *intensive* variables, and thus proves inapplicable to many interesting applications (including the study of isochoric freezing). Currently, no standard generalized form of this rule exists, and the formulation of such a rule has not proven a priority of the community. However, re-examining Gibbs' original geometric interpretations of the energy surfaces of materials, a generalized rule can easily be envisioned which starts from the extensive variables of the system, is extensible to N-dimensions, and can describe arbitrary intensive or extensive phase-coexistence by virtue of the convex-hull approach used in section 2.1 for the derivation of the *T-V* phase diagram.

The issue at hand in this example is not that phase coexistence in increasingly complex thermodynamic contexts *cannot* currently be predicted, but instead that current methods are

sufficiently complex and obtuse to prevent the establishment of any base intuition about said phase equilibria. This intuition, the founding physical principles that guide our expectations about how material systems will behave, is essential to increasing our capacity for materials discovery and understanding, and expanding our ideas of what may be possible.

This base intuition is furthermore essential to the cross-pollination of materials thermodynamics with other fields (for example cryobiology and medicine), whose ultimate application of advanced thermodynamic principles will scale with their relative simplicity, accessibility, and ease of computation. Thus, future work should set about developing a new generation of generalized classical theory for the description of equilibrium and kinetic phenomena in alternative thermodynamic contexts, shaking the century-old yoke of the Gibbs free energy and enabling a ushering in a new era of classical thermodynamic research.

Chapter 3. Applied thermodynamics of metastable, non-equilibrium, and multiphase isochoric freezing processes

In the preceding sections, we have concerned ourselves principally with the theoretical machinations of isochoric systems and the tools used to probe said machinations. However, the overarching goal of this thesis remains unchanged: to apply the rich thermodynamics of confined systems to practical cryopreservation. Thusly, and equipped with the base intuitions developed in the preceding chapter, we will now embark upon a series of applied and experimental investigations aiming to clarify the thermodynamic and kinetic effects of isochoric confinement on real systems that may plausibly be deployed for cryopreservation.

Of particular interest are phenomena which do not lend themselves to convenient or definitive theoretical prediction, namely those observed in metastable supercooled isochoric systems, vitrifying isochoric systems, and isochoric systems comprising multiple chemical constituents. In the pages to follow, we report studies in each of these domains, each performed with an eye trained on downstream biological applications. We hope these investigations will serve as phenomenological foundations for significant further research in non-equilibrium isochoric research, and that the greater cryobiology community may promptly apply the thermodynamic observations reported herein to all manner of cryopreservation protocols.

3.1 Enhanced supercooling stability in aqueous systems under isochoric confinement

As detailed in Chapter 1, effective preservation of complex organ and tissue systems is essential to a wide range of 21st century medical and research efforts[16], including expanding access to lifesaving organ transplantations, enabling the storage and transportation of engineered tissues for drug-testing, etc. While classical approaches to preservation have often included high doses of cryoprotectant chemicals and ultralow cryogenic temperatures, a new generation of protocols is leveraging thermodynamic supercooling to dramatically enhance the duration and quality of biopreservation while operating in the high-subzero centigrade regime (between -20°C and -3°C) and minimizing cryoprotectant concentrations[29,30,46,102].

Although this approach has produced strong early biological results in the laboratory, the reduction of these protocols to practice in a clinical or industry setting faces a fundamental limitation: thermodynamic stability[33]. Supercooling is a metastable thermodynamic state, in which a substance remains liquid at temperatures lower than its freezing point due to a lack of sufficient kinetic stimuli. Upon even slight agitations, a supercooled system can rapidly and destructively freeze, returning to thermodynamic equilibrium and destroying any preserved biologics. Thus, in order to develop supercooling preservation protocols that are practicable outside a highly controlled laboratory environment, transportable, and clinically convenient, new methods but be sought to enhance the stability of supercooled systems.

In this section, we introduce isochoric (constant-volume) supercooling, a simple thermodynamic alteration to standard supercooling techniques that significantly enhances the stability of supercooled water in the face of a range of mechanical and thermal disturbances. We furthermore develop several hypotheses concerning the fundamental mechanisms contributing to this enhancement, unifying factors that stem from thermodynamics, fluid dynamics, and kinetics. While a complete theoretical explanation is outside the scope of this experimental validation, the results herein may be put to immediate practical use in high-stability supercooling of sensitive biological matter.

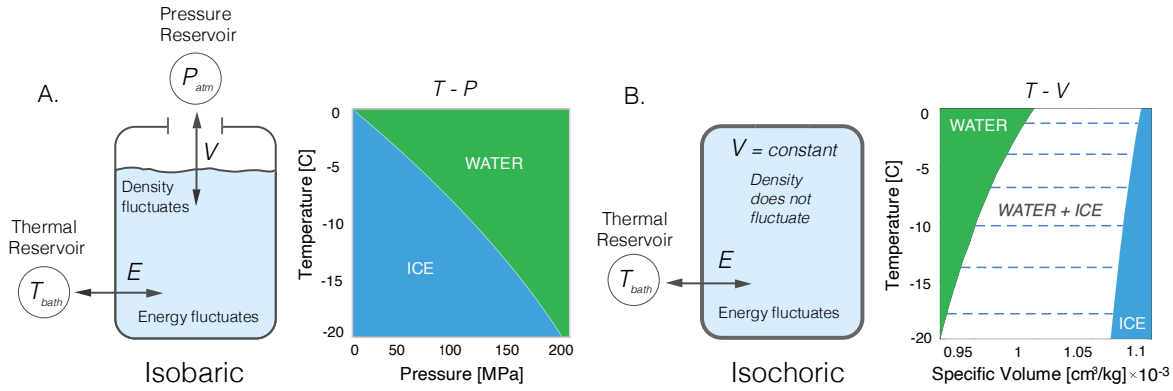

Figure 3.1. Comparison of isobaric (T-P) and isochoric (T-V) thermodynamic conditions for water and ice. A. Isobaric systems maintain contact with a pressure reservoir (the atmosphere in the context of this work), and thus fluctuate constantly in density at the microscopic scale. At atmospheric pressure, water in an isobaric system will transform entirely to ice-1h at sub-zero centigrade temperatures. B. Isochoric systems are held at constant-volume, isolated from the atmosphere, and thus do not fluctuate in density. Water in an isochoric system will not freeze entirely at sub-zero centigrade temperatures, instead forming a two-phase water-ice equilibrium.

3.1.1. Thermodynamic arguments for enhanced supercooling stability

Nucleation of a stable ice phase from supercooled (metastable) water occurs when a perturbation within the system proves sufficiently large to drive the free energy of a cluster of liquid molecules over the nucleation barrier[103]. Such perturbations can stem from the constant microscopic fluctuations undergone by any system with finite temperature, or from macroscopic mechanical or thermal agitation[104]. Thus, for a supercooling-based preservation technique to become practical or clinically relevant, it must maintain stability not only when experiencing microscopic fluctuations, but also when experiencing the macroscopic agitations that characterize practical use and mobility, including motion, macroscopic vibration, impact with rigid surfaces, temperature swings, etc.

Most supercooling preservation protocols operate under isothermal (constant temperature) and isobaric (constant pressure) conditions. According to statistical thermodynamics, systems in contact with a temperature reservoir (such as a cooling bath) and a pressure reservoir (the atmosphere) are free to fluctuate in energy and volume[105] (or density if mass is constant), the extensive conjugates of temperature and pressure (Fig. 3.1A, left). Thus, systems under isobaric conditions are constantly undergoing microscopic density fluctuations due to the random motion of particles, which can lead to the formation of ice clusters that meet and exceed the critical size required for nucleation. Furthermore, when exposed to macroscopic perturbations, isobaric

systems in contact with the atmosphere are susceptible to bulk fluid motion and bulk mixing with air, which can also lead to nucleation through cavitation or the introduction of new nucleation sites[102,104,106].

Isochoric (constant-volume) systems however, by their very definition, do not microscopically fluctuate in density[105] (Fig. 3.1B, left), and restrict bulk motion of the contained liquid. Furthermore, we have shown in our previous work[1,101] (Ch. 2.1) that both the process of ice nucleation and growth and the fundamental water-ice phase equilibria are different under isochoric conditions: As seen by comparing the T-P and T-V phase diagrams for pure water (Fig. 3.1A/B, right), nucleation at constant pressure yields complete freezing, while nucleation at constant volume yields only partial freezing, resulting in a two-phase water-ice equilibrium. This ultimate two-phase equilibrium has myriad useful consequences, and prior works have theoretically predicted that amongst these consequences may be heightened nucleation barriers and reduced thermodynamic driving forces for nucleation[1,39]. Additionally, isochoric conditions inherently eliminate the air-water interface, which has been suggested to facilitate heterogeneous nucleation[102]. Based on the sum of these thermodynamic considerations, we hypothesized that isochoric conditions should yield enhanced supercooling stability.

3.1.2. Supercooling stability testing

In order to test this hypothesis, we supercooled deionized water in identical rigid glass chambers (Fig. 3.2B/C) under three sets of conditions:

1. Standard isobaric conditions, in which the chambers were filled to approximately 95% volume and capped, leaving a bulk layer of air approximately 2cm in height to function as an effective atmospheric pressure reservoir.

2. Oil-sealed isobaric conditions, in which chambers were filled as in (1) but sealed with an approximately 2mm tall layer of mineral oil before capping, maintaining isobaric conditions while completely eliminating the air-water interface[102].

3. Isochoric conditions, in which chambers were assembled using a simple cap modification that enabled filling and sealing of the jars without the introduction of any air (details in Methods), leaving a totally constrained liquid volume incapable of any manner of visible flow when turned upside down.

All systems were initially supercooled to -3 +/- 0.01 C in a constant-temperature circulating bath and then exposed to various macroscopic perturbations (shown schematically in Fig. 3.2A), including drop-impact from a height of 1ft onto a hard acrylic surface, 2.2g vibrational loading on a rotary shaking table, ultrasonication in a cooled bath at 55 kHz, and continuous thermal cycling between 0 and -6C for 24 hours (experimental details available in Methods). For mechanical and acoustic perturbation testing, nucleation was evaluated visually (as in Fig. 3.2B). When nucleation was observed in isochoric systems, care was taken to warm the nucleating chamber immediately, as prolonged ice growth under isochoric conditions will produce pressures capable of shattering the glass chambers[101]. For thermal perturbation testing (occurring over 24 hours), breakage of the chamber was also used as an indicator of nucleation.

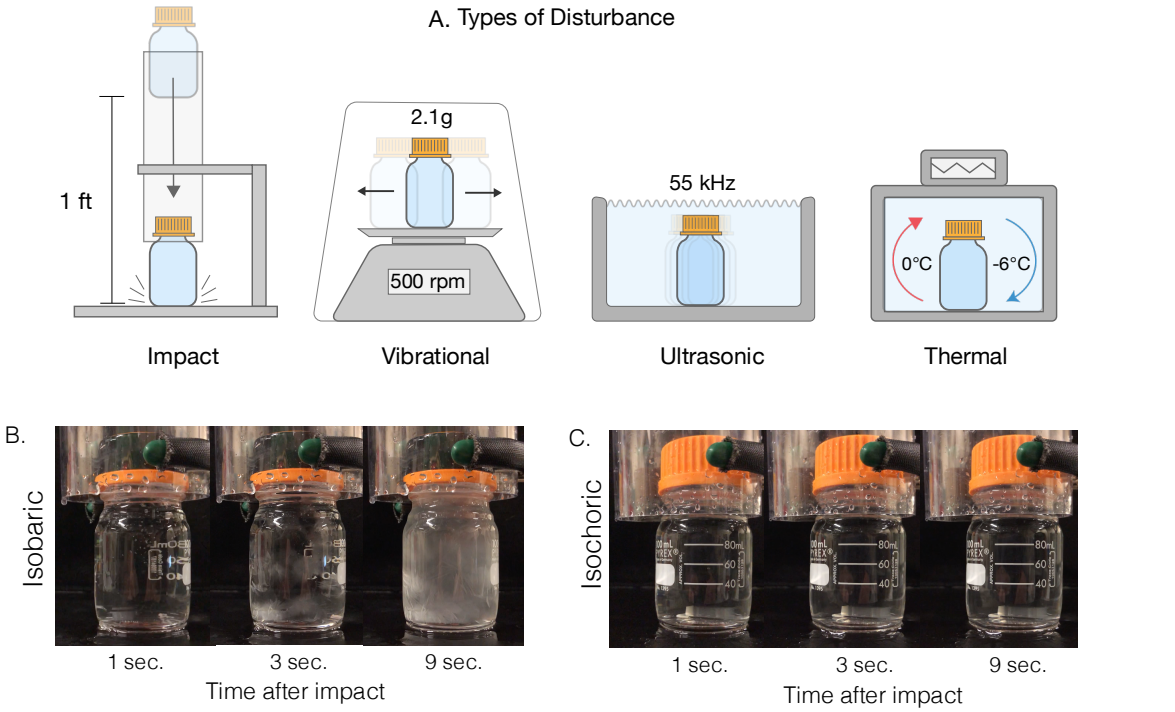

Figure 3.2. Disturbance experiments to evaluate supercooling stability. A. Schematic representation of each of the four disturbance experiments. Full experimental descriptions available in Methods. B. Timelapse photo series of an isobaric chamber following impact from a drop height of one foot. Ice nucleation proceeds quickly and can be easily visually detected. C. Timelapse photo series of an isochoric chamber following impact from a drop height of one foot. Supercooling remains stable and ice does not nucleate.

The nucleation frequency was recorded as the number of chambers per group that experienced ice formation. All tests were conducted in n = 6 trials of N = 12 chambers, and repeated in two sizes (approximately 65 ml and 130 ml) of borosilicate glass media bottles with rigid threaded polypropylene caps. In order to ensure the relevance of these tests to preservation protocols of interest, which invariably involve the introduction of other potential nucleation sites into the system, a PDMS-on-glass chip was also added to each container (visible in Figs. 3.2B/C), representative of the lab-on-a-chip systems used to house engineered tissue constructs[107].

The nucleation frequency as a function of disturbance type is plotted for all three chamber configurations in Fig. 3.3A, and comparisons between chamber configurations for each disturbance type are presented individually in Fig. 3.3B-E for statistical evaluation. As demonstrated in Fig. 3.3A, isochoric conditions afford greatly enhanced supercooling stability across all perturbation types, at both volume scales. Notably, isochoric supercooling at a 65 ml volume remained stable in 90% of trials when exposed to ultrasonication, which is perhaps the most universal and sure-fire trigger of ice nucleation[84,108,109], and remained stable in all trials when exposed to vibrational loading comparable to that encountered during commercial flight. Standard isobaric conditions yielded the least stability by comparison, while oil-sealing provided statistically significant stability enhancements during exposure to macroscopic vibrational loading and acute impact, but did not significantly affect resistance to ultrasonic or thermal perturbation.

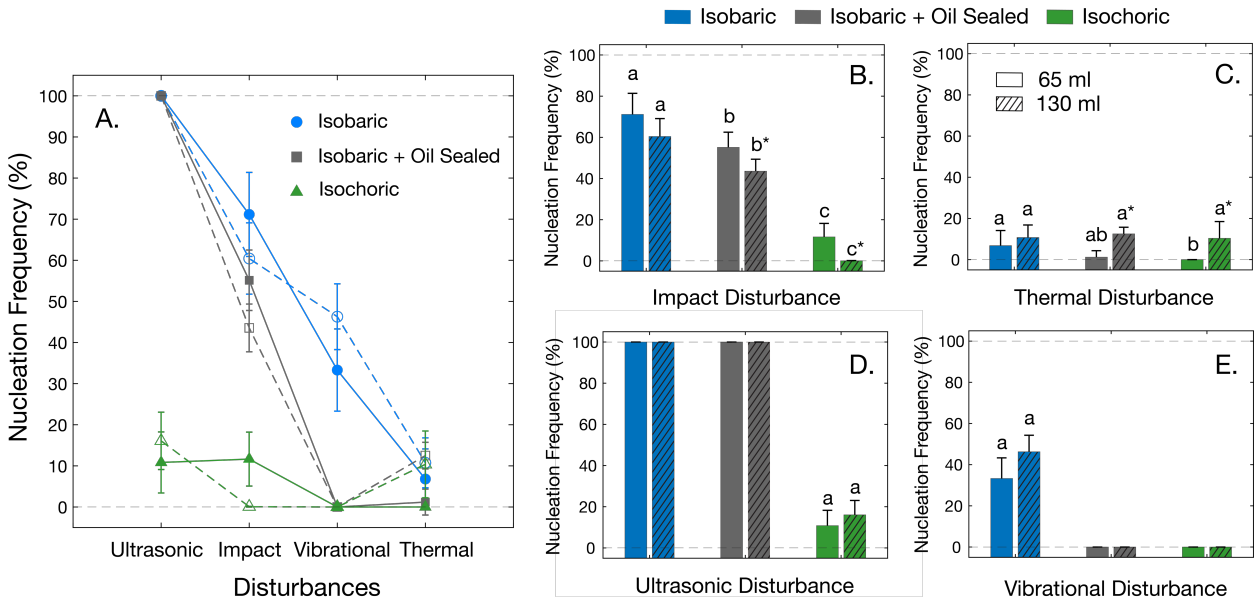

Figure 3.3. Nucleation frequency upon exposure to external disturbances for conventional isobaric, isobaric oil-sealed, and isochoric systems. A. Nucleation frequency for all systems as a function of disturbance type. Solid markers and lines represent 65 ml chambers, hollow markers and dotted lines represent 130 ml chambers. Lines between markers are plotted for visual assistance, and to not indicate a quantitative trend. B-E. Results for each disturbance type grouped by system type and volume. Statistically significant differences ($P < 0.05$) between system types at a given volume are marked by differing letters. Significant differences between volumes of a given system type are marked by an asterisk (*). Marked values provide the mean and error bars provide the standard deviation.

3.1.3 Potential mechanisms driving enhanced stability during isochoric supercooling

Previous work has suggested that the removal of the air-water interface is responsible for the vibrational stability enhancement experienced during oil-sealed supercooling[102]. The results presented in Figures 3.3B/D therefore confirm that the stabilizing effect realized under isochoric conditions must transcend the simple removal of air as a nucleation site, given the relative superiority of stability between isochoric and oil-sealed chambers. Furthermore, the fact that oil-sealing affects stability in the face of bulk vibrational loading and acute impact, both of which can result in bulk motion of the supercooled water under isobaric conditions, suggests that the effect of oil-sealing itself may be more complex than previously considered, resulting to some degree due to immobilization of the water phase. In order to clarify this prospect, we further examined the behavior of the free water surface during vibration under isobaric conditions with and without oil sealing.

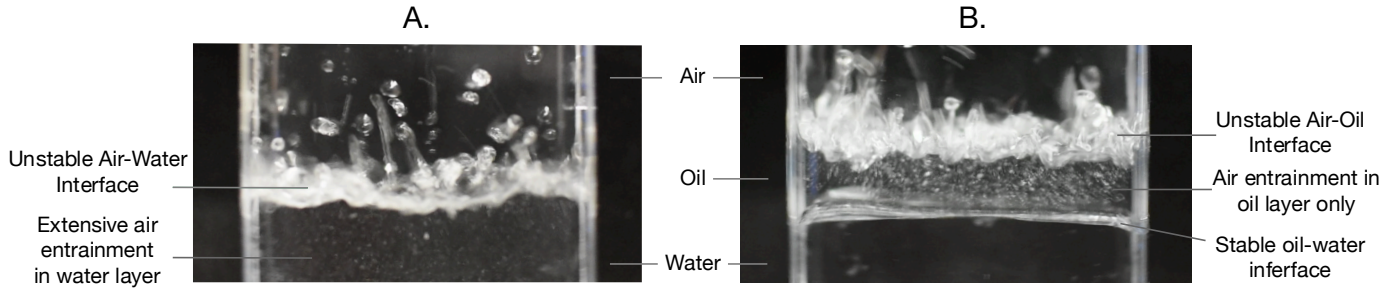

Figure 3.4. Comparison of the stability of the free water surface in vibrating systems under standard isobaric conditions and isobaric oil-sealed conditions. A. Standard isobaric conditions. The water-air interface is observed to be highly unstable, and extensive entrainment of air is evident in the water layer. B. Isobaric oil-sealed conditions. The oil-air interface is observed to be highly unstable, but the water-oil interface remains stable. Extensive entrainment of air is observed in the oil layer, but the water layer remains air-free.

The results of this examination are featured in Figure 3.4, and clearly represent a previously-unaccounted for phenomenon. In Fig. 3.4A, when the unconstrained water surface interfaces directly with air, unstable turbulent behavior is observed at the surface, due in principal to the Faraday instability[110]. However, when an oil layer is added atop the water, as in Fig. 3.4B, this extreme instability is observed only to occur at the oil-air interface, whilst the water-oil interface remains stable. This phenomenon is caused principally by the high kinematic viscosity of the oil relative to the air, and is observable for vibrations that occur at frequencies beneath a characteristic cutoff[110–112]. Surface instabilities of this nature in multi-layer fluid systems are a contemporary area of research[110,111,113].

Mechanical stimuli have long been known to induce ice nucleation[85], and the last century of research into the topic has clarified that cavitation is the most prominent responsible mechanism[106,109,114,115]. While cavitation is frequently associated with ultrasonication, it can also be caused by all manner of shockwaves[116] and by vibrational surface effects such as the Faraday instability[112] displayed in Figure 3.4.

The results obtained in this study demonstrate that isochoric supercooling is significantly more stable than its isobaric counterparts when exposed to mechanical stimuli of any kind, and it is thus suggested that one fundamental mechanism driving this isochoric stability is a reduced likelihood of cavitation. By totally constraining the liquid volume, isochoric conditions eliminate opportunities for cavitation from effects that require bulk fluid-fluid interfaces (such as the Faraday instability or analogous effects), and eliminate opportunities for cavitation from bulk motion of the stored water. They furthermore present two thermodynamic obstacles to cavitation from shockwaves or ultrasonication: firstly, because there is no bulk air anywhere in the system, cavitation must occur in dissolved air that is first forced out of solution with the supercooled water; secondly, the formation of a low-density air bubble in a constrained volume of water will create a positive pressure due to Le Chatelier's principle, increasing its energetic barrier to formation. The limiting effects of isochoric confinement on cavitation-induced nucleation were clarified in fundamental single-bubble analyses in Ch. 2.2.

This cavitation-centered explanation is also consistent with the observed behaviors of the oil-sealed chambers, which showed some enhancement of vibrational stability as compared to their un-sealed counterparts. In effect, oil-sealing reduces the likelihood of cavitation at the free water surface by removing direct contact with air and stabilizing the interface (Fig. 3.4B), but does not otherwise energetically deter cavitation throughout the liquid volume.

In total, the superior supercooling stability experienced in isochoric systems is likely a composite effect, reflective of the complex thermodynamic and kinetic factors driving ice nucleation in systems of bulk volume. Thermodynamic factors such as the reduction or elimination of microscopic density fluctuations and the increase of the ice nucleation barrier (as discussed in Ch. 2.1) under isochoric conditions likely contribute[1,39]; the elimination of the air-water interface as a nucleation site likely contributes[102]; and an increased resistance to cavitation may play a central role. While these effects must be independently clarified in future theoretical and experimental work and may reveal routes to further stability enhancement, the experimental reality of enhanced supercooling under isochoric conditions may be employed immediately for low-risk preservation and transportation of sensitive biological matter.

Finally, it should be noted that the sealed chambers employed in this work are of course only capable of producing approximately isochoric conditions; both the glass chambers themselves and the rigid polypropylene caps have finite stiffness, and thus minor changes in volume due to deformation or thermal expansion effects may occur during cooling. We therefore anticipate that additional enhancements in supercooling stability may be elicited in chambers of increasing rigidity, and future theoretical and experimental work should examine the chamber rigidity range over which isochoric supercooling effects may be observed.

3.1.4 Materials and methods for supercooling stability tests

Chamber preparation

Isoabaric Chambers
Isobaric chambers were filled to approximately 95% volume with de-ionized water pre-chilled to 4°C. After the initial pour, the open chamber was ultrasonicated in order to remove any air bubbles that may remain within the bulk liquid. The chamber was then capped, leaving a bulk layer of air approximately 2cm in height atop the liquid, ensuring isobaric conditions. Oil-sealed isobaric chambers were filled according to the same procedure, but sealed via syringe with a layer of mineral oil (Sigma-Aldrich, USA) approximately 2mm in height before capping. Care was taken to ensure that the entire water-air interface was eliminated, as per the protocol outlined by Huang et al[4].

Isochoric Chambers
For assembly of isochoric chambers, the same pre-chilling and post-pour ultrasonication procedures were employed, but an aluminum plug approximately 1.5 ml in volume was press-fit into the cap of each chamber, which served to displace excess air and liquid as the cap was turned onto the threads of the chamber and ensure that no air remained upon sealing of the system. Photos of this cap modification are included in Figure 3.5. After sealing, isochoric chambers were turned

upside down and shaken in order to visually verify that no air bubbles remained within in the system.

In order to ensure that hyperbaric conditions are not unintentionally produced during sealing of the isochoric chamber, the volume of the completely filled chamber was evaluated once before capping and a second time after the cap was removed. The difference in volumes was then determined to be equal to the volume of the plug, verifying that no extra volume of water was trapped and compressed during sealing.

It should be noted further that thermal expansion effects may also cause a slight increase in pressure (<1 MPa) upon supercooling of the isochoric chambers. This pressure is considered thermodynamically negligible for the purposes of nucleation, resulting in a maximum freezing point depression of -0.05°C.

In all three cases, a 3 x 1.5 x 1.5cm PDMS-on-glass chip was also added to each system as a potential heterogeneous nucleation surface in order to ensure that observed effects were not products of the surfaces of the specific containers being employed.

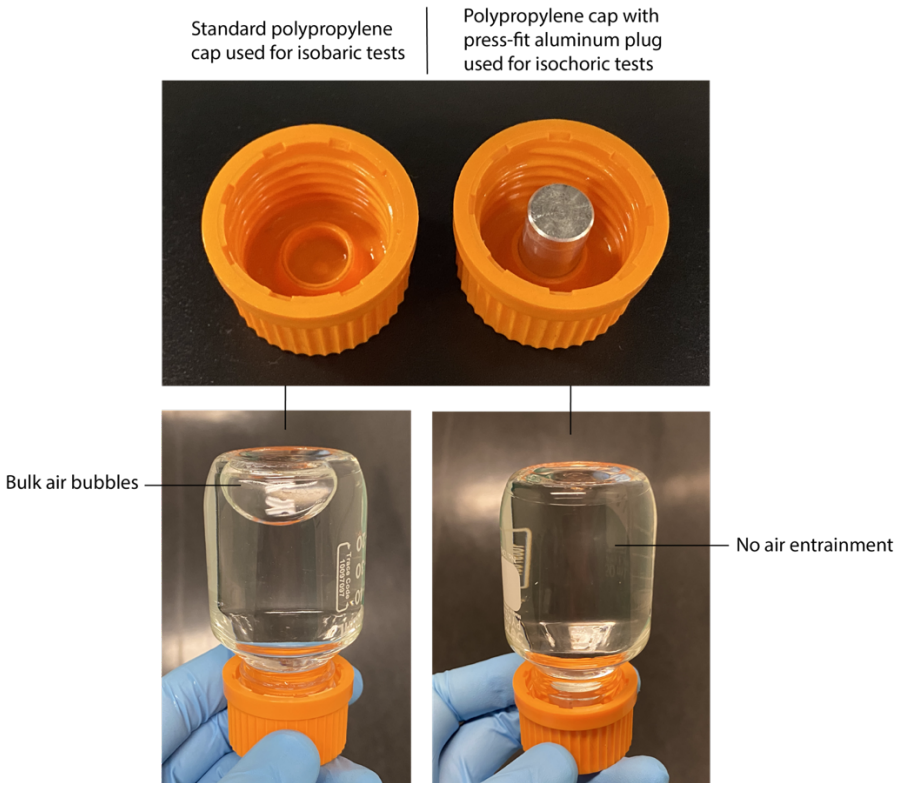

Figure 3.5: Cap modification to allow effective air removal in sealing of isochoric chambers. *Left top:* Standard polypropylene cap, as used for assembly of isobaric chambers. *Left bottom:* inverted chamber after assembly with standard cap. Bulk pockets of air can be observed. *Right top:* Polyprolyene cap with press-fit aluminum plug, as used for assembly of isochoric chambers. As the cap is threaded onto the chamber, the plug displaces a small volume of water, which forces out any air remaining in the mouth of the chamber or trapped in the cap itself. This displaced liquid and air is able to escape past the threads as the cap is being tightened, until the final point of closure, at which the roof of the lid meets the lip of the chamber and forms a rigid seal. *Right bottom:* inverted

chamber after assembly with modified cap. No air bubbles can be seen, and no bulk motion of the fluid can be observed during inversion.

Mechanical Disturbances

For all non-thermal disturbance scenarios, chambers were first supercooled to -3 +/- 0.01 °C in a programmable constant-temperature circulating chiller bath (PolyScience, USA) for four hours. They were then removed and immediately exposed to one of the following disturbances:

Impact: Chambers were dropped from a height of one foot onto a hard acrylic plate of 0.5" thickness. As per the schematic in Figure 2A, a clear acrylic tube of slightly larger diameter than the chambers was used to ensure a straight and repeatable drop trajectory. In isobaric oil-sealed chambers, no disruption of the oil-water interface was visually observed upon inspection post-impact.

Vibration: Chambers were mounted to a covered rotary shaking table (ThermoFisher, USA) and shaken for 60 seconds at a rate of 500 rpm and a rotary radius of 8mm, yielding acceleration magnitudes of approximately 2.2g. Chambers were mounted in an insulating foam rack, and the atmosphere within the covered shaking table was maintained at -3 +/- 0.5 °C via circulation of cold CO_2 vapor. During initial experimental design, the temperature inside the chambers was confirmed via thermocouple to remain consistent within 0.1°C over the 60 second shaking period. In isobaric oil-sealed chambers, no disruption of the oil-water interface was visually observed upon inspection post-vibration.

Ultrasonication: Chambers were moved directly from the circulating chiller to an ultrasonic bath (Fisher Scientific, USA), submerged completely, and sonicated at 55 kHz for 30 seconds. The bath was filled with 10% w/v NaCl solution pre-chilled to -3°C to ensure temperature consistency. In isobaric oil-sealed chambers, no disruption of the oil-water interface was visually observed upon inspection during or after ultrasonication.

Thermal Disturbance

Chambers were submerged fully in the -3°C bath directly following assembly. The chilling bath then was programmed to ramp continuously between 0°C and -6°C on a one hour period for 24 hours (constituting twelve cycles between the two temperatures), maintaining an average temperature of -3°C. This range was chosen to reflect the temperature oscillation encountered in standard on/off vapor-compression refrigeration units. After 24 hours, chambers were carefully removed and evaluated for ice nucleation.

Nucleation evaluation

In all disturbance scenarios, ice nucleation was evaluated visually, as shown in Fig. 3.2B, and recorded as a binary pass/fail for the purposes of calculating the nucleation frequency.

Furthermore, when ice nucleation was detected in isochoric systems exposed to non-thermal disturbances, care was taken to immediately warm the nucleating chamber; as ice grows in an

isochoric system, significant hydrostatic pressures can develop[12], which will lead to fracture or shatter of the glass chambers given sufficient time.

For thermal disturbances, because the tests were conducted over a 24-hour period, isochoric chambers that experienced ice nucleation invariably shattered. Breakage of the chamber was used as an alternative method of nucleation verification in these cases.

Examination of fluid-fluid interfaces under vibration

In order to enable clear photo capture of the interface behaviors displayed in Figure 3.4, alternative containers made of optically-clear virgin polystyrene with a rectilinear profile were used (T75 cell culture flask, ThermoFisher, USA). 45 ml of DI water was added to each container, with careful avoidance of air bubbles during filling. 10 ml of mineral oil was then added to one container, completely sealing the free water surface. The two chambers were then vibrated on a vertical-action vortex mixer (ThermoFisher, USA) and video of the interface behavior was captured at 1080p resolution and a speed of 30 frames-per-seconds on a Nikon D3400 camera.

Statistical Analysis

Each experimental group, defined as the chambers exposed to a given disturbance (e.g. impact, vibration, ultrasonication, thermal) at a given container volume (e.g. 65 or 130) under a given loading condition (e.g. isobaric, isobaric oil-sealed, or isochoric), was comprised of 72 chambers divided into n = 6 groups of N = 12 chambers. Values plotted in the results represent means, while error bars represent standard deviations. Statistically significant differences between groups were evaluated using paired-sample *t*-tests computed using MATLAB, with a standard significance threshold of $P < 0.05$.

3.2 Enhanced vitrifiability of aqueous solutions under isochoric confinement

In addition to short-term preservation interventions in the high-subzero regime (such as the supercooling method discussed in the previous section), there is sustained interest in developing technologies for long-term preservation of biological materials at cryogenic temperatures [16]. Vitrification, the transformation of liquid water into a glass, provides one of the most promising approaches, and vitrification protocols that are scalable to large volumes have been a landmark goal of the field for many decades. Luyet was the first to attempt cryopreservation by vitrification, in the 1930's, and reported successful vitrification with: moss [117], frog sperm [118], chick embryo heart [119], vinegar eels [120] and other small biological constructs. Luyet also studied the effect of high pressure on cells [121–124] during this period, presumably as a means to improve the probability for vitrification, and reported ultimately detrimental biological effects of sustained high pressure. In 1985, Rall and Fahy reported the successful preservation of murine embryos by vitrification, which heralded a new era of research in the field [125], and was supported by fundamental work on vitrification by Fahy and MacFarlane reported in two seminal publications [126,127].

Several competing factors affect the probability for vitrification. Luyet focused principally on the cooling rate during cooling to cryogenic temperatures, which much be sufficiently high to reduce the probability for ice nucleation in the temperature regime between the freezing point and the glass transition. However, while rapid cooling is effective for very small volumes, it is unsustainable at larger volumes, such as those required for full-organ preservation, due to thermal diffusion limitations in water. Fahy's group took an alternative approach and focused on developing vitrification solutions, which replace part of the water in the organ with glass-promoting solutes and thereby facilitate vitrification at lower cooling rates [128], which has thus far proven to be a more effective approach. Fahy and colleagues proposed that another effective way to improve the probability for vitrification may be to increase the hydrostatic pressure within the system [127]. Using visual inspection to detect crystallization, they compared the concentration of vitrification solutions required for vitrification at one atmosphere of pressure and at 1000 atmospheres. They found that an increase in pressure substantially reduces the concentration of chemical additives required to induce vitrification [127], consistent with the depression effect of pressure on the freezing point. They reported that the concentration of Propane-diol and Me_2SO required to induce vitrification at 1 atm are 44% (w/v) and 49% (w/v) respectively, while the concentrations required at 1000 atm are 39% and 44% respectively. This study served as an initial experimental validation of the assumed effect of pressure on vitrification, and will be discussed further in later sections.

In this study, we introduce the notion of vitrification under isochoric (constant-volume) conditions. Based on the myriad isochoric thermodynamic arguments developed so far, including the heightened-stability supercooling, heightened ice nucleation barriers, and two-phase water-ice equilibrium encountered in isochoric systems, we hypothesize that isochoric confinement should enhance the vitrifiability of aqueous systems by decreasing the likelihood of ice nucleation in a given time period. Furthermore, we anticipate that evaluating vitrification in isochoric systems will take on a much more quantitative flavor than in conventional isobaric systems; instead of attempting to evaluate vitrification visually, it can be detected by an increase in hydrostatic pressure within the system, which must accompany the crystallization and expansion of ice-1h.

The goal of this report is to present experimental data of relevance to vitrification in an isochoric system and to convey a fundamental understanding of the principles of vitrification in an isochoric system, in the context of our previous work on isochoric thermodynamics. In anticipation of future applications for tissue and organ banking, the experiments reported here were carried out by incorporating the cryoprotectants Propane-diol and Me_2SO in Unisol®, which is an established proprietary preservation solution [129–136].

3.2.1 Materials and Methods for Isochoric Vitrification

Isochoric system and experiments

The isochoric freezing system is a simple constant-volume metallic chamber, capable of withstanding with minimal deformation the tremendous pressures that can develop during constant-volume ice formation. As illustrated in Figure 3.6a, the isochoric chamber is a 2 ml 316 stainless steel commercial micro-reactor (total inner volume with fittings 3 ml, working pressure

60,000 psi) custom designed by High Pressure Equipment Company (Erie, PA, USA) to withstand high pressures and cryogenic temperatures. The chamber has an inner diameter of 3/16", an outer diameter of 9/16", an inside depth of 4", and an overall length of 7". The chamber is connected to an ESI Technology Ltd HP1100 0-4000 bar (0-60,000 psi) pressure transducer, routed to a DATAQ Instruments Model DI-245 Voltage and Thermocouple DAQ 4 channel data logger and connected to a laptop running DATAQ Instruments Hardware Manager. The stored data was viewed and exported from the WinDAQ Waveform browser, installed on the laptop. The pressure transducer is comprised of a Silicon-on-Sapphire sensor combined with a diaphragm machined from a single piece of titanium alloy. In these experiments, to minimize inflow heat flux through the pressure transducer, we used polyethylene pipe insulation fixed with electrical tape to insulate the pressure transducer. For safety, the system employed a safety head equipped with a rupture disk for a limiting pressure of 4000 bar. It should be noted that because these transducers are designed to accommodate such high pressures (up to 4000 bar), they lose sensitivity at pressures close to atmospheric (less than approximately 50 bar). Omega T-type thermocouples connected to a Extech Instruments EasyView™ 15 Thermometer Datalogger were also attached to the outside of the isochoric chambers as a second check to verify the set temperatures. The T-type thermocouples were attached on the isochoric micro-reactors using copper foil tape with conductive adhesive. No temperature measurement was made inside the vessels.

Two different experimental procedures were performed with this chamber. In the first, the isochoric system was placed in a program-controlled rate freezer (Planer Kryo 10 series III), capable of reaching liquid nitrogen temperatures at a pre-programmed rate of cooling (Figure 3.6b). In the second, the isochoric system was immersed in a 2L stainless steel thermos-flask (Thermo Scientific Thermoflask 2123) of liquid nitrogen at -196 °C, in order to achieve maximal cooling rates.

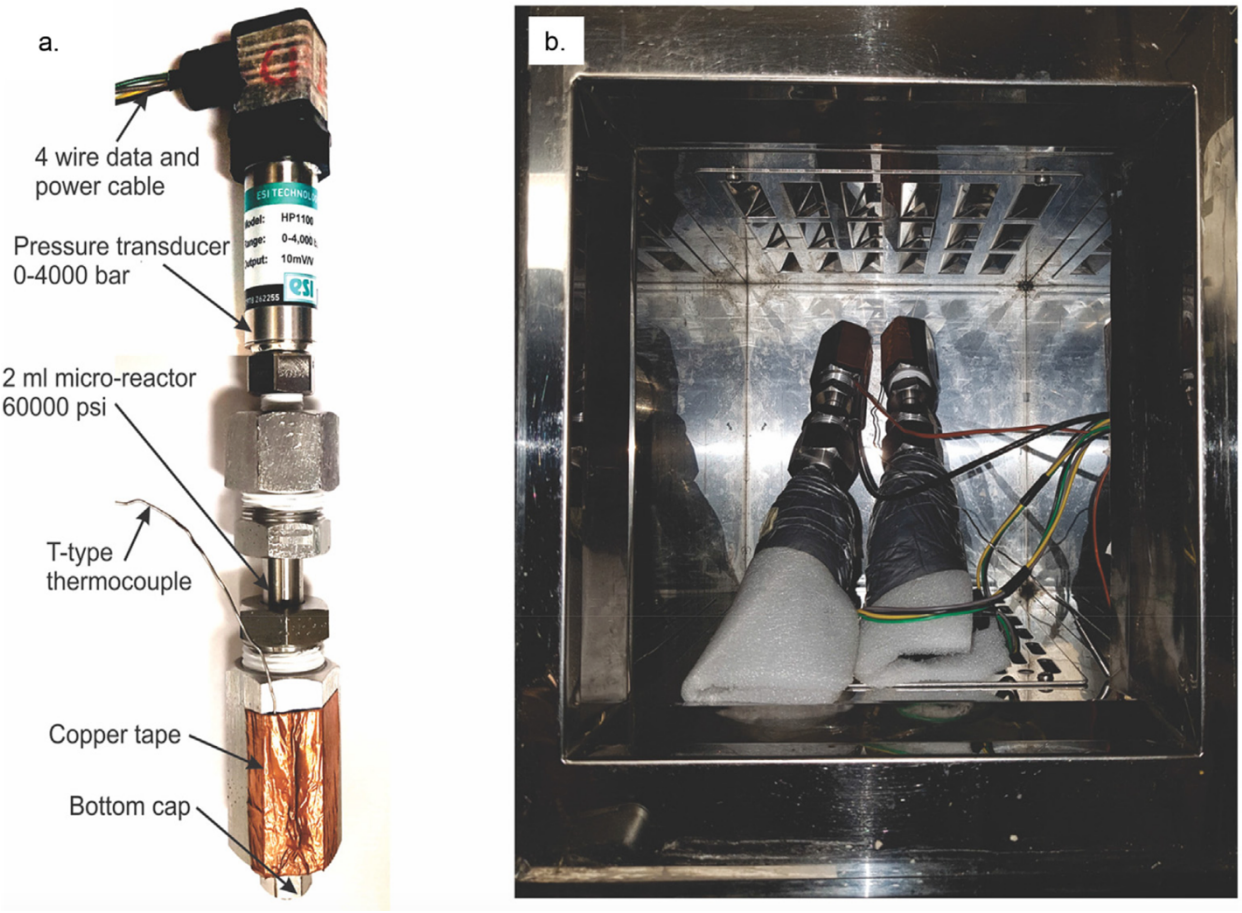

Figure 3.6. Elements of isochoric system and experimental setup. a) Isochoric chamber with pressure transducer and thermocouple. b) Two Isochoric systems in the Planer controlled rate freezer before the start of an experiment.

Vitrification Solutions

Experimental solutions comprising various concentrations of the commonly used cryoprotectants 1,2-propane-diol (also known as Propane-diol [PD]) or dimethyl sulfoxide (Me_2SO) were prepared in a proprietary vehicle solution (Unisol-CV; Tissue Testing Technologies, LLC). Specifically, isochoric measurements were carried out using propane-diol (0%; 10%; 20%; 30%; 40% and 44% (w/v), or Me_2SO (0%; 10%; 20%; 30%; 35%, and 49% (w/v) prepared in Unisol-CV [130–132,137].

Experimental protocols

Slow Cooling Protocol: For the first series of controlled-rate cooling experiments, three identical chambers were bottom-filled, tightly sealed and placed in the controlled rate freezer (Planer). It is important to emphasize that care must be taken to eliminate air in gaseous form from the system [138], as even minimal air infiltration will substantially modify the thermodynamics of the system that we seek to study [138]. The freezer was used to cool and heat the chambers following the pre-programmed temperature profile shown in Figure 3.7c. As shown, for Propane-diol (PD), the chambers were cooled from 20°C to -40°C at a rate of -20° C/min and held at -40 °C for 30 minutes.

Next, the chambers were cooled in -40 ˚C decrements down to -160 ˚C at a rate of -20 °C/min and held at each temperature for 30 mins. After 30 mins at -160 °C, the chambers were warmed in a reverse manner to the cooling. From -160 ˚C the chambers were heated to -120°C at 20°C/min and held at -120°C for 40 minutes. The chambers were then heated in 40˚C increments up to -40 °C at a rate of 20 °C/min and held at each temperature for 40min. From -40°C the chambers were then warmed to 20°C at a rate of 20 °C/min at which point the program stopped. Pressures were measured throughout each experiment, each of which was repeated in triplicate.

Similarly, For the Me_2SO series, the chamber was cooled from 20°C to -10°C at a rate of -20 °C/min and held at -10 °C for 30 minutes. Next, the chambers were cooled in -10˚C decrements down to -40˚C, then the chambers were cooled in -40˚C decrements to -160˚C at a rate of -20 °C/min and held at each temperature for 30 mins. After 30 mins at -160 °C, the chambers were warmed in a reverse manner to the cooling. From -160˚C the chambers were heated to -120 °C at 20 °C/min and held at -120 °C for 40 minutes. The chambers were then heated in 40 degree increments up to -40 °C at a rate of 20 °C/min and held at each temperature for 40min, and then the chambers were heated to -10 °C at a rate of 20 °C/min and held at each temperature for 40min. From -10 °C the chambers were then warmed to 20 °C at a rate of 20 °C/min at which point the program stopped.

Rapid cooling protocol: For the second series of experiments, the chambers were cleaned and dried before being charged with fresh experimental solution. The chambers were then immersed for 15 minutes in a Thermoflask (Thermo Scientific) filled with liquid nitrogen, which was continually replenished as necessary to maintain the required level in the flask. The cooling rate measured by the thermocouple on the isochoric chamber averaged approximately 53.2 ℃ / min (Fig 3.7). It should be noted that in the experiments of Fahy, the cooling rates used were from 5 to 30 ℃ / min. Our cooling rates during the rapid freezing are higher, as constrained by the dimensions of the isochoric device. After 15 minutes in liquid nitrogen, the isochoric system was removed and warmed in air for 60 minutes. The thermal history during cooling and warming was recorded and a typical result is displayed in Figures 3.7a,b. The pressure was measured while the device was immersed in liquid nitrogen and while it was being warmed. Measurements were made for the series of propane-diol concentrations specified above and each experiment was repeated three times. Data was collected using the data logging system described above and analyzed using MATLAB.

3.2.2 Baseline isochoric pressure-temperature measurements in the absence of cryoprotectants

Figures 3.8a,b show the pressure profiles recorded for pure Unisol solution during the two experimental protocols described above. This experiment was performed to serve as a baseline for the effect of the addition of Propane-diol and Me_2SO. Panel 3.8a shows the pressure changes as a function of temperature during controlled-rate freezing and thawing. The experiments were performed by first setting a constant temperature within the cooler and monitoring the pressure until it leveled, at which point the temperature-pressure condition was taken to represent a state of thermodynamic equilibrium in the isochoric system. While calculations show that the entire thermal mass of the chamber is in thermal equilibrium with the prescribed Planer temperature at

the point in time at which the pressure stabilizes, we do not know if the equilibrium is stable or metastable. Nevertheless, the temperature and pressure recorded when the pressure measurements level define the thermodynamic state of the system. It should be noted however that these experiments will contain a systematic variance in pressure due to the shrinkage of the metal walls of the chamber upon cooling, though based on thermal contraction calculations, we estimate that the volume change of the isochoric chamber is on the order of 1% at -200°C, and as such, we assume that the approximation of constant-volume conditions will hold.

The overall behavior observed in these baseline tests is comparable to our previously published observations for pure water in [37], the thermodynamic significance of which is discussed in detail in that work. In brief, Figure 3.8 demonstrates that the pressure increases during freezing to temperatures below the eutectic. The pressure peaked when the temperature of the Planer was set to – 80 ˚C and then began to drop as the temperature was further decreased to – 160 ˚C. It was observed that in all the temperature segments, the pressure changed until it reached a plateau. Upon warming the pressure increased until the set temperature at – 80 ˚C, and then decreased at the set temperature of – 40 ˚C. It is also interesting to note that the pressure/temperature relationship measured during freezing is mirrored during the thawing phase. This suggests that the data has thermodynamic significance and is not a random occurrence. Panel 3.8b shows the pressure changes during freezing by immersion of the isochoric chamber in liquid nitrogen followed by thawing in air. The temperature change of the chamber during cooling and warming is shown in Figures 3.7a,b. Upon freezing to liquid nitrogen temperatures, the pressure increased to a peak and then began to decrease when liquid nitrogen temperatures were reached. Two interesting observations can be made during this sequence. First, the peak pressure in the immersion in liquid nitrogen experiment is comparable to the peak pressure in the Planer experiment, and is consistent with the maximum pressures that can be produced by the growth of ice-1h under isochoric conditions. Second, the pressure drops and levels as the temperature of the chamber reaches liquid nitrogen temperatures. The pressure during thawing in air also exhibits a similar pattern to that previously reported [37] and is comparable to that observed in the Planer experiment.

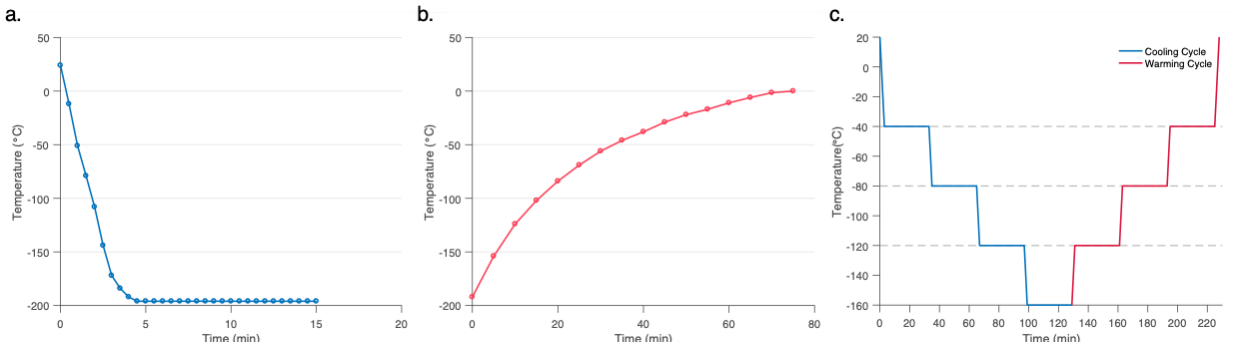

Figure 3.7. Typical (a) cooling and (b) warming temperature history. Representative plots of temperature measured during immersion of isochoric chambers in liquid nitrogen for 15 min and warming in air at room temperature, respectively. The average cooling rate during immersion was 53.2 °C/min, and the average warming rate was 2.9 °C/min. (c)The pre-programmed temperature profile in the Planer controlled rate freezer for the slow cooling protocol. The freezing and warming rate between set temperatures was 20 °C/min.

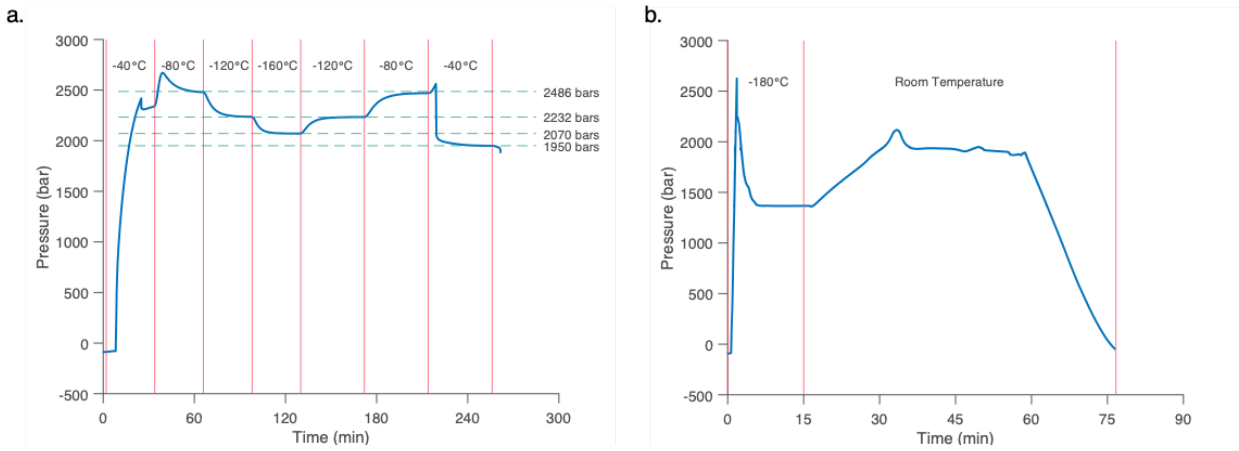

Figure 3.8: Typical pressure measurements in the isochoric chamber for pure Unisol solution. The pressures achieved during cooling and during warming are almost the same, indicating that those measurements are during thermodynamic equilibrium. These experiments established the baseline for interpreting the effect of adding Propane-diol and Me_2SO. **A)** Cooling in steps from room temperature down to -160˚C and warming back to room temperature, and **B)** For rapid cooling in liquid nitrogen for 15 minutes followed by warming in air.

3.2.3 Isochoric pressure-temperature measurements in the presence of propane-diol

Figures 3.9a,b show pressure profiles for a Unisol solution containing 10%(w/v) PD processed in the same way as described above. Figure 3.9a shows results with the Planer device. It was observed that: a) the maximal pressure was reached when the planer was set to – 80 ˚C, b) the pressure decreased with a decrease in temperature from – 80 ˚C to – 160 ˚C, c) the pressure first increased during the warming stage to – 80 ˚C and then decreased, d) the pressure leveled at thermodynamic equilibrium and, e) the equilibrium pressure was the same for a given temperature during both the freezing and thawing stages. The main difference from Fig 3.8a for Unisol without CPA, is that the maximum pressure was lower, likely due to the freezing point depression effect of PD. Additionally, in the pure Unisol tests, the pressure did not return to atmospheric in the final warming stage of the Planer experiment, likely because there was more water in the solution and we did not record the complete melting. Figure 3.9b, depicting freezing in liquid nitrogen and thawing at room temperature, showed similar responses to that in Figure 3.8b: a) a high-pressure peak occurs during the early stages of cooling, followed by b) a partial reduction of pressure while reaching thermodynamic equilibrium in liquid nitrogen, and c) an increase in pressure at the beginning of the thawing process, followed by a reduction in pressure to atmospheric as the thawing is completed. Interestingly, the maximal pressure in the Planer freezing is comparable to that in the liquid nitrogen freezing. In Figures 3.9c,d, equivalent pressure profiles for the freezing and thawing of a solution of 20% (w/v) PD in Unisol are presented, showing trends qualitatively identical to Figures 3.9a,b but reaching once more a lower maximal pressure due to the enhanced concentration of PD.

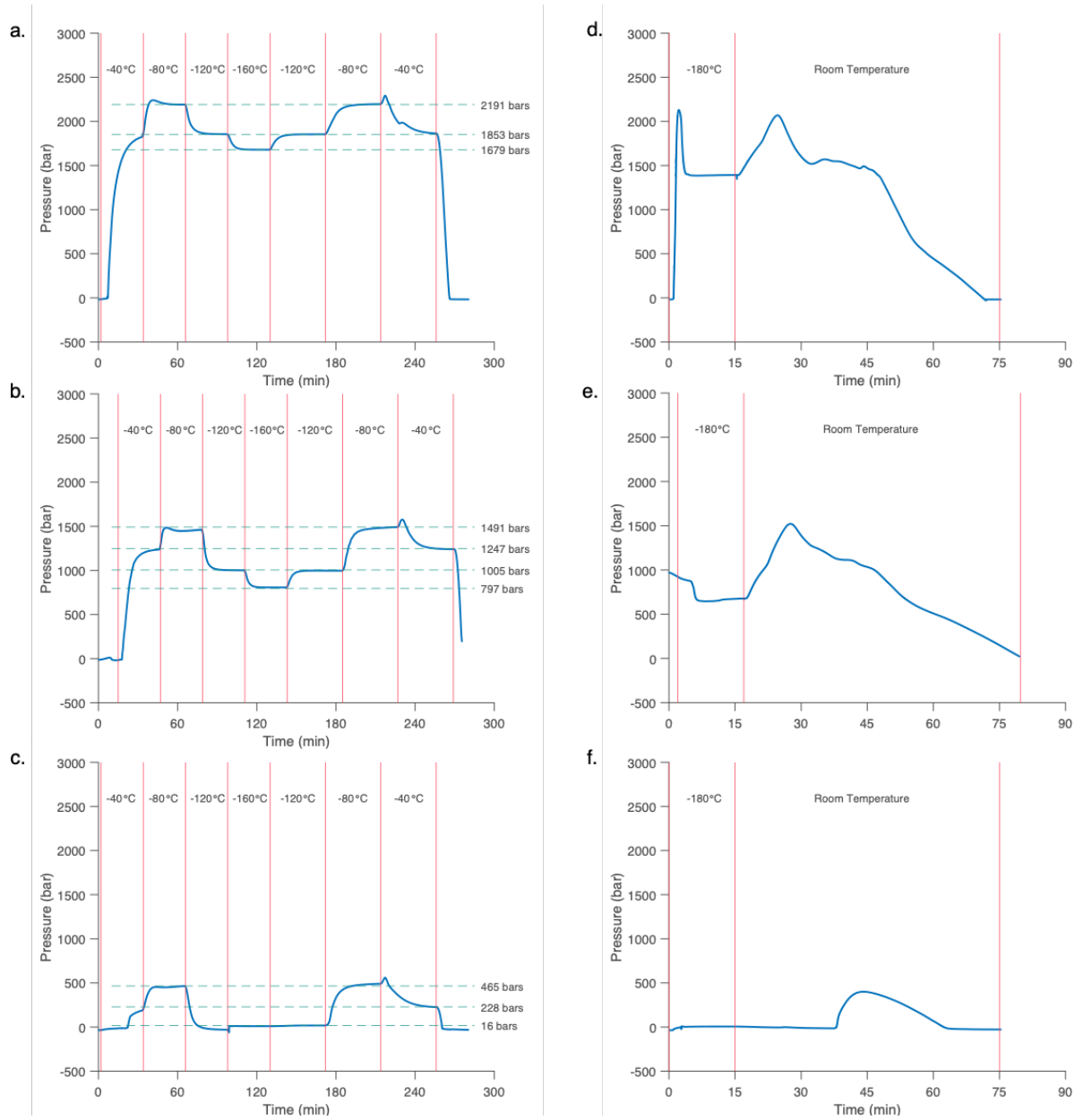

Figure 3.9: Typical pressure measurements in the isochoric chamber for Unisol mixed with propane-diol in various concentrations. Vitrification, denoted by no pressure increase, is observed in the 30% (w/v) Propane-diol (PD) solution during the rapid immersion in liquid nitrogen. Devitrification can be seen during the warming when the pressure is observed to increase. A) 10% (w/v) PD in Unisol cooled in steps from room temperature down to -160˚C and warmed back to room temperature. B) 10% (w/v) PD in Unisol rapidly cooled in liquid nitrogen for 15 minutes and warmed in air. C) 20% (w/v) PD in Unisol cooled in steps from room temperature down to -160˚C and warmed back to room temperature. D) 20% (w/v) PD in Unisol rapidly cooled in liquid nitrogen for 15 minutes and warmed in air. E) 30% (w/v) PD in Unisol cooled in steps from room temperature down to -160˚C and warmed back to room temperature. F) 30% (w/v) PD in Unisol rapidly cooled in liquid nitrogen for 15 minutes and warmed in air.

A notable change in behavior begins with a concentration of 30% (w/v) PD, as shown in Figures 3.9e,f. In Figure 3.9e, freezing and thawing in the Planer device is qualitatively similar to the previous figures. Here also, the pressure increases during the freezing stage, reaching a maximum

at a Planer setting of -80 ˚C. The pressure decreased as the temperature was further reduced, albeit to atmospheric now. It should be noted that a slight increase in pressure was observed at the transition between -120 ˚C and -160 ˚C in Figure 3.9e, though meaningful interpretation of this observation is limited within the context of these studies, as the pressure transducers employed have substantially reduced sensitivity at pressures below 50 bar. Upon thawing, the pressure increased again at the -80 ˚C setting, after which it decreased with an increase in temperature. Here also the pressure levels suggested a state of thermodynamic equilibrium.

As we have established previously, the increase in pressure during freezing is a consequence of the formation of ice [37]. However, a new type of behavior was manifest during rapid cooling in liquid nitrogen. While there was an increase in pressure with slow freezing (Fig. 3.9E), the pressure in the isochoric system during freezing in liquid nitrogen (Figure 3.9F) did not increase whatsoever. It is obvious from the Planer freezing experiment that the 30% (w/v) solution can freeze at the prescribed rate of cooling, and that the pressure will indeed increase upon freezing. Therefore, a reasonable explanation for the absence of an increase in pressure during cooling in liquid nitrogen is that the solution has vitrified, and no ice was formed for cooling at this rate. This is supported by the observation that during the slow thawing in air, the pressure increases to the value recorded during the thawing in the Planer system. This suggests that the solution devitrified during the thawing process, forming ice as the system traveled more slowly through the temperature range between the glass transition and the melting point. Importantly, these observations suggest that it may be possible to achieve vitrification in an isochoric system at substantially lower cooling rates than previously observed, and with a CPA concentration as low as 30 % (w/v). Previous work has shown that vitrification of a solution with similarly low concentrations of CPAs under conventional isobaric conditions (at atmospheric pressure) would require cooling rates on the order of 100 °C/s, or alternatively, that a concentration of approximately 50 % (w/v) would be required to vitrify a solution at the cooling rate employed in this study[139]. Furthermore, it is important to note that when vitrification conditions occur in an isochoric chamber, the pressure does not increase. Therefore, a properly designed isochoric chamber must be rigid and maintain a constant volume, but it need not be designed to withstand the high pressures for which a hyperbaric vitrification system is designed (see [127]).

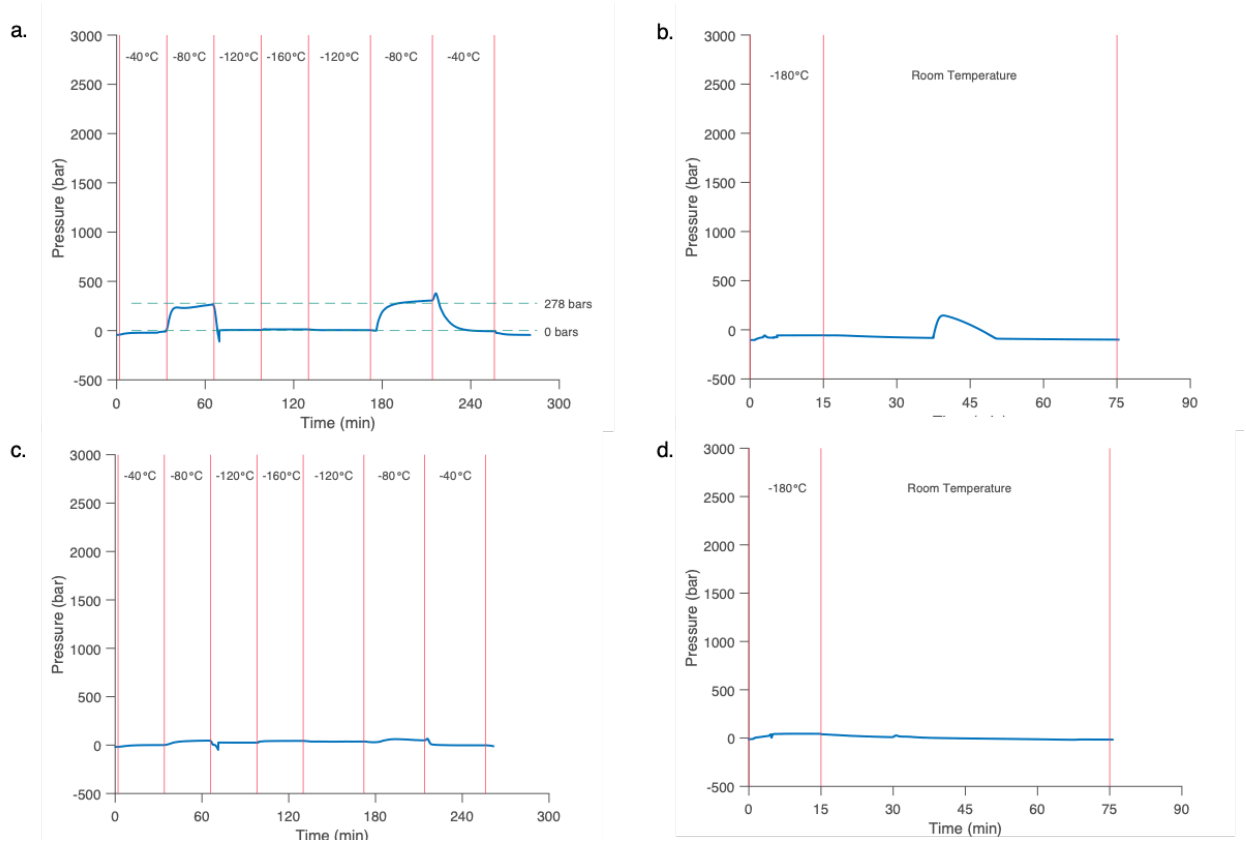

Figure 3.10: Typical pressure measurements in the isochoric chamber for Unisol mixed with Propane-diol (PD) in various concentrations. Vitrification, denoted by no pressure increase, can be seen in the 40% (w/v) PD solution during the rapid immersion in liquid Nitrogen. Devitrification can be seen during the warming when the pressure increases again. Vitrification, known to occur at 44% (w/v), can also be seen by no pressure change. A) 40% (w/v) PD in Unisol cooled in steps from room temperature down to -160˚C and warmed back to room temperature. B) 40% (w/v) PD in Unisol rapidly cooled in liquid nitrogen for 15 minutes and warmed in air. C) 44% (w/v) PD in Unisol cooled in steps from room temperature down to -160˚C and warmed back to room temperature. D) 44% (w/v) PD in Unisol rapidly cooled in liquid nitrogen for 15 minutes and warmed in air.

Figures 3.10a,b shows the pressure changes in relation to temperature changes for a concentration of 40% (w/v) PD in Unisol. The results are comparable to those in Figures 3.9e and 3.9f. In the Planer freezing and thawing system, there was an increase in pressure during both, freezing and thawing, at the Planer temperature of -80 ˚C. This indicates that ice formed in this composition. However, when the isochoric chamber was immersed in liquid nitrogen, there was no increase in pressure during freezing, i.e. vitrification. It is noted however, that there was an increase in pressure during thawing, suggestive of devitrification. Parenthetically, it should be reiterated that the interpretation of pressure changes observed below 50 bar are limited due to the decreased sensitivity of pressure transducers used in this study within this pressure range.

Figures 3.10c,d represent plots for a small increase in CPA concentration to 44% (w/v) PD. This was selected for study as it is the value that Fahy and his colleagues determined to be the limit for onset of vitrification, from visual inspection[126,127]. Our measurements show no increase in pressure, neither during freezing with the Planer nor by immersion in liquid nitrogen, and thereby support findings of Fahy et al., who used visual inspection to determine vitrification.

The research by Fahy et al on the effects of pressure[126,127] found that a hyperbaric increase in pressure to 1000 atmospheres will reduce the PD concentration required for vitrification to 39% (w/v). It is important to recognize, from the data presented so far, that such an increase in pressure does not occur during isochoric vitrification. Isochoric vitrification is largely thermodynamically distinct in nature from hyperbaric vitrification. Isochoric vitrification does not operate through an elevation in pressure, but instead by reducing the bulk likelihood of ice formation, as discussed in Chapters 2 and 3.1. The current study shows that even for an isochoric chamber of bulk (mL) volumes, vitrification is possible already at a concentration of 30% (w/v), significantly less than the 39% (w/v) required for hyperbaric vitrification. However, it should be noted that the cooling rate employed in the present study (53.2 ℃/min) is higher than that employed by Fahy and colleagues (30 ℃/min) in their hyperbaric system, this may attenuate the differences in concentrations required for vitrification somewhat.

3.2.4 Isochoric pressure-temperature measurements in the presence of dimethyl sulfoxide

Similar results were found in the studies with Me_2SO in Unisol. The equilibrium pressures observed at each temperature step for Me_2SO are presented in Table 3.1, alongside the pressures observed in Propane-diol and Pure Unisol (as depicted in Figures 3.8a, 3.9a – c, 3.10a, and 3.10c). The results for 10% and 20% (w/v) Me_2SO closely resemble those for propane-diol, in which the following was observed: In the Planer experiments a) the maximum pressure was reached when the Planer was set to -80 ˚C, b) the pressure decreased with a decrease in temperature from -80 ˚C to -160 ˚C, c) the pressure first increased during the increase of temperature stage from -160 ˚C to -80 ˚C and then decreased after -80 ˚C , d) the pressure leveled at thermodynamic equilibrium and e), the equilibrium pressure was the same for a given temperature during both freezing and thawing. During immersion in liquid nitrogen, the pattern was equally similar: a) a high-pressure peak occurred during the early stages of cooling, followed by b) a reduction of pressure to a value above atmospheric while reaching thermodynamic equilibrium in liquid nitrogen, c) an increase in pressure at the beginning of the thawing process, followed by a reduction in pressure to atmospheric as the thawing was completed. Interestingly, the maximal pressure in the Planer freezing is comparable to that in the liquid nitrogen freezing. Furthermore, although the trends between propane-diol and Me_2SO were consistent, in some cases slight asymmetry was observed in the steady state pressure values observed at fixed temperatures during cooling versus during warming. Similar asymmetries have been observed previously [28], and it is unclear in the context of this study whether they represent experimental artifacts or genuine thermodynamic or kinetic phenomena, and should be examined further in future work.

Table 3.1. Hydrostatic pressures of cryoprotective solutions at sub-zero temperatures under isochoric conditions.

Temperature		Pressure (kbar)			
		−40 °C	−80 °C	−120 °C	−160 °C
Pure UNISOL		1.97	2.67	2.25	2.01
UNISOL Base + Me_2SO	10%	1.95	2.57	2.13	1.92
	20%	0.96	1.23	0.69	0.40
	30%	0.14	0.17	0.06	0.05
	35%	0.03	0.04	0.01	0.02
	49%	0.02	0.03	0.03	0.03
UNISOL Base + Propane-Diol	10%	1.84	2.19	1.85	1.68
	20%	1.25	1.49	1.01	0.80
	30%	0.23	0.47	0.02	0.01
	40%	0.0	0.28	0.01	0.01
	44%	0.0	0.05	0.03	0.04

As with PD, the isochoric system began to behave differently at a concentration of 30% (w/v) Me_2SO, as presented in Figures 3.11a-d. Figure 3.11a shows the pressure profile observed during cooling in the Planer device, in which the pattern is seen to be similar to the results from the lower concentrations. However, an interesting phenomenon emerged within the triplicate liquid nitrogen immersion results. Figures, 3.11b, 3.11c and 3.11d show the three repeats of the immersion experiments; Note that 3.11b and 3.11d behave similarly to the general observations concerning the lower concentrations, described above. However, in Figure 3.11c, the pressure did not increase, and it resembled the pattern in Figures 3.9f and 3.10b, in which vitrification occurred. A likely explanation is that this composition represents the critical limit for vitrification at these cooling rates, and is thus dominated by stochastic kinetic effects which may vary run-to-run.

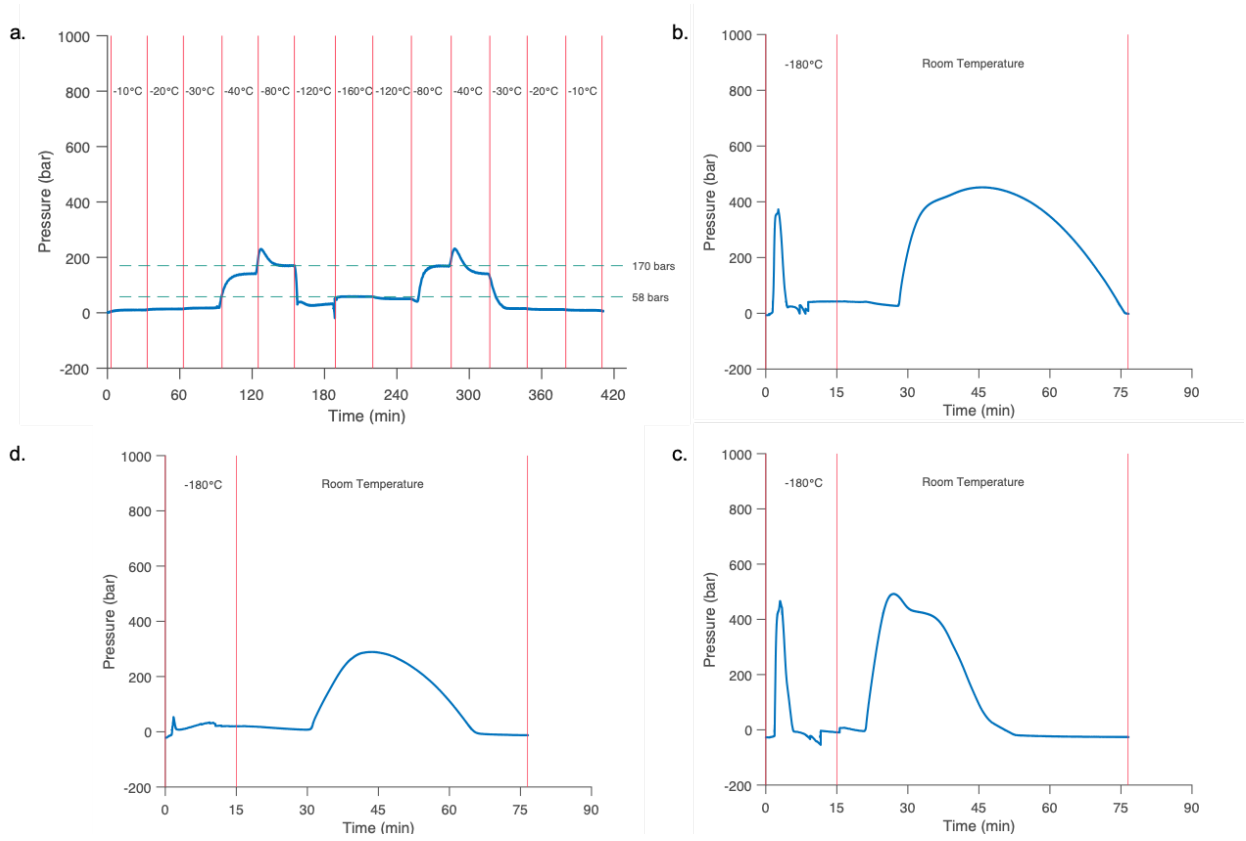

Figure 3.11: Typical pressure measurements in the isochoric chamber for Unisol mixed with 30% (w/v) Me_2SO. A) Cooled in steps from room temperature down to -160˚C and warmed back to room temperature. **B), C) & D)** Rapidly cooled in liquid nitrogen for 15 minutes and warmed in air. No pressure increase in one of the three rapid cooling runs which suggests this concentration is on the limit for vitrification in isochoric conditions, which is much lower than the 49% (w/v) Me_2SO concentration observed at atmospheric pressure.

Finally, Figures 3.12 a,b represent observations for a concentration of 35% (w/v) Me_2SO in a Planer cooling system and by immersion in liquid nitrogen, respectively. Figures 3.12c,d are for a concentration of 49% (w/v) Me_2SO in a Planer cooling system and by immersion in liquid nitrogen, respectively. In all of the above, there is no evidence for a significant increase in pressure (reiterating once more that our pressure transducers do not provide reliable data at pressures under 50 bars). As discussed earlier, the absence of a significant increase in pressure in systems in which more than half of the solution is water indicates an absence of freezing. Again, our results are consistent with the results of Fahy et al obtained from visual inspection [126,127]. Also, in accordance with the reports of Fahy et al., the current study using pressure measurements suggest that a concentration of 49% (w/v) is a vitrification composition at atmospheric pressure [126,127]. Fahy et al. also showed that at a hyperbaric pressure of 1000 atmospheres, the required vitrification concentration is reduced to 45% (w/v). Interestingly, our results show that in an isochoric chamber, in which the volume is constrained, but the pressure remains atmospheric, the required vitrification concentration is reduced to 35% (w/v), and potentially even lower. This supports the hypothesis advanced by Szobota and Rubinsky [140] and explored in the previous chapters of the current work, that isochoric thermodynamic conditions may energetically discourage ice formation and thus promote vitrification.

We would like to re-emphasize that isochoric vitrification is thermodynamically distinct from hyperbaric vitrification; the first requires a rigid-walled chamber that need only sustain very low pressures, while the second requires a source of enhanced constant pressure and an accordingly pressure-resistant container. In a hyperbaric system, the elevated pressure is used to decrease the probability for ice nucleation, whereas in an isochoric system the confined volume is used to decrease the probability for ice nucleation. These represent two different thermodynamic mechanisms, the former dependent on the Gibbs free energy and the latter dependent on the Helmholtz free energy. In comparison with data from the literature, we show that isochoric chambers are much more effective in promoting vitrification than hyperbaric pressure chambers, and are obviously also expensive, easier to design, and easier to use.

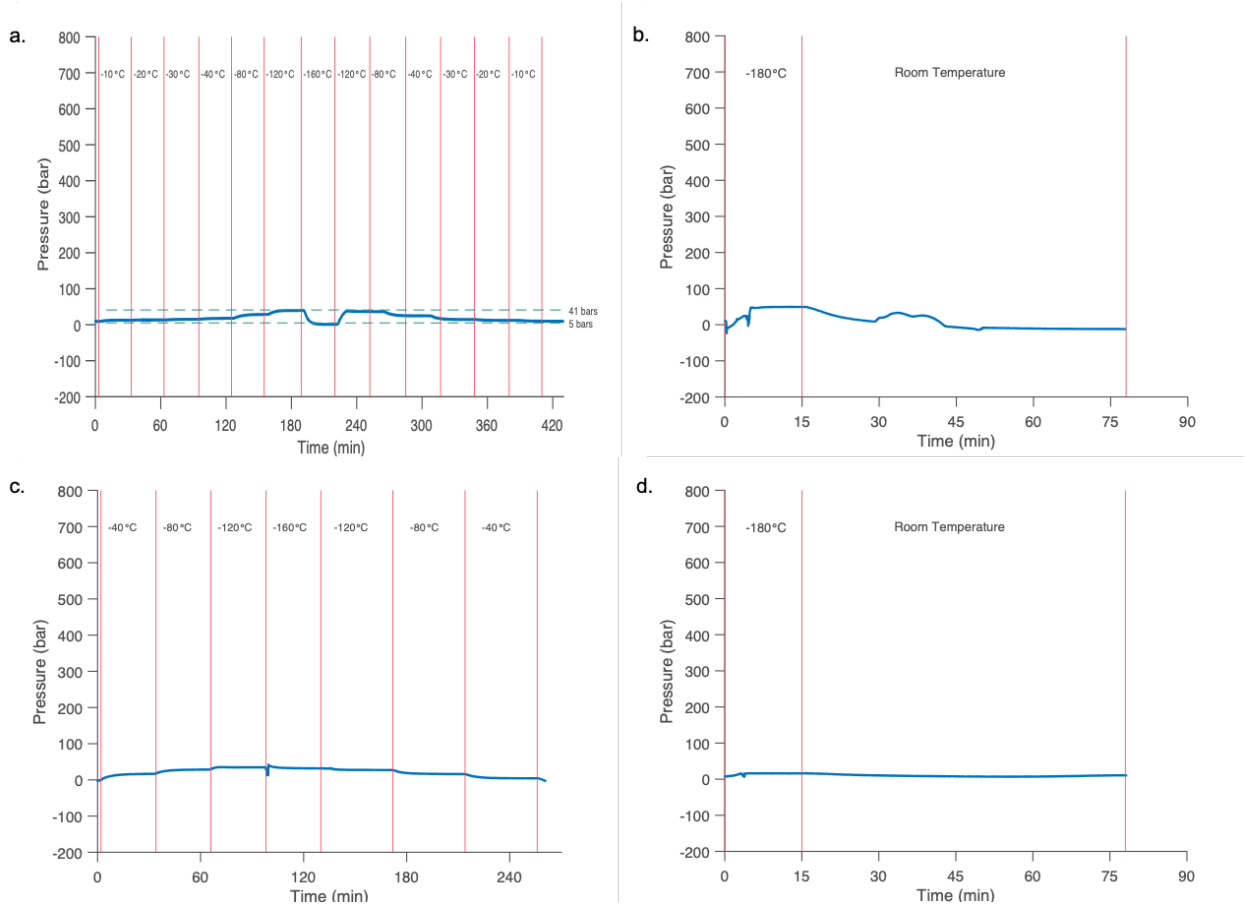

Figure 3.12: Typical pressure measurements in the isochoric chamber for Unisol mixed with Me_2SO in various concentrations. Vitrification, indicated by no change in pressure, can be seen in the 35% (w/v) Me_2SO solution during the rapid immersion in liquid Nitrogen. Vitrification, known to occur at 49% (w/v) Me_2SO, can also be seen by no pressure change. **A)** 35% (w/v) Me_2SO in Unisol cooled in steps from room temperature down to -160˚C and warmed back to room temperature. **B)** 35% (w/v) Me_2SO in Unisol rapidly cooled in liquid nitrogen for 15 minutes and warmed in air. **C)** 49% (w/v) Me_2SO in Unisol cooled in steps from room temperature down to -160˚C and warmed back to room temperature. **D)** 49% (w/v) Me_2SO in Unisol rapidly cooled in liquid nitrogen for 15 minutes and warmed in air.

This study represents but a first-order proof-of-concept, and much more research (both experimental and theoretical) is needed to generate a rounded understanding of the significance of the data presented in this study. In order to fully contextualize the experimental results reported in this work, a detailed thermodynamic analysis is required which rigorously considers thermal expansion and contraction effects, kinetic effects, thermal diffusion effects. At this stage, the focus of this research is to glean some empirical understanding of the process of vitrification in an isochoric chamber, and to clarify early routes towards clinically-relevant isochoric vitrification protocols for the cryopreservation of bulk-scale biological constructs. Despite the first-order nature of the results described and discussed herein, the results display a consistent overall trend consistent with high-level thermodynamic understanding of the system, and the observed consistency suggests that the observed behaviors are of a fundamental nature worthy of more in-depth investigation in further studies. In summary, we believe that isochoric vitrification should be given serious consideration in future attempts of cryopreservation by vitrification.

3.3 Isochoric freezing processes involving multiple chemical constituents

At constant atmospheric pressure, when the temperature of biological matter is reduced below the freezing point of physiological saline (-0.57C), ice formation may occur. Due to its crystallographically pure structure, ice-1h readily rejects solutes as freezing progresses, increasing the concentration of the remaining solution and modulating its chemical potential.

In cellular, tissue, and organ systems preserved in solution at sub-freezing temperatures, ice nucleation typically occurs first in the large extracellular space[11,12], while the probability of intracellular ice nucleation is much lower due to the much smaller intracellular volume. Furthermore, even on the occasion that a given cell might freeze, the ice will not necessarily trigger ice formation in other cells. Thus, during freezing of biological materials, the ice and solution in the extracellular space are in thermodynamic equilibrium, but the yet-unfrozen cells are in a thermodynamically metastable supercooled state.

In order to equilibrate the difference in chemical potential which emerges between the interior of the cell, in which the solution is supercooled, and the exterior of the cell, in which ice is in thermodynamic equilibrium with the extracellular solution, water will leave the cell through the water-permeable cell membrane. Consequently, the intracellular solution will become hypertonic. It was originally proposed by Lovelock [141] and later incorporated in his comprehensive theory by Mazur [11,12] that the increased hypertonic intracellular solution is damaging to cells, and indeed experiments employing conventional isobaric freezing show that damage to cells increases both as the temperature decreases below the freezing point (thus increasing the solute concentration and hypertonicity) and as the exposure time increases.

Isochoric freezing was originally introduced by Rubinsky et al. with the goal of reducing the damaging effects of freezing; and while we have focused thus far on its prevention of the morphological disruption that can occur due ice expansion and growth, isochoric freezing also significantly reduces the aforementioned cytotoxicity of hypertonic intracellular solutions.

Recall that in an isochoric freezing system, the volume is constrained as the temperature is reduced, freeing to the pressure to vary as necessary as ice forms and compresses the remaining liquid phase. On the common T-P phase diagram of water, it has been shown that freezing in an isochoric system will follow precisely the liquidus line between ice-1h and water[142], up to the triple point of water, ice-1h, and ice-III, implying that at all temperatures between 0 and -21.985ºC the equilibrium contents of an isochoric system will be comprised of a two-phase solution of ice and liquid (for reference, at -21.985°C only approximately 56% of the volume of the system is frozen).

This overall reduction in ice formation results in an according reduction in the difference in chemical potential between the intracellular and extracellular volumes, and thus significantly reduces migration of water and intracellular hypertonicity, with both models and experiment demonstrating that the percentage increase in concentration of a solution frozen to -20°C is more than an order of magnitude less in an isochoric system than in a standard isobaric system[142]. Thus, in isochoric freezing experiments, sensitive biological matter stored in the portion of the system that remains in the liquid state endures significantly less hypertonicity than experienced during conventional freezing, whilst being simultaneously protected from the direct mechanical damage of ice crystallization.

Isochoric preservation studies operating at equilibrium have thus far considered or employed a single homogeneous solution (phase) of constrained volume. In such “single-phase” systems, while the increase in concentration is substantially reduced compared to conventional freezing, it nevertheless increases as the temperature descends. Furthermore, the concentration increase is an immutable function of the employed solution and desired subfreezing temperature. In this work, we propose a new, improved approach to the equilibrium isochoric method: multiphase isochoric freezing. We hypothesize that by employing multiple chemical phases within the same system, separated by a membrane impermeable to mass transfer but open to equilibration of pressure and temperature, it is possible to completely eliminate harmful concentration increases in the phase in which biological matter is preserved. Herein we develop a mathematical model to describe the equilibrium thermodynamic behaviors of such a system, validate this model with experimental data, and demonstrate the versatility of the multiphase approach from a protocol design perspective. Multiphase results are compared to single-phase isochoric and conventional isobaric results, suggesting a superior method of avoiding hypertonic cytotoxicity during preservation of biological matter.

3.3.1 Conceptual overview of multiphase isochoric freezing

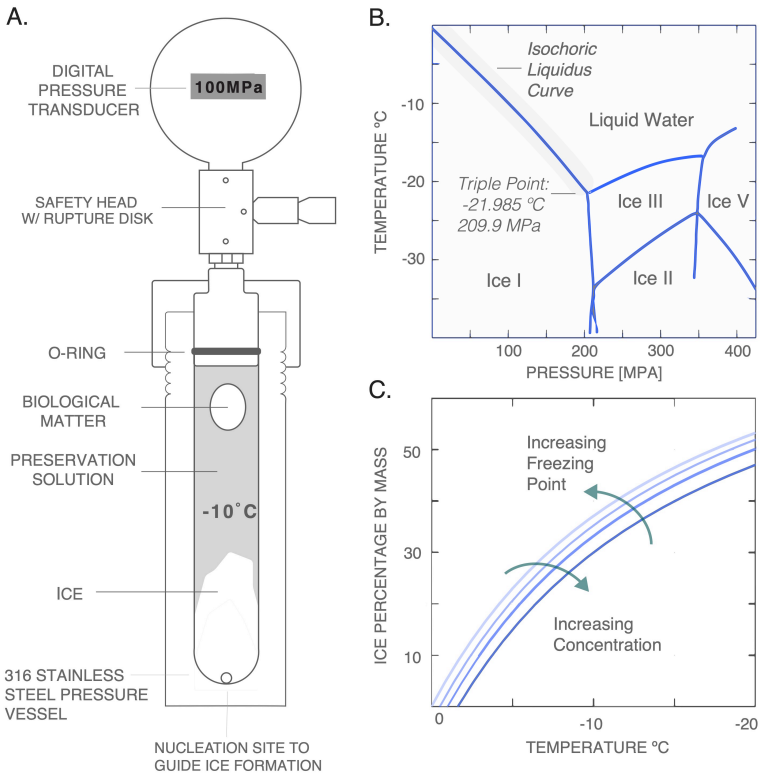

Figure 3.13. **Single-phase isochoric freezing. A**. Schematic of an experimental isochoric chamber, loaded with a single homogeneous solution. Cross-sectional view depicts the two-phase liquid-solid equilibrium characteristic of isochoric freezing. **B.** Phase diagram of pure water. The equilibrium states of an isochoric system occupy the labeled liquidus curve between ice-1h and water between 0°C and the triple point of water, ice-1h, and ice III. **C.** Ice percentage vs. temperature for a generic series of solutions of varying solute concentration in an isochoric system. As the solute concentration increases, the freezing point of the solution will decrease and the ice percentage curve will shift deeper in temperature.

A single-phase isochoric system employs a single aqueous solution held at subfreezing temperatures in a rigid, sealed container (Fig. 3.13A). As described, the equilibrium states of this system will occupy the liquidus curve of the solution phase diagram (Fig. 3.13B for water), holding the contents in a constant two-phase, liquid-solid equilibrium, and enabling ice-free cryopreservation of sensitive biological matter in the liquid phase (Fig. 3.13C). At a given system specific volume, this system can be characterized by three thermodynamic variables: pressure, temperature, and concentration, which, in a single-phase system, are all interdependent. Speaking generally, as the equilibrium temperature is decreased in a single-phase isochoric system, the pressure and concentration will increase, depressing the freezing point of the liquid phase to match the equilibrium temperature and maintaining two-phase ice-solution equilibrium.

A multiphase isochoric system operates under the same basic premises, but affords access to a substantially wider array of equilibrium states and complete or partial elimination of concentration increases by incorporating two chemically independent aqueous phases within a given isochoric

enclosure. Formally speaking, as depicted in Fig. 3.14, a multiphase isochoric system is a system of constrained volume comprised of two distinct aqueous phases with different initial compositions and osmolalities. They are separated by a boundary, Γ, which is impermeable to matter but completely malleable and able to transmit heat and pressure (in the experimental work to follow, this boundary is realized using a latex balloon). For clarity, we will assume that one phase is completely encased by the other, and we will refer to them as the external and internal phases respectively (implying position external to or internal to the boundary Γ). The composite system shares a universal temperature T and pressure P, but the concentrations C_{ext} and

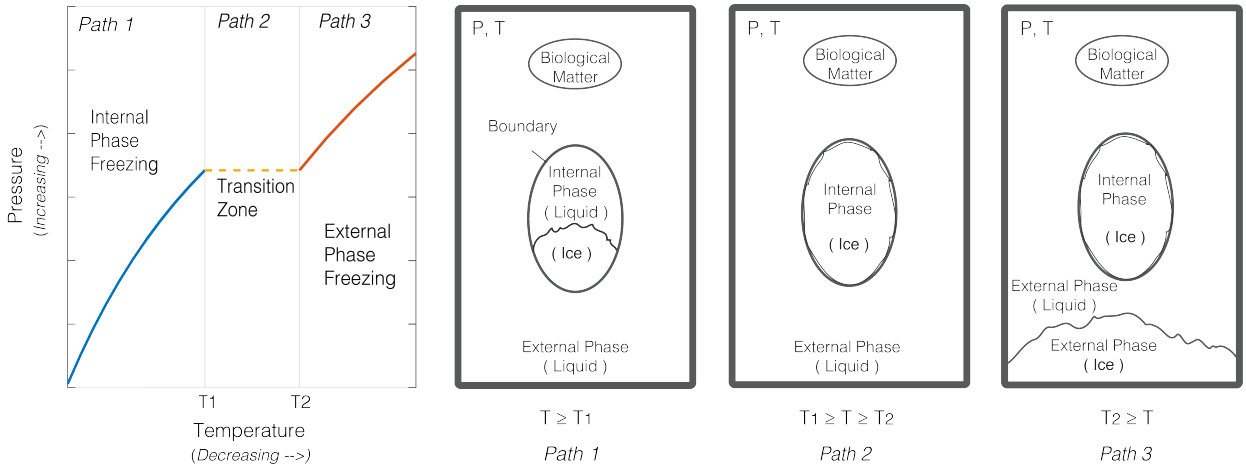

Figure 3.14. Multiphase isochoric freezing. A. Pressure-temperature diagram depicting the equilibrium states occupied by a system consisting of two distinct aqueous phases, one internal to and one external to the mass-impermeable boundary Γ. The system will follow three distinct paths as temperature decreases, presented conceptually in schematics B – D: On Path 1 (B), only the internal phase forms ice. This path is identical to the liquidus curve of the phase diagram of the internal phase. Path 2 (C) covers the temperature range between the temperature at which the internal phase has frozen completely and the pressure-adjusted freezing point of the external phase. On Path 3 (D), the external phase also forms ice. This phase represents a pressure-adjusted liquidus curve for the external phase.

C_{int} of the external and internal phases remain independent of each other due to the mass-impermeable nature of the boundary Γ.

Given the same constant-volume constraint on the system as a whole, the thermodynamic behaviors of single phase and multiphase systems are fundamentally similar—but while the equilibrium states of single-phase isochoric systems can be described by the liquidus curve of a single phase diagram, the equilibrium states of a multiphase isochoric system will navigate between the liquidus curves of multiple phase diagrams, depending both on the solutions employed in each phase and the volume ratio between them.

The equilibrium states that a multiphase isochoric system will occupy at subfreezing temperatures can be broken into three distinct paths, as indicated in Fig. 3.14A. Assuming without the loss of generality that the internal phase has a higher initial freezing point than the external phase, the equilibrium states the system will occupy on Path 1 will follow the liquidus line of the phase diagram of the internal phase, and the system will behave identically to a single-phase isochoric system (it is important to note that this statement is only rigorously correct when the compressibility of the external phase is not significantly lower than that of the internal). However,

provided that the volume of the internal phase is sufficiently small (less than roughly 56% for pure water), at sufficiently low temperatures, its entire volume will freeze. At these temperatures, the equilibrium states of the system will then deviate from the internal phase liquidus curve, and will enter a "transition zone." This second path is described thusly because it represents a unique space in temperature over which the system can be said to transition from the liquidus curve of the internal phase to the liquidus curve of the external phase. As highlighted in Fig. 3.14, this path is unique in that it permits the system to further decrease in temperature without an according increase in pressure and concentration. This is the result of a temperature gap that emerges between the point at which the internal phase has frozen completely and the point at which the external phase will first freeze. Based on the earlier assumption that the osmolality of the external phase is greater than that of the internal, its freezing point is lower by definition; however, it should be noted that in practice the freezing point of the external phase will be further depressed by the pressure exerted by the now-frozen internal phase. Thus, the final thermodynamic path begins at the phase transition temperature of the external phase at some transition pressure P_t, and follows a pressure-adjusted liquidus curve for the external phase.

3.3.2 Multiphase Thermodynamic Model

In order to theoretically model these multiphase equilibrium pathways, we herein extend the single-phase model developed by Rubinsky[143] to include multiple phases that do not exchange mass, but share a common temperature and pressure. In the name of brevity, the single-phase model in its entirety is not reproduced here, but can be found in full detail in [6]. The goal of this model is to fully specify the thermodynamic equilibrium state of an isochoric system by determining the values of interdependent variables temperature T, concentration c, pressure P, and quality or phase fraction Z (the mass ratio of ice to liquid water in the two-phase system), given prior knowledge of only one (henceforth we will assume the pressure to be the initially specified variable).

The first and most conceptually important component of this task is calculation of the equilibrium temperature. Recalling that a single-phase isochoric system will exist in two-phase solid-liquid equilibrium at all temperatures between 0°C and -21.985°C (the triple point), the equilibrium temperature is necessarily a function of the freezing point depression caused by the increases in pressure and concentration which accompany the formation of ice. Herein we assume the depression contributed by pressure and that contributed by increased solute concentration to be linearly additive and mutually independent, and furthermore that the effects of each chemical species can be considered independently of one another. This is a well-known approximation commonly used in cryobiology research, e.g.[144]; we anticipate that this assumption is correct at lower concentrations, and that at higher concentrations the effects may not be linearly additive. The equilibrium temperature $T(P, c)$ in an isochoric system at a given pressure and concentration can thus be written as:

$$T(P, c) = T^0 + \Delta T(P) + \Delta T(c) \qquad (3.1)$$

in which T^0 is the initial freezing temperature of the solution, $\Delta T(P)$ is an experimentally derived function relating the freezing point depression caused by pressure P, and $\Delta T(c)$ is an experimentally derived function relating the freezing point depression caused by solute

concentration (see Appendix A1 for more detail). As stated earlier, depending on the solution, $\Delta T(c)$ may itself be a linear combination incorporating the independent freezing point depressions of multiple chemical species, such that

$$\Delta T(c) = \Delta T(c_1) + \Delta T(c_2) + \Delta T(c_3) \dots \Delta T(c_n) \qquad (3.2)$$

Armed with the pressure and temperature and incorporating the principles of conservation of mass, experimental data relating the specific volumes of ice and water as a function of temperature, and coefficients of thermal expansion and isothermal compressibility, the quality Z of the system can be calculated. The derivation and mode of calculation can be found in Appendix A1.

Finally, from the quality of the system and principles of conservation of mass of solutes, the concentration in the unfrozen volume can be calculated. This concentration is a direct product of the degree of ice formation, as ice forms a pure crystal and thus rejects solutes into the remaining liquid phase [143] . A simple relation between the quality Z, the concentration c_1 at some subfreezing temperature T_1, and the initial concentration c_0 at the atmospheric freezing point T_0 can be given as

$$c_1 = \frac{c_0}{Z} \qquad (3.3)$$

This value c_1 can then be substituted into eq. (3.1), and the temperature, quality, and concentration can be recalculated iteratively until convergence is reached. The process of fully specifying the equilibrium thermodynamic state of an isochoric system can thus be summarized in the following steps:

Single-Phase Algorithm

1. Specify an initial freezing point T_0, concentration c_0, and a desired pressure P. Initially the quality Z will be equal to zero, as the entire system is liquid.
2. Calculate the freezing point depression using Eq. (3.1). An initial guess of $c = 0$ may be used in the first iteration.
3. Based on the pressure and temperature, calculate the quality of the system Z.
4. Calculate the new concentration using eq. (3.3).
5. Iteratively repeat steps 2 – 4 using the new concentration until convergence is reached to a desired tolerance.

This process enables calculation of the equilibrium state variables for a single-phase isochoric system. The process for a multiphase system is directly analogous, but requires sequential calculations to specify each path described in Figure 3.14. Assuming similarity of compressibilities between the internal and external phases of the system, Path 1 is calculated in the exact manner described above, functioning essentially as a single-phase isochoric system. Recalling that the quality Z is defined as the ratio of ice mass to total system mass $\frac{m_{ice}}{m_{total}}$, Path 1 is valid in the quality range

$$0 \leq Z \leq Z_1 \qquad (3.4)$$

in which $Z_1 = \frac{(m_{ice} = m_{internal})}{m_{total}}$, or Z_1 is the quality of the state at which the entire mass of the internal phase has frozen. After the system has reached the temperature T_1 at which Z_1 occurs, the system follows Path 2, entering the transition zone. Recalling that the transition zone represents the temperature gap between T_1 and the freezing point T_2 of the external phase, in order to calculate the range over which the transition zone will extend, T_2 must be calculated. This is done using equation (3.1), with $P = P_1$ (the pressure experienced at (T_1, Z_1)) and $c = c^0_{ext}$, or the initial concentration of the external phase:

$$T_2(P = P_1, c = c^0_{ext}) = T^0_{ext} + \Delta T_{ext}(P_1) + \Delta T_{ext}(c^0_{ext}) \qquad (3.5)$$

Note that the subscript "ext" is incorporated here to specify that the freezing point depression relations employed in eq. (3.5) pertain to the solution that comprises the external phase of the system, which will differ from those used previously to describe the internal phase.

With calculation of T_2, the temperature span of the transition zone can now be defined as

$$T_1 < T_{transition} < T_2 \qquad (3.6)$$

Note that within the transition zone, only the temperature varies, because the entire mass of the internal phase has frozen and the system has not yet reached the pressure-adjusted freezing point of the external phase, and thus no changes in pressure or concentration should be expected.

The final thermodynamic path of the system, describing states in which the external phase will also freeze, begins at $T = T_2$, and is calculated using the same single-phase algorithm employed previously, with slight modification. Given the impermeable membrane Γ between the internal and external phases, the external and internal solute concentrations are independent, and thus the single-phase algorithm can be initiated for the external phase using the initial concentration of the external phase only. However, the pressure is common to the whole system, and thus the algorithm for the external phase will begin at a pressure P_1, instead of at atmospheric pressure.

This multiphase model is thus a logical extension of that developed in [143], which has shown good agreement with experiment over a range of solutions. Of course, the treatment of the thermodynamic approach provided herein is conceptual in nature; a rigorous mathematical treatment for both single-phase and multiphase systems can be found in Appendix A1.

3.3.3. Experimental Validation

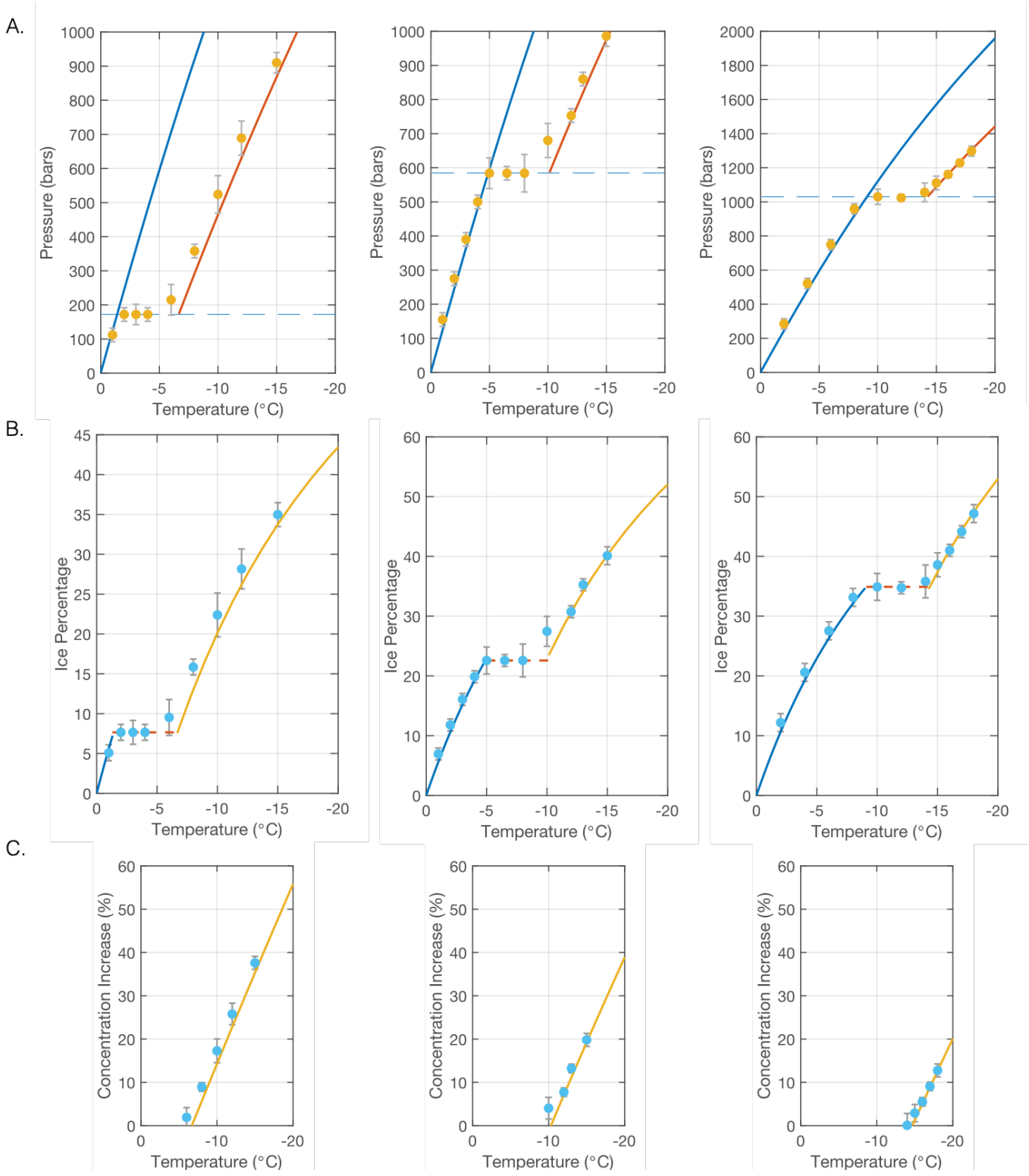

Figure 3.15. Experimental results (markers) and theoretical predictions (curves) for a multiphase isochoric system employing an external phase of 2M glycerol and 0.9% physiological saline and an internal phase of pure water. Three internal phase volumes are presented: 12%, 24% 36% (presented left to right). **A.** Pressure data (measured directly). The theoretical internal phase liquidus

line (blue) is extended over the entire temperature range for easy reference to single-phase isochoric behavior. **B.** Ice percentage data (calculated from pressure data). **C.** Percent increase in concentration (calculated from pressure data).

Experimental results and theoretical predictions for the equilibrium states occupied by a multiphase isochoric system containing pure water as the internal phase and a solution of 2M glycerol and phosphate-buffered saline (PBS) as the external phase are presented together in Fig. 3.15 for three different internal phase volumes. As described in the Methods section at the end of the chapter, the data in Figure 3.15A (the pressure-temperature behavior) were obtained directly using the experimental setup depicted schematically in Figure 1, and Figures 3.15B (ice percentage increase) and 3.15C (concentration increase) are calculated from this data using the thermodynamic model described previously. Experimental results agree well with the modeled predictions, suggesting that the iterative approach developed herein is sufficiently accurate to predict the behavior of these systems.

Of particular importance, Figure 3.15C depicts the increase in concentration with decreasing temperature. No increase in concentration is observed until deep sub-zero temperatures are reached, well past the atmospheric freezing points of both the internal and external phases. Additionally, the total concentration rise observed over the temperature range from 0 to -20°C is a strong function of the volume of the internal phase, which ultimately dictates the point at which the external phase will begin to freeze and increase the solute concentration.

Furthermore, the solutions employed as the internal and external phases in these experiments were chosen for conceptual and experimental convenience, and are otherwise entirely arbitrary. Any solution can be employed in either phase, in any volume ratio. Thus the temperature span over which freezing in each phase occurs, and the temperature span of the transition zone, in which the temperature decreases without an according pressure or concentration increase, can be adjusted at will. This permits tailored selection of the composition in which biological matter might be stored without the sacrifice of desired thermodynamic parameters, which enables use of preservation solutions that include minimal or no cryoprotective chemical additives.

3.3.4 Advantages of a multiphase approach

The unique thermodynamic behaviors observed in the multiphase isochoric system provide several potential benefits to cryopreservation protocols. Firstly and most importantly, the multiphase system allows for the complete elimination of solute concentration increases over a wide temperature range. Presented in Figure 3.16A is a comparison

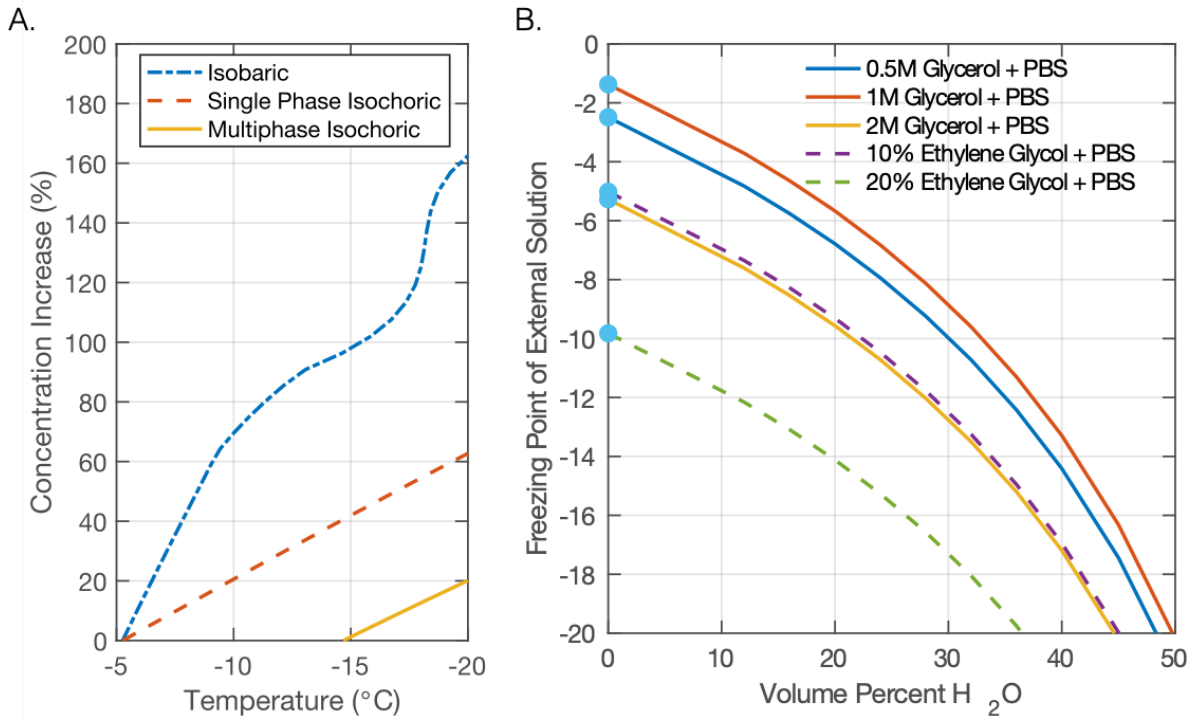

Figure 3.16. Comparison of thermodynamic behaviors between single-phase isochoric and isobaric systems and a multiphase isochoric system. A. Comparison of the concentration increase experienced in a solution of 2M glycerol and 0.9% saline in an isobaric, single-phase isochoric, and multiphase isochoric system. B. Calculated freezing point curves for various solutions of interest to cryopreservation in a multiphase isochoric system, as a function of internal water phase volume. The freezing points of the solutions in a single-phase isochoric system can be found intersecting the y-axis (at 0% internal water volume).

of the concentration increases observed in a conventional isobaric system (any system frozen at atmospheric pressure and unconstrained volume), a single-phase isochoric system, and a multiphase isochoric system, all employing a preservation solution comprised of 2M glycerol and PBS (with the multiphase including a 36% v/v internal water phase, as explored experimentally above). The capacity of multiphase isochoric systems to temper increases in solute concentration proves vastly superior to both isobaric and single-phase isochoric systems, and the period over which no increase is observed is both lengthy and adjustable. Solute cytotoxicity, alongside mechanical damage from ice crystallization, represents one of the most significant modes of damage imparted on biological materials during cryopreservation[11,12,145,146,147,148]—and while standard cryopreservation techniques frequently employ high concentrations of chemical cryoprotective agents[14] to combat ice formation, these agents themselves prove toxic to cells[15], creating a circular cytotoxicity issue. Very few current methods allow minimal or no use of chemical CPAs while enabling subfreezing-temperature preservation without ice damage (a notable exception includes emergent techniques based on systems held in a metastable, supercooled state, though such non-stable equilibrium systems can be difficult to transport and very sensitive to disturbance). Upon review of present literature, it appears that the complete elimination of ice-based solute effects in a cryopreservation system held at stable equilibrium at deep subzero temperatures without the requirement of cryoprotective agents is heretofore

unprecedented, and this achievement may have strong implications for the long-term storage of cellular solutions and organ and tissue systems.

The introduction of multiple phases to isochoric preservation also opens a new thermodynamic frontier for protocol design and versatility. In a single-phase system, be it isobaric or isochoric, a given preservation solution is constrained to one freezing point, and in the isochoric context, one pressure-temperature trajectory. However, with multiple phases that interact thermodynamically but not chemically, a given preservation solution (the external phase) can be made to take on an infinitum of freezing points and pressure-temperature profiles, based on the chemically-independent internal phase. In order to demonstrate this point, Figure 3.16B presents the calculated effective freezing points of various external phase solutions in a multiphase isochoric system, as a function of the volume of an internal phase consisting of pure water. The points intercepting the y-axis represent a single-phase isochoric system, the behavior of which, like a typical isobaric system, is fully constrained. While it is evident in Fig. 3.16B that the combination of any given external phase with an internal water phase allows for a wide range of thermodynamic scenarios based on the volume ratio of the phases, it is also important to note that the choice of water as the internal phase was made for conceptual simplicity—in practice, the internal phase can include any arbitrary substance, and thus composition of the internal phase introduces yet another degree of freedom in the design of a tailored preservation protocol.

This protocol modularity comes at no additional cost or complexity to the system, and allows for the careful optimization of a preservation protocol based on the biological entity to be preserved. At this juncture in cryopreservation progress, this flexibility may prove essential— with the acknowledged insufficiency of current preservation techniques, efforts to explore the mechanisms of damage which drive failure during cryopreservation of complex biological systems are being redoubled. While many methods walk the tight-rope between necessarily low-temperatures and necessarily high concentrations, multiphase isochoric experimentation allows the dynamic incorporation of a third thermodynamic variable, pressure, adding a flexible new dimension to existing approaches. While this study provides a conceptual introduction and proof-of-concept for multiphase isochoric preservation, future work can easily extend the method to develop new cryopreservation protocols with as-of-yet unseen flexibility in their thermodynamic parameters, balancing the positive and negative effects of temperature, concentration, and pressure simultaneously in an inexpensive and mechanically simple system.

Furthermore, while this method can be applied immediately as-is in the creation of new tailored cryopreservation protocols, the thermodynamic behaviors detailed herein are all equilibrium behaviors—and given the unique trajectory of the equilibrium states of the multiphase isochoric system, non-equilibrium thermodynamics in these systems may also provide new and useful behaviors. In particular, future work should investigate possible augmentation of supercooling in the external phase due to pre-pressurization provided from the freezing of the internal phase (effectively an extension in temperature of the transition zone), and possible augmentation of vitrification of the external phase as a result of the same pre-pressurization.

As a final piece of context, it should be noted that the multiphase isochoric system presented in this work is incredibly physically simple. It consists of a rigid container, capable of withstanding an internal design pressure without deforming, filled completely with liquid and monitored via a

single pressure transducer. The stark simplicity and low cost of these devices highlights the fact that the isochoric method is purely thermodynamic in nature, and can be generalized to any enclosed aqueous system. This versatility may prove essential in the long-term goal of developing an overarching cryopreservation technique that proves applicable to all biological systems, as opposed to developing independent techniques and devices for each biological model.Furthermore, organ and tissue replacement procedures such as transplantation are currently overwhelmingly cost-prohibitive, and thus available to only a very small economic strata of the population. In looking towards the ultimate clinical goal of organ transplantation (saving and improving lives), practical aspects affecting the ultimate consumer cost (and thus availability) of organ replacement must be considered—and in this regard, the simplicity of the multiphase isochoric approach could translate to a much clearer road toward clinical adoption and widespread use.

3.3.5. Multiphase Isochoric Freezing: Materials and Methods

1. Isochoric chamber materials

The isochoric chamber employed in this study is a modified OC-1 cylindrical 316 stainless steel pressure vessel (volume 125 ml, working pressure 20,000 psi) with a threaded cap closure and one standard 1⁄4”O.D. threaded connection, custom designed by High Pressure Equipment Company (Erie, PA). A schematic is provided in Figure 3.13A. A durometer 70A EPDM O-Ring was employed for effective sealing (McMaster-Carr Supply Co., Santa Fe Springs, CA). As a safety precaution, a 29,000 psi rupture disk was also employed. The chamber was cooled by a programmable circulating bath (PolyScience, AD15R-40-A11B) with a rated resolution of 0.1C, employing a 50% ethylene glycol, 50% water composition as the bath fluid. The internal pressure of the chamber was monitored using an Ashcroft 2174 digital pressure gauge (4e20 mA loop-powered, 20,000 psi) at a sampling rate of 100Hz, and recorded via a NI myDAQ data acquisition device (National Instruments, Austin TX) in conjunction with LabVIEW 2016 software.

2. Loading protocol

In this study, a 2M glycerol in 1X PBS solution was chosen as the external phase and pure water was chosen as the internal phase. The glycerol-PBS solution was chosen for its relevance to tissue and organ preservation, and water was chosen for conceptual simplicity and to provide a sufficient contrast in freezing points between the two phases. Both fluids were prepared and pre-chilled to 0°C in an ice bath, in order to minimize thermal contraction during consequent low-temperature testing. A 260Q latex balloon (Kadbaner, US) was evacuated of air and filled with one of three volumes (15ml, 30ml, 45ml) of pure deionized water via syringe and secured with a knot. For clarity, this balloon functions as the mass-impermeable membrane Γ depicted in Figure 3.14A, chemically separating the internal and external phases whilst allowing transmission of temperature and pressure. The balloon was weighed to verify the volume of water and visually inspected to ensure that no air bubbles were present. Excess latex was removed with a pair of scissors and the balloon was placed in the ice bath. Working quickly to prevent the chilled liquids from warming during loading, the isochoric chamber was filled to the rim with the glycerol-PBS solution before and the balloon was placed in the center of the chamber. Care was taken to prevent the introduction of stable bubbles into the glycerol solution during the above steps, as the presence of even small amounts of air can significantly alter observed pressure data.

3. Testing protocol

After loading, the chamber was sealed and plunged to -18°C, inducing two nucleation events: one within the balloon and one in the surrounding glycerol solution. The pressure was allowed to stabilize, and a stepwise warming routine was then initiated in 2°C increments, allowing two hours of equilibration for each step in the range (-18°C to -1°C). The discrete temperatures selected in that range were chosen in accordance with the freezing point depression anticipated in the external solution as a result of varying balloon (i.e. pure water) volume. Each series was repeated (n = 3) for each of the three water volumes (15 ml, 30 ml, 45 ml). As an initial control, a single-phase isochoric system was also prepared using the glycerol-PBS solution and checked against theoretical predictions.

4. Statistical analysis

All marked experimental values in Figure 3.15 represent the mean value across (n = 3) tests, and error bars represent the standard deviation.

5. Theoretical predictions

The theoretical curves presented alongside the experimental data in Figure 3.15 were generated using the approach developed in the "Concepts and Modeling" section and covered in detail in Appendix A1.

3.4 Looking Forward: Mastering non-equilibrium processes is isochoric systems

Each of the investigations detailed in this chapter highlights features of the rich and unexplored thermodynamic terrain accessible to isochoric systems—but as the first studies of their kind, they barely scratch the surface of what may be possible. Cryobiologists have studied the vitrification and supercooling of water for decades, but exclusively under constant-pressure conditions. We hope that this suite of proof-of-concept studies will thus lay the foundation for a new generation of non-equilibrium cryobiological research that questions not only how these oft-studied processes might vary under constant volume, but how alternative thermodynamic boundary conditions as a whole might affect the grander cryopreservation process.

In order to reduce these principles to useful clinical practice, future researchers must rise to several distinct challenges. Firstly, theoretical tools must be developed to describe the passage of a confined solution through the metastable supercooled phase and into the glass phase. Given the ultimately limiting effect that confinement has on ice formation and the competing effects of increasing internal pressure and decreasing temperature on the thermodynamic driving forces for crystallization, modeling of isochoric vitrification presents an exceptionally involved hybrid modeling problem requiring the coupling of thermal transport theory with nucleation and kinetic theory. Furthermore, the "all-or-nothing" approach that has largely defined cryobiological vitrification efforts in the past (i.e. the requirement of protocols that result in complete vitrfication

of the system) may prove unnecessary in an isochoric context; because the phase fraction of ice 1h is ultimately limited in an isochoric system, it may be possible to develop partial-vitrification protocols which allow controlled crystallization in certain regions of the system to ensure that the region of the system in which the biologic is stored vitrifies. Such protocols would be nigh-impossible to design or realize at the macroscale under isobaric conditions, but may well be achievable under isochoric conditions.

The work presented in this section (and indeed the thesis as a whole) has largely focused on isolating general thermodynamic and kinetic effects that are agnostically applicable to different system chemistries. This approach is valuable in the initial discovery of new phenomena, but of course must be followed by an intimate exploration of how system chemistry might be manipulated to interact with these effects. In particular, the effects of various solutes on the supercooling capacity of isochoric systems must be probed, and compared to isobaric equivalents in order to probe fundamental mechanisms at play. Similarly, exploration of isochoric vitrification with solutions not traditionally considered to be prime glass formers may reveal that the material properties and physical phenomena dominating the tendency for glass formation in isochoric systems may be different than in isobaric systems.

Finally, the multicomponent isochoric system described herein, for which equilibrium behaviors were detailed, may also be tailored for use in stable supercooling or multicomponent vitrification. The ability to dynamically pressurize a selected constituent phase by strategically freezing a different constituent phase raises new questions about the potential role of dynamic pressurization during vitrification, and the role of enhanced pressure in stable supercooling. Furthermore, not only may potential cryopreservation protocols benefit from these explorations, but the isochoric system as an experimental apparatus also provides a platform from which to study the effects of high-magnitude enhanced pressure with incredible ease, which may lead to findings applicable to all manner of solid-liquid phase transitions.

The findings in this chapter present several newly-discovered water-ice phase change phenomena, and point to isochoric confinement as a potentially effective non-chemical method of inhibiting ice formation in various capacities. These findings furthermore illustrate an acute need for advances in thermodynamic modeling of non-equilibrium phase change processes in systems under alternative thermodynamic boundary conditions, and the author hopes that future cryobiologists will be equal to the challenge.

4. Cryopreservation of whole organs and tissues using single-solution equilibrium isochoric freezing

At long last, we arrive dear reader at the chapter most intimately aligned with the ultimate goal of this thesis: to develop new protocols for the cryopreservation of whole mammalian organs and tissues, based upon isochoric freezing. We will relate herein a series of studies employing two biological constructs of great importance to the modern transplantation community: hearts and pancreatic islets. We will describe what we understand to be the first-ever sub-zero centigrade preservation and revival of a whole mammalian heart in the absence of cryoprotectants, explore the time-dependent effects of enhanced pressure on complex biological systems, and report an effective and transportable method for multiday preservation of pancreatic islets. However, before delving into the data to follow, the reader should prepare for a certain degree of discontinuity between the protocols applied herein and the various thermodynamic studies described in the preceding chapters.

The notion of isochoric freezing (and its application to cryopreservation) is very young. Envisioned first theoretically in 2005, no cryopreservation of biological matter was attempted experimentally until 2016, and the studies to follow in this chapter represent the very first experimentation on mammalian tissues and organs. Thus, it may rightfully be argued that biological validation of isochoric freezing has for some time lagged behind the accompanying theoretical thermodynamic vision, and the investigations reported here do not attempt to defy this trend.

We have discussed in the preceding sections various thermodynamic *extensions* of the core isochoric freezing concept – supercooling, vitrification, and multicomponent methods – each motivated by various desired use cases (transportable short-term preservation, ultra-long-term "banked" preservation, etc.) and theorized opportunities for improvement. However, in the according evaluation of the relative *biological* efficacy of these techniques, understanding of the "baseline" performance of isochoric freezing is needed. In other words, before we can truly determine the relative value of a multi-solution isochoric protocol or a metastable supercooling protocol, we must first evaluate the efficacy of the core isochoric freezing concept, i.e. the single-solution, equilibrium method.

This baseline evaluation is what we attempt in this chapter. Near identical protocols and experimental devices are used in the three studies to follow, and the goal at hand is not only to determine the efficacy of single-solution equilibrium isochoric freezing for whole-organ and tissue preservation, but to also decompose the end preservation result and identify specific aspects of the isochoric process that may be helpful (e.g. avoidance of mechanical ice damage and reduced osmotic toxicity) or harmful (e.g. exposure to enhanced pressure).

We therefore aim for this chapter to provide the baseline biological data required to efficiently iterate design of future isochoric freezing protocols, and to clarify potential advantages or pitfalls

of the next-generation techniques explored thermodynamically in the preceding chapters of this thesis.

4.1 Preservation of rat hearts at various subfreezing temperatures under equilibrium isochoric conditions: Initial experimental validation

The need for superior *ex vivo* biopreservation techniques discussed throughout this work is perhaps no more apparent than in the case of thoracic (heart) transplantation. Heart transplantation is a well-established surgical solution for the treatment of end-stage heart failure or severe coronary artery disease, with a ten-year rate of survival in adults of more than 60%, and often represents the only life-saving alternative available to patients with advanced cardiological conditions[149]. However, there is a severe lack of hearts available for transplantation. This shortage is fueled in large part by the inability to preserve organs outside the body for periods of time sufficient for harvesting, transportation, and transplantation, a hurdle which leads to approximately 70% - 80 % of thoracic donor organs going untransplanted each year[16]. Thus, there is an acute need for technology that will extend the extracorporeal preservation period for organs. Hypothermic preservation of hearts at 4 ℃ in solutions that mimic the intracellular composition, such as the University of Wisconsin (UW) solution, has become the clinical gold standard for transplantation purposes[150]. However, the period of time hearts typically survive in these conditions is limited to approximately six hours, which severely limits heart transplantation procedures and frequently proves prohibitive for organ transportation, geographically limiting the usability of donor hearts[151].

This study is the first to investigate subfreezing-temperature isochoric preservation of whole mammalian organs, namely rat hearts. The effects of this method on hearts preserved in UW solution at temperatures down to -8 °C are investigated, and compared to hearts stored in UW solution on ice, as is the current clinical standard. Heart viability and functional parameters following preservation were determined using a Langendorff perfusion system and effects at the cellular level were examined through histology.

4.1.1 Materials, Methods, and Experimental Protocol

Isochoric Preservation System

The isochoric system in which the hearts were preserved consists of a simple, rigid, constant-volume chamber held at constant subzero temperatures. The chamber itself (Figure 1A) is a modified OC-1 cylindrical 316 stainless steel pressure vessel (volume 125 ml, working pressure 13,800 psi) with a threaded cap closure and one standard ¼” O.D. connection, custom designed by High Pressure Equipment Company (Erie, PA). A durometer 70A EPDM O-Ring was employed for effective sealing (McMaster-Carr Supply Co., Santa Fe Springs, CA). As a safety precaution, a 29,000 psi rupture disk was also employed. An Ashcroft 2174 digital pressure gauge (4-20 mA loop-powered, 20,000 psi) was used to monitor the internal pressure of the chamber at a sampling

rate of 2 Hz, and data was recorded via a NI myDAQ data acquisition device (National Instruments, Austin TX) in conjunction with LabVIEW 2016 software. The isochoric chamber was cooled and held at temperature using a Nestlab RTE-140 Refrigerated Bath/Circulator with a rated accuracy of 0.1°C (Thermo Scientific, Waltham, MA), with a 50/50 mixture of water and ethylene glycol as the liquid medium.

Langendorff system

A custom made isolated heart perfusion system was used to evaluate the performance of the preserved heart as a function of preservation temperature. The principle of the Langendorff system is to provide the isolated heart with oxygen and metabolites by means of a cannula inserted into the ascending aorta. In this constant pressure system, an oxygenated perfusate is driven towards the heart from a constant elevation reservoir. Prior to entering the heart, the perfusate is heated to 37 °C using a counter-flow heat exchanger and is oxygenated with a mixture of 95% oxygen and 5% CO_2. The retrograde perfusion closes the aortic valve and forces fluid into the coronary arteries during the diastolic period as occurs in the normal cardiac cycle. Flow then continues through the coronary system and eventually exits via the coronary sinus in the right atrium. Heart viability is compared between conditions by recording the rate of contraction (beats per minute) and flow rate (mL per minute) of isolated hearts.

Experimental protocol

Heart Removal

The animals received humane care with oversight and approval from the Animal Care and Use Committee at the University of California, in compliance with the ‘‘Principles of Laboratory Animal Care’’ and the ‘‘Guide for the Care and Use of Laboratory Animals’’ prepared and formulated by the Institute of Laboratory Animal Resources and published by the National Institute of Health (NIH Publication No 86-23, Revised 1985). Isolated hearts were obtained from Sprague–Dawley male rats (250– 350 g), which were anesthetized by 5% isoflurane with an isoflurane precision vaporizer and given intraperitoneal injection heparin (500 U/kg). A midline abdominal incision was performed and the anterior chest wall was separated from the diaphragm. The anterior rib cage was divided with heavy scissors, exposing the heart. The heart was rapidly excised and placed in ice-cold saline. The heart was then connected by the ascending aorta to a perfusion apparatus and flushed with 7 ml ice-cold University of Wisconsin (UW) solution (Belzer UW Cold Storage Solution, Bridge to Life LLC, Columbia, SC). The harvested heart was submersed in UW solution pre-cooled to 4 °C and transported in an insulated ice bath to the isochoric preservation laboratory (15 minutes).

Isochoric Preservation

For each heart preservation study, the isochoric chamber was pre-cooled to 4 °C in a refrigerator and filled with pre-cooled UW solution upon arrival of the heart. A small, rough-surfaced metallic agent was placed at the bottom of the chamber to dictate the location of initial ice nucleation. The

heart was then placed in a porous thin-walled plastic vessel to ensure flotation at the top of the chamber volume and the chamber was sealed, taking special care to ensure that no air bubbles are trapped within.

The sealed chamber was then fully submersed in a cooling bath held at the target temperature and the internal pressure was recorded. To ensure consistent nucleation and pressure trajectories, the bottom of the chamber was agitated every 60 seconds after submersion until the pressure rise associated with nucleation is observed. After one hour in the cooling bath, the chamber was transferred to a water bath at room temperature and allowed to warm until no ice remained internally, as indicated by complete dissipation of the internal pressure. The heart was then removed from the chamber and perfused immediately using the Langendorff system.

A.

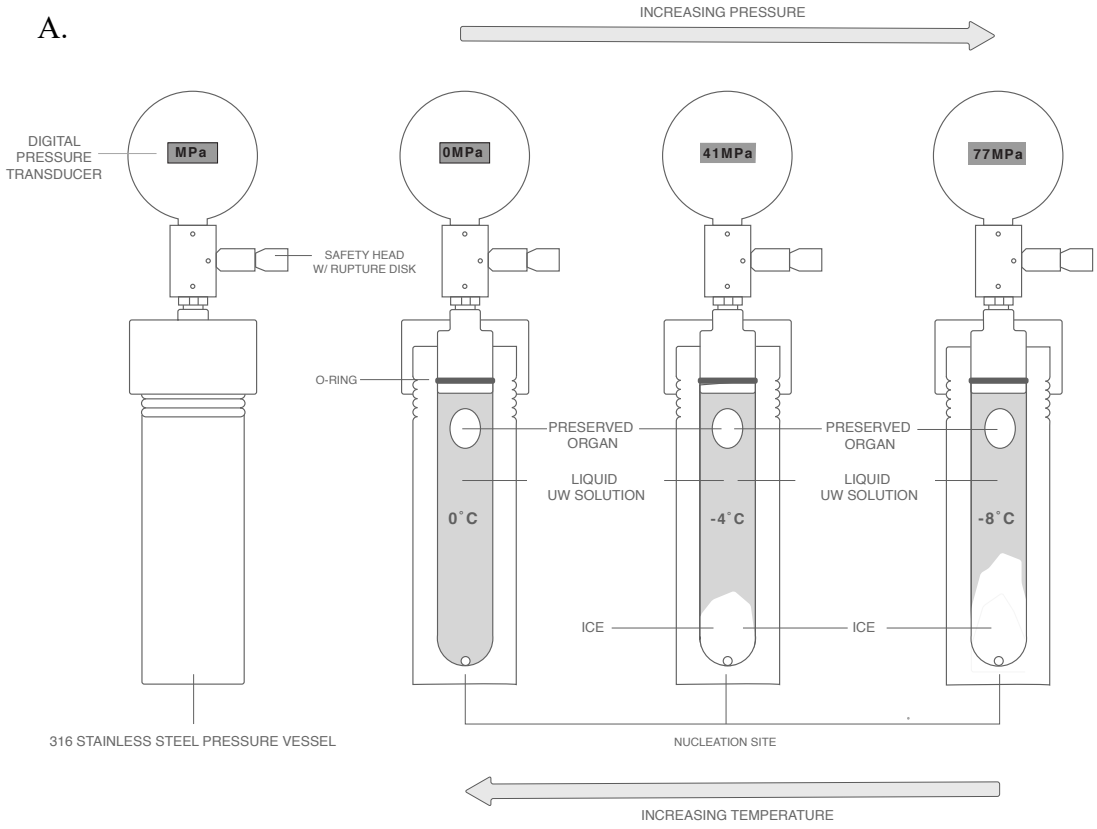

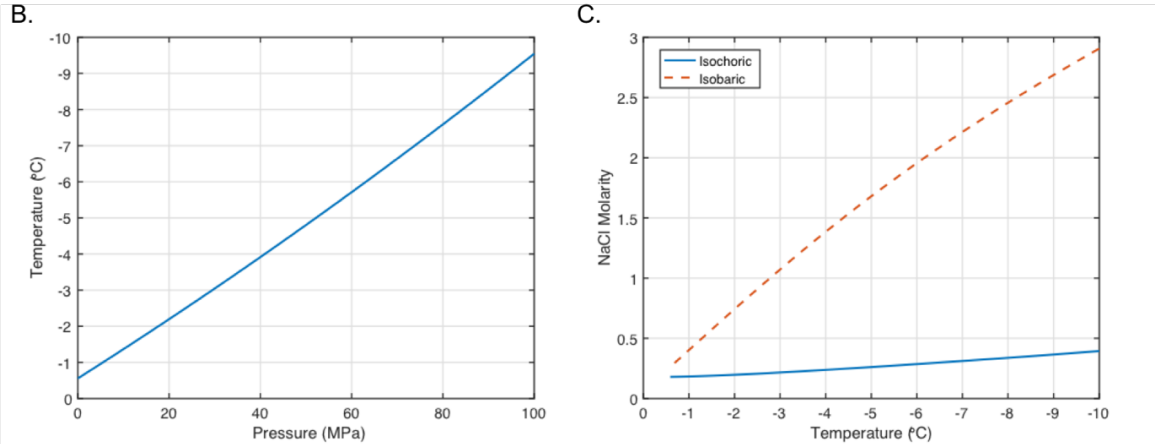

Figure 4.1 Process and principles of isochoric preservation. (A) Schematic of isochoric preservation apparatus in exterior and cross-section views at various subfreezing temperatures. (B) Temperature-pressure relations in an isochoric system at subfreezing temperatures. (C) Comparison of NaCl concentration as a function of temperature during isochoric and atmospheric isobaric freezing of a NaCl solution, which at a pressure of 1 atm had a physiological concentration of 0.9% w/w[143].

Perfusion

Hearts were connected to the Langendorff system after 1h preservation. Perfusion was initiated using filtered and oxygenated (95% O_2 + 5% CO_2) Krebs–Henseleit solution (Sigma-Aldrich, St. Louis, MO) at 37 °C. This fluid was delivered by a peristaltic pump to an elevated reservoir, and then allowed to perfuse the heart in a retrograde direction through the ascending aorta at a constant hydrostatic pressure (80-90 mmHg) determined by the elevation of the reservoir. The coronary flow was determined by timed collection of effluent from the heart and the heart rate was counted.

Histological Evaluation

Following perfusion, hearts were removed from the Langendorff system and immediately fixed in formalin, and then embedded in paraffin. Transverse sections were cut at the mid-ventricle level and stained with hematoxylin and eosin. Slides were coded and then evaluated for injury in a blinded fashion. Four areas from the left ventricular free wall were randomly selected from each slide and scored by an experienced pathologist based on an injury scale from 0 to 4, with 0 representing normal myocardium and 4 representing complete disruption of morphology. The injury score considered integrity of myocyte structure, including regular arrangement of sarcomeres, interstitial edema, presence of contraction bands, and myocyte swelling. Slides from hearts stored on ice and at -4 °C were further analyzed for percent area of interest occupied by edema using Image J software.

Statistical analysis

Four hearts were tested for each experimental condition. One additional fresh heart (fixed immediately without preservation) was used to provide a normal, reference appearance for histological comparison. Pressures recorded in the isochoric system are grouped by target temperature and reported as the means ± standard deviation. Heart rate and coronary flow rate data are also grouped and reported as means ± standard deviation, and a parametric one-way ANOVA

was used to confirm significance of difference between groups. Injury scores were analyzed using the Kruskal-Wallace non-parametric ANOVA with Dunn's test for multiple comparisons. Interstitial edema data were analyzed using an unpaired Student's t-test, with $p < 0.05$ considered to be significant. Contingency tables were analyzed using the Fishers exact test.

4.1.2 Heart Preservation Results

Table 4.1 Perfusion performance of hearts grouped by preservation conditions

Preservation Conditions		**Perfusion Performance**	
Temperature (°C)	Pressure (MPa)	Heart Rate (beats/min)	Flow Rate (mL/min)
0 (on ice)	0.1 Mpa (atmospheric)	93.75 ± 10.5	26.25 ± 4.50
-4	40.62 ± 0.71	91.50 ± 12.6	20.25 ± 1.94
-6	59.84 ± 0.72	76.50 ± 23.6	13.50 ± 3.0
-8	77.71 ± 0.85	0	0

The perfused heart beat rate and the coronary flow rate results for all samples are presented in Table 4.1 . Additionally, hearts preserved on ice and at -4 °C appeared soft upon gross examination after preservation, and beat steadily in both the atria and ventricles upon perfusion with the Langendorff device. Heart beat rates were comparable between these two groups ($p > 0.05$), while flow rates were slightly reduced after preservation at -4 °C. In contrast, hearts preserved at -6 °C and -8 °C appeared firm upon gross examination. Upon perfusion, hearts preserved at -6 °C beat exclusively in the atria and experienced reduced beat and flow rates, while hearts preserved at -8 °C failed to beat at all.

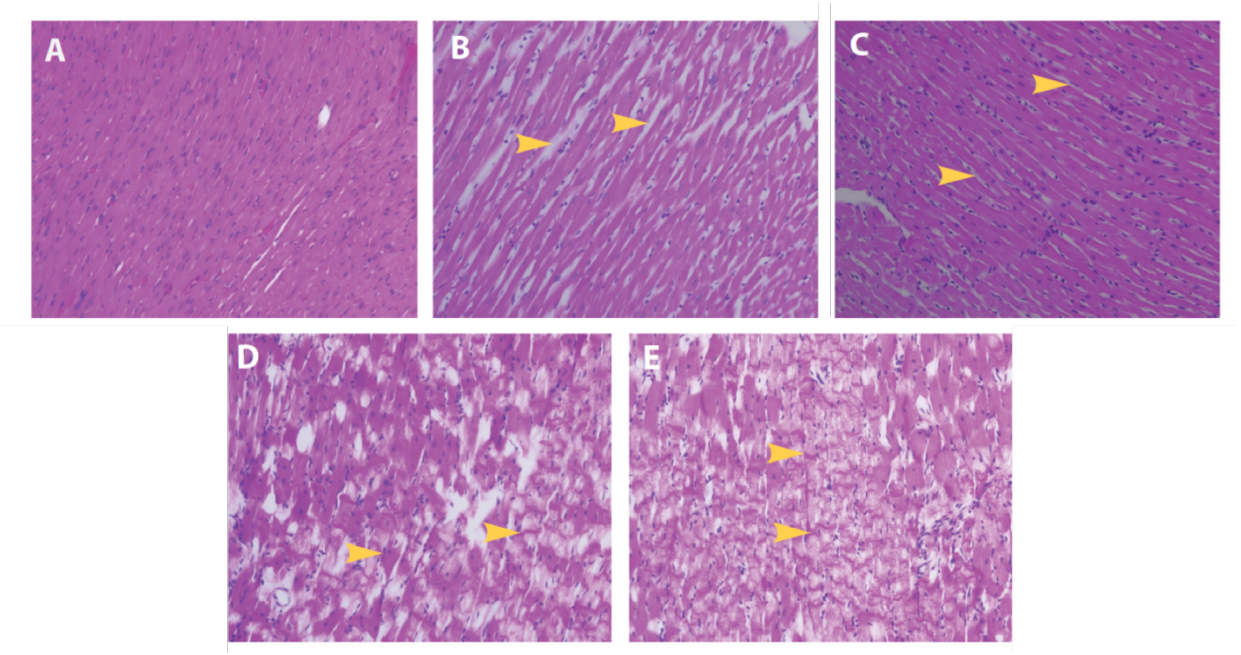

Figure 4.2. Hematoxylin & eosin stains of tissue taken from the left ventricle of hearts preserved under a variety of conditions. Images captured at a 20x objective. (A) Fresh, healthy heart. (B) Heart preserved on ice at atmospheric pressure for one hour. Arrows identify points of interstitial edema. (C) Heart preserved at -4 °C (40.62 MPa) under isochoric conditions for one hour. Arrows identify points of interstitial edema. (D) Heart preserved at -6 °C (59.84 MPa) under isochoric conditions for one hour. Arrows identify example contraction bands. (E) Heart preserved at -8 °C (77.71 MPa) under isochoric conditions for one hour. Arrows identify example contraction bands.

Histology of a fresh control heart showed normal morphology, with regularly aligned myocytes with well-organized sarcomeres and scant interstitial spaces between myocytes (Figure 4.2A). Hearts preserved on ice for one hour in UW solution showed essentially normal myocyte structure, but displayed extensive interstitial edema (Figure 4.2B). Hearts preserved at -4 ºC (40.62 MPa) under isochoric conditions showed myocyte structure similar to that of hearts preserved on ice (Figure 4.2C); while there was a trend indicating a slightly less severe injury score, it was not statistically significant (Figure 4.3A). However, upon gross examination of the histological slides, the extent of interstitial edema evident in the -4 ºC isochoric group appeared to be lesser compared to storage on ice. Sections from each heart were thus subjected to quantitative analysis of the percent area occupied by interstitial space using Image J software (Figure 4.3B). One hour of preservation at -4 ºC under isochoric conditions resulted in a highly significant decrease in edema ($p = 0.0009$) compared to conventional preservation on ice, suggesting protection from increased vascular permeability following preservation and reperfusion.

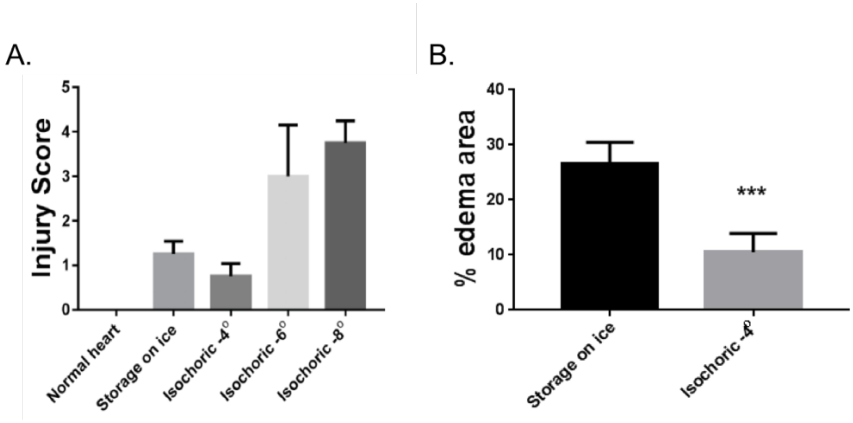

Figure 4.3. Histological evaluation. (A) Overall injury scores considering integrity of myocyte structure, including regular arrangement of sarcomeres, interstitial edema, presence of contraction bands, and myocyte swelling. (B) Percent area occupied by interstitial edema in hearts preserved on ice in atmospheric conditions and at -4C (40.62 MPa) under isochoric conditions.

In contrast, hearts preserved under isochoric conditions at -6 °C (Figure 4.2D) and -8 °C (Figure 4.2E) showed extensive disruption of myocytes, with disorganized sarcomeres and extensive contraction bands indicative of pathological contracture. This is consistent with the hardness of the hearts observed by gross inspection. The injury scores of both of these groups were significantly worse than those for the hearts stored on ice or under isochoric conditions at -4 °C.

4.1.3. Discussion of Functional and Histological Observations

Low temperatures are employed in the preservation of transplantable organs because they reduce the rate of metabolism. Under constant atmospheric pressure, freezing begins when the temperature is reduced below the freezing point of the intra- and extracellular fluids of the tissue, and continues until the vast majority of the liquid has frozen. Freezing introduces mechanisms of damage that include solute concentration effects and intracellular ice formation[11,12]. Larger organs are particularly affected by the former, which occur during freezing with low cooling rates and are induced by the increase in extracellular concentration caused by the removal of water from the liquid solution in the form of ice. A commonly used method to avoid damage during freezing is the addition of select chemicals, known as cryoprotective agents, that modify the composition in order to colligatively depress the freezing temperature[10,152]. A major deficiency of cryoprotectants is the difficulty of introducing and removing them from preserved tissue, in addition to their potential toxicity. While numerous cell types can be preserved with cryoprotective agents, these drawbacks have thus far precluded their successful use for whole organ preservation.

Theoretical and experimental studies have shown that the concentration of solutes resulting from freezing in isochoric systems is an order of magnitude lower than the concentration of solutes resulting from freezing in an atmospheric isobaric system (Figure 4.1C). Considered alongside the capacity of an isochoric system to store biological matter at subfreezing temperatures in an ice-free liquid phase, this observation highlights the potential benefits of isochoric systems as significantly superior to conventional preservation approaches for storage of transplantable organs. However, the increased hydrostatic pressure introduced in subfreezing temperature isochoric systems may have detrimental effects on preserved biological matter [153]. Isobaric systems at

elevated pressures and subzero ℃ temperatures have been investigated previously for preservation and transplantation of livers in the absence of ice[34,154,155]. It was observed that all rats receiving transplanted livers preserved for one hour at 0 ℃ and pressures lower than 40 MPa (n=6) or livers preserved at – 2 ℃ and pressures of 5 MPa survived for at least two weeks. Informed by these findings and the phenomena presented in Figure 4.1C, the study presented herein investigated one-hour isochoric heart preservation at - 4 °C (40.62 MPa), - 6 °C (59.84 MPa) and – 8 °C (77.1 MPa), and compared the results to conventional heart preservation on ice in order to establish a baseline for future research on isochoric heart preservation.

As detailed in the results section, hearts preserved at -4 °C (40.62 MPa) under isochoric conditions proved the highest quality, with myocyte structure and physiological performance comparable to that of hearts preserved on ice but significantly reduced interstitial edema, which indicates reduction of vascular injury. The improved tissue morphology observed at -4 °C is a promising indicator of the potential of isochoric systems to improve overall preservation quality. Furthermore, the high quality of hearts preserved at -4 °C (40.62 MPa) and the decreasing quality of hearts preserved at - 6 °C (59.84 MPa) and – 8 °C (77.1 MPa) appears consistent with the discussed observations of the pressure tolerance of other organs[34,154,155]. Given that the anticipated principal sources of damage in an isochoric system are heightened extracellular solute concentrations and increased hydrostatic pressure, the relatively modest increase in concentration predicted in Figure 4.1C suggests that the pressure increase, which is substantial, is likely the cause of the severely disrupted morphology and impaired physiological function observed in the hearts preserved at - 6 °C (59.84 MPa) and – 8 °C (77.1 MPa).

This is a preliminary study of subfreezing temperature isochoric preservation of organs, intended to demonstrate the viability of the method and establish a baseline for future work. According to the observations presented herein, isochoric preservation at -4 °C yields a better-preserved organ than conventional preservation on ice over a one hour period. This advantage of organ preservation at – 4 ℃ over conventional on-ice preservation is consistent with previous findings[81], in which a liver was preserved at – 4 ℃ using an active perfusion method for the liver and supercooling. It should also be noted that one hour of preservation by conventional means typically results in adequate functional recovery of human hearts. As such, it is not surprising that myocyte integrity after -4 °C preservation was not significantly improved, as it was not significantly compromised in the hearts stored on ice. It is likely that the benefits of the greater metabolic depression achieved at lower temperatures would manifest more strongly given longer storage times. It also appears that further elevation of pressure is detrimental to the viability of the organ. This suggests that in designing isochoric preservation protocols, the beneficial effects of reduced metabolism and minimal extracellular solute concentration must be balanced with the detrimental effect of elevated pressure. Furthermore, any reduction of temperature should increase organ preservation quality if the detrimental effects of pressure can be mitigated. For instance, it has been observed that the liver shows sensitivity to the rate of increase and reduction in pressure [22, 23]; these parameters should be evaluated and optimized for the heart in future studies. It has also been shown that introducing relatively low concentrations of cryoprotectants, such as Me_2SO, ethylene glycol, or glycerol, works synergistically with isochoric freezing to reduce the pressure at any subzero temperature. A possible approach to minimizing pressure-related damage in subfreezing temperature isochoric preservation may be to add low concentrations of cryoprotectants to the preservation solution. Chemical additives that improve resistance to elevated pressure may be also

of interest, and in fact, many known cryoprotectants also act in this mode. This study is a first report to demonstrate the viability of subfreezing temperature isochoric preservation of organs, and much research remains to be done.

4.2 Time-dependent effects of pressure on isochoric preservation of rat hearts

In our initial feasibility study on isochoric cryopreservation of the heart, described in the previous section, rat hearts were preserved in a University of Wisconsin (UW) intracellular solution for one hour under isochoric conditions at: 0 ºC (atmospheric pressure, 0.1 MPa), - 4 ºC (41MPa), - 6 ºC (60 MPa) and -8 ºC (78 MPa) [5]. The viability of the heart was evaluated using Langendorff perfusion and histological examination. While the functional performance of hearts preserved at - 4 ºC (41MPa) was comparable to that of a heart preserved on ice at atmospheric pressure, the hearts preserved at −4 °C displayed substantially reduced interstitial edema, suggesting significant protection from increased vascular permeability following preservation. Hearts preserved at – 6 °C (60 MPa) suffered injury from cellular swelling and extensive edema, and at – 8 °C (78 MPa) hearts experienced significant morphological disruption. This study was designed as a continuation of the initial investigation with the goal of generating additional insight into the time-dependent effects of pressure during preservation of hearts under isochoric freezing conditions, and to explore means to improve preservation quality.

4.2.1 Experimental Protocol

This study employed devices, techniques and approved animal research protocols identical to those described in the previous section.

Experimental Design
Groups of (rat) hearts (n = 4) were preserved in the isochoric chamber pictured in Figure 4.1 at a given temperature-pressure for varying durations until the pressure-time threshold (PTT) was reached. The PTT is defined by the pressure-time condition under which a majority of hearts performed marginally during functional evaluation (Langendorff perfusion), as characterized by ventricular fibrillation or beating confined only to the atria. The hearts performance evaluation in the Langendorff system was divided into three categories: functional, marginally functional and non-functional. The experimental data was analyzed in three groups: a) the histology of the marginally functional hearts; H&E staining was used in order to evaluate whether common indicators of cell death or morphological disruption could be observed between marginally functional hearts stored at different temperatures and pressures. b) the histology of hearts stored at -2 ºC (20 MPa) as a function of time of storage; H&E staining was used in order to determine whether temporal evolution of morphological disruption could be observed and c) a first study on the possible use of isochoric freezing protective chemicals: hearts were preserved at -4 ºC in solution including 1M glycerol, which functions to reduce the pressure experienced at a given temperature. Hearts were preserved for 1 and 2 hour periods and compared both functionally and histologically to hearts preserved for the same time and temperature without the addition of glycerol.

Statistical analysis

Four hearts were tested for each experimental condition. Pressures recorded in the isochoric system are grouped by target temperature and reported as the means ± standard deviation. Heart rate and coronary flow rate data are also grouped and reported as means ± standard deviation, and a parametric one-way ANOVA was used to confirm significance of difference between groups, with $p < 0.05$ considered to be significant.

4.2.2 Functional and Histological Results

Pressure-temperature-time threshold results are presented in Figure 4.4, indicating the functional evaluation observed at each pressure-temperature condition for each duration. Functional evaluations are divided into three categories based on behavior during perfusion: Optimal, as characterized by regularly beating hearts, sup-optimal, as characterized by ventricular fibrillation or beating confined strictly to the atria, and compromised, as indicated by hearts which do not resume any sort of beating upon perfusion. A clear decreasing trend is visible, suggesting that the exposure period the heart can sustain decreases in a rapid non-linear fashion with increasing pressure. The heart beat rates and flow rates for each preservation condition are tabulated in Table 4.2.

In Figure 4.5, sample histological sections from hearts held at -2 ºC (21MPa), -4 ºC (41 MPa), and -6ºC (59 MPa) until reaching the pressure-temperature-time threshold are compared. Regardless of peak pressure, the modes of damage observed (which include contraction band necrosis, mild disruption of sarcomeres, and mild vacuolization) are consistent in nature and apparent prevalence across the samples. This suggests that within the pressure range examined herein, pressure damage to the heart is a function of both pressure magnitude and exposure duration, and does not appear to vary in nature after any discrete peak pressure/time of preservation threshold.

Similarly, Figure 4.6 displays the temporal evolution of hearts held under consistent temperature-pressure conditions (-2 ºC [21MPa]) for increasing durations until the PTT threshold is reached. No statistically significant variance is observed in functional evaluations (heart beat rate and flow rate) until the onset of ventricular fibrillation at the PTT threshold, and nor do histological indicators of pressure damage emerge until that time. This suggests that morphological damage of significant enough magnitude to disrupt function must emerge over a relatively short time period, in this case between 4 hours preservation (at which point no significant damage is observed histologically and hearts beat healthily when (perfused) and 6 hours preservation (at which point contraction bands and disruption of sarcomeres can be observed and ventricular fibrillation occurs upon perfusion). Speaking practically, this suggests that while there may not be a narrow peak pressure threshold for morphological damage, there may exist a relatively discrete *time* threshold for a given pressure-temperature *before which* an organ can be preserved without accruing appreciable damage. Further clarification of this notion and understanding of the time threshold and activation of cell death mechanisms will be essential to designing preservation protocols, isochoric or otherwise, that utilize augmented hydrostatic pressure in hypothermic preservation.

Table 4.2 Perfusion performance of hearts grouped by preservation conditions

Preservation Conditions		**Perfusion Performance**	
Temperature (°C)	Pressure (MPa)	Heart Rate (beats/min)	Flow Rate (mL/min)
-2 (1 hour)	21.11 ± 0.63	86.25 ± 8.62	21.38 ± 8.34
-2 (2 hour)	"	94.50 ± 3.87	16.75 ± 6.80
-2 (4 hour)	"	102.0 ± 18.97	9.38 ± 0.75
-2 (6 hour)	"	VF	
-2 (8 hour)	"	0	
-4 (1 hour)	40.62 ± 0.71	91.50 ± 12.6	20.25 ± 1.94
-4 (2 hour)	"	VF	
-4 (4 hour)	"	0	
-4 (2 hour + 1M Glycerol)	29.93 ± 0.96	96.00 ± 12.0	12.50 ± 3.13
-6 (1 hour)	59.22 ± 0.72	VF	
-6 (2 hour)	"	0	
-8 (1 hour)	77.34 ± 0.85	0	

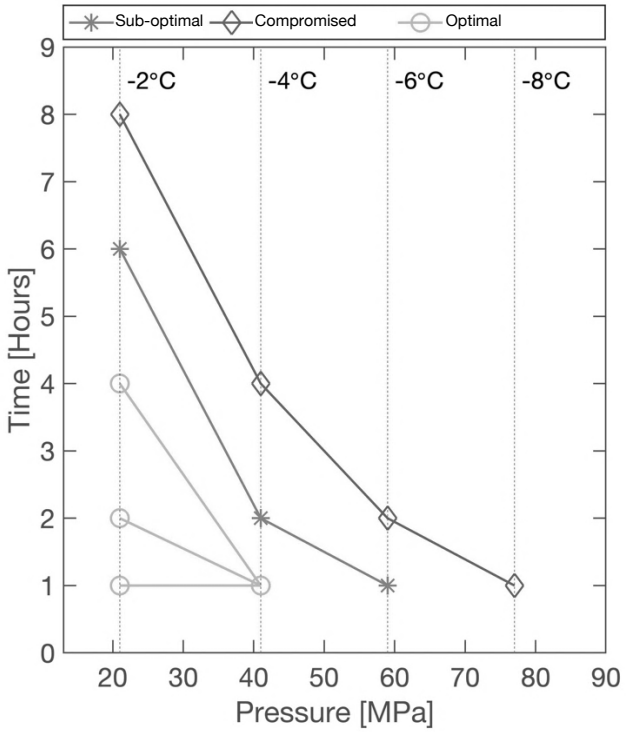

Figure 4.4. Pressure-time dependence of hearts based on functional evaluations. Healthy, rhythmically beating hearts are classified as optimal, hearts experiencing ventricular fibrillation or otherwise irregular beating are classified as sup-optimal, and hearts that failed to revive at all upon perfusion are classified as compromised.

Based on the prevailing assumption that reduced temperature enhances preservation quality due to the slowing of metabolism [156], it has been assumed thus far in this work that damage observed in preserved hearts is caused exclusively by increased pressure. In order to solidify that notion, a final set of experiments were performed with the addition of 1M glycerol to the UW preservation solution. Glycerol is a natural cryoprotectant, functioning in this context to reduce the pressure observed in an isochoric system at a given subfreezing temperature [35]. Figure 4.7 compares sample histological sections from hearts preserved at -4 ºC for 2 hours with glycerol (yielding 29.93 MPa) and without glycerol (yielding 41 MPa). It can be seen that the reduction in pressure afforded by the addition of glycerol has a significant positive effect on the preserved tissue, preventing formation of contraction bands, disruption of sarcomeres, and vacuolization over the given time period. Similarly, in functional evaluation hearts preserved without glycerol experience ventricular fibrillation upon perfusion, while hearts preserved with glycerol beat healthily. Our hypothesis thus is that glycerol (and cryoprotectants generally) offer a protective effect by reducing the pressure at each preservation temperature. This finding represents first-order evidence that if the pressure in an isochoric system can be reduced (via cryoprotectants or other means), preserved organs can be held longer at colder temperatures. However, glycerol may have other cryoprotective effects in an isochoric freezing system, and this hypothesis must
be verified with other cryoprotectants or chemical additives.

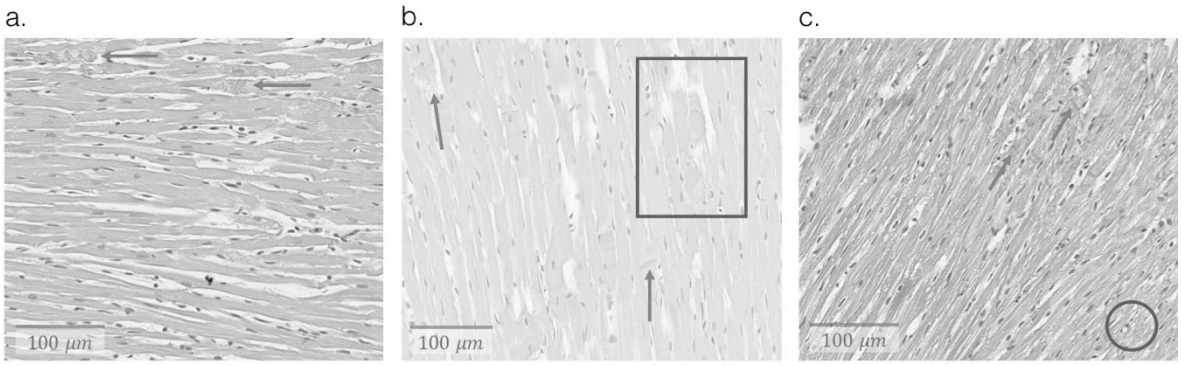

Figure 4.5. Histological sections at 20x magnification from the left ventricular wall stained with Hematoxylin & Eosin. Hearts were classified as sub-optimal after exhibiting ventricular fibrillation upon perfusion after preservation under the following conditions: **a.** -2 ºC, 21 MPa, 6 hours. **b.** -4 ºC, 41MPa, 2 hours. **c.** -6 ºC, 59MPa, 1hour. Examples of contraction bands are marked by arrows, an example of disrupted sarcomeres is marked by the rectangular box, and an example of vacuolization is marked by the circle.

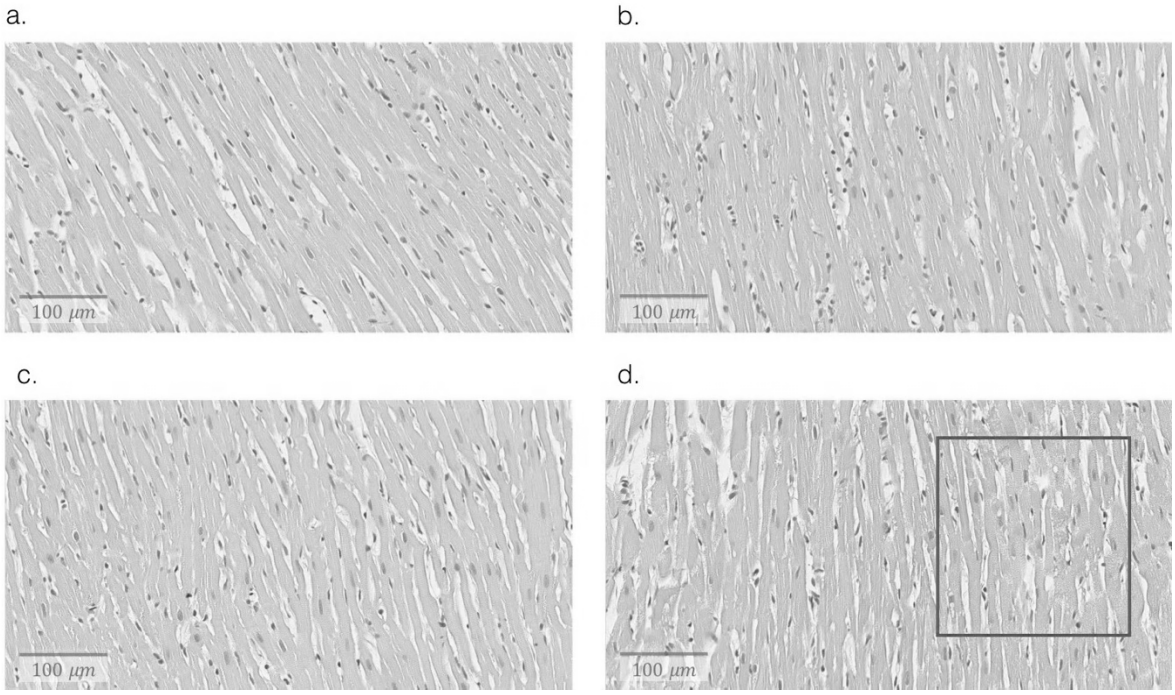

Figure 4.6. Histological sections at 20x magnification from the left ventricular wall stained with Hematoxylin & Eosin, taken from hearts preserved at -2 ºC and 21MPa for the following periods: a. 1 hour. **b.** 2 hours. **c.** 4 hours. **d.** 6 hours. Samples **a – c** exhibit healthy myocytes and beat regularly upon perfusion. Sample **d** exhibited ventricular fibrillation upon perfusion, and the emergence of contraction bands and sarcomere disruption can be observed within the rectangular box.

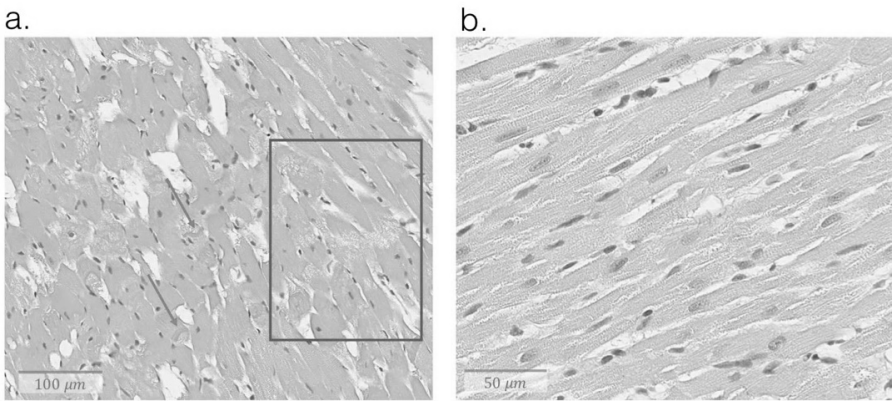

Figure 4.7. Histological sections from the left ventricular wall stained with Hematoxylin & Eosin, taken from hearts preserved at -4 ºC for 2 hours in **a,** pure UW solution (41 MPa) and **b**, UW solution with 1M added glycerol (29.93 MPa). Clear differences in myocyte health can be seen between the two cases, with the rectangular box marking disrupted sarcomeres and arrows identifying contraction bands.

Our studies represent early-stage research on isochoric preservation. Surveying the literature to date, data available on the effects of non-physiological high hydrostatic pressure in biological systems pertains almost exclusively to isolated cells. The responses of whole-organ or bulk tissue systems to elevated pressures, subfreezing temperatures, and exposure periods such as those examined in this work are largely unexplored. The work of Ueno et al [157] presents one of the few whole-organ studies to date, which investigated pressurized preservation of rat livers at elevated pressures with and without reduced temperatures, finding a survival threshold of 30 MPa for a 1 hour preservation period, and a survival threshold of -2 ºC and 5 MPa, which agrees loosely with the time-pressure findings reported in this study. It is important to note however that several non-physiological hydrostatic pressure studies involving isolated mammalian cells rather than whole-organ systems report pressure tolerances of 100 MPa and above, before which cell viability is not compromised (though few of such studies examine longer length scales, see review in [1]). This fact suggests that the modes of damage at play in pressurized whole-organ systems may well occur at a higher functional level, affecting the viability of organ-specific multi-cellular structures. If this is indeed the case, the pressure limitations clarified in this work may well be surmountable barriers to successful high-pressure preservation, with potential solutions available by manipulating cellular mechano-transduction and signaling pathways or other systemic means.

The results presented in this work suggest a strong time dependence of pressure damage in isochoric high-pressure organ preservation, and the need for further clarification of the modes of hydrostatic pressure damage in bulk biological systems. Furthermore, this work suggests that the use of cryoprotectants as pressure-reducing agents in isochoric preservation systems may present a possible pathway to successful preservation protocols, and merits additional study.

4.3 Isochoric preservation of rat pancreatic islets

Preservation of pancreatic islets for transplantation is of substantial clinical interest for the treatment of type 1 diabetes, and presents unique challenges due to the compact organization and extreme fragility of islet clusters. Current islet preservation methods can be subdivided into three domains: culture (at temperatures ranging from 22°C to 37°C), hypothermic non-freezing preservation (4°C to 1°C), and extreme cryogenic preservation (-80°C to -196°C), each with notable advantages and drawbacks[159]. Ice formation is of critical concern in the low-temperature preservation of islets, which are exceptionally fragile, and thus current low-temperature techniques must resort either to preservation at temperatures above the freezing point of water or the use of chemical cryoprotectants such as DMSO or ethylene glycol, which are themselves toxic to islets and have been demonstrated to adversely affect both islet viability and transplant success[160]. There is thus an obvious need for a method of islet preservation that avoids the deleterious effects of CPAs while capturing the benefits of low temperature storage. Therefore, this preliminary study explores the potential of high subzero isochoric freezing preservation of pancreatic islets.

4.3.1 Materials, Methods, and Experimental Protocol

In this study, pancreatic islets were isolated from Sprague-Dawley rats weighing 250–350g and preserved in University of Wisconsin solution at -3°C +/- 0.1 ºC in a custom isochoric chamber (Fig. 4.1). All animals received humane care from properly trained professionals in compliance with both the Principles of Laboratory Animal Care and the Guide for the Care and Use of Laboratory Animals, published by the National Institute of Health (NIH publication no. 85-23, revised 1985), and treated according to an animal protocol approved by the Animal Care and Use Committee of the University of California, Berkeley. The rats were anesthetized, and the peritoneal cavity was entered via a midline incision of the abdomen. The common bile duct was cannulated and injected with digestion solution-containing collagenase P (Roche, # 11249002001). The pancreas was excised and put into a 50 ml centrifuge tube. The centrifuge tube was incubated in a 37°C water bath for 20 minutes. Digestion was then terminated by adding cold washing buffer containing HBSS (Hyclone SH3058802), 1% Pen-Strep (Invitrogen, 15070063), 1% 1M Hepes (Invitrogen, 15630080), 0.1% Dnase I, 1.7ml 1M CaCl2/ 1000ml and 1.2ml 1M MgCl2/ 1000ml. After being washed several times and filtered by a strainer, the digested islets were separated on a Histopaque (Sigma-Aldrich, 11191) density gradient. The islets were then handpicked for purity in samples sizes of 50 ± 5 and preserved in the isochoric chamber. A few sample fresh islets from each isolation were stained with dithizone (DTZ) to confirm their purity. Stock solution of DTZ (0.5 mg/ml) was prepared in DMSO. In use, the stock solution was diluted five times in DPBS solution. One ml DTZ working solution was added to 1 ml islet solution and allowed to stain for 1- 2 minutes at room temperature before imaging.

For each preservation study, the isochoric chamber was pre-cooled to 4 ºC in a refrigerator and filled with pre-cooled University of Wisconsin solution (Belzer UW Cold Storage Solution, Bridge to Life LLC, Columbia, SC) upon arrival of the islets. A small, rough-surfaced metallic agent was placed at the bottom of the chamber in order to dictate the location of initial ice nucleation. Islet samples were placed in open-topped 1 ml centrifuge vials to ensure flotation at the top of the chamber volume while allowing for uniform hydrostatic pressure. The chamber was then sealed, taking special care to ensure that no air bubbles were trapped within. The sealed chamber was fully

submersed in a cooling bath held at the target temperature, -3 ºC +/- 0.1 ºC, and the internal pressure was recorded in order to confirm isochoric behavior and monitor internal temperature consistency (because in isochoric systems temperature and pressure vary in tandem). To ensure consistent nucleation and pressurization trajectories between experiments, the bottom of the chamber was agitated every 10 minutes after submersion until the pressure rise associated with nucleation was observed. After 24, 48, or 72 hours in the cooling bath, the chamber was transferred to a water bath at room temperature and allowed to warm until no ice remained internally, as indicated by complete dissipation of the internal pressure.

After preservation for 24, 48, or 72 hours, the islets were removed from the chamber and viability was evaluated using FDA/PI immunofluorescent staining and image analysis. Islets were assessed for cell viability using Fluorescein Diacetate/Propidium Iodide (FDA/PI). Following removal from the preservation environment, the islets were washed with DPBS three times, and 920 µl DPBS was added to a single well of a culture plate, followed by 40 µl of islets suspension, 20ul of 750 µM PI, and 20ul of 24 µM FDA. The plate was gently swirled in a circular fashion to concentrate the islets in the center of the well. The fluorescent microscopic images were captured at 20X magnification (Eclipse TE300, Nikon, Japan). Freshly isolated islets and islets exposed hydrogen peroxide for 60 minutes were also stained, in order to provide positive and negative controls respectively.

Images were opened in ImageJ software (NIH, Bethesda, MD) and denoised as necessary using the "Color Balance" feature. Images containing FDA staining were then traced using the "Wand" tool until the stained areas were completely enclosed, providing a sharp outline of each islet. The "Measure" feature was then used to calculate FDA fluorescence per unit selected (i.e. islet) area. The selection was then saved as a mask file and overlaid on the corresponding denoised PI stained image, ensuring that identical areas are considered for live and dead evaluations. The "Measure" feature was used once more to calculate PI fluorescence per unit islet area. In order to calculate the viability, the PI fluorescence per unit area value for the preserved islets was divided by the according value for the negative control, effectively yielding a percentage of compromised cells. This percentage was then subtracted from 1 to give the percentage of intact cells, or the overall reported viability. For each experimental condition at least six live and six dead images were analyzed, and results were averaged. Reported uncertainty values represent the standard deviation. Parametric one-way ANOVA was used to confirm significance of difference between viability values for different experimental conditions, with $p < 0.05$ indicating significance.

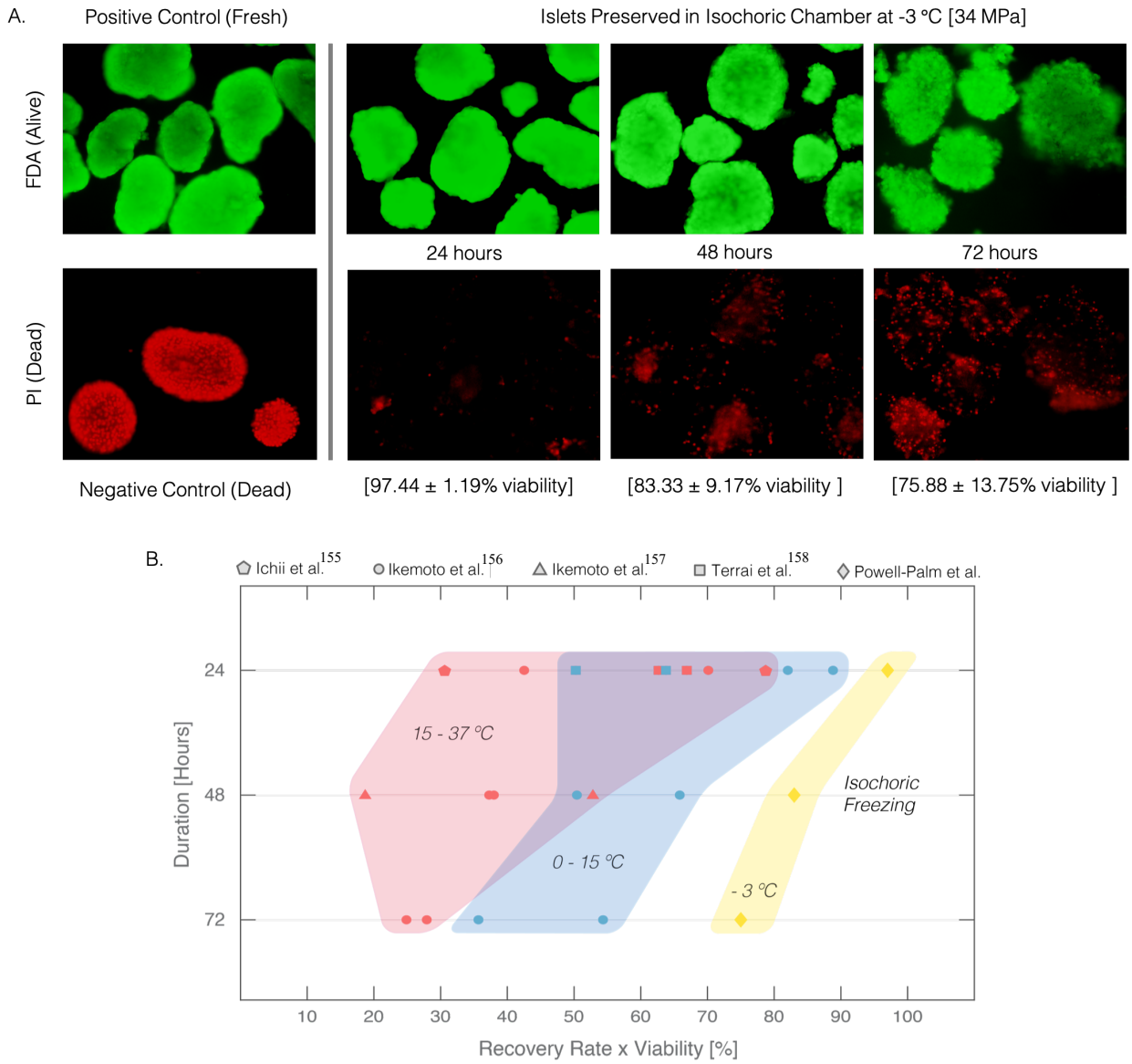

Figure 4.8. **Islet preservation results. A.** Islets preserved in an isochoric freezing system at -3°C [34 MPa] for 24, 48, and 72 hours, compared to positive and negative controls. All preserved islets maintained good morphological integrity, and no dissociation of the cell clusters was observed. **B.** Comparison of current results to previous work investigating the same time range and reporting fluorescence-based viabilities. Recovery rate was multiplied by viability on the x-axis to yield an average viability across the entire preserved islet population. Each color group contains results performed within the labeled temperature range. It should be noted that only those works using directly comparable evaluation methods were considered in this figure, and that this comparison should by no means be considered exhaustive.

4.3.2 Preservation Results and Discussion

Viability results and sample fluorescence images are featured in Figure 4.8A. At -3.0 ± 0.1 ºC and the accompanying hydrostatic pressure of 34 ± 3.4 MPa, isochoric freezing yielded 97.44 ± 1.19% viability after 24h (n = 3), 83.33 ± 9.17% after 48h (n = 3), and 75.88 ± 13.75% after 72h (n = 3). The 48h and 72h viabilities did not vary significantly ($p = 0.29$). Furthermore, many previous studies have had to filter out damaged or dissociated islets prior to evaluating viability, requiring

additional reporting of an islet "recovery rate"[161–164]. Critically, herein all preserved islets were recovered at all time intervals, appearing visually intact, not dissociated, and easily evaluable by fluorescence.

In order to contextualize these results against the broader islet preservation effort and highlight the beneficial nature of reaching subzero temperatures without ice formation or CPAs, our results are plotted in Figure 4.8B alongside several previous works, all employing different methods to investigate the same time range and reporting both recovery rates and fluorescence-based viabilities[161–164]. It is important to note that the x-axis features the reported recovery rate multiplied by the reported viability. This combined term, interpretable as an average total viability, more accurately reflects the survival of the total initial population of islets, rather than simply the viability of those that survived preservation without gross morphological disruption or cluster disassociation. Results are further color-grouped by preservation temperature regime, and a distinct increasing trend in preservation quality is visible as temperature decreases. It should be further noted that the temperature regime accessed in this work, the "high subzero Centigrade" regime, has never before been accessed in ice-free islet preservation, and is of increasing interest due to impressive recent successes such as four-day preservation of rat livers at -4°C using thermodynamic supercooling and continuous machine perfusion[81].

The results presented in this work show marked improvement over existing methods, and it is important to emphasize further that this improvement was enabled inexpensively by a very simple modification of standard preservation protocol: use of a closed volume system rather than an open one. Furthermore, isochoric systems may improve islet preservation by imparting a high degree of physical immobility on preserved matter. Islets are notoriously delicate clusters of cells, and frequently lose functionality upon dissociation or loss of bulk structure. The constrained and pressurized liquid volume in which islets are stored during isochoric freezing restricts bulk fluid motion, preventing simple jostling or mechanical agitation from causing islets to de-cluster. These inherent traits render isochoric freezing systems well suited to islet preservation. However, of comparable clinical importance is the remarkable simplicity of the physical system. Scientific solutions in the transplant preservation domain must be practical in order to advance to clinical use. Isochoric freezing chambers are simply rigid containers capable of withstanding a designated internal pressure, containing no air. They have no moving parts, consume no electricity directly, and are simple to manufacture, assemble, and use. They are exceptionally insensitive to external fluctuations in temperature and pressure, in no way physically delicate, and lend themselves to easy transportation. Furthermore, they require no harmful chemical additives, reducing potential regulatory hurdles. Given the prevalence of type 1 diabetes in the US, low-cost, easily deployable preservation methods are needed to enable widespread islet transplantation. While this study is preliminary, isochoric freezing may offer one such method and warrants significant further research.

4.4 Looking Forward: Improving single-solution equilibrium isochoric preservation and exploring derivative non-equilibrium techniques

Two principle conclusions can be drawn from the biological studies relayed herein. Firstly, it is clear that enhanced hydrostatic pressure yields an as-of-yet poorly understood, time-dependent injurious effect on complex biological constructs, especially at pressures exceeding approximately 40 MPa. Secondly, it is clear that the reduction of preservation temperature even a few degrees below 0°C can significantly enhance preservation quality. Thus a clear objective emerges for continued to isochoric cryopreservation research: to minimize the pressure experienced at a given subzero temperature.

Within the single-phase equilibrium approach, we have demonstrated herein that minimally toxic classical cryoprotectants such as glycerol may be used to this end. Future research may thus immediately expand upon the approach detailed in section 4.2 to achieve longer preservation times at higher qualities, without any deviation of technique. However, nearly all cryoprotectants are accompanied by some degree of cytotoxicity at the relevant concentrations, and thus an arguably more promising approach is to leverage additional non-chemical thermodynamic effects to avoid hydrostatic pressure damage.

Of the alternative thermodynamic approaches discussed in this thesis, isochoric supercooling stands out as the technique best suited to produce superior results based on these baseline biological studies. Metastable supercooled preservation affords the modest reduction in temperature required to significantly enhance preservation quality whilst resisting ice formation, and thus the development of enhanced hydrostatic pressure, entirely. The sacrifice of stable-equilibrium must of course be made however, and thus, while our initial theoretical and experimental efforts demonstrate high supercooling stability at the subzero temperatures of interest, additional testing is needed to verify that isochoric supercooling will remain stable in the dynamic transportation and clinical environment.

In concert with efforts to evade injurious pressures and improve pre-clinical isochoric preservation protocols, we must further clarify the precise *mechanisms* of pressure damage in complex organ and tissue systems, which are both unclear and dramatically understudied. Given the relative pressure insensitivity of individual mammalian cells up to relatively high pressures (100 MPa), our data anecdotally suggests that distinct mechanisms of pressure damage may emerge with increasing complexity of the construct, affecting multicellular structure-function relationships at the structural level.

Given the pressing nature of the clinical problem of organ preservation, efforts should remain focused first and foremost on development of an effective preservation protocol applicable to human organs. However, isochoric protocols introduce enhanced hydrostatic pressure as a relatively unfamiliar variable in the study of human biology, and thus concurrent opportunities to

glean fundamental insight into the tolerances and reactions of our organs to sustained pressure stimuli should simultaneously be seized.

5. Applications of isochoric freezing in the food industry

While the ongoing organ preservation crisis provided the impetus for the development of isochoric cryopreservation, the principle of low-temperature metabolic reduction can be applied agnostically to any biological system, human or otherwise. Thus, in the final chapter of this thesis, we will explore an additional application of isochoric freezing: food preservation.

In spite of a skyrocketing global population and according global hunger, the U.N. Food and Agriculture Organization (FAO states that up to one third of all harvested food is spoiled or squandered before consumption. This represents an incredible waste of not only essential nutrients, but also the labor, water, energy, land, and other resources that required for the production of the food. Of all food groups, fruits and vegetables have the highest wastage rates, approximately 40-50%, whilst often being the least accessible in economically and nutritionally underserved communities.

For thousands of years, societies have recognized cold storage as an exceptionally effective method of extending the shelf-life of consumables. Historically, this storage was typically achieved at temperatures somewhere above the freezing point of water, roughly analogous to the modern household refrigerator. However, with the advent of mass-produced vapor-compression freezers, sub-zero centigrade, long-term storage of many foods has become the norm, and frozen foods now comprise an essential part of the societal food chain. However, as we will discuss further in the coming sections, the freezing process yields the same mechanisms of mechanical and osmotic cellular damage to food that it does to human tissues and organs, and in many cases (particularly in fruits and vegetables), this damage can critically corrupt not only the textural integrity of the foods, but the nutritional content.

This inability to effectively preserve fresh fruits and vegetables via freezing contributes heavily not only to massive global food waste, but also to the relative inaccessibility of the related nutrients to many underserved populations isolated from agricultural points of production, such as in the inner-city of Detroit, the Northern Cheyenne Reservation of Montana, and myriad other socioeconomically disadvantaged population centers across the globe.

I will thus herein relate a series of studies investigating the potential of isochoric freezing to remedy these cold storage issues. We will present first-of-their-kind studies of whole-fruit isochoric preservation with Reinier sweet cherries and grape tomatoes, develop thermodynamic and heat transfer analyses to demonstrate that isochoric freezing could yield significant energy savings compared to conventional freezing, and show that the enhanced pressures and reduced temperatures encountered during isochoric preservation yield a unique sterilizing effect on various dangerous food-borne bacteria.

5.1 Preservation of sweet cherries by isochoric freezing

The USDA's Economic Research Service (2014) reported that food loss in the United States in 2010 was estimated to be 31 percent at the retail and consumer levels, which corresponded to approximately 133 billion pounds and $161 billion worth of food. This degree of waste has far-reaching impacts on food security, resource conservation, and climate change. Fruits and vegetables experienced the highest losses at $49.8 billion, consistent with their highly perishable nature and limited postharvest life. Consequently, preservation technologies play an essential role in extending the shelf life and ensuring the quality and safety of perishable fruits and vegetables. Various forms of freezing at atmospheric pressure comprise the principle processes used for long-term preservation and storage of all manner of food. However, while sub-freezing temperatures and crystallization of water can slow deterioration reactions such as senescence, enzymatic decay, chemical decay and microbial growth, freezing also causes chemical and mechanical damage to cellular tissues via cell dehydration, localized increases in solute concentration, and ice crystal formation. The efficacy of conventional atmospheric freezing of fruits and vegetables has thus been acutely limited due to the resultant nutritional loss, color changes, and textural degradation[165,166]. Given the limitations presented by conventional freezing, the protection from ice-related mechanical and osmotic damage afforded by isochoric freezing suggests that it may prove a superior method for the low-temperature preservation of sensitive fruits, vegetables, and any otherwise sensitive foodstuffs.

One promising potential candidate for isochoric freezing is the sweet cherry (*Prunus avium*). One of the most popular fruits in the world with a global production of roughly 2.25 million tons (2014), sweet cherries are rich in beneficial phytochemicals such as ascorbic acid, anthocyanins, β-carotene and phenolic compounds[167–169], and are reported to possess anti-oxidant, anti-inflammatory, anti-cancer, anti-diabetic and anti-obese properties[170]. However, the extremely short cherry season and their highly perishable nature severley limit the market availability of fresh cherries and augment end-of-season cherry spoilage. We therefore anticipate that the use of isochoric freezing to extend the preservable lifetime of the sweet cherry could lead to increased marketability and consumption and reduced spoilage.

In this study, we demonstrate the first use of isochoric freezing on perishable fruits. We preserve whole Rainier cherries at sub-zero centigrade temperatures, characterize their post-preservation physical integrity and nutritional properties, and compare the effects of isochoric freezing to parallel experiments conducted using conventional isobaric freezing and individual quick freezing (IQF), two current industry standards.

5.1.1 Materials and Methods

Fruit material

Fresh Rainier cherries (6-7 g) were obtained from a local supermarket and local growers in Marin County (CA). Cherries were stored at 5 °C before subsequent sample processing. The samples were used within one week.

Isochoric system

The isochoric system consisted of an R1 pressure chamber from High Pressure Equipment Company (Erie, PA, USA). The chamber was made of 4340 alloy steel. It had an inner diameter of 1 inch, an outer diameter of 3.1/5 inches and an inner length of 6 inches. The total volume capacity was 66 ml. The constant volume chamber was closed with a screw and metal seal. Sealing was accomplished by a combination of O-ring and separate metal back-up ring. The back-up ring was designed to expand and contract as pressure increased or decreased in value. The pressure chamber was connected to an electronic pressure transducer (Stork Solutions Ltd, Hampshire, UK) that was connected to a laptop. The system was cooled in a recirculating bath (VWR AP 15R-40, Radnor, PA, US) filled with a water and ethylene glycol (50:50) solution.

Experimental protocol

Three different methods were used to preserve fresh cherries: preservation for 24 hours at -4°C or -7°C in an isochoric system, preservation for 24 hours at -4°C or -7°C in an isobaric system, and individual quick freezing (IQF). For isochoric treatment, a metal ice nucleating piece was placed at the bottom of the isochoric chamber to ensure that ice formation started far from the sample, which was placed at the top of the chamber. The isochoric chamber was filled with 17.5 °Brix sucrose solution and then sealed. The chamber was completely immersed in a recirculating cooling bath at 0°C and cooled at 0.25 °C/min to -4°C or -7°C. The pressure reached 29.5 MPa at -4°C and 62.1 MPa at -7°C. The cherries remained at the set temperatures for 23 hours. After this time, the chamber was heated back to 0°C at 0.25 °C/min. The chamber was taken from the bath and opened once it reached room temperature. The principle of operating the isochoric chamber is illustrated in Fig. 5.1. The isobaric treatment followed the same procedure as the isochoric treatment except that the cherries were placed in a Ziploc bag and then immersed in the recirculating bath. After freezing, samples were thawed at room temperature for 30 minutes. IQ freezing was performed in a cryogenic freezer using liquid nitrogen (Custom biogenic systems, MI, US). Fresh cherries were frozen to ensure freezing throughout the whole cherry using the following protocol: (a) cooling to -25°C at 25 °C/min, (b) cooling from -25°C to -40°C at 1 °C/min and (c) cooling to -90°C at 25 °C/min. The total processing time was 20 mins. The frozen fruits were collected and directly stored in a conventional freezer at -20 °C for 24 hours. The mass change of the samples was determined gravimetrically, °Brix of the juice expressed from cherries was determined with a refractometer and the pH values of cherries were measured using a pH meter (Beckam Coulter, Indianapolis, US).

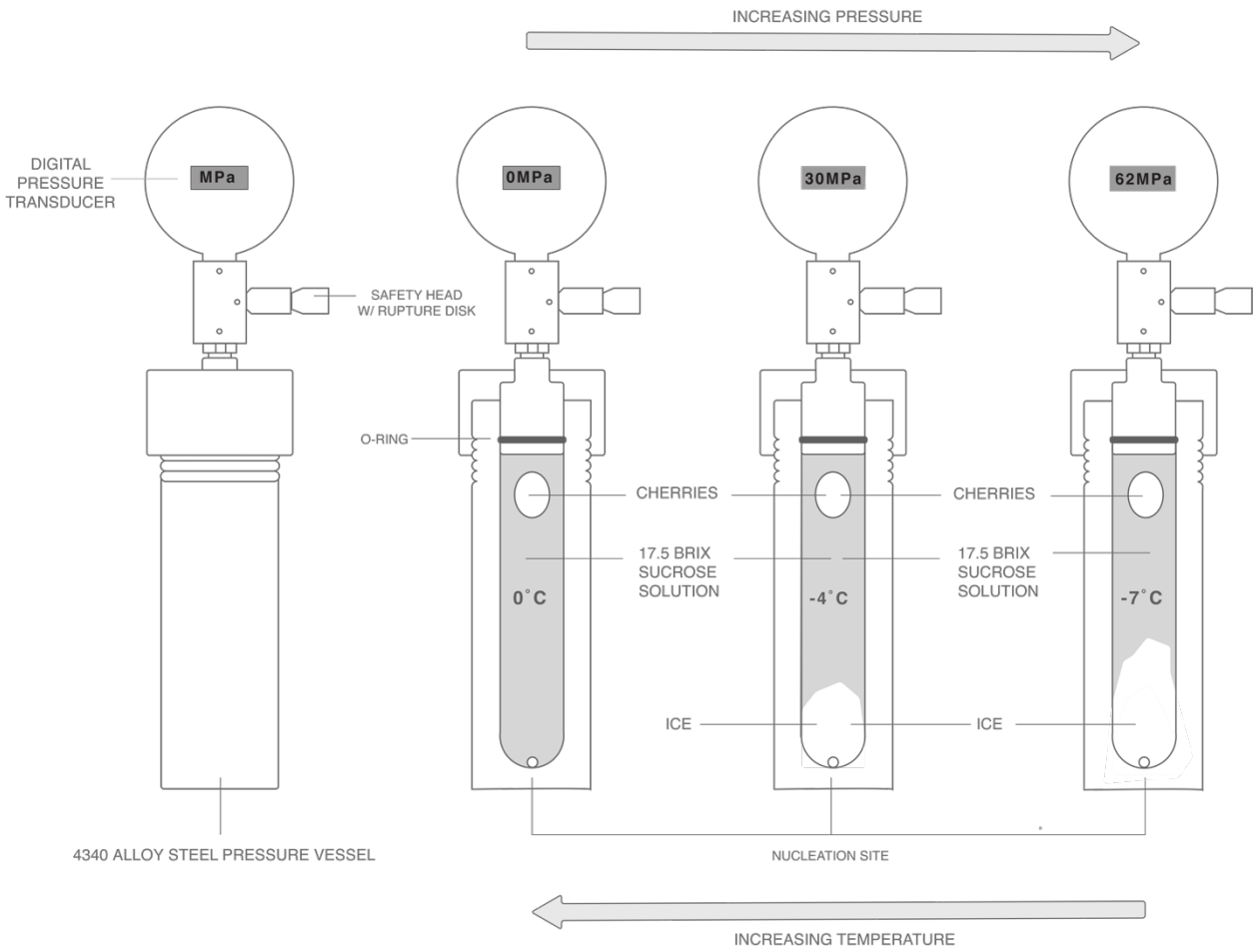

Figure 5.1. Schematic of isochoric chamber and generalized freezing process. In a system of constrained liquid volume with rigid walls and no air pockets, ice expansion will generate hydrostatic pressure, which depresses the freezing point of the system. The pressure will continue to rise until the freezing point of the system becomes equal to the system temperature. At this point, liquid and solid phases will exist in equilibrium. Approximately 12% and 23% of the total volume will be frozen at -4°C and -7°C, respectively.

Drip loss Analysis

Three cherries per treatment were cut in half and used to analyze drip loss. Each half cherry was placed in a 45 mL plastic centrifuge tube suspended on a perforated support. The samples were centrifuged at 4000 rpm for 10 min. Measurements were done at room temperature. Drip loss of cherry samples was measured as the percentage difference between the weight of the cherry after freezing and the weight of the cherry after centrifugation (Eq. 5.1).

$$\% \text{ drip loss} = (\text{initial wt} - \text{final wt})/\text{initial wt} \times 100 \qquad (5.1)$$

Color

Rainier cherries have yellow skin blushed with varying levels of red pigment. The color of the cherries was measured in the yellow areas of the skin. A high-resolution digital camera (Nikon-7000) was used to measure color by capturing the color image of the cherry fruits under constant

lighting. The color was analyzed with Photoshop, in which the Histogram Window was used to find the average Lightness, a and b values for an area of 5625 pixels. This was done twice for each fruit. The values were then converted into the standard L*, a*, b* values using Equations 5.2, 5.3 and 5.4, respectively.

$$L^* = 100 * \text{Lightness}/255 \quad (5.2)$$

$$a^* = 240a/255 - 120 \quad (5.3)$$

$$b^* = 240b/255 - 120 \quad (5.4)$$

L* is the lightness, a* represents the green-red color axis (redness) and b* is the blue-yellow axis (yellowness). The total chromatic difference with respect to the fresh cherry sample (ΔE) was calculated using Equation 5.5.

$$\Delta E = (\Delta L^2 + \Delta a^2 + \Delta b^2)^{0.5} \quad (5.5)$$

Mechanical properties

Mechanical tests were performed with a Texture Analyzer (Stable Microsystems Ltd., TA-XT2i, UK) at 23 °C. A probe (3 mm diameter stainless steel cylinder) with a trigger force of 5 N penetrated the sample to a depth of 8 mm at a speed of 1 mm/s. It returned to its original height at a speed of 10 mm/s. Five or six cherries were measured for each treatment and each cherry was punctured twice, resulting in 10 or 12 measurements. Hardness was calculated as the peak compression force during cherry penetration. Stress as a function of strain curves were analyzed and Young's modulus or modulus of elasticity (E) was obtained from the slope of the curve in the elastic region. The fracture strain (ε_f) was the strain at which the cherry failed via fracture.

Ascorbic acid determination

Ascorbic acid was extracted from the cherries immediately after processing and thawing for 30 mins by blending edible tissue with cold metaphosphoric and acetic acid (MPA) solution at a ratio of 1:2.5. The metaphosphoric acid solution consisted of 30 g metaphosphoric acid, 0.5 g EDTA and 80mL glacial acetic acid diluted to 1L with distilled water. The blended sample was centrifuged for 15 min at 10,000 rpm in a cold centrifuge (4 °C) and the supernatant was collected. Samples (3mL) were passed through C-18 Sep-Paks that was preconditioned with 2mL acetonitrile followed by 3mL distilled water. All samples were kept on ice and HPLC analysis was performed on the same day as the extraction. Ascorbic acid was analyzed by injecting 20µl of the sample into an Agilent HPLC 1100 series liquid chromatograph (Agilent Technologies, Wilmington, DE, USA). A 20 mM H_2SO_4 solution was used as the mobile phase at a flow rate of 0.3mL/min. A ICSep ICE-ION-300 (300 x 7.8 mm) column with guard column from Transgenomics was used in conjunction with an Agilent diode array detector set at 265 nm. Ascorbic acid standards ranging from 25 to 100 mg/mL were used for calibration and sample peaks were identified according to HPLC retention times and absorbance spectra in comparison with authentic standards. Ascorbic acid determination was performed in triplicate.

Total soluble phenolic content

Total soluble phenolic (TSP) content was determined through the Folin–Ciocalteu assay as described by Singleton and Rossi (1965). HPLC grade methanol (20 mL) was added to one gram of pitted cherry in a 45 mL centrifuge tube. Tubes were capped, vortexed for 15 s and then stored at 4 °C overnight. The next day, the sample was vortexed for 15 s and then clarified by centrifugation (15,600 rpm, 15 min at 4 °C) using a SORVALL RC 5C Plus centrifuge (Kendro Laboratory Products, Newtown, CT). A total of 150 µL methanol extract was removed from the clear supernatant and then diluted with 2400 µL nanopure water. After this, 150 µL of 0.125 mol L^{-1} Folin-Ciocalteu reagents was added and the sample was incubated for 3 min at room temperature. The reaction was stopped by adding 300 µL of 0.5 mol L^{-1} Na_2CO_3 and the mixture was incubated for an additional 25 min. Absorbance readings at 725 nm were taken using a Shimadzu PharmaSpec UV-1700 spectrophotometer (Shimadzu Scientific Instruments, Inc., Columbia, MD). A blank prepared with methanol was used as control. The total amount of phenols was determined using a gallic acid standard curve and results were expressed as milligrams of gallic acid equivalent (GAE) per gram of fresh weight. Three replicates were performed for each sample.

Antioxidant activity analysis

The same methanol extract prepared during TSP analysis was used to determine the antioxidant activity (AOX) of fresh and treated cherries. Duplicate samples were used for analysis from each extract. Sample aliquots of 50 µl were taken from the clear supernatant and reacted with 2950 µl of 2,2-diphenyl-1-picrylhydrazyl (DPPH, 103.2 µM in methanol, and absorbance of ∼1.2 at 515 nm) in a covered shaker at room temperature. The samples were allowed to react for 20 hours. Absorbance at 515 nm was recorded using the spectrophotometer. The antioxidant activity was calculated by measuring the decrease in the sample absorbance compared to a methanol sample and quantified from a standard curve developed for Trolox (0–750 µg/ml). Antioxidant (AOX) values were expressed as milligrams of trolox equivalent (TE) per gram of fresh weight. Three replicates were performed for each sample.

Cryo-SEM observations

Some samples were processed to observe microstructure changes. Immediately after treatment, cherries were cut parallel to the longitudinal axis using a scalpel. The sample was placed in the SEM sample holder and plunged into subcooled nitrogen (-210 °C). The frozen sample was transferred to the cryo-stage and then freeze fractured and gold coated. The samples were viewed in a field emission scanning electron microscope JEOL 7900F (JEOL, Kyoto) using a Quorum PP3010T cryo system.

Statistical Analysis of Data

Data were analyzed by one-way analysis of variance and Tukey's multiple comparison tests at 95% confidence level using Minitab version 14.2 statistical software (Minitab Inc., State College, PA).

5.1.2 Textural and nutritional quality after 24-hour preservation

Effects of freezing on mass change, °Brix, pH and drip loss

The mass of cherry samples before and after freezing as well as sensory attributes such as °Brix (related to sweetness) and pH (related to acidity) are shown in **Table 5.1.**

Table 5.1. Effect of freezing on mass change (%),°Brix, pH and drip loss (%)

Sample	ΔM (%)	°Brix	pH	Drip loss (%)
Fresh		22.6 ± 4.5a	3.99 ± 0.14a	23.2 ± 2.1d
Isochoric -4°C	2.99 ± 0.73	18.4 ± 3.6a	4.05 ± 0.15a	32.2 ± 1.6d
Isochoric -7°C	2.27 ± 0.84	17.6 ± 2.7a	3.91 ± 0.13a	50.1 ± 3.5b
Isobaric -4°C	0.02 ± 0.03	18.0 ± 1.1a	3.91 ± 0.11a	43.5 ± 0.1c
Isobaric -7°C	-0.45 ± 0.56	17.6 ± 2.7a	3.76 ± 0.22a	47.8 ± 1.4b
IQF	-0.36 ± 0.33	23.0 ± 0.5a	3.87 ± 0.07a	58.4 ± 1.0a

IQF= Individual Quick Freezing
Letters following values in the same column show homogeneous groups at 95% confidence interval (C.I.)

Freezing under isobaric conditions or individual quick freezing did not result in significant mass changes. In comparison, the cherries preserved under isochoric conditions showed a slight gain in mass (<3%) due to the impregnation of the cherry with the external sucrose solution. °Brix and pH values for all cherry samples did not change significantly due to freezing.

Freezing cherries under isochoric conditions resulted in a significantly lower rate of drip loss compared to IQ freezing, and in fact at -4°C showed no significant differences in drip loss compared to fresh cherries. The increase in drip loss at -7°C may be due to the higher hydrostatic pressures experienced, which can alter cell permeability in fruit tissues (and thus the movement of water from within the cell) and may potentially damage the cellular structure at sufficiently high values[171].

Mean drip losses of cherries frozen under conventional isobaric conditions were significantly higher than drip losses in the fresh samples, indicating that appreciable cell damage occurred during the isobaric freezing process, as drip loss is physical evidence of the inability of water that osmotically exits the cell during freezing to return to the cell upon thawing.

Of the methods investigated, IQ frozen cherries showed the greatest drip loss upon thawing. While it is well known that rapid freezing results in smaller and less damaging ice crystals, small crystals are more to grow via recrystallization than larger crystals, due to their high surface free energy[11]. Consequently, recrystallization growth may have occurred in these samples, especially if temperature fluctuated during storage, and the resultant larger ice crystals may have exerted sufficient force to rupture cell membranes[11]. During thawing, water will then leak out of the cellular matrix and manifest as significant drip loss.

Color analysis

Appearance and color is the single most important attribute determining whether a product is accepted as fresh in an industrial or consumer context, and thus represents one of the most critical quality attributes for foods[172]. The appearance and color of fresh and post-preservation cherries are shown in Figure 5.2 for all preservation types, and Figure 5.3 provides the L*-a* and a*-b* color space for the fresh and thawed samples.

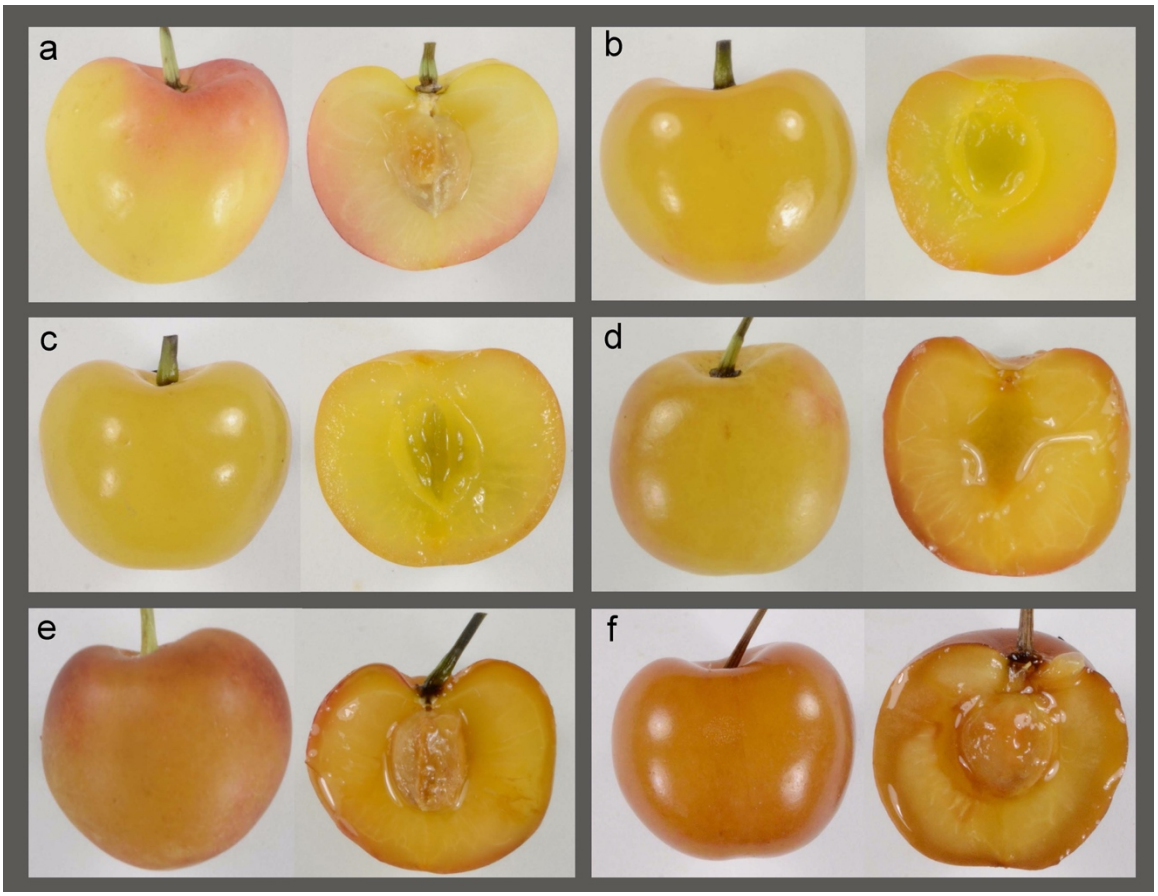

Figure 5.2. Photographs of (a) fresh cherry, (b) thawed cherry frozen to -4ºC in an isochoric system, (c) thawed cherry frozen to -7ºC in an isochoric system, (d) thawed cherry frozen to -4ºC in an isobaric system, (e) thawed cherry frozen to -7ºC in an isobaric system and (f) thawed cherry from IQF.

As evident in Figure 5.2, isochoric freezing yielded a small effect on the color attributes of the cherries, slightly enhancing slighlty their darkness (-L* values), redness (a* values), and yellowness (b* values). This slight shift is likely due to infiltration of the porous cherry tissue structure by the surrounding sucrose solution, resulting in cherries with a somewhat more translucent appearance. Samples at -4ºC and -7ºC showed no significant variations in color, indicating that changes in hydrostatic pressure over the experimental range considered did not affect degradation of β-carotene (the major compound contributing to the yellow quality of Rainier cherries) or phenolic compounds. This observation is consistent with previous work[173] showing

that hydrostatic pressures up to 600 MPa had little influence on β-carotene content in carrots and broccoli minimal effect on the phenolic content of various fruits[174].

By comparison, for isobaric and IQ frozen samples, lightness (L*) and b* values decreased significantly, while a* values increased in value relative to fresh samples, a result that grew more distinct at lower freezing temperatures. The observed degradation of β-carotene was likely related to enzymatic oxidation caused by native enzymes such as lipoxygenase[175]. Additionally, enzymatic browning may have occurred due to the degradation of polyphenols by enzymes such as polyphenol oxidases and peroxidase[176]. These degradation reactions were most likely accelerated due to membrane damage, which can assist enzyme-substrate interactions that lead to color changes in cherries.

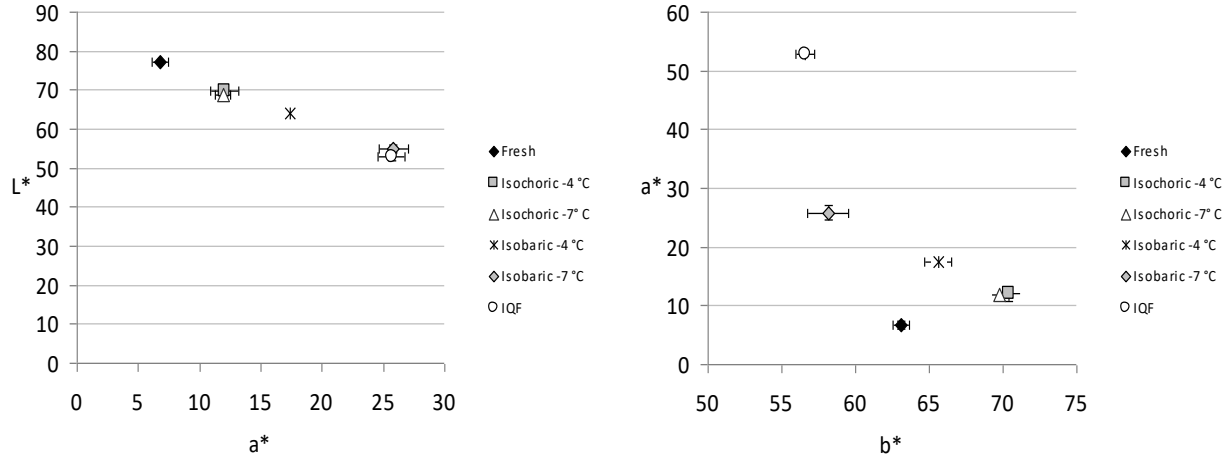

Figure 5.3: L*-a* and a*-b* color space of fresh and thawed cherries frozen under different conditions.

Finally, the chromatic difference (ΔE) values confirmed significant differences in the color of the cherries between preservation modes: isochoric preservation at -4ºC and -7ºC induced the lowest chromatic difference (12%), whereas IQ freezing induced the largest (32%) and samples frozen at -4ºC and -7ºC in an isobaric system induced differences of 17% and 30% respectively.

Mechanical properties

Consumers often purchase a product for the first time based on appearance, but repeat purchases are driven by additional quality factors such as texture[172]. Thus, preserved cherries should have comparable texture to fresh cherries in order to ensure consistent customer appeal. As shown in Figure 5.4, cherries preserved under isochoric conditions yielded the best mechanical properties (Fig. 5.4), showing no significant differences in the maximum force, elasticity modulus, and strain fracture values when compared to their fresh counterparts. Decreasing the temperature from -4°C to -7°C resulted in a slight decrease in sample firmness and rigidity, likely due to the capacity of high hydrostatic pressures to break cell structures and reduce membrane permeability[177].

Conversely, freezing under isobaric conditions and IQ freezing produced extreme changes in textural properties (Fig. 5.4). The firmness of these samples was significantly lower than those of fresh cherries, indicating weakened the integrity of the cell membranes and walls, and the elastic

modulus also decreased significantly, indicating enhanced elasticity associated with a loss in turgidity. During compression tests, these samples failed entirely to fracture, lacking sufficient structure or integrity to provide a discrete rupture or breaking event. The firmness and modulus values observed between isobaric and IQ freezing showed no statistical ($P > 0.05$) differences. This indicates that both slow and fast freezing rates produce considerable sample softening due to cell lysis and subsequent leakage of water and cellular components, consistent with previous studies: Kong et al. observed that thawed cherries stored at -20°C for 31 days became extremely mushy in texture with a complete loss of firmness to touch[178]; Alonso et al. found that IQF cherries showed a decrease in firmness and elasticity modulus values[179]; and Alonso et al. found that a major contributor to the loss of firmness was due to leakage of intracellular pectin that resulted in the damage of calcium bridges and the loosening of cell tissue[180]. Our mechanical results in sum indicate that preservation under isochoric conditions is distinctly preferable to conventional isobaric and IQ freezing from a textural standpoint, and that minimal textural changes occur relative to fresh Rainier cherries.

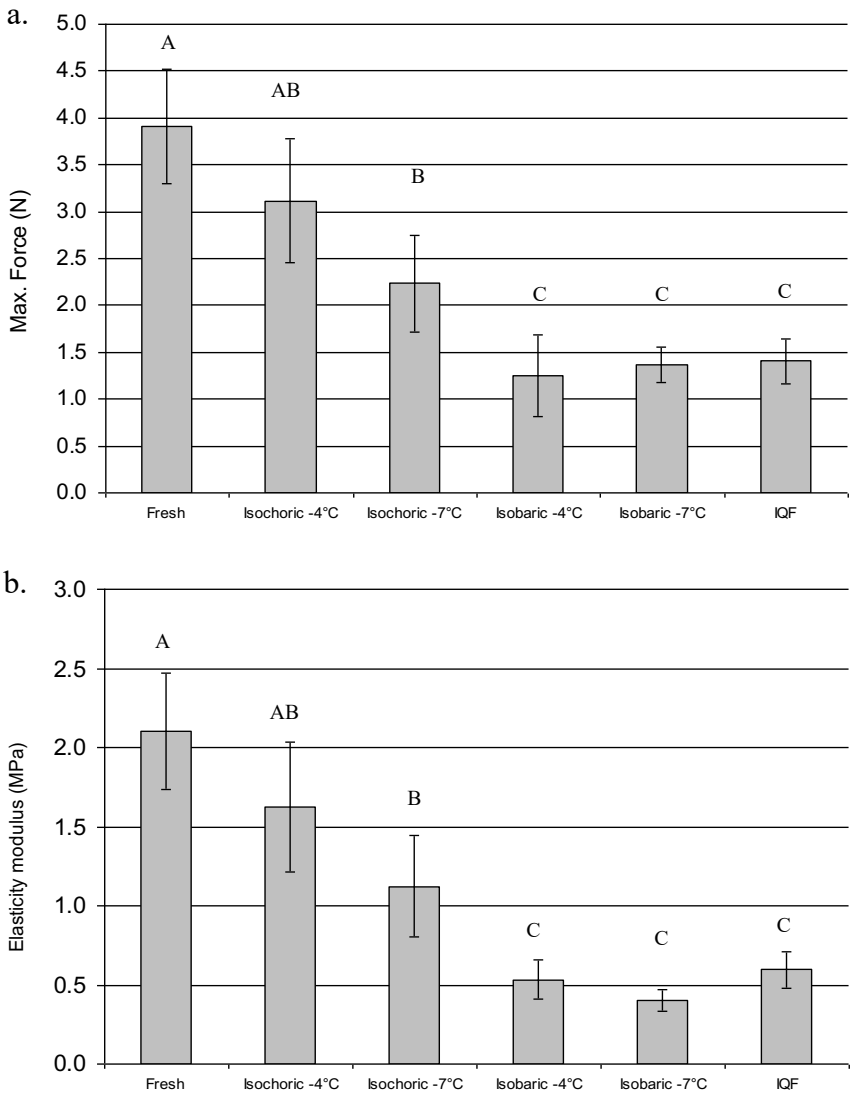

Figure 5.4. Effects of freezing methods on the (a) maximum force and (b) elasticity modulus of thawed cherries under different freezing conditions. The same letter indicates no significant differences between treatments at 95% confidence interval.

Ascorbic acid content

The total ascorbic acid content of fresh Rainier cherries was 5.3 ± 0.8 mg/100 g. Cherries preserved under isochoric conditions retained their ascorbic acid contents (Fig. 5.5), with the increase in pressure from 30MPa to 62MPa yielding no significant effect, consistent with previous studies that have shown that hydrostatic pressure does not generally affect low molecular weight food compounds[181]. By comparison, isobaric freezing and IQF led to significant ascorbic acid losses, including a 63% loss at -4°C under isobaric freezing and a 72% loss after the IQF process (Fig. 5.5). This ascorbic acid degradation was likely due to enzymatic oxidation (via ascorbic acid oxidase). In frozen products enzymatic reactions are slowed but not completely eliminated, and cell damage due to ice formation can furthermore augment enzyme substrate-interactions during the thawing process.

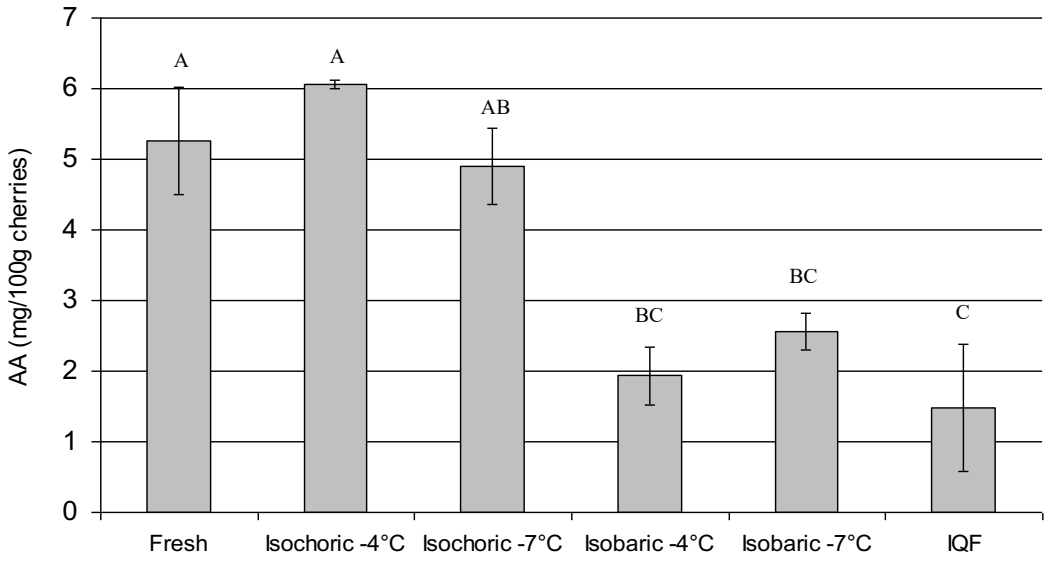

Figure 5.5. Ascorbic acid contents of fresh and thawed cherries using different freezing methods. The same letter indicated no significant differences between treatments at 95% confidence interval.

Total soluble phenolics (TSP)

Fresh cherry samples had a TSP value of 0.52 ± 0.03 mg GAE.g^{-1}, somewhat lower than previously reported values of 0.65 ± 0.05 mg GAE.g^{-1} and 1.42 ± 0.05 mg GAE.g^{-1} for flesh and skin, respectively[168]. Cherries preserved under isochoric conditions showed apparent increases in TSP values (Fig. 5.6), with preservation at -4°C showing a 19% increase and samples at -7°C showing a 27% increase. This increase in phenolic compounds at lower temperatures (and higher

pressures) may be due to an increase in extractability of phenolics from damaged cells. However, the TSP content also increased in value at higher temperature (lower pressure), at which cells remained intact. This might be due to the response of the cherry cells to pressure/temperature stresses under isochoric conditions, which may have synthesized phenolic acids to protect against these stressors. If this is the case, higher processing pressures at lower temperatures would logically increase TSP values, though more conclusive experiments are needed to validate this theory.

Cherries subjected to isobaric freezing and IQF treatment meanwhile showed a significant decrease in TSP content (Fig. 5.6). The formation of ice might have caused damage to the delicate organelle and membrane structures of the cells and dislocated the enzyme systems, particularly polyphenoloxidase system, which has been shown to be very active in the flesh and skins of cherries[182]. Polyphenoloxidase activity is temperature-dependent and consequently, polyphenol degradation can be minimized at lower freezing temperatures. Several authors have reported a decrease in TSP content of cherries due to freezing: Poiana et al., found a 7% decrease in ascorbic acid content immediately after freezing at -18°C [183]; Chaovanalikit and Wrolstad reported a 25% decrease in TSP content of Bing cherries frozen under liquid nitrogen and stored for 3 months at -23°C [168]; and Kong et al reported 50% degradation of soluble phenolics after storage for one month at -20 °C [178].

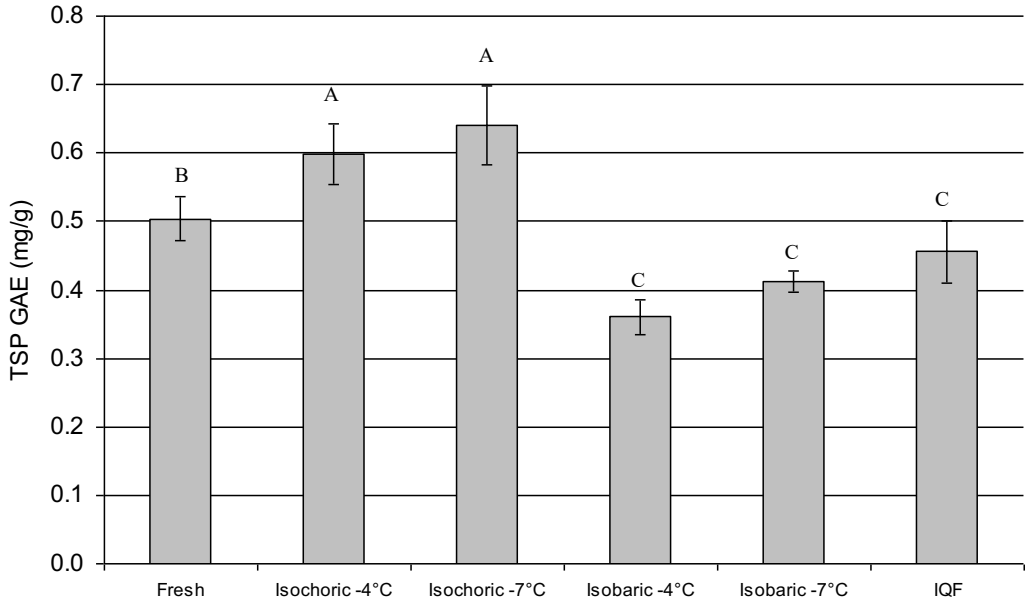

Figure 5.6. Total soluble phenolic contents of fresh and thawed cherries using different freezing methods. The same letter indicated no significant differences between treatments at 95% confidence interval.

Antioxidant activity (AOX)

Studies show that antioxidant compounds can have positive effects on human health due to their ability to scavenge free radicals and thus inhibit the oxidative mechanisms that led to degenerative

diseases[170]. Cherry is one fruit with high antioxidant activity, related principally to anthocyanins, flavonoids and total phenolics content[169,184].

The antioxidant activity of our fresh cherries was determined to be 1.9 ± 0.1 mg TE.g^{-1} in the flesh and skin respectively. Freezing at -4°C under isochoric conditions did not result in significant changes in antioxidant activity (Fig. 5.7) However, cherries preserved at -7°C under isochoric conditions showed an apparent increase in antioxidant activity, which might be related to the increase in TSP content discussed previously (Fig. 5.6).

By comparison, cherries subjected to freezing under isobaric conditions showed a slight reduction in antioxidant activity (Fig. 5.7), a change of lesser magnitude than its shifts in ascorbic acid and total phenolics. One possible explanation could be that antioxidant activity is correlated with the concentration of all bioactive compounds, and some polyphenolic degradation products still retained antioxidant activity. Previous studies have provided comparable results to those found here[168,183].

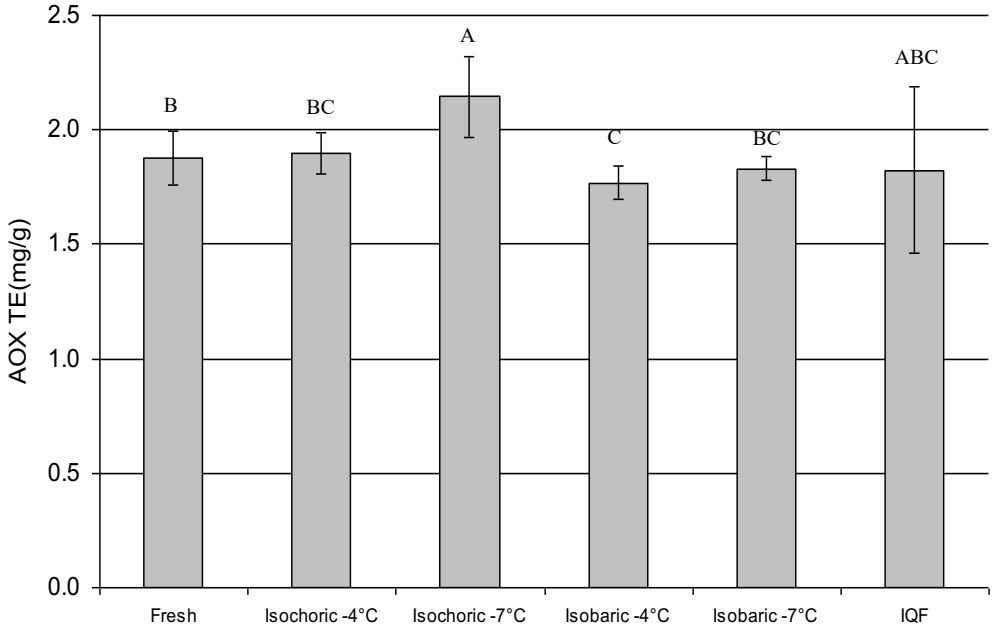

Figure 5.7. Effects of freezing methods on the antioxidant activity of thawed cherries under different freezing conditions. The same letter indicates no significant differences between treatments at 95% confidence interval.

Cryo-SEM images

To better understand the effects of freezing on cherry structure, cryo-SEM images were taken to visualize the tissue structure at the cellular level. The effects of freezing on the cell structures of thawed cherry parenchyma are shown in Figure 5.8. For comparison, fresh cherry tissue is also shown in Fig. 5.8a.

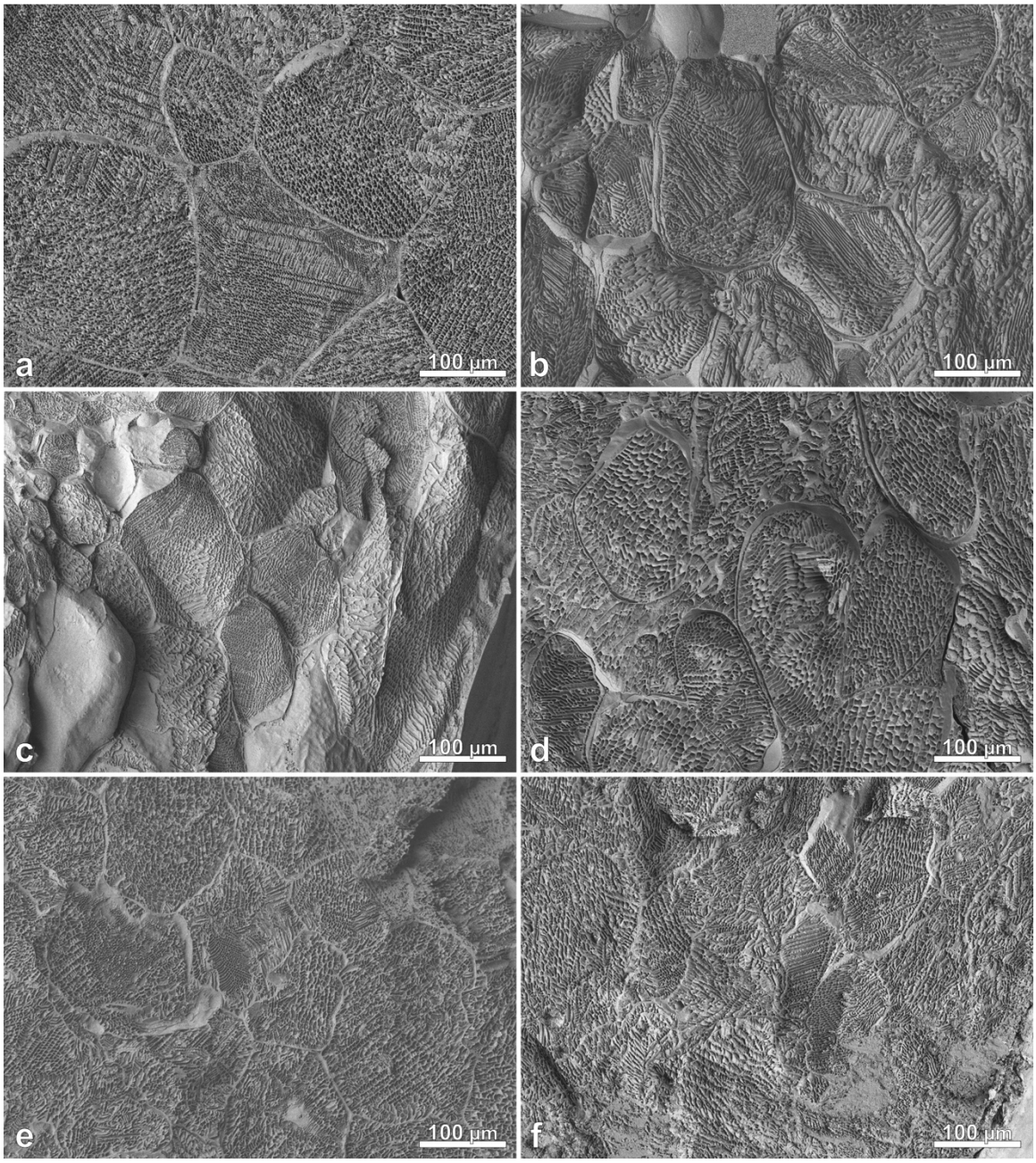

Figure 5.8. Cryo-SEM images of cherry parenchyma tissue in (a) fresh cherry, (b) thawed cherry frozen to -4ºC in an isochoric system, (c) thawed cherry frozen to -7ºC in an isochoric system, (d) thawed cherry frozen to -4ºC in an isobaric system, (e) thawed cherry frozen to -7ºC in an isobaric system, (f) thawed cherry from IQF.

The cells of fresh cherry appeared compact and turgid. Some intercellular spaces filled with air could also be observed in the image. Cherries frozen at -4°C under isochoric conditions (Figure 5.8b) had cells that maintained intact membranes and walls. Intercellular spaces appeared to be filled with the external sugar solution, but the physical structures of the cherry remained unharmed. The sample frozen at -7°C under isochoric conditions (Figure 5.8c) had tissue with a patchwork appearance that contained areas of well-preserved cells as well as areas with a vitrified

homogenous aspect due to the loss of cell permeability and compartmentalization. This could potentially have been caused by the different compressibilities of the cellular materials under pressure[177].

By comparison, freezing at -4°C or -7°C under isobaric conditions (Figure 5.8d and 5.8e) induced large changes in the cellular structures, and fluid was observed in the intercellular spaces due to migration of cellular components. Furthermore, certain cells appeared loose with abnormally large intercellular spaces, likely due to the loss of intracellular pectin, and dehydration appears to have caused buckling and folding of the cell walls. IQ freezing similarly induced major morphological damage to the tissue (Fig. 5.8f). In the provided sample, some cell walls could be identified as irregular shapes by their lighter coloration, but the tissue appeared largely homogenous and it was difficult to differentiate between intra- and extracellular volumes, as both became filled with a blend of liquid and solids due to the release of intracellular content.

Results in Sum

Rainier cherries preserved at -4°C in an isochoric system possessed similar quality and nutritional properties to those of fresh cherries, with well-maintained texture and minimized drip loss. We attribute this effectiveness of preservation to the absence of ice crystallization within the fruit tissue, which functioned to minimize morphological damage relative to traditional freezing methods, as confirmed by cryo-SEM. Isochoric freezing somewhat enhanced the apparent translucency of the cherries' appearance, likely due to infiltration of the surrounding isotonic sucrose solution, but color attributes were otherwise directly comparable to fresh cherries. At a holding temperature of -4°C, this novel preservation method furthermore maintained ascorbic acid levels, phenolic compounds, and antioxidant activity in cherries, ostensibly because cell compartmentalization remained intact during the freezing process. Reducing the temperature from -4°C to -7°C in an isochoric system led to decreases in firmness, rigidity and water holding capacity of the cherries, suggesting that cellular damage may develop after a relatively discrete threshold in pressure. Nonetheless, freezing at -7°C in an isochoric system preserved the quality and nutritional properties of the cherries to a greater extent than freezing under conventional isobaric conditions or via IQ freezing, indicating strong potential for improvement over currently-employed industrial standards. In summary, the deployment of isochoric freezing for the extension of shelf life may enable production of more widely acceptable frozen fruit products with higher textural and nutritional quality, and a concomitant reduction in fruit waste.

5.2 Preservation of grape tomato by isochoric freezing

Building upon the initial effort to preserve whole fruit products described in the preceding section, which yielded exceptional preservation quality but over only a brief time period (24 hrs), we will next examine isochoric freezing of another difficult difficult-to-preserve fruit, the grape tomato, at time scales of practical industrial relevance (4 weeks). Tomatoes contribute significantly to human nutrition due to their high vitamin C, phenolic and carotenoid (primarily lycopene) contents, and epidemiological studies have shown that tomatoes may yield a protective effect against various forms of cancer (especially prostate cancer), atherosclerosis and cardiovascular diseases[185]. Despite their established position in the global human diet and the incredible volume of global tomato production however, methods of significantly extending the postharvest shelf life of all

manner of tomatoes (including grape tomatoes) have yet to be identified. This preservation difficulty can be attributed to their acute sensitivity to *mild* cold; tomatoes must be stored at 10°C or higher to avoid chilling injury[186], a catchall term for myriad modes of damage that can occur in the temperature ranges between normothermic and sufficiently hypothermic (i.e. frozen) states. However, tomatoes also prove unsuitable for traditional freezing, which results in considerable texture degradation, color alteration and nutritional loss during both the initial freezing process and the subsequent frozen storage period[187].

Tomatoes thus present an optimal candidate for further exploration isochoric fruit preservation. In this study, we examine the effects of isochoric freezing at -2.5°C on the textural and nutritional quality of grape tomatoes and compare the results with other preservation techniques often used in the tomato industry: Cold storage at 10°C and 85% relative humidity (RH) and individual quick freezing (IQF) followed by storage at -20°C. In order to make additional fundamental comparisons, we also preserved tomatoes under isobaric conditions at -2.5°C and atmospheric pressure.

5.2.1. Materials and Methods

Fruit material

Red, ripe grape tomatoes were purchased from a local produce distribution center in Berkeley (CA).

Isochoric system

An OC-9 pressure chamber from High Pressure Equipment Company (Erie, PA, USA) was used in the isochoric system. The chamber was made of 316 stainless steel. It had an inner diameter of 5.08cm, an outer diameter of 11.11 cm and an inside depth of 25.4 cm. The total volume capacity was 500 mL. The chamber was closed with a screw and metal seal and connected to an electronic pressure transducer (Stork Solutions Ltd, Hampshire, UK). The system was cooled in a recirculating bath (VWR AP 15R-40, Radnor, PA, US) filled with a water and ethylene glycol (50:50) solution.

Experimental protocol

Four different methods were used to preserve fresh tomatoes for up to four weeks: cold temperature (10°C) and 85% RH, -2.5°C in an isochoric system, -2.5°C in an isobaric system and individual quick freezing (IQF) followed by storage at -20°C. For the isochoric treatment, an ice nucleating piece (screw) together with SnoMax protein were placed at the bottom of the isochoric chamber to ensure that ice formed far from the sample, which was placed at the top of the chamber. The isochoric chamber was filled with 6.5 °Brix sucrose solutions and then sealed. The chamber was completely immersed in a recirculating cooling bath at –2.5°C. The pressure reached 24.7 ± 0.7 MPa. The tomatoes remained at the set temperatures for 1, 2, 3 or 4 weeks. Different tomato batches were used for each time period. Once the trial was complete, the chamber was placed in a room temperature bath for 30 minutes before being opened. The isobaric treatment followed the same procedure as the isochoric treatment except that the tomatoes were placed in a mylar bag filled with 6.5 °Brix sucrose solutions and then immersed in the recirculating bath. After freezing,

samples were thawed at room temperature for 30 min. IQ freezing was performed in a cryogenic freezer using liquid nitrogen (Custom Biogenic Systems, MI, US). Fresh tomatoes were frozen to ensure freezing throughout the whole tomato using the following protocol: (a) cooling to -25°C at 25 °C/min, (b) cooling from -25°C to -40°C at 1 °C/min and (c) cooling to -90°C at 25 °C/min. The total processing time was 20 min. The frozen tomatoes were then collected and directly stored in a conventional freezer at -20 °C for 24 h. Tomatoes with fractures due to thermal shock were discarded. For all preservation studies, tomatoes with an initial mass of 7-7.5g were used to determine mass and volume changes. The mass change of the samples was determined gravimetrically and the volume change was determined using a digital caliper micrometer and the assumption that the grape tomatoes have an ellipsoid shape. The moisture content of about 5 g of blended tomato was determined by drying the sample at 85 °C until constant weight. °Brix of the juice expressed from tomatoes was determined with a refractometer.

Color

Surface color of tomatoes was measured using a spectrophotometer (CM508D, Konica-Minolta Inc., Ramsey, NJ, USA) with an 8 mm CM-A196 Target Mask. Measurements were taken on six tomatoes and reported in CIELAB color scales where L* described the lightness of the sample, a* described the intensity in red (a*>0), and b* described the intensity in yellow (b*>0).

Cryo-SEM

Scanning electron microscopy was used to analyze microstructural changes after 4 weeks of preservation. The sample was placed in the SEM sample holder and plunged into subcooled nitrogen (-210 °C). The frozen sample was transferred to the cryo-stage and then freeze fractured and gold coated. The samples were viewed in a JEOL 7900F field emission scanning electron microscope (JEOL, Kyoto) using a Quorum PP3010T cryo system.

Mechanical properties

Mechanical properties were obtained by a compression test using a Texture Analyzer (Stable Microsystems Ltd., TA-XT2i, UK) at 23 °C. Six tomatoes with an initial weight between 7 and 7.5 g were tested for each treatment. The tomatoes were compressed to 50% deformation in a single compression-decompression cycle at a steady speed of 0.1 mm/s using a 50 mm diameter circular flat plate (TA-25 probe). The fracture force was determined to be the force at which the tomato failed via fracture. Young's modulus or modulus of elasticity (E) was obtained from the slope of the stress-strain curves in the elastic region.

Ascorbic acid determination

Ascorbic acid was extracted and analyzed by HPLC using a method previously described in Bilbao-Sainz et al. (2019). Samples for ascorbic acid determination were prepared in triplicate immediately after each treatment.

Determination of lycopene content

Lycopene content was determined spectrophotometrically following the methodology proposed by Fish et al. (2002). The absorbance of the extracts was measured at 503 nm using hexane as a blank. The amount of lycopene was determined by the following formula:

$$lycopene\ \left(\frac{mg}{kg}\right) = \frac{x}{y} \times A_{503}\ \times 3.12 \qquad (5.6)$$

where x is the amount of hexane (ml), y the weight of tomato tissue (g), $A503$ the absorbance at 503 nm and 3.12 is the extinction coefficient of lycopene.

Total soluble phenolic content and antioxidant activity

The total soluble phenolic (TSP) content was determined according to the Folin-Ciocalteau assay as described by Singleton and Rossi[188]. Absorption was measured at 725 nm using a Shimadzu PharmaSpec UV-1700 spectrophotometer (Shimadzu Scientific Instruments, Inc., Columbia, MD, USA). The total amount of phenols was determined using a gallic acid standard curve and results were expressed as milligrams of gallic acid equivalent (GAE) per gram of tomato in dry basis. Three replicates were performed for each sample. The same methanol extract from TSP analysis was used to determine the antioxidant capacity (AOX) using the 2,2-diphenyl-1-picrylhydrazyl radical (DPPH$^{\bullet}$) scavenging activity assay. The assay was based on the method of Brand-Williams et al[189]. DPPH$^{\bullet}$ scavenging activity was expressed as mg of Trolox equivalents (TE) per g of tomato in dry basis.

Statistical Analysis of Data

Analysis of variance (ANOVA) and Tukey multiple range tests ($\alpha = 0.05$) were used to determine statistically significant differences using Minitab version 14.2 statistical software (Minitab Inc., State College, PA).

5.2.2 Textural and nutritional quality after 4-week preservation

Effects of preservation method on mass, volume, water content and °Brix.

The mass change of tomato samples, volume of tomato samples, water content, and °Brix over 4 weeks preservation time are shown in Table 5.2. Freezing under isochoric conditions did not result in significant mass or volume changes, and neither water content nor °Brix values changed significantly, indicating that the employed 6.5 °Brix sucrose solution was in osmotic equilibrium with the tomato samples. By comparison, the tomatoes stored via all other methods gradually lost mass (up to 16.7% for IQF) and volume (up to 9.6% for cold storage at 10°C) over time, principally due to respiration. Table 5.2 further shows that IQ and isobaric freezing significantly reduced the water content of the tomatoes, by 79% and 76% respectively. Ice crystal growth during initial freezing or longer-term recrystallization may have led to degradation of cell constituents or cellular structure and caused leaking of cell contents during thawing.

Table 5.2. Effect of preservation on mass change, volume, water content and °Brix.

Sample	Time	Mass change (%)	Volume (cm^3)	Water content (%)	Brix
Fresh			57.7 ± 4.7 [a]	92.1 ± 0.2 [a]	6.93 ± 0.39 [a]
Isoch. -2.5°C	1 wk	0.6 ± 1.1[a]	56.6 ± 4.9 [a]	92.7 ± 1.1 [a]	6.28 ± 0.71 [a]
	2 wk	1.2 ± 0.3[a]	56.9 ± 2.9 [a]	92.6 ± 0.2 [a]	8.48 ± 1.26 [a]
	3 wk	0.2 ± 0.6[a]	57.8 ± 1.9 [a]	90.8 ± 0.3 [a]	7.30 ± 0.62 [a]
	4 wk	0.2 ± 1.1[a]	58.1 ± 3.5 [a]	91.1 ± 0.1 [a]	7.35 ± 0.39 [a]
Cold storage	1 wk	-2.9 ± 0.7 [b]	57.6 ± 3.8 [a]	89.2 ± 0.7 [a]	7.03 ± 0.31 [a]
	2 wk	-4.5 ± 0.8 [c]	50.3 ± 4.2 [b]	87.6 ± 0.8 [b]	7.13 ± 0.26 [a]
	3 wk	-6.6 ± 1.2 [d]	52.8 ± 2.8 [b]	85.5 ± 1.2 [c]	6.33 ± 0.39 [a]
	4 wk	-8.6 ± 0.9 [d]	48.0 ± 7.3 [bc]	86.0 ± 2.2 [bc]	7.00 ± 0.28 [a]
IQF	1 wk	-5.5 ± 3.8 [bcd]	51.8 ± 5.1 [bc]	86.6 ± 1.8 [bc]	7.00 ± 0.70 [a]
	2 wk	-12.1 ± 3.1 [d]	50.1 ± 4.6 [bc]	81.7 ± 2.8 [cd]	7.45 ± 0.48 [a]
	3 wk	-15.7 ± 5.2 [d]	49.5 ± 3.4 [bc]	76.5 ± 5.2 [d]	7.75 ± 0.38 [a]
	4 wk	-16.7 ± 3.3[d]	48.3 ± 4.9 [bc]	79.4 ± 4.1[cd]	7.55 ± 0.37 [a]
Isob. -2.5°C	1 wk	-6.5 ± 1.8 [cd]	50.3 ± 3.0 [bc]	85.6 ± 1.8 [bc]	7.57 ± 1.16 [a]
	2 wk	-6.6 ± 1.6 [cd]	48.5 ± 3.9 [bc]	85.5 ± 1.6 [bc]	7.80 ± 0.79 [a]
	3 wk	-11.9 ± 2.3 [d]	44.2 ± 4.0 [c]	80.2 ± 2.3 [d]	6.40 ± 0.72 [a]
	4 wk	-16.3 ± 1.1 [d]	44.4 ± 3.4 [c]	75.8 ± 1.1 [d]	5.97 ± 0.76 [a]

IQF= Individual Quick Freezing
For each column, values followed by the same letter (a–d) are not statistically different at $p < 0.05$

Appearance and color analysis

The appearance and color of fresh and preserved grape tomatoes are shown in Figure 5.9. No perceptible difference in visual appearance was observed between whole fresh tomatoes and whole tomatoes preserved under isochoric conditions for 4 weeks. The transverse section of the isochoric tomatoes revealed presence of some free water, likely a result of the fact that pressure can change cell permeability in vegetable tissues, enabling movement of water from inside the cell to the extracellular environment and resulting in a wetted appearance[171]. In contrast, cold-stored tomatoes became shriveled and dehydrated after 3 weeks due to the greater susceptibility of small grape tomatoes to water loss during storage. By the third week, almost all cold-stored tomatoes were deemed below marketable quality, consistent certainly with previous reports[186] that the visual quality of grape tomatoes stored at 10°C is maintainable for up to 12 days. Samples frozen via IQF or conventional isobaric means demonstrated further visual degradation, yielding a mushy appearance and apparent detachment of the skin of the tomato from its flesh. The adverse effect of freezing on tomato appearance was more pronounced for isobaric than for IQ freezing.

Figure 5.9. Photographs of fresh grape tomato and preserved tomatoes after four weeks.

For color, isochoric freezing and cold storage had only small effects on the L* a* b* values (Table 5.3), indicating consistency of color between fresh and preserved tomatoes across the whole preservation period. By comparison, IQ frozen and isobaric samples grew yellower (increased b* values) when compared to fresh samples, especially after IQF. Color changes during frozen storage has been reported in tomatoes and tomato products previously, typically characterized as an increase in yellowness and a simultaneous lightening of color[190,191]. These changes have been attributed to a decrease in carotenoid content in frozen tomatoes due to enzymatic oxidative reactions, and the higher b* values observed for IQF samples compared to isobaric samples may be due to greater carotenoid oxidation in IQF samples due to air circulation during frozen storage at -20°C.

Table 5.3. Effect of preservation conditions on CIE L*, a*, b* parameters.

Sample	Time	L*	a*	b*
Fresh		31.4 ± 0.8 ^{ab}	8.8 ± 1.8 ^{ab}	11.1 ± 0.9 ^{d}
Isoch. -2.5°C	1 wk	31.8 ± 0.9 ^{ab}	6.7 ± 1.0 ^{b}	12.3 ± 1.2 ^{bcd}
	2 wk	29.8 ± 0.9 ^{bc}	6.6 ± 1.1 ^{b}	10.0 ± 1.6 ^{d}
	3 wk	31.0 ± 0.4 ^{b}	8.2 ± 1.2 ^{ab}	11.4 ± 1.2 ^{d}
	4 wk	30.1 ± 0.7 ^{c}	7.7 ± 1.3 ^{ab}	11.2 ± 1.1 ^{d}
Cold storage	1 wk	31.1 ± 1.3 ^{abc}	7.0 ± 1.0 ^{ab}	10.6 ± 1.8 ^{d}
	2 wk	30.6 ± 0.6 ^{bc}	7.4 ± 0.6 ^{ab}	10.5 ± 0.7 ^{d}
	3 wk	30.6 ± 0.3 ^{bc}	8.3 ± 0.3 ^{a}	11.1 ± 0.7 ^{d}
	4 wk	30.2 ± 0.6 ^{bc}	7.2 ± 1.7 ^{ab}	9.7 ± 1.6 ^{d}
IQF	1 wk	32.3 ± 0.9 ^{a}	8.5 ± 2.3 ^{ab}	15.3 ± 2.1 ^{abc}
	2 wk	32.6 ± 1.0 ^{a}	7.7 ± 1.4 ^{ab}	16.2 ± 0.4 ^{a}
	3 wk	32.7 ± 1.2 ^{a}	7.6 ± 1.6 ^{ab}	16.0 ± 0.9 ^{ab}
	4 wk	32.6 ± 0.6 ^{a}	8.2 ± 1.9 ^{ab}	15.5 ± 2.5 ^{abc}
Isob. -2.5°C	1 wk	31.8 ± 1.9 ^{abc}	8.9 ± 1.7 ^{ab}	15.3 ± 1.3 ^{abc}
	2 wk	32.4 ± 1.2 ^{a}	6.6 ± 1.7 ^{ab}	14.3 ± 1.0 ^{bc}
	3 wk	29.5 ± 2.5 ^{abc}	7.8 ± 1.8 ^{ab}	13.8 ± 0.3 ^{bc}
	4 wk	31.3 ± 1.2 ^{abc}	7.3 ± 1.5 ^{ab}	12.5 ± 1.4 ^{bc}

IQF= Individual Quick Freezing
For each column, values followed by the same letter (a–d) are not statistically different at $p < 0.05$

Cryo-SEM images

Cryo-SEM images were taken to visually probe the effects of different preservation techniques on tomato cell structure after 4 weeks preservation. Figure 5.10 shows the transverse section of a fresh tomato fruit with both the skin and inner parenchyma cells. Tomato "skin" or peel is composed of a thin layer of epidermal cells and several layers of relatively small, flattened cells. Parenchyma cells are polyhedral, and manifest in various sizes and shapes. They appear much larger than skin cells and are separated by several intercellular spaces. The tissue of tomatoes preserved under isochoric conditions was similar to that of the fresh sample; the cells remained intact, although the intercellular spaces appeared filled with fluid, likely indicating the occurrence of some degree of cell injury (Fig 5.11A). The microstructure of samples stored for 4 weeks at 10°C is presented in Fig. 5.11B., and clearly displays extensive folding and corrugation of the cells and collapse of nearly all intercellular spaces. For IQF samples, some cells in the parenchyma tissue appeared completely disrupted, whereas others appeared to maintain their structure (Fig. 5.11C). Finally, complete morphological disruption occurred for tomatoes preserved under isobaric conditions (Fig. 5.11D).

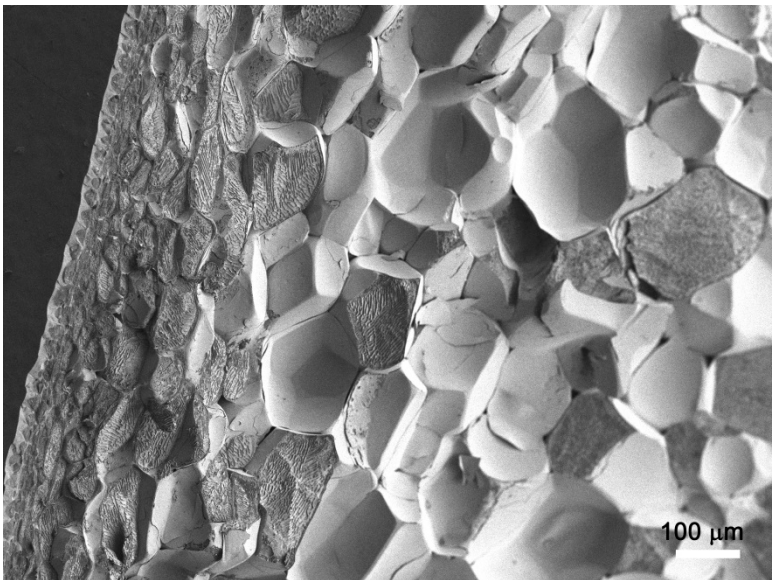

Figure 5.10. Cryo-SEM image of fresh grape tomato tissue.

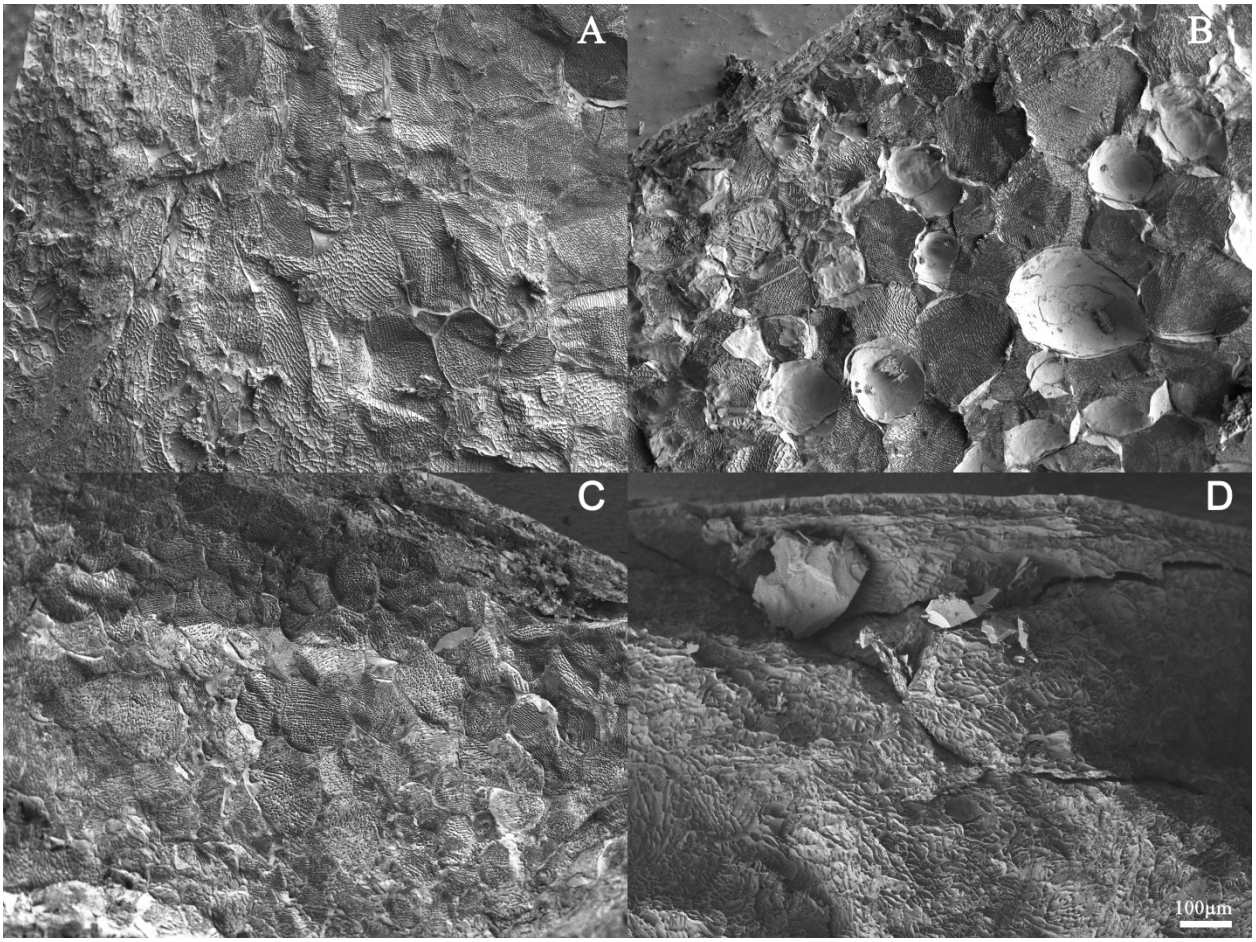

Figure 5.11. Cryo-SEM images of tomato tissue preserved for four weeks (A) in an isochoric system at -2.5°C, (B) in cold storage at 10°C and 85% RH, (C) in a freezer at -20°C after IQ freezing, (D) in an isobaric system at -2.5°C.

Texture

The fracture force and elasticity of fresh grape tomatoes were determined to be 26.3 ± 7.7N and 0.16 ± 0.06MPa, respectively. As shown in Fig. 5.12, isochoric tomatoes retained an acceptable degree of mechanical integrity. The fracture force decreased in value by roughly 20% after the first week of preservation, and no further significant changes in this value were observed during the ensuing three weeks of preservation (Fig. 5.12A). Furthermore, tomatoes preserved under isochoric conditions showed no significant difference in elasticity values when compared to that of fresh tomatoes (Fig. 5.12B). Tangwongchai, Ledward and Ames demonstrated that textural damage in tomatoes increased with higher hydrostatic pressures in the pressure range 200-600 MPa[192], concluding that initial damage was caused by the greater compressibility of the gaseous phase (air) present within the fruit compared to the liquid−solid components. They suggested that when the pressure is released, the rapid expansion of the air may damage the compressed matrix and yield an increase in membrane permeability, permitting egress of water and enabling enzymatic action that causes further cell damage and softening. Therefore, the initial softening of the isochoric tomato samples may be due to a change in cell membrane permeability, resulting in mild loss of cell turgor. However, the stability of the textural properties over time may also indicate low enzymatic action, and further study is needed to clarify the pressure-dependent mechanisms of damage at these comparatively low pressures.

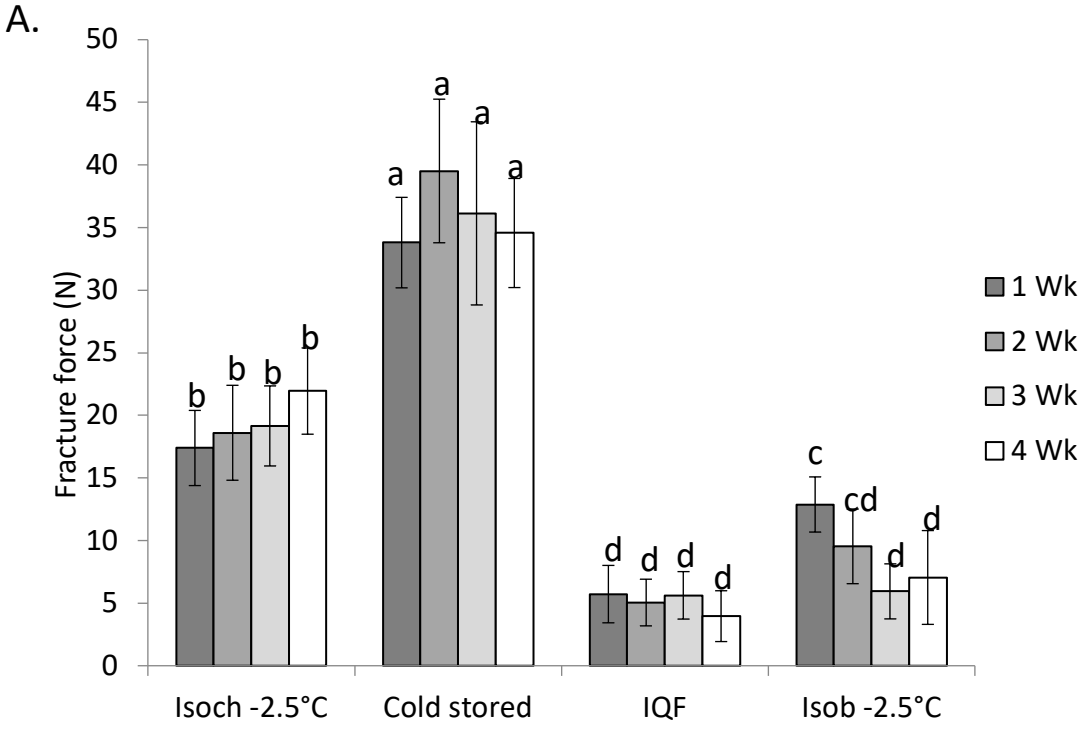

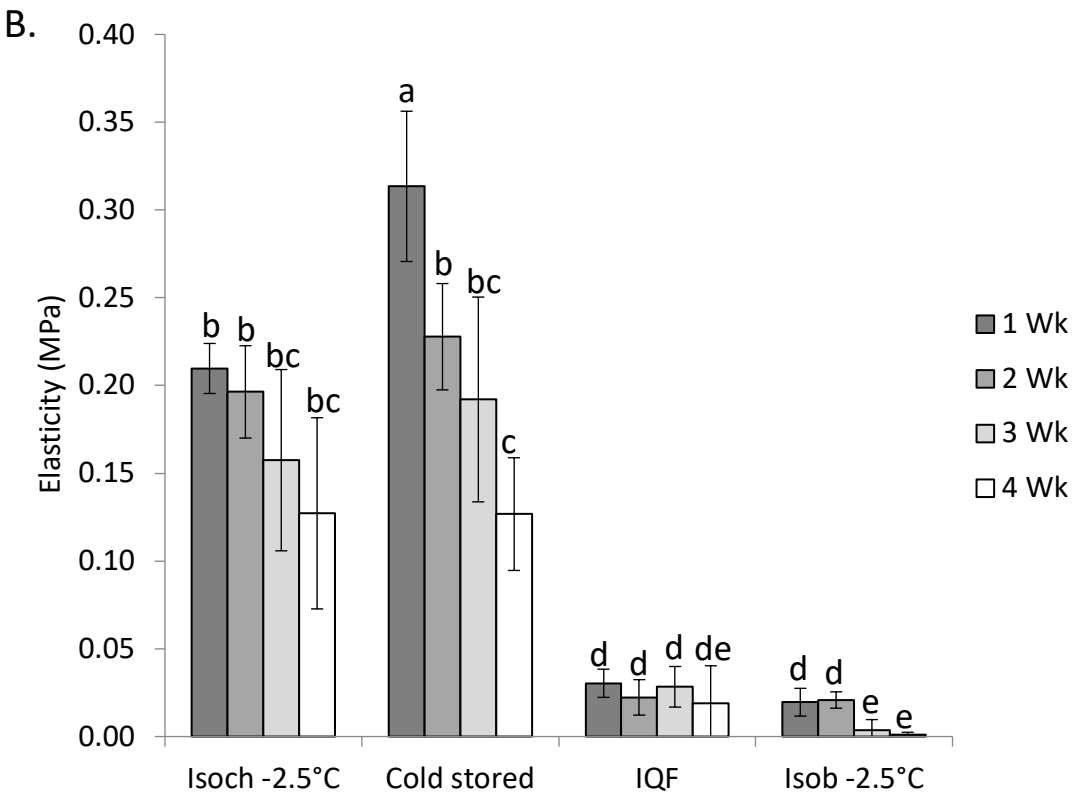

Figure 5.12. Effects of preservation methods on the (A) fracture force and (B) elasticity of preserved tomatoes under different conditions. The same letter indicates no significant differences between treatments at 95% confidence interval.

Figure 5.12 also shows that tomatoes preserved for one week in 10°C cold storage grew harder and more elastic than fresh tomatoes. However, these samples then softened with continued storage, suggesting two potentially opposing factors that might have affected their texture: Firstly, an increase in sample consistency due to the loss of water may have contributed to an increase in fracture force and elasticity. Secondly, softening due to natural ripening may have decreased these same properties. Therefore, the prolonged effects of ripening may have counteracted the effects of the increased consistency developed after the first week. Chylinska et al. reported that softening during ripening occurs due to the breakdown of carbohydrates in the cell wall and the increase in soluble pectin substances, resulting in weakening of the cell walls and reduction of cohesive forces binding the cells together[193].

IQF and isobaric freezing caused the greatest change in textural properties, with tomatoes showing serious morphological damage and exhibiting lower fracture forces and greater elasticity losses (Fig. 5.12), likely due to the ice-related disruption of cell membranes and tissue integrity. To this effect, Lisiewska & Kmiecik reported significant reduction of protopectin and pectin levels in tomato tissue after freezing and subsequent frozen storage[190], and Fuchigami, Miyazaki, & Hyakumoto also observed that the inferior texture of frozen tomatoes was accompanied by a decrease in the content of pectic compounds[194]. Although rapid freezing (as achieved in IQF) is generally regarded as the best technique to maintain the texture of frozen food products, recrystallization could have occurred during prolonged storage, and freeze-thaw cycles can lead to

further release of pectin and reduction in the degree of esterification due to activation of pectin methylesterase via cell damage, resulting in softening of the fruit[195].

Ascorbic acid content

The ascorbic acid content of fresh grape tomatoes was determined to be 196 ± 21 mg/100g d.m., consistent with values previously reported in literature[196]. Tomatoes preserved under isochoric conditions fully retained their ascorbic acid contents over four weeks (Fig. 5.13). By comparison, samples under cold storage showed a slight increase in ascorbic acid content after 2 weeks, potentially due to the ripening process[187,197], and thereafter remained constant; IQF samples lost 17% ascorbic acid content after 2 weeks, and thereafter remained constant; and isobaric samples retained only 10% of their initial ascorbic acid content by the end of the 4-week storage period. This reduction in vitamin C content after conventional freezing could be due to ascorbic acid degradation via ascorbic acid oxidase, as well as due to drip losses after thawing, in which water may act as a carrier agent[190].

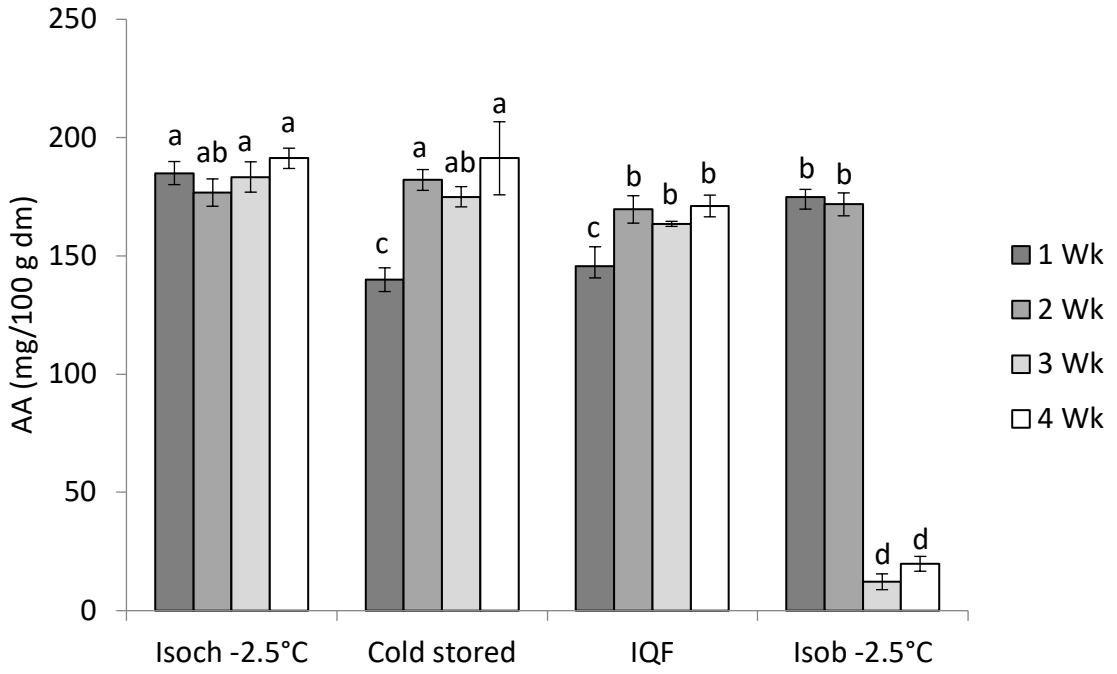

Figure 5.13. Ascorbic acid contents of preserved tomatoes using different preservation methods. The same letter indicates no significant differences between treatments at 95% confidence interval.

Lycopene content

Lycopene content is an important contributor to the nutrition index of tomato products due to its strong antioxidant activity[198], and it furthermore provides the signature red color expected of tomatoes. The lycopene content of fresh grape tomatoes was determined to be 675 ± 18 mg/ kg d.m., consistent with previous reports[190]. Tomatoes preserved under isochoric conditions retained 90% lycopene content after 4 weeks of treatment (Fig. 5.14), indicating that prolonged exposure

to enhanced hydrostatic pressure applied does not significantly affect lycopene degradation. By comparison, lycopene content decreased by 25% after two weeks of cold storage (with no significant changes thereafter), and lycopene losses after the full preservation period reached 67% and 52% for the IQF samples and isobaric samples respectively. This reduction in lycopene content may be related to the changes in color discussed previously; within the literature, 48% to 59% lycopene losses had been reported for tomatoes stored at -20°C for 12 months[166], and it has been suggested that the losses are due to enzymatic activity, particularly in oxygen-containing environments[199]. Lycopene is highly unsaturated and is susceptible to oxidation in the presence of enzymes such as peroxidase, catalase and lipase in tomatoes[166,200].

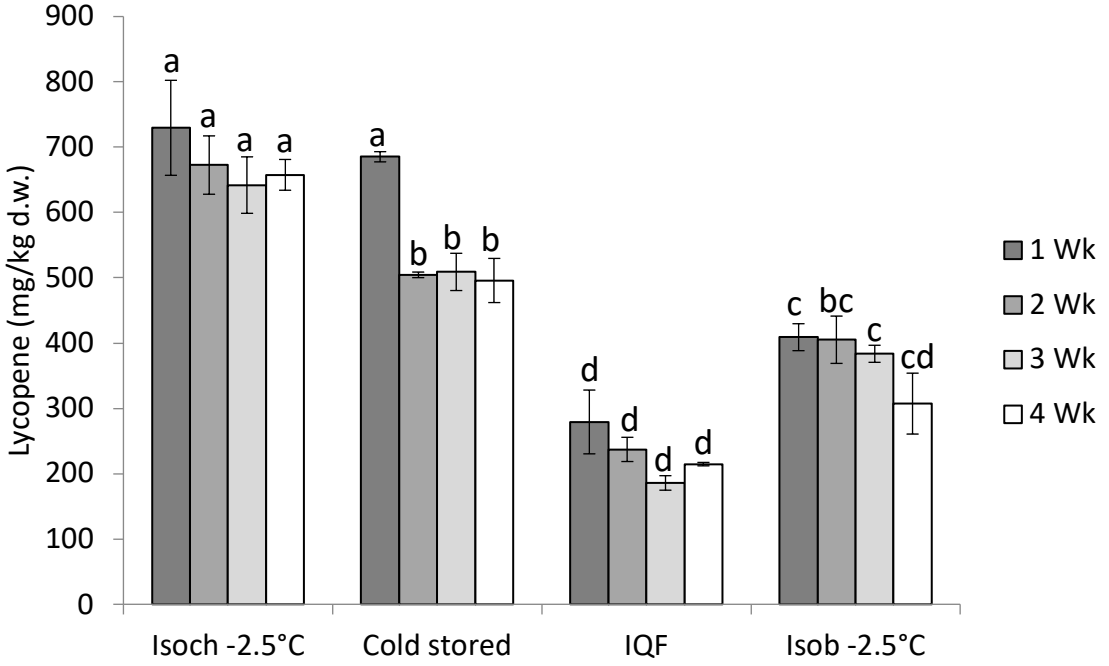

Figure 5.14. Lycopene contents of preserved tomatoes using different preservation methods. The same letter indicates no significant differences between treatments at 95% confidence interval.

Total soluble phenolic content and antioxidant activity

Fresh grape tomatoes were found to have a TSP value of 6.2 ± 0.7 mg GAE/g d.m, consistent with previous reports[201]. Isochoric tomatoes showed a statistically insignificant decrease in TSP value (12%) after 4 weeks of treatment (Fig. 5.15A), while final TSP retention after the same period was 52%, 40% and 18% for cold storage, IQF and isobaric samples respectively. During cold storage and freezing, the structure of the tomato became disrupted, driving the liberation of peroxidative and hydrolytic enzymes such as peroxidase and polyphenoloxidase, which reduce TSP content.

Antioxidant activity in fresh tomatoes was determined to be 16.6 ± 2.3 mg TE/g d.m. Toor & Savage[202] reported that soluble antioxidants, principally ascorbic acid and soluble phenolics, contributed 92% of the total antioxidant activity of tomatoes, whereas the lipophilic antioxidants,

mainly lycopene and lipophilic phenolics, contributed only about 8% of the total antioxidant activity. Freezing at -2.5°C under isochoric conditions did not result in significant changes in antioxidant activity (Fig. 5.15B), while samples preserved using all other techniques showed a gradual decrease in antioxidant activity over time due to the degradation of bioactive compounds.

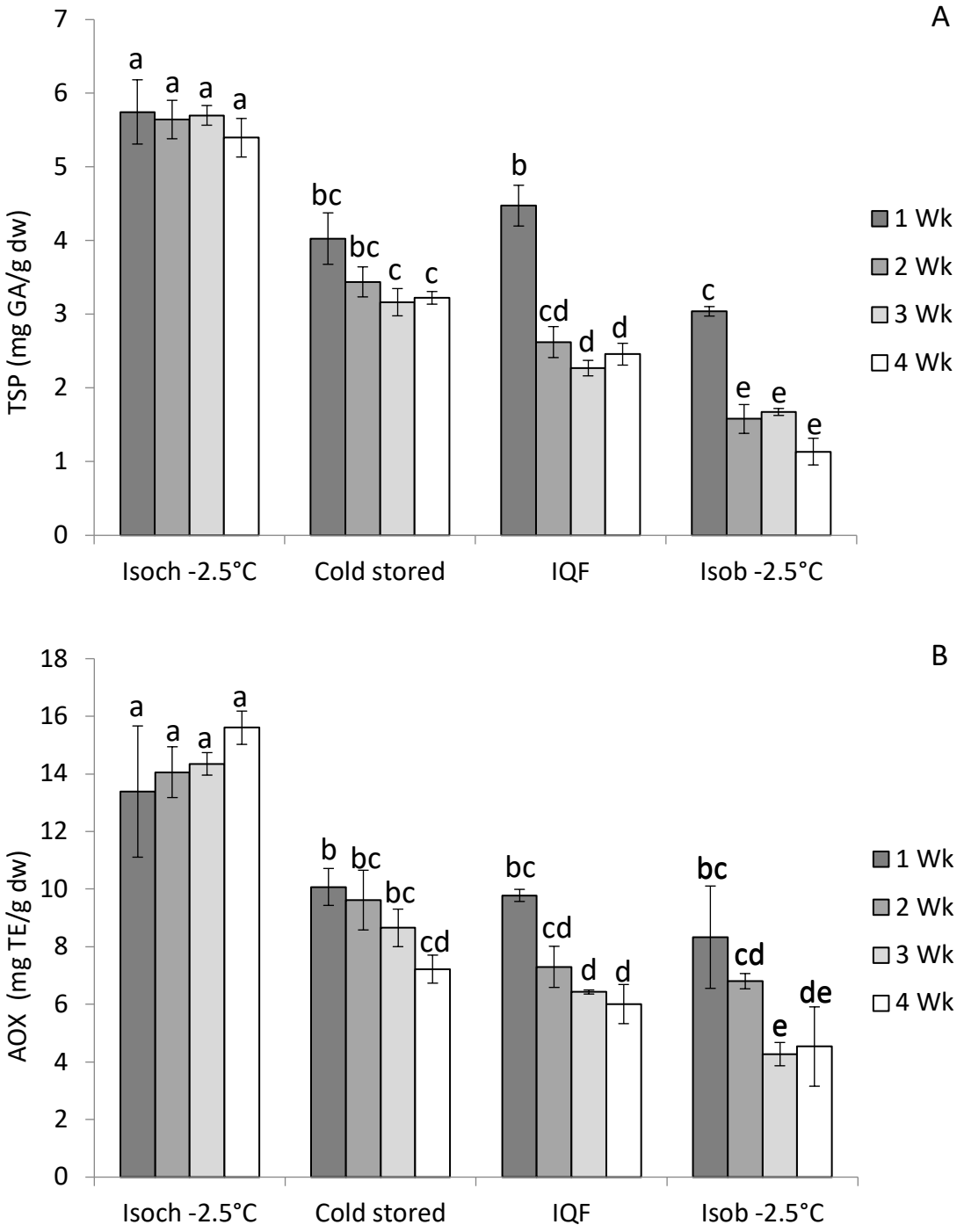

Figure 5.15. Total Soluble Phenolic (TSP) contents (A) and Antioxidant activity (AOX) of preserved tomatoes using different preservation methods. The same letter indicates no significant differences between treatments at 95% confidence interval.

Results in Sum

Isochoric preservation yielded significant improvements in the long-term stability of tomato quality compared to various conventional preservation techniques currently employed in industry, including cold storage at 10°C and individual quick freezing (IQF). Tomatoes preserved at -2.5°C in an isochoric system showed the most desirable sensory characteristics in terms of mass, shape, volume, color and textural properties, with minimal deviations from the fresh unpreserved fruit, and isochoric freezing further preserved tomato ascorbic acid content, lycopene content, phenolic compounds, and antioxidant activity. in tomatoes since cell compartmentalization remained in place during preservation. The success of this preservation method is driven by the absence of ice crystal formation and the low processing pressures required, which served to minimize cell damage and maintain sufficient cellular compartmentalization, as observed under cryo-SEM. To our knowledge, isochoric freezing represents the first stable method of preserving tomatoes at this degree of quality for a 4-week time scale.

5.3 Inactivation of foodborne bacterial populations during isochoric freezing

Frozen foods, while essential to the national food chain in hundreds of countries, are a continual driver of foodborne illnesses in the United States and abroad. Frozen berries have been linked to largescale outbreaks of norovirus[203,204] and hepatitis A[205–207], frozen vegetables have been associated with outbreaks of *Listeria monocytogenes*[208–210], and *Salmonella enterica* outbreaks have been previously linked to frozen poultry[211] and seafood[212]. While reduction of temperature can slow bacterial growth and osmotic stresses induced by ice formation can affect the integrity of bacterial cellular structures, freezing on its own does not reduce bacterial populations to unrecoverable levels. Thus, other methods of enhancing bacterial inactivation generally, and in frozen food products specifically, are sought.

In this work, we leverage the unique coupling of reduced temperature and augmented hydrostatic pressure experienced within isochoric systems to investigate the effects of combined hypothermic-hyperbaric conditions on the viability of two pathogenic bacteria often associated with foodborne illness, *L. monocytogenes* and *S.* Typhimurium. Our results reveal a striking enhancement in log-reduction of the bacterial population when moderate low temperatures and moderate elevated pressures are applied simultaneously, demonstrating that the two conditions work synergistically to destroy bacterial populations at rates far greater than those achieved by the application of one condition or the other independently.

5.3.1 Experimental Overview

A full accounting of the materials and methods employed in this study can be found in the Materials and Methods at the end of this section, but will be provided in brief as follows. Bacterial cultures from strains *L. monocytogenes* serotype 4b (ATCC 19115) and *S. enterica* serovar

Typhimurium (ATCC 14028) were grown, washed, and diluted to ~7 log CFU/ml in sterile PBS. One milliliter aliquots of prepared culture were placed in Costar Spin-X centrifuge tubes (Corning) equipped with 0.22 μm flexible nylon membranes to allow for the equilibration of hydrostatic pressure and exchange of fluids during treatments while retaining the bacteria within the tubes. The sample tubes were then sealed in a 316 stainless steel isochoric chamber (pictured schematically in Fig. 5.16a-b) filled entirely with sterile PBS, following the methodology outlined in Bilbao-Sainz et al.[213] with slight alterations. In all experiments, the chamber was submerged in a cooling bath held at constant subzero temperatures +/- 0.1C, and the internal pressure was monitored via digital pressure transducer (Stork Solutions Ltd.). In the first set of experiments, designed to gauge sensitivity to temperature/pressure conditions, bacterial samples were stored at -4 ºC (30 MPa), -7 ºC (65 MPa), and -15 ºC (135 MPa) for 24 hours each. In the second set, designed to gauge sensitivity to exposure time, samples were stored at -15 ºC for 1, 2, 3, 6, 12, and 24 hours. For the purpose of direct comparison, concurrent experiments were conducted for each temperature and time condition under conventional isobaric conditions (e.g. exposed to atmospheric pressure). After treatment, the chamber was warmed for 30 minutes in air at room temperature, and the bacterial solution samples were serially diluted and plated on PALCOM-TAL or XLD-TAL for *L. monocytogenes* or *S.* Typhimurium, respectively. Log reduction of pathogen concentration was then determined by subtracting the concentration of viable bacteria measured post-treatment from the initial concentration measured before treatment. Finally, untreated bacteria samples (controls) and samples frozen at -15ºC for 24 hours under isochoric and isobaric conditions were imaged using transmission electron microscopy (TEM) and field emission scanning electron microscopy (FE-SEM) in order to evaluate any morphological changes or damage to the cell wall. Full sample preparation procedures available in the Materials and Methods.

5.3.2 Bacterial Reduction Results and Hypothesized Mechanisms

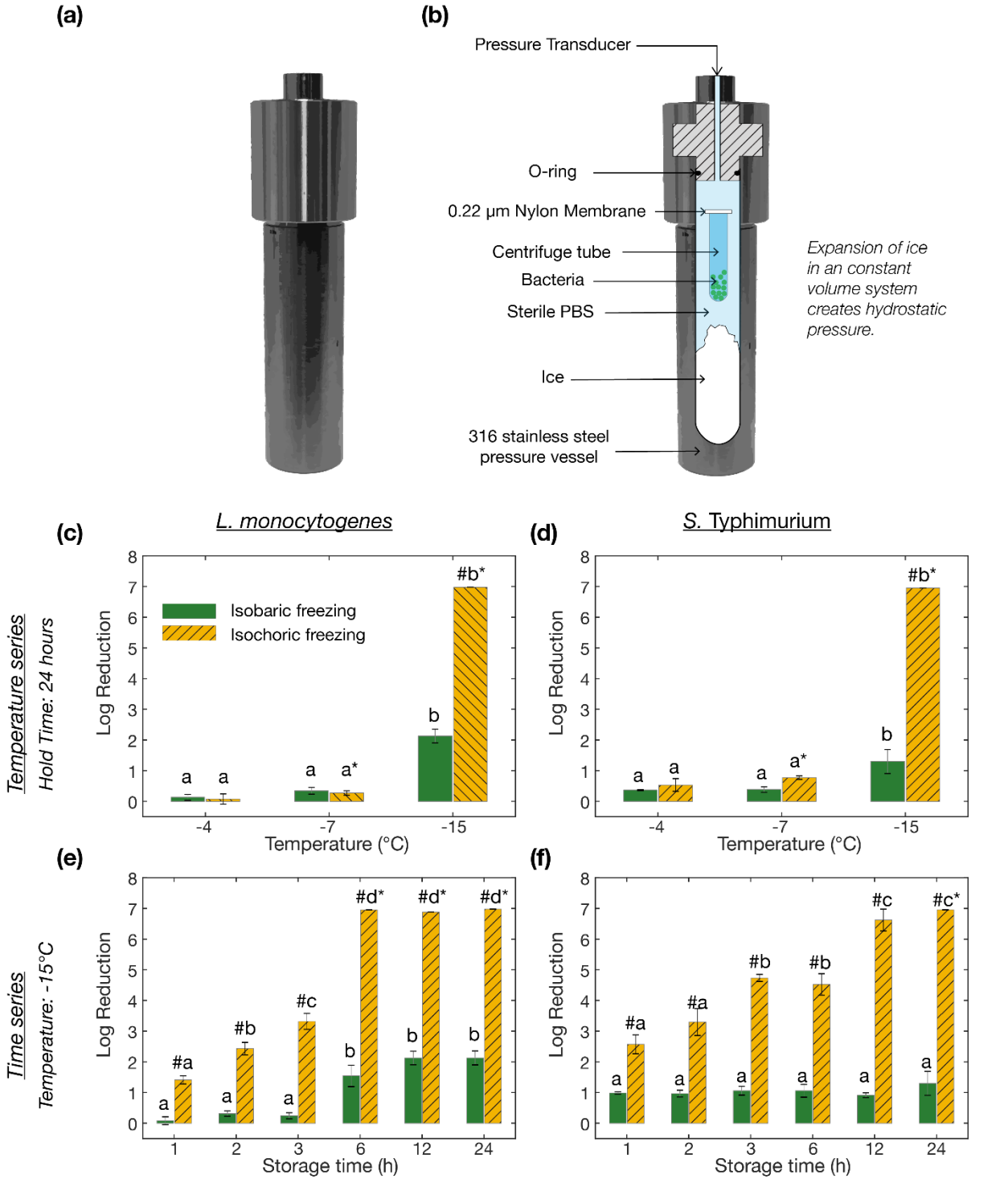

Figure 5.16. Impact of isochoric freezing on bacterial populations. (a) Photo and (b) schematic of a prototypical isochoric chamber. (c) Reduction of *L. monocytogenes* or (d) *S.* Typhimurium after isobaric or isochoric freezing at various temperatures for 24 hours. (e) Reduction of *L. monocytogenes* and (f) *S.* Typhimurium after isobaric or isochoric freezing at -15 ºC for various storage times. Statistically significant ($P < 0.05$) differences in bacterial reduction between the two freezing methodologies at each temperature

are indicated by the # symbol. Significant differences in bacterial reduction observed between exposure temperatures for each methodology are signified by differing letters (a or b). Reduction of bacteria below recoverable levels are noted with a * symbol.

Bacterial reductions after isochoric and isobaric freezing at -4 ºC, -7 ºC, and -15 ºC for 24 hours are shown in Figures 5.16c and 5.16d. At -4 ºC and -7 ºC reduction of both *L. monocytogenes* and *S.* Typhimurium were < 1 log for both isochoric and isobaric freezing methods. However, at -15 ºC (135 MPa) the isochoric system reduced both pathogens to below recoverable levels (> 7 log), while conventional isobaric freezing at atmospheric pressure yielded average log reductions of only 2.1 for *L. monocytogenes* and 1.3 for *S.* Typhimurium. Bacterial reductions as a function of storage time at -15 ºC are shown in Figures 5.16e and 5.16f. Maximum reductions of *L. monocytogenes* and *S.* Typhimurium under isochoric conditions were achieved after for 6 and 12 hours, respectively. Furthermore, isochoric freezing at -15 ºC (135 MPa) achieved dramatically higher levels of bacterial reduction at all tested timepoints for both species of bacteria compared to conventional freezing at -15C and atmospheric pressure, which failed across test conditions to produce reductions approaching the 5 log measure recommended as sufficient by the FDA.

TEM and FE-SEM images of *S.* Typhimurium cells that were untreated (nonfrozen control) and cells frozen (24 h at -15 ºC) under isobaric or isochoric conditions are presented in Figure 5.17. Overall, no morphological differences can be detected between the healthy controls and samples frozen under conventional isobaric conditions. However, *S.* Typhimurium cells exposed to isochoric freezing were noticeably deformed and shriveled (FE-SEM), and featured regions in which the cytoplasm had separated from the cell wall (TEM). Isochoric freezing of *L. monocytogenes* did not appear to cause same level of cellular deformity (Fig. 5.18), despite the similar reduction in population, which could be due to the fundamental differences between the *L. monocytogenes* (gram positive) and the *S.* Typhimurium (gram negative) cell wall structures.

The distinct inability of conventional isobaric freezing to significantly reduce bacterial population suggests that neither cold stresses nor the osmotic gradients encountered during the freezing process nor mechanical interactions with ice crystals provide substantial mechanisms of damage to either of the bacteria considered. Conversely, treatments with enhanced pressure (e.g. high-pressure processing) are well known to have a strong antimicrobial effect and are employed in a variety of industry contexts, but typically require 400-600 MPa to achieve bacterial reductions below recoverable limits[214–216]. Thus we conclude that the reduced temperature and enhanced pressure encountered in the isochoric system work synergistically to yield bacterial reductions disproportionate to those provided by either condition independently.

The precise mechanism of hypothermic-hyperbaric damage is unclear, but may be due to competing physiological responses to cold and pressure. In bacteria, the cold shock response is highly conserved and is characterized by homeoviscous adaptation. This results in an increase in the proportion of unsaturated fatty acids in membrane lipids, which helps the membranes to retain adequate fluidity at lower temperatures[217]. Pressure tolerance is also influenced by membrane fluidity however, and the proportion of *saturated* fatty acids, specifically cyclopropanes, is thought to enhance resistance to high pressures[216]. While the cumulative susceptibility of a bacterial cell to these combined stresses of course cannot be explained simply by the fatty acid composition in the cell membrane, this suggests that physiological responses due to distinct stressors (e.g. cold and pressure) may yield mutually antagonistic or compromising effects. It should be further noted

that treatments with high pressure in industry are typically short (on the order of minutes minutes), and it is unclear what relative role the prolonged exposure (>1 h) used in this study may have had on bacterial mortality.

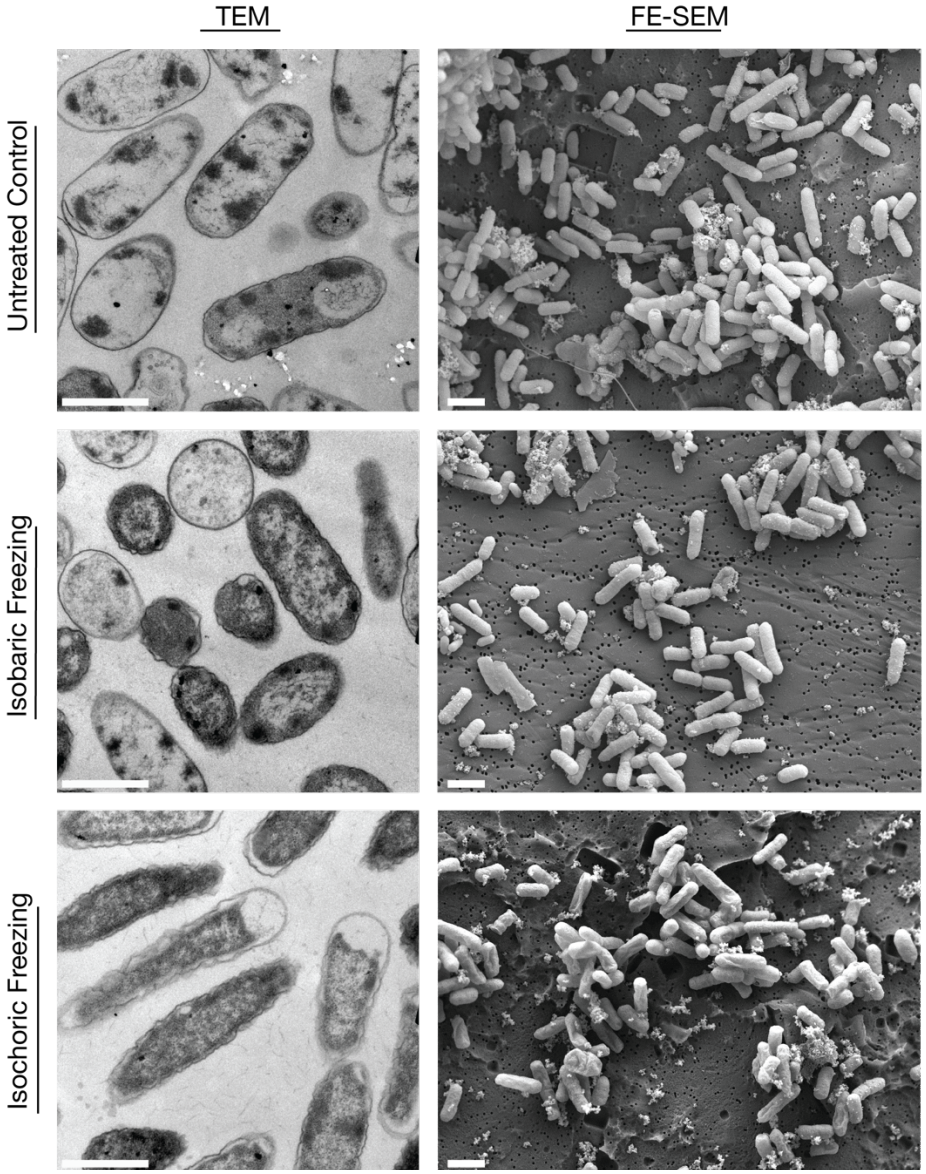

Figure 5.17. Transmission electron microscopy (TEM) (left) and field emission scanning electron microscopy (FE-SEM) (right) images of *S.* Typhimurium after (a) overnight growth (no treatment), (b) isobaric freezing at -15°C for 24 hours, or (c) isochoric freezing at -15°C (135MPA) for 24 hours. Bacteria subjected to isochoric freezing show cytoplasmic separation and bulk morphological deformation. Scale bars indicate 1 μm for TEM images and 2 μm for FE-SEM images.

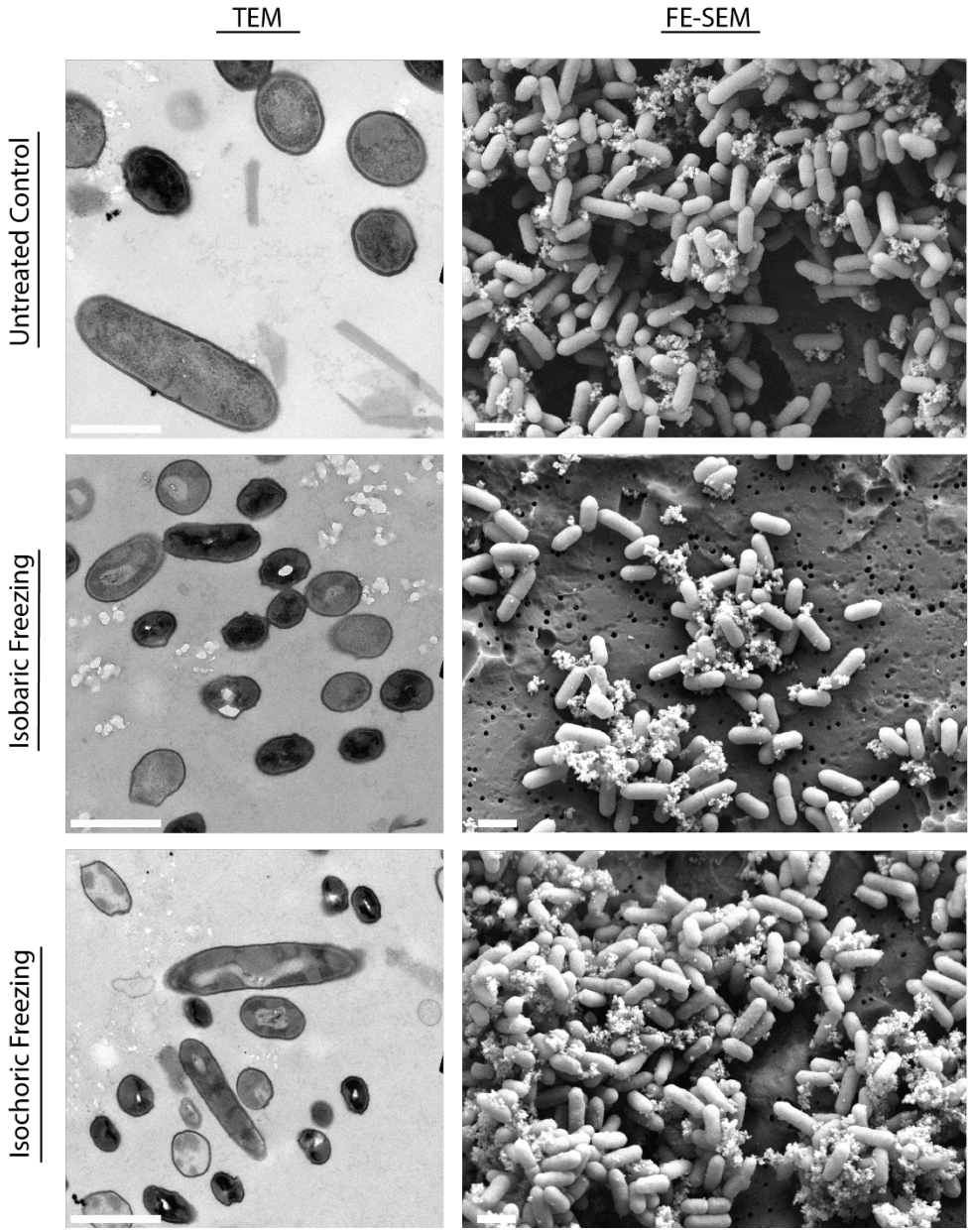

Figure 5.18. Transmission electron microscopy (TEM) (left) and field emission scanning electron microscopy (FE-SEM) (right) images of *L. monocytogenes* after (a) overnight growth (no treatment), (b) isobaric freezing at -15°C for 24 hours, or (c) isochoric freezing at -15°C (135MPA) for 24 hours. Scale bars indicate 1 μm for TEM images and 2 μm for FE-SEM images.

The results of this study suggest the existence of a previously unrealized mechanism of hypothermic-hyperbaric damage that may help to inform next-generation sterilization protocols for frozen food products. Furthermore, the easy experimental realization of enhanced pressures at reduced temperatures in isochoric systems, coupled with recent studies demonstrating their potential for high-quality food preservation, suggest that isochoric freezing may present a method with which sterilization and long-term preservation may be combined. Future work should both further probe the exact hybrid mechanism of cellular damage, incorporate bacterial inactivation studies into long-term isochoric preservation protocols of various food models of interest, and

examine potential energy savings that may be gleaned by the elimination of separate sterilization and preservation processes.

5.3.3 Materials and Methods

Bacterial strains

L. monocytogenes serotype 4b (ATCC 19115) and *S. enterica* serovar Typhimurium (ATCC 14028) were transferred from a frozen stock maintained at -80 ºC to tubes of tryptic soy broth (TSB) and grown overnight at 37 ºC. Overnight cultures were then streaked on slants of tryptic soy agar (TSA) and kept at 4 ºC throughout the study. Before experimentation, 10 ml tubes of TSB were inoculated with either *L. monocytogenes* or *S.* Typhimurium and grown overnight at 37 ºC. The following day, the cultures were centrifuged at 10,000 xg for 15 min and the resultant pellet was resuspended in 1x phosphate buffered saline (PBS). This washing step was repeated and the bacterial concentration (log CFU/ml) of the washed cultures were measured via streak-plating on PALCAM agar or xylose lysine deoxycholate agar (XLD) for *L. monocytogenes* and *S.* Typhimurium, respectfully. Throughout the study, selective agars were overlayed with TSA (TAL method) to help recover sub-lethally injured bacteria as described previously by Wu et al[218].

Isochoric system

The isochoric system used in this study was previously described in detail by Bilbao-Sainz et al[219]. In short, the chamber was made of steel alloy and had a 1 inch (2.54 cm) inner diameter, a total capacity of 66 ml, and was graded for use ≥ - 15 ºC. The pressure in the chamber was actively measured using an electronic pressure transducer (Stork Solutions Ltd) and the system was cooled with a recirculating water bath (VWR AP 15R-40) filled with a water and ethylene glycol (50:50) solution.

Experimental protocol

Bacterial cultures were grown and washed as previously described and diluted to ~7 log CFU/ml in sterile PBS. One milliliter aliquots of prepared culture were placed in Costar Spin-X centrifuge tubes (Corning) equipped with 0.22 µm nylon membranes to allow for the movement of fluid during treatments while keeping bacteria within the tubes. Preliminary work was done to ensure that there was no measurable level of bacterial escape from the tubes during treatment. Following the methodology outlined in Bilbao-Sainz et al[219]. with slight alterations, the treatment column was filled with sterile PBS and the tubes of bacteria with inserted and sealed within the column. The first set of experiments were performed testing microbial reduction in the isochoric system at -4 (30 MPa), -7 (65 MPa), and -15 ºC (135 MPa) for 24 h. Next, the antimicrobial effect of the isochoric system was tested at -15 ºC for 1, 2, 3, 6, 12, and 24 h. For comparison, *S.* Typhimurium and *L. monocytogenes* were concurrently treated with conventional (isobaric) freezing for the same temperatures and treatment times as listed above.

Bacterial recovery and enumeration

After treatment the samples were thawed for 30 min at room temperature and the tubes were removed from the isochoric system. The bacterial solutions were serially diluted and plated on PALCOM-TAL or XLD-TAL for *L. monocytogenes* or *S.* Typhimurium, respectfully. Log reduction of pathogen concentration was then determined by subtracting the concentration of viable bacteria measured post-treatment from the initial concentration measured before treatment.

Transmission electron microscopy (TEM) preparation and imaging

Bacteria without treatment (control) and those frozen using isochoric or isobaric methods at -15 ºC for 24 h were selected for transmission electron microscopy (TEM) examination. Bacteria samples were preserved overnight in standard fixative (2.5% glutaraldehyde, 2% formaldehyde, 2.5 mM $CaCl_2$, in 0.1 M sodium cacodylate; pH 6.9), washed with 0.1 sodium cacodylate for 20 min three times, and stained with 1% osmium tetroxide for 2 h. After staining, the samples were washed with 0.1 sodium cacodylate for 20 min three times and dehydrated with an acetone series (30%, 50%, 75%, 95%, 100%, 100%, 100%; 30 min each). The dehydrated samples were embedded in Spurr's resin and hardened for 1 day at 40 ºC followed by 1 week at 60 ºC. Ultrathin-sections were made of the embedded samples using a microtome and transferred to 200-mesh copper grids. The sections were stained with 2% uranyl acetate for 30 min in the dark followed by 0.5% lead citrate for 1 min. After staining, the samples were viewed using a JOEL 1200 transmission electron microscope.

Field emission scanning electron microscopy (FE-SEM) preparation and imaging

Bacteria without treatment (control) and those frozen using isochoric or isobaric methods at -15 ºC for 24 h were selected for field emission scanning electron microscopy (FE-SEM) examination. The samples were preserved, rinsed, and stained with OsO_4 as described previously , dehydrated with an ethanol series (30%, 50%, 75%, 95%, 100%, 100%, 100%; 30 min each), filtered onto 0.22 µm polycarbonate filters, and dried in CO_2 with a Tousimis AutoSamdri Critical Point Dryer. After drying, the bacterial samples where sputter-coated with gold/palladium using a Denton Desk II Sputter Coating Unit and viewed using a JOEL 7900F (JEOL) field emission electron microscope.

Statistical analysis

All experiments were performed in triplicate and statistical analysis was performed using JMP (ver.12) software with $\alpha = 0.05$. One-way ANOVAs coupled with Tukey's HSD post-hoc tests were used to determine significant differences in reductions across treatment temperatures or hold times for each freezing methodology. The antimicrobial efficacies of isochoric and isobaric methodologies were compared at each treatment condition using paired t-tests.

5.4 Energy use reduction via isochoric freezing in the food storage domain

In addition to enhancing the efficacy of low-temperature food preservation techniques from a biological stand-point, which may reduce food waste and help to ease market constraints on the fresh fruits and vegetables essential to global nutrition, we must also consider the efficiency of cold storage from an energy consumption standpoint.

Cold storage is the most prominent method of preventing post-harvest food losses and the spread of foodborne disease globally, with an estimated 1.6 billion refrigeration and freezing units deployed for this purpose. It accounts for roughly 8% of global electricity consumption [220,221] and given rapid population growth and the economic advancement of large developing countries, this number is expected to rise sharply in the near future [220]. Furthermore, increasing global temperatures exacerbate the need for cold storage while simultaneously highlighting the importance of reducing its carbon footprint [222]. It is thus recognized that increasing the energy efficiency of food cold storage processes should be a key goal for both the public and private sectors [220–223].

The efficiency of frozen food storage can be considered in two phases: the freezing efficiency and the storage efficiency. The freezing efficiency is characterized by the energy required to bring a mass to thermal equilibrium at a given subfreezing temperature. For water-based systems such as food, freezing is a much more energy intensive process than simple cooling—the energy required to freeze a unit mass of water (the latent heat of fusion) is nearly 100 times that required to cool the same unit mass one degree Centigrade. Thus freezers experiencing frequent additions of unfrozen mass, such as those used during industrial food processing, experience lower efficiencies than those used in domestic contexts [224,225]. The storage efficiency is characterized by the energy required to hold a mass of food at a desired subfreezing temperature over long periods, both at permanent storage sites and during transportation, and in the face of controlled and uncontrolled ambient temperature fluctuations. These fluctuations are a principal source of inefficiency in long-term food storage, and also contribute to various detrimental phenomena including moisture migration, bulk weight loss, disruption of microstructure, and poor retention of food-specific nutritional qualities [226–231].

Recent efforts to address these issues have focused primarily on improving heat pump technology [232]. Though vapor-compression devices remain the most common choice for closed-loop cycling of heat, in light of their relatively low efficiencies and the environmentally harmful nature of the required refrigerants, many alternative technologies are being investigated, including those based on caloric effects, thermoelectric, thermoacoustic, and magnetic effects, air cycle and Stirling cycle refrigeration, etc [232,233]. In this study however, we aim to take a fundamentally different approach: instead of trying to increase the efficiency of discrete refrigeration technologies, a method is proposed to alter the fundamental thermodynamics at play in the freezing process itself, increasing the efficiency and temperature stability of cold storage regardless of the device used to facilitate it.

We have discussed at length in this thesis the apparent potential of isochoric to enhance the preservation quality of myriad biological matter, including cherries and tomatoes in the preceding sections of this chapter. Additional recent work from our laboratory, not covered in detail herein for the sake of brevity, has also demonstrated significant enhancement of the preservation quality of potatoes and spinach, and we have furthermore demonstrated in the previous section that isochoric cold storage has the capacity to eliminate potentially harmful bacteria (which we also demonstrate for *E. coli* elsewhere[234]), based on its unique combination of low temperatures and augmented pressures. In the present section, we will present an additional theoretical study of two unique and previously unrealized energetic behaviors of isochoric systems, with the potential to significantly improve the energy efficiency of frozen food storage in both the initial freezing and long-term storage phases. For the initial freezing phase, we demonstrate through fundamental thermodynamic analyses that up to 70% less energy is required to bring isochoric containers with relevant food contents to equilibrium at subfreezing temperatures compared to traditional isobaric containers. For the long-term storage phase, we develop a novel heat transfer model to reveal unique phase change phenomena that enable the coupling of latent and sensible heat effects, effectively increasing the thermal mass of a quantity of food held in an isochoric container by two orders of magnitude relative to the same quantity in an isobaric container. These phenomena provide isochoric systems with exceptional temperature stability when exposed to external temperature fluctuations, which in turn has been shown to reduce the energy consumption of long-term storage and substantially improve the quality of the preserved food.

The simple change in the thermodynamic state in which frozen food is stored, from isobaric to isochoric, requires relatively small changes to current worldwide refrigeration infrastructure, and has the potential to substantially and immediately reduce the energy consumption of frozen food storage while simultaneously improving the quality of the preserved food. The analyses detailed herein present a novel potential path forward in the effort to improve global cold storage, rooted in the fundamental thermodynamics of the freezing process of water.

5.4.1. Principles of freezing food in an isochoric system

The goals of cold storage of food are twofold: to reduce the rate of metabolism, the temperature-dependent process which drives biological degradation, and to provide an environment inhospitable to harmful microorganisms. Traditional freezing often achieves these goals, but at the cost of significant energy consumption, reduced food quality, and bulk weight loss. The root cause of these negative effects is the formation of ice crystals within the food matter, which cause mechanical damage, osmotic damage, dehydration, etc [235]. Isochoric cold storage (ICS) was thus developed with the goal of protecting stored food matter from ice damage while retaining the beneficial effects of storage at temperatures below the freezing point of water.

The traditional thermodynamic premise upon which the modern freezing industry is built considers systems under isobaric conditions; systems at (constant) atmospheric pressure in which the two remaining state variables, temperature and volume, then vary in tandem. Within such a system, an unrestricted volume of water or aqueous solution (or the total water content within a given solid mass of food) will freeze almost completely when held below its phase transition temperature (freezing point). In an isochoric system however, the *volume* is held constant (physically

constrained by a rigid container) and the *temperature* and *pressure* are left to vary in tandem. This fundamental remix of state variables leads to a very different freezing process, as detailed in Chapters 2 and 3 and highlighted conceptually in Fig. 5.19 below.

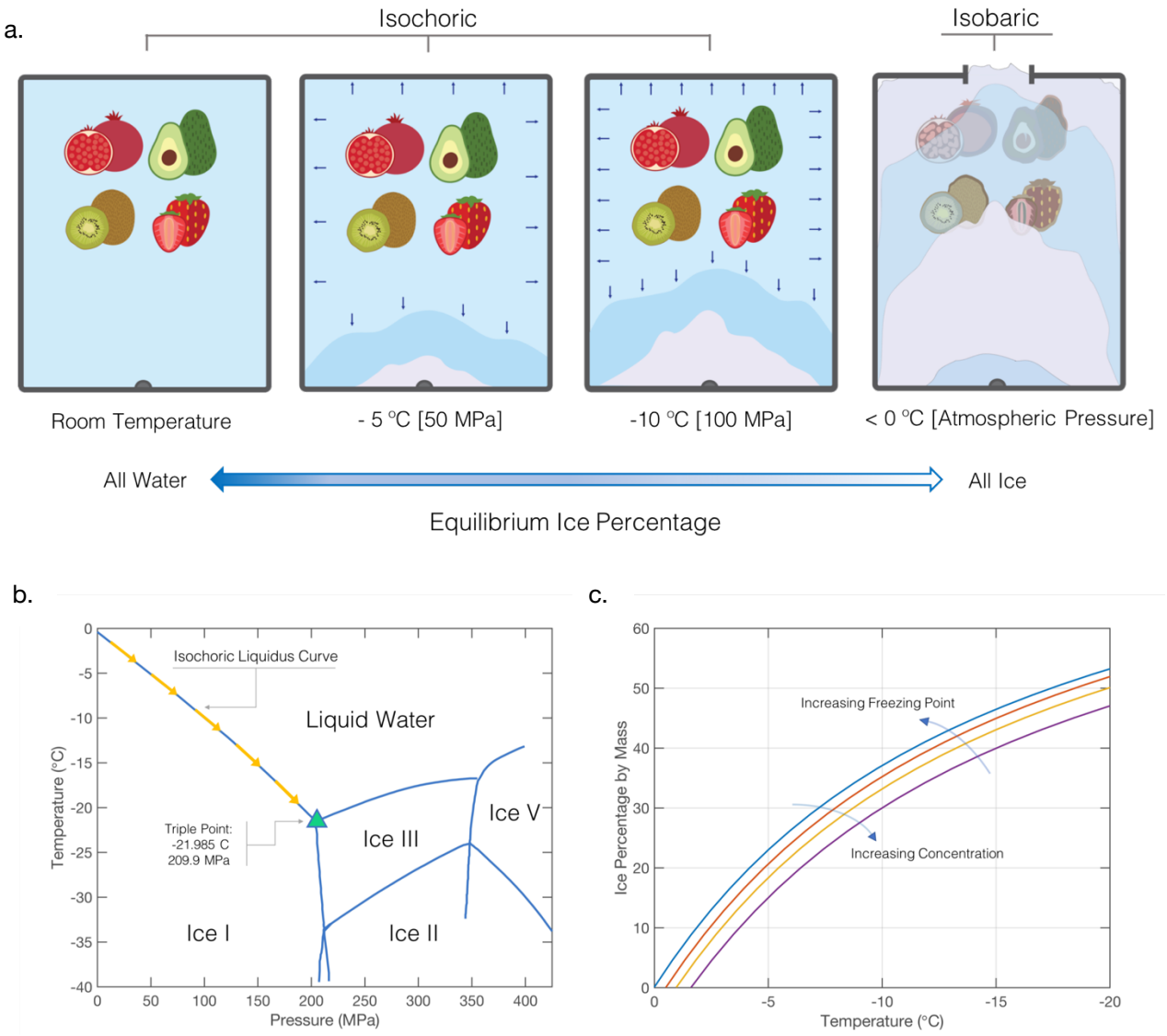

Figure 5.19. Equilibrium states of isochoric systems at various temperatures and comparison to a standard isobaric system frozen at atmospheric pressure. a. Conceptual schematic. b. Phase diagram of water and ice, with the thermodynamic path followed during isochoric freezing indicated by the yellow arrows. c. Variation of the ice mass phase fraction with temperature for solutions of increasing solute concentration.

In practice, isochoric thermodynamic conditions can be achieved in any rigid container that can withstand high pressures (the exact magnitudes of which will vary depending on the target preservation temperature, according to the path highlighted in Fig. 5.19b). Food is typically stored in an isotonic solution inside the isochoric container (a saline solution for meats and fish or a sugar solution for fruits and vegetables, see Fig. 5.19c), and no air is allowed inside the chamber (due to its immense compressibility). While the research-grade isochoric containers used to date are

typically built from thick-walled stainless steel cylinders, there is ample opportunity to design containers out of lighter materials (such as carbon fiber composites or hard phenolic thermosets), depending on the target temperature and pressure, and such containers need not employ a pressure transducer. Essential to understanding the premise of isochoric food storage however is the fact that the thermodynamic conditions described above can be achieved by a very simple transition from an unconstrained volume to a constrained volume— no electricity or moving parts are required, simply ample rigidity and the absence of air within the container.

5.4.2. Comparative thermodynamic analysis of energy consumption during isobaric and isochoric freezing

In this work, the fundamental thermodynamics of isochoric freezing are examined to show that freezing an isochoric system to a given temperature is significantly less energy intensive than freezing a traditional (isobaric) system to the same temperature. For conceptual simplicity we consider herein a mass of water, but it should be noted going forward that these thermodynamic analyses can be applied to any solid food product with high water content (such as fruits or meats) or any liquid food product (such as milk or juices).

To bring a mass of water to equilibrium at a subfreezing temperature in a conventional isobaric system at atmospheric pressure, the following energetic quantities must be considered: the sensible heat required to bring the mass of water from some initial temperature to its freezing point (0°C at atmospheric pressure), the latent heat required to freeze the mass of water at its freezing point, and the sensible heat required to bring the resulting mass of ice to the final subfreezing temperature. If the mass of water is assumed to be pre-chilled to 0°C , the calculation simplifies to:

$$E = m_{total} L(T_0) + m_{total} \int_{T_0}^{T_1} c_{p\_ice}(T)\, dT \qquad (5.7)$$

where E is the energy required to reach equilibrium at a subfreezing temperature T_1, $L(T_0)$ is the latent heat of fusion for water evaluated at 0°C , m_{total} is the total mass of system, and $c_{p\_ice}(T)$ is the temperature-dependent isobaric specific heat capacity of ice. Note that because under isobaric conditions the entire phase transition takes place at the atmospheric freezing point, the temperature-dependent latent heat need not be integrated.

In an isochoric system however, the freezing point decreases as the phase transition progresses, due to the discussed development of internal pressure, and only a portion of the initial mass of water is able to freeze (Fig. 1b). In previous work, a thermodynamic method was developed to calculate the percentage of the total system mass that is converted to ice as a function of temperature, henceforth referred to as $mp_{ice}(T)$ (see Methods for additional detail) [35]. Using this function to relate temperature to the mass percent of ice, an energy statement equivalent to eqn. (5.7) can be developed for an isochoric system:

$$E = \int_{m_1}^{m_2} L(T)\, dm + \int_{T_0}^{T_1} c_{v_{water}}(T) \times m_{total}\left(1 - mp_{ice}(T)\right) dT + \int_{T_0}^{T_1} c_{v_{ice}}(T) \times m_{total} mp_{ice}(T)\, dT \quad (5.8)$$

where it is first recognized that the differential mass dm in the integrated latent heat of fusion term can be rewritten as $dm = m_{total}\, mp_{ice}^{'}(T)\, dT$, allowing integration over the temperature domain:

$$E = \int_{T_0}^{T_1} L(T)\, m_{total}\, mp_{ice}^{'}(T)\, dT + \int_{T_0}^{T_1} c_{v_{water}}(T) \times m_{total}\left(1 - mp_{ice}(T)\right) dT + \int_{T_0}^{T_1} c_{v_{ice}}(T) \times m_{total} mp_{ice}(T)\, dT \quad (5.9)$$

Term by term, eqn. (5.9) thus represents: the integrated latent heat of fusion, the integrated sensible heat loss of the portion of the system that remains liquid, and the integrated sensible heat loss of the portion of the system that becomes ice. It should further be noted the use of the isochoric heat capacity c_v, which differs insignificantly from the isobaric equivalent at 0°C.

To evaluate the potential for energy savings, the ratios of the energy required to freeze identical masses in an isochoric system and an isobaric system were calculated. Fig. 5.20a presents these ratios as a function of final temperature for several solutions of relevance to the food industry. The energy required in an isochoric system is observed to be significantly less than that required for an isobaric system of identical mass. This phenomenon can be attributed to two physical effects: the reduction in total frozen mass and the temperature dependence of the latent heat of fusion of water. As established previously, at any subfreezing temperature higher than the triple point only a portion of the mass in an isochoric system will actually freeze (Fig. 5.19a/b), and thus there is a drastic reduction in the overall energy required for ice fusion. However, the energy required to freeze even that limited portion is also less than would be required for the same portion in an isobaric system, because the latent heat of fusion decreases with temperature. This temperature dependence does not benefit isobaric systems because, as highlighted previously, the entire phase transition takes place at the atmospheric freezing point. In an isochoric system, the freezing point decreases as the phase transition progresses, and thus the energetic requirements of freezing are reduced. At a high level, in terms of latent heat, atmospheric isobaric systems naturally *maximize* the amount of energy required to freeze. Conversely, isochoric systems naturally reduce this energy.

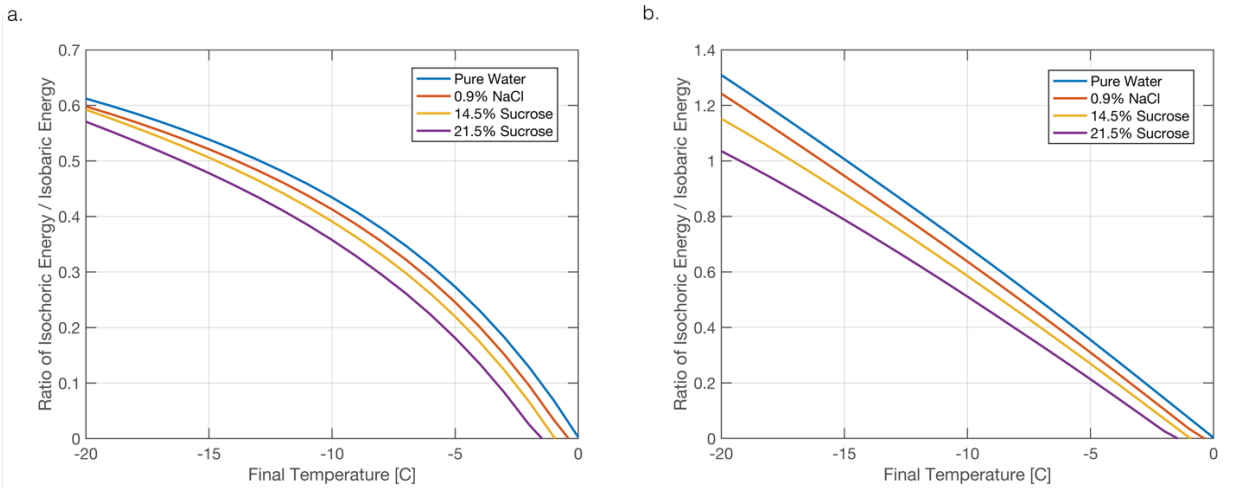

Figure 5.20. Ratio of the energy required to bring a system to equilibrium at subfreezing temperatures between 0 and -20°C under isochoric and isobaric conditions (isochoric/isobaric) for different solutions, including: pure water, saline solution of concentration equivalent to fresh meat or fish, sucrose solution of concentration equivalent to cherries (14.5 brix), and sucrose solution of concentration equivalent to pomegranate (21.5 brix). **a**, Ratios considering two systems of identical size. **b**, Ratios considering an isochoric system sized such that the portion remaining unfrozen at a given temperature is equal to the total size of the isobaric system.

As stated, a central goal of isochoric cold storage at subfreezing temperatures is the protection of preserved food matter from ice formation. However, in the scenario considered in Fig. 5.20a, the isobaric and isochoric system masses are equal, which implies that at subfreezing equilibrium some percentage of the isochoric system will be frozen. Thus in a practical food storage context, the effect of the isochoric system would be to protect only *some portion* of the preserved food matter from ice damage. While this scenario is certainly of industrial relevance, a means of conserving energy while reducing (rather than eliminating) damage, an additional comparison is required to evaluate the energy needed to protect the entire mass of food matter. A new isochoric system is thus considered, incorporating two mass terms: a food mass m_F, defined as the mass of food matter to be protected from ice formation, and a design mass m_D, defined as the total system mass required such that a portion equal to the food mass will remain unfrozen, or $m_D = \frac{m_F}{1-mp_{ice}(T)}$. Substituting m_F and m_D for m_{total} in eqns. (5.8) and (5.9) respectively, the energy requirements are recalculated for an isobaric system of mass m_F and an isochoric system of mass m_D and presented in Fig. 5.20b. This figure reveals an interesting temperature threshold after which the effect of increased total mass overcomes the effect of ice reduction in the isochoric system, making it less efficient than the isobaric. It also further highlights the significant potential for energy savings in isochoric systems in the high subzero temperature range, where the difference in the total degree of ice formation will be most extreme between isochoric and isobaric systems. Differences observed between solutions in both figures are attributed to the freezing point depression that accompanies increased concentration [236].

5.4.3. Heat Transfer with Phase Change Model of Isochoric Freezing

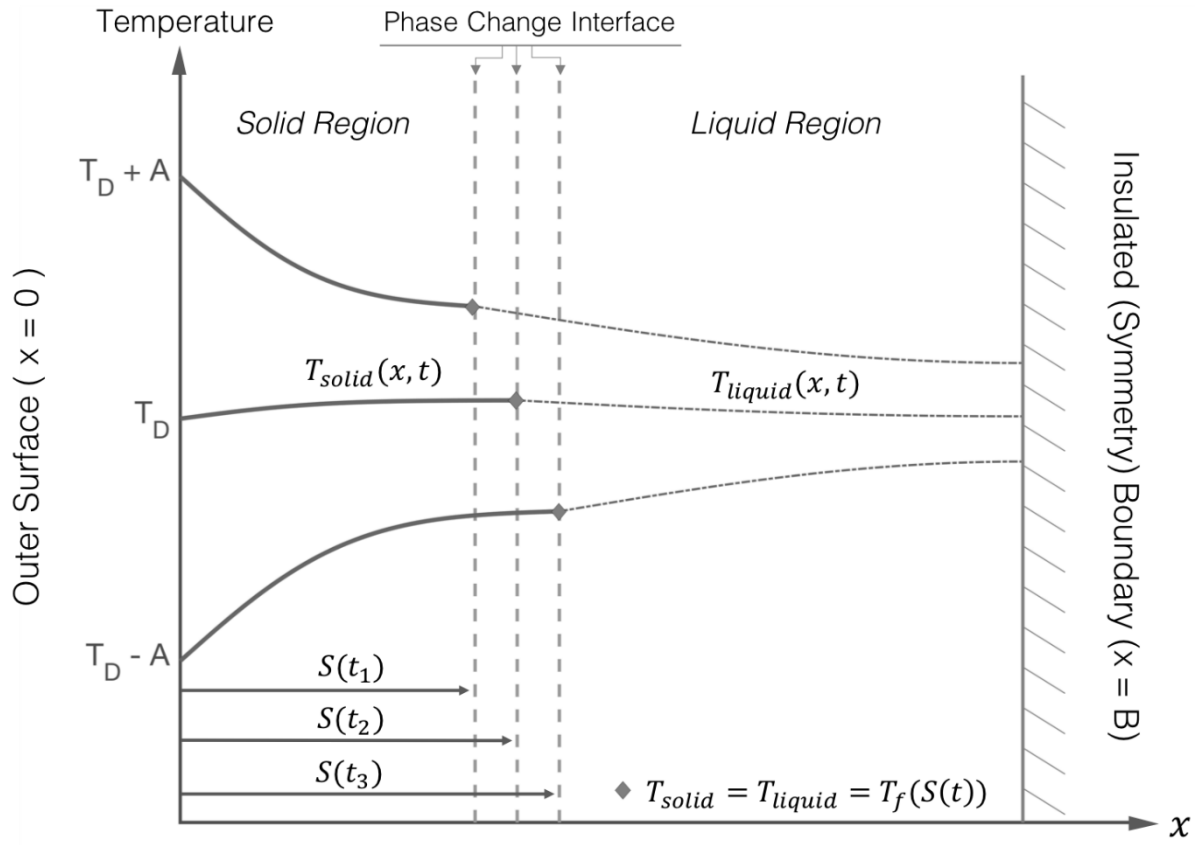

Figure 5.21. Isochoric Phase Change Model: A finite, one-dimensional, two-phase system is considered, bounded by an outer surface with an oscillating prescribed temperature and an insulated (symmetry) boundary. The time-dependent position of the phase change interface is marked by $S(t)$. The domain $0 < x < S(t)$ represents the solid (frozen) region, and the domain from $S(t) < x < B$ represents the liquid (unfrozen) region. The temperature at the interface is the phase change temperature of the system, which varies with interface position.

A novel 1D phase change model is now developed to explore the effects of a steadily fluctuating external temperature on an isochoric system, after the completion of the initial freezing process (Fig. 5.21). The mathematical formulation of this problem for the solid phase is given as:

Solid Region: $$\frac{\partial^2 T_s}{\partial x^2} = \frac{1}{\alpha_s}\frac{\partial T_s(x,t)}{\partial t} \quad \text{in} \quad 0 < x < S(t), \quad t > 0 \qquad (5.10)$$

$$T_s(x = 0, t) = T_D + A\cos(wt) \qquad (5.11)$$

while the liquid phase is given as:

Liquid Region: $$\frac{\partial^2 T_l}{\partial x^2} = \frac{1}{\alpha_l}\frac{\partial T_l(x,t)}{\partial t} \quad \text{in} \quad S(t) < x < B, \quad t > 0 \qquad (5.12)$$

$$\frac{dT_l(x=B,t)}{dx} = 0 \tag{5.13}$$

$$T_l(x, t = 0) = T_s(x, t = 0) = T_D \tag{5.14}$$

The coupling conditions at the interface are:

$$T_s(x = S(t), t) = T_l(x = S(t), t) = T_f(\bar{S}) \tag{5.15}$$

$$k_l \left.\frac{\partial T_l}{\partial x}\right|_{x=S(t)} - k_S \left.\frac{\partial T_s}{\partial x}\right|_{x=S(t)} = \rho L(T_f) \frac{dS(t)}{dt} \tag{5.16}$$

Here the subscripts *s* and *l* indicate properties of the solid and liquid regions respectively, and the parameters are: thermal conductivity k, thermal diffusivity α, liquid density ρ, freezing point T_f, temperature-dependent latent heat of fusion $L(T_f)$, target storage temperature T_D, amplitude of external boundary temperature fluctuation A, frequency of external boundary temperature fluctuation w, and non-dimensional position of the freezing front $\bar{S} = S(t)/B$, in which B is the characteristic length of the system. These formulations resemble those of classic solidification problems in most regards, but feature two key adaptations to reflect isochoric conditions: In isobaric systems, the freezing point T_f is treated as constant, due to the fact that the entire solidification process is assumed to occur at the atmospheric T_f. Here (similar to the previous section), T_f varies as freezing progresses, in 1D as a function of the position of the freezing front $\bar{S}$. The relation $T_f(\bar{S})$ for pure water is calculated using the method of Rubsinky (see Methods) [35]. The temperature dependence of the latent heat $L(T_f)$ is also introduced, which is otherwise typically considered constant.

The problem formulated above was solved using an approximate finite difference approach, (see Methods), ultimately yielding transient temperature profiles for an isochoric system exposed to external periodic temperature fluctuations.

5.4.4. Temperature Stability Results

Steady temperature fluctuations were calculated for dimensionally identical isobaric and isochoric systems of pure water at thermal equilibrium for varying input parameters, including the amplitude A and frequency w of the external temperature oscillation, the desired storage temperature T_D, and the characteristic length of the system (Fig. 5.22a – 5.22c). Calculations for isochoric systems use the specialized model formulated in the previous section, because even at a steady subzero temperature, an isochoric system will consist of two phases in thermodynamic equilibrium with a liquid/solid phase boundary between them. In isobaric systems however, at subzero-temperature equilibrium the entire volume will have frozen, eliminating the need to consider a phase boundary and enabling use of standard steady-periodic slab solutions.

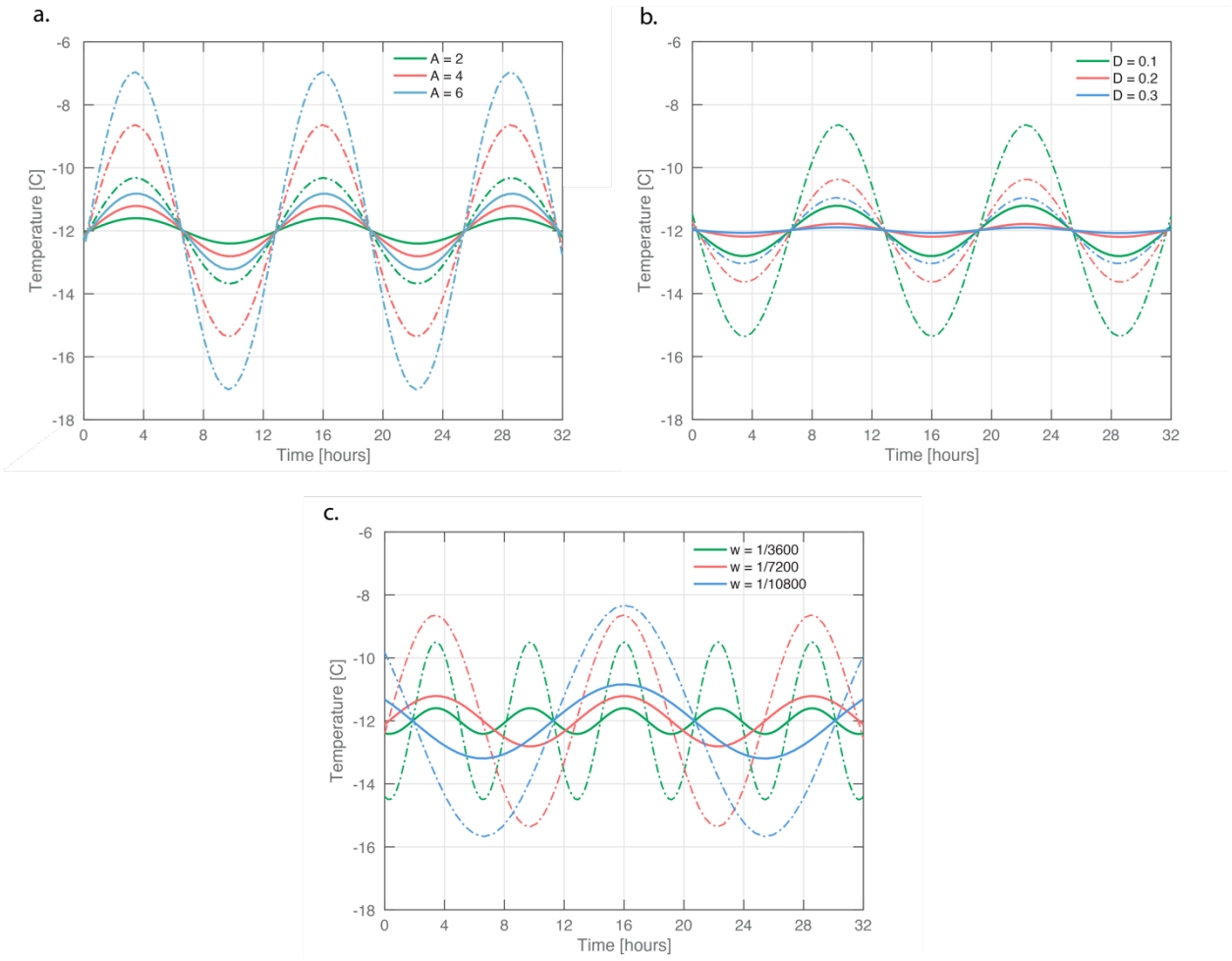

Figure 5.22. Internal temperature fluctuations experienced under isochoric (solid line) and isobaric (dashed line) conditions for various input parameters: **a**, Amplitude is varied. D = 0.1 m; w = 1/7200 s, T_D = -12C. **b**, Characteristic system length is varied; w = 1/7200 s, A = 4C, T_D = -12C. **c**, Frequency is varied; D = 0.1 m; A = 4C, T_D = -12C. *Note: all curves have been phase-shifted in time for ease of comparison.*

Using the data showcased in Fig. 5.22, the effective amplitude of the temperature fluctuation experienced at the center of each system was measured, and ratios of isochoric to isobaric amplitudes are presented in Fig. 5.23a and 5.23b. Both figures reveal that isochoric systems experience *up to an order of magnitude less* internal temperature fluctuation than isobaric systems, and both show a consistent dependence on system size. This is a general reflection of the underlying principal governing the observed temperature stability: because the temperature of an isochoric system held at subzero°C equilibrium will always equal its phase change temperature, the majority of any imparted energy change will be consumed directly by phase change, not sensible temperature change. Thus, as the mass available for freezing increases, the energetic weight of this phase change buffer increase accordingly.

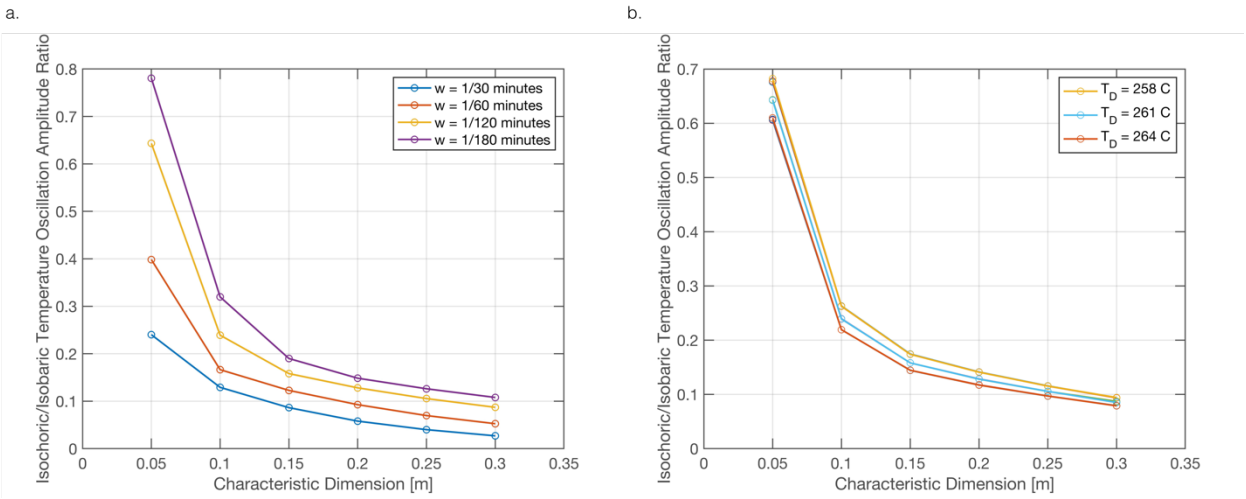

Figure 5.23. Ratios of the amplitude of temperature fluctuation experienced within identical systems under isochoric and isobaric conditions (isochoric/isobaric). **a**, Ratios for an applied amplitude of A = 4C and design temperature T_D = -12C, with varying frequency and characteristic length. **b**, Ratios for frequency w = 1/7200 s, with varying applied amplitude A, design temperature T_D, and characteristic length. Note that curves for varying values of A at a given design temperature appear indistinguishable.

Fig. 5.23a showcases the dependence of the amplitude ratio on the frequency of the applied external temperature fluctuation, suggesting that isochoric systems are increasingly protected against temperature swings as the frequency increases. While food matter will typically encounter lower frequencies (cycles of two or three hours) during long-term storage, exposure to high frequency temperature changes is often experienced during transitions in storage conditions/locations, as food matter moves through the distribution process [237,238]. In Fig. 5.23b, the applied external amplitude appears not to appreciably affect the internal amplitude ratios, but sensitivity to the desired storage temperature is observed, with relative isochoric stability decreasing as T_D decreases. This behavior results from the temperature dependence of the latent heat of fusion, as discussed for the thermodynamic model; because the energy required for phase changes decreases with temperature, the temperature buffer afforded to an isochoric system by continuous phase change also decreases with temperature.

5.4.5. Discussion of implications on industrial cold storage

The thermodynamic considerations of Figure 5.22 reveal that freezing efficiency is substantially increased in isochoric systems, based principally on the naturally reduced ice formation inherent to water-based systems of constrained volume. At -5°C , storage in an isochoric container designed to fully isolate food matter from ice crystallization (Figure 5.22b) could yield up to a 70% decrease in the energy required to freeze meat or fish, with even greater savings available for high sugar foods such as fruits and berries. Furthermore, in an industrial context, these savings represent a lower bound, as they consider only traditional slow freezing; in industry, many foods are first frozen via flash freezing, an energy intensive method employing deep cryogenic temperatures to reduce the size of ice crystals in the interior of the frozen matter [239], and then allowed to warm back to typical freezer temperatures. Because no ice will form within food stored in an isochoric system, such processes would prove unnecessary preceding isochoric storage, yielding further energy savings.

Isochoric cold storage was also found to provide exceptional temperature stability relative to isobaric storage (Fig. 5.23a and 5.23b), reducing the temperature fluctuation experienced by stored food matter by up to an order of magnitude. This stability is the product of a thermodynamic behavior unique to isochoric systems which has not been previously investigated: in an isochoric system, the phase change temperature will always equal the bulk system temperature at equilibrium, effectively coupling latent and sensible heat consumption at all subzero temperatures. In other words, any input of energy into a subzero-temperature isochoric system will cause phase change, no matter the precise subzero value. This differs fundamentally from conventional isobaric systems, in which phase change will only occur at the fixed atmospheric phase change temperature (0°C for pure water), and functions to effectively increase the thermal mass of the isochoric system by two orders of magnitude, or the ratio between the latent heat of fusion and sensible heat capacity of water.

The use of phase change as a buffer against temperature change is well-established in the field of thermal management, and furthermore, exterior phase change materials (PCMs) have recently been proven to increase the efficiency of vapor-compression freezers by increasing thermal mass and reducing the amount of time the compressor must run [240]. These exterior PCMs must be tailored to a specific system based on freezing point however, and introduce new complexity to freezer design. By comparison, the thermal mass effects discovered in this study show that an isochoric system behaves like an inherently optimized version of a traditional phase change material, in which the phase transition temperature dynamically varies alongside the system temperature, maximizing the amount of energy consumed by phase change relative to temperature change for a given energy input. Isochoric storage thus offers the unique advantage of effectively transforming *stored food* contents into phase change materials; in conventional isobaric systems, the stabilizing effects of phase change are lost after initial freezing around 0°C, but in isochoric systems, phase change and temperature change are permanently coupled. Under isochoric conditions, water itself (including that found within solid food products) becomes an effective phase change material (PCM) at all temperatures between 0°C and the triple point, capable of significantly stabilizing temperature and increasing efficiency.

Various studies on increasing the efficiency of refrigeration systems by employing PCMs have demonstrated that by roughly halving temperature fluctuation, energy consumption can be reduced on the order of 10% [241–244]. While a rigorous study of long-term storage efficiency is outside the scope of the present work, the order-of-magnitude reduction in temperature fluctuation seen herein suggests that long-term isochoric cold storage has the potential for exceptional additional energy savings. Furthermore, increased temperature stability has been shown to yield a plethora of other advantages, including resilience during power outages (of particular importance to the economically disadvantaged countries estimated to require the largest future growth in refrigeration infrastructure [220]) , increased ability to avoid power consumption during peak hours, reduction of food spoilage, and protection of food contents from moisture migration, freezer burn, weight loss, and loss of nutritional value [226–229,240].

Although the chief goal of this study is to mathematically demonstrate the existence of these unique thermodynamic features, it is also valuable to view the presented findings in a greater industrial context: ICS presents a method by which global cold storage might be improved without replacing the world's current 1.6 billion food refrigeration and freezing units. From a discrete technological perspective, ICS systems are simply rigid containers filled entirely with a given solution (containing less than 1% air) and capable of withstanding a design pressure based on the desired final temperature; these devices contain no moving parts or electronics and are easily

constructed [5,35,230,231]. Thus, ICS capabilities could potentially be added to any existing freezer—a means of increasing the efficiency and quality of frozen food storage without generating significant appliance waste or requiring major infrastructural changes. ICS is distinct from most emergent refrigeration technologies in this way— it aims to increase efficiency by altering the fundamental thermodynamics at play *within the contents* of the freezer, as opposed to altering the freezer itself.

Conclusions

In this work we present thermodynamic analyses and a heat transfer phase change model to demonstrate mathematically that preserving food matter in an isochoric container can significantly reduce the energy requirements of frozen food storage. This is accomplished by two newly realized thermodynamic phenomena that arise in isochoric systems: the prevention of total freezing of a liquid volume at temperatures between 0 °C and -20 °C and the marriage of latent and sensible heat effects. The energy required to completely freeze a mass of water is nearly 100 times that required to simply cool it to a subfreezing temperature—thus by preventing a large percentage of the water content of stored food matter from freezing in an isochoric system, the energy expenditure of the cold storage process is reduced. Furthermore, we show that within an isochoric container, the internal temperature cannot change without some amount of ice also forming or melting. Thus the contents stored within an isochoric container, which can include liquid food products (such as milk or juice) or solid food products of high water content (such as meat, fish, vegetables, or fruits) immersed in solution, behave like optimized phase change materials, maximizing their effective thermal mass. This increase in thermal mass dramatically increases the temperature stability of the system as a whole, not only improving the storage quality of the products by combatting fluctuation-dependent effects like moisture migration, but also enhancing the efficiency of the freezer in which the isochoric container is stored.

In light of growing food storage demands and increasing global temperatures, new solutions for improving frozen food storage are keenly needed. The unique fundamental thermodynamics of isochoric freezing present a potential pathway toward both more efficient and higher quality food preservation, and warrant significant further research.

5.4.6. Mathematical Methods

Isochoric ice percentage correlations

The function employed to relate ice percentage to equilibrium temperature in the thermodynamic model of isochoric freezing, $mp_{ice}(T)$, was calculated using the method of Rubsinky et al. This method incorporates known pressure-temperature relations for pure water (as available in the phase diagram of water, Fig. 2A) alongside standard compressibility and thermal expansion data in order to estimate the percentage of ice that will exist in an isochoric system at a given equilibrium temperature (and thus pressure) between 0C and the triple point of water, ice I, and ice III. With the addition of solutes the freezing point depression caused by increasing concentration is also incorporated, and the model has been experimentally validated for both pure water and multiple solutions. For easy reproduction, the ice percentage correlation for pure water is provided here:

$$mp_{ice}(T) = -0.0002T^4 - 0.0107T^3 - 0.3088T^2 - 5.8734T. \quad (5.17)$$

The same method is used to produce the function $T_f(\bar{S})$ relating phase transition temperature to freezing front position in the phase change model of isochoric freezing, with slight differences. For the 1D formulation employed, the mass percentage should be converted to a volume percentage in order for $\bar{S} = S(t)/B$ to be equivalent, and the ice volume-temperature data should then be correlated to produce $T_f(\bar{S})$. Note that the temperature values used in this correlation can only be interpreted as phase change temperatures in an isochoric system, in which the equilibrium temperature of the system will always equal its phase change temperature in the temperature domain from 0°C to -21.985°C .

Adaptation of thermodynamic approach for aqueous solutions

In order to apply the thermodynamic approach described in the text to aqueous solutions, the thermal mass of the solutes must also be considered. The presence of solutes will adjust the ice percentage correlation due to the freezing point depression effect associated with increased concentrations, as shown in Fig. 5.20b. The method detailed by Rubinsky [35] includes the capability to account for this effect. Furthermore, the mass considered in eqns. (1 – 3) must be amended to reflect only the mass of water, and an additional integrated sensible heat term should be added to account for the thermal mass of the solute. For example, for a solution of 21.5% sucrose by mass, initially chilled to 0°C , eqn. (3) will be adjusted to:

$$E = \int_{T_0}^{T_1} L(T)\, m_{water}\, mp_{ice}'(T)\, dT + \int_{T_0}^{T_1} c_{v_{water}}(T) \times m_{water}\left(1 - mp_{ice}(T)\right) dT + \int_{T_0}^{T_1} c_{v_{ice}}(T) \times m_{water} mp_{ice}(T)\, dT + \int_{T_0}^{T_1} c_{v_{sucrose}}(T) \times m_{sucrose}\, dT \quad (5.18)$$

Here, the mass of the water plus the mass of the sucrose is equal to the total mass of the system. It should be noted that this method assumes the thermal mass of water and a given solute to be linearly additive. While this is often not strictly the case, small variation in the magnitude of the sensible heat terms will not significantly affect the outcome, as the process of ice 1 freezing in water-based systems is dominated by latent heat effects (ste ~ 0.1).

Solution of the Heat Transfer Model

The model schematic is featured in Figure 5.21. Standard analytical solutions (available in any graduate level heat transfer text) for the temperature distributions in each region are employed, consistent with the governing equations and boundary conditions outlined in eqns. (4 – 8). For the purposes of evaluating these distributions, S is employed as a discrete dimensional parameter that is not time-dependent, which implicitly implies a quasi-steady assumption—e.g. the assumption that the position of the phase front changes much slower than the sensible temperature distribution. This assumption is valid when the Stefan number is low, as it is in the subfreezing-temperature, water-based isochoric systems considered herein (ste ~ 0.1). The spatial derivatives of these distributions can then be inserted into the energy balance at the phase change interface (eqn. (10)), providing a non-linear first order equation for its position that is solvable using finite differences. An iterative approach was used to solve this equation, in which a guess for the position $S(t)$ was used to evaluate T_f, L, and the requisite spatial derivatives, and the two sides of eqn. (10) were

compared. Iteration in S for a given time point t continued until the interface energy balance was satisfied to within 1%. Standard mesh halving was used to confirm convergence. Considering a mesh of N steps, at an arbitrary point in time $t = N\Delta t$ with $N \geq 3$, the velocity $\frac{dS(t)}{dt}$ of the freezing front was approximated using the following three-point second-order backward difference scheme:

$$\frac{dS(t)}{dt} = \frac{3S_N - 4S_{N-1} + S_{N-2}}{2\Delta t} + O(\Delta t^2). \qquad (5.19)$$

For N = 2, a standard two-point first-order backwards difference was employed. This iterative procedure can be initialized in one of two ways. If investigating the non-steady initial freezing process, in order to avoid singularities, the marching of time is started at $t = 0.01$, and an initial guess of very small S is employed, which can after-the-fact be improved using a four-point forward difference once sufficient marching in time has occurred. Varieties of this approach are commonly employed in similar contexts, including by Savovic [245] and Rizwan-uddin [246,247]. If investigating only the steady-periodic domain however (after all transients have died out), an initial position of S can be determined by setting the $T_f(\bar{S})$ function equal to the final desired temperature T_D and solving for S, a technique unique to isochoric analysis.

In order to generate the temperature curves featured in Figure 5.22, the temperature was sampled at the insulated (symmetry) boundary and in the center of the domain, and a spatial average over the entire domain was also taken. In the steady-periodic regime considered, differences of sampling location and averaging yielded differences of less than 1% on the observed amplitude, period, and frequency of the temperature fluctuations, so all of the results presented in this work were measured at a single location, arbitrarily chosen to be the insulated boundary.

5.5 Looking Forward: Reducing isochoric freezing to practice within the food industry

In this chapter, we have presented experimental demonstrations of the potential of isochoric preservation to maintain the quality of otherwise-unpreservable fruits at subfreezing temperatures, experimental demonstrations of the anti-bacterial effects of combined hypothermic-hyperbaric conditions, and theoretical analyses showing that isochoric freezing may also significantly enhance the energetic efficiency of subzero-centigrade food storage. These early explorations of the potential roles that isochoric freezing might play in modern food storage are very promising, but significant further study is required to understand the potential of this technology to penetrate the food industry.

First and foremost, the biological efficacy of isochoric freezing must be determined for a much wider range of food products, including both currently unfreezable products such as fruits, berries, leafy greens, and fish, and products that are frequently frozen currently but stand to gain significant value from improvements in preservation quality, such as meat products at the whole carcass scale. Optimal temperatures and preservation solutions must be identified, and the pressure dependence

of damage to various classes of food tissues must be clarified, alongside its fundamental mechanisms. Early interpretation of the limited data available, including the studies relayed herein in addition our work on spinach leaves[248] and peeled potato cubes (unpublished), suggests that isochoric preservation performs extremely well for food products with robust exterior skins or peels and foods preserved "whole", i.e. foods that have not been additionally wounded or processed before preservation. This observation is largely anecdotal at this early stage of investigation, but may provide a sound basis from which to prioritize those food products that should be studied with the most urgency, based on likelihood of success— or, one might say, a basis from which to identify the "low-hanging fruit".

Assuming continued positive results with any food product of interest, the next most pressing obstacle to investigate is the economic reality of isochoric preservation, which of course hinges upon efficient chamber design. Current research-grade vessels are designed with extreme conservatism, often covering pressure ranges up to 250 MPa and being crafted from hefty steel alloys. Based on the findings relayed herein, it may well be preferable to conduct isochoric preservation at temperatures as high as -2.5°C, which yield pressures only on the order of 30 MPa. Thus, design and economic analysis of isochoric chambers tailored to this low-pressure scenario are urgently needed.

It is also important to acknowledge the shifting landscape of global food production and storage. The trials of COVID-19 have demonstrated on the national and international scale that our current food production and storage infrastructure is woefully ill-equipped for disaster or crisis scenarios, which, with ever-increasing global population, global temperatures, and climate instability, are likely to continue increasing in frequency and severity. The early months of 2020 have seen millions of pounds of fresh produce fall to waste in the United States due to supply chain disruptions, delivering a potent testament to the need to re-think our long-term preservation capacity for fresh food, which is currently all but non-existent. Analogous to the temporary storage of charge by electrical capacitance, a national "food capacitance" must be developed to ensure continued food security in an increasingly insecure world, and acknowledgement of this reality may alter current calculus regarding the economic value of prolonged food storage technologies.

6. Conclusions and Future Directions

In the three years separating the initiation and conclusion of the studies detailed in this thesis, our understanding of the constant-volume phase transitions of water has expanded radically, in terms both of their thermodynamic foundations and their varied applications. In these concluding pages, I will briefly summarize the most significant findings and outline promising avenues for continued research.

Thermodynamics and Kinetics

Isochoric freezing presents a uniquely rich and unstudied thermodynamic terrain, largely because it is not simply a new thermodynamic *technique*, but instead a new *context* in which to develop thermodynamic techniques. As detailed in Chapters 2 and 3, the foundational intuitions governing the thermodynamic and kinetic behaviors of water and its solid polymorphs in isochoric systems are fundamentally distinct from those governing systems exposed to the atmosphere, and we have barely scratched the surface of theoretical description of these systems.

Herein we derived a new isochoric nucleation theory, which takes volume as a natural variable of the system an allows continuous evaluation of system kinetics from nano- to macro-scale volume. This analysis, which gives nanoscale insights without resorting to atomistic computational arguments, revealed the existence of a critical confinement volume at which ice-1h may thermodynamically allowed whilst kinetically prohibited. This analysis was conducted at the single-nucleus scale, but the conceptual notion, like the nucleation theory itself, is applicable across the spectrum of volume: confinement at constant-volume will introduce kinetic resistance to the formation of ice (or of any expanding solid phase for that matter). This conclusion should of course feel natural and simple to the physical thinker, which highlights the importance of developing accordingly simple theory to describe it.

The implications of this kinetic limitation are far-reaching and as-of-yet only minimally explored. I have shown in this thesis that it serves (via several discrete but related mechanisms) to dramatically enhance the stability of metastable supercooled systems, which may prove transformative in the search for entirely ice-free cryopreservation techniques, and that it serves to enhance the vitrifiability of aqueous solutions. These early experimental demonstrations benchmark the need for significantly more advanced theoretical descriptions of these non-equilibrium systems.

In order to accurately model macroscale supercooling effects, the nucleation theory derived in section 2.1 must be expanded from single-nucleus analysis to multi-nucleus analysis. This expansion is conceptually straightforward whilst technically challenging; in a pure material under isobaric conditions, nuclei growing simultaneously (assuming sufficient physical distance to prevent thermal interactions) do not readily influence one another. However, in an isochoric context, every growing cluster within the system affects every other cluster through the lever of hydrostatic pressure, which is both uniform in the liquid phase and incredibly fast-acting as compared to thermal effects. Thus an interacting-cluster theory must be developed to accurately describe the nucleation rate, induction time, etc. at the macroscopic scale.

More challenging still is an adequate theoretical description of isochoric vitrification, which must also of course incorporate nucleation rate analysis, in addition to transient and highly complex heat transfer analysis. In a vitrifying system, the cooling rate is paramount, and at any discrete point within the system it represents a complex function of system geometry, thermal forcing parameters, and the thermal and phase change history of all surrounding points. Crystallization of ice at the edge of a vitrifying system will both produce pressure, affecting the kinetic driving forces for nucleation and growth, and significantly alter the thermal conductivity of the system in real time. Thus theory must be developed which fully couples a phase-change transport method (for instance the common enthalpy method) with isochoric nucleation analysis. Surprisingly, many (if not most) transport-based methods for studying phase change exist in open defiance of the physical realities of nucleation kinetics (for instance, the assumption of constant-temperature phase fronts and no local supercooling), and many classical nucleation theories fail to account for rigorous thermal transport effects. Thus a coupled transport-kinetics description of isochoric vitrification may well aid the broader field of phase-change analysis in presenting fully coupled, physically consistent theory.

Likely hinging upon the successful description of the above scenarios for pure water, both theoretical and experimental advances must then be made in the translation of these notions to arbitrary aqueous solutions. The general effects of different classes of solutes on solution metastability (e.g. supercooling) are poorly understood even under isobaric conditions, but the systematic probing of supercooling stability as a function of solute concentration compared under isobaric and isochoric may help to yield fundamental insights into the material parameters affecting aqueous metastability. In the myriad freezing literature produced within the last century, freezing point depression and supercooling capacity are nearly always considered coincident. I would argue that these effects are likely in fact quite distinct, with the former rooted in thermodynamic limitations and the later rooted in kinetic, and probing under isochoric conditions may help us to reduce kinetic effects and further clarify this distinction.

Finally, taking a wider view of the state of modern thermodynamics, the desired analyses and insights described in the last few paragraphs must then be generalized to materials systems of arbitrary natural variables. Herein we've seen the fertile terrain and technical challenge presented by swapping pressure for volume as a natural variable of a given system, but this represents only the simplest possible deviation from the *T-P* framework that has largely dominated modern thermodynamics. Many 21st century materials systems can be described by several additional natural variables (electric and magnetic fields, epitaxial strains, etc.), and thus generalized, multi-dimensional tools are needed to analytically predict the effects of the infinite set of available thermodynamic contexts on phase change phenomena. Performing this grand generalization is an essential step forward in the description of our modern material reality, and this task now falls to you, dear reader.

Organ and tissue cryopreservation

Fundamental thermodynamic advancements are of course only as compelling as the applications that they enable. Isochoric cryopreservation provides a novel and scalable means of maintaining large organ and tissue constructs at sub-zero centigrade temperatures with no threat of damaging ice formation and minimal osmotic toxicity. However, at equilibrium, these benefits are

accompanied by an enhancement of hydrostatic pressure, which itself can prove damaging to the biologic. Thus a calculus is required which considers how best to modulate these benefits and dangers, and weighs the relative advantages of stable equilibrium against metastable or non-equilibrium isochoric techniques.

From a conceptual standpoint, perhaps the greatest potential advantage of cryopreservation approaches driven by *non-chemical* modulation of freezing phenomena is the opportunity to develop *model-agnostic* techniques, or techniques which may be generically applied to a wide variety of biologics without significant variation. In conventional techniques powered by cryoprotectant agents (CPAs), a wealth of background data on the toxicity and diffusibility of a given CPA (or cocktail of CPAs) within a given organ or tissue system is typically required in order to design a given preservation protocol, and in the case of full organs intended for transplantation, careful additional attention must be paid to complete removal of often-high concentrations of CPAs post-preservation. In principle, techniques driven by non-chemical thermodynamic factors (such as physical confinement) may be applied more or less agnostically to any biological construct.

Within this thesis, we have generated early data in pursuit of this principle using two very different complex biological models, whole rat hearts and rat pancreatic islet clusters. Our successful 1-hour preservation and revival of whole rat hearts at -4°C, which resulted in reduced vascular permeability and interstitial edema compared with controls held using clinical static cold storage at +4°C, is to our knowledge the first demonstration of sub-zero centigrade heart preservation in the absence of non-physiological cryoprotectants. While the preservation period was brief and time-dependent pressure toxicity effects will emerge at longer preservation periods, this result demonstrates empirically that cryoprotectant agents are not a definitive pre-requisite of cryopreservation. We then, using a functionally identical, CPA-free preservation protocol, preserved pancreatic islets at high viability 72 hours, improving upon previous techniques by roughly 25% at that time point. Whole hearts and pancreatic islet clusters provide exceptionally different biologics, hailing from different organ systems, with different chemical, electrical, and mechanical functionalities; and while clear differences in their tolerance of prolonged pressure exposure are obvious, both proved preservable at some time scale using the same simple isochoric procedure, providing a very preliminary indication that model-agnostic preservation may be achievable using isochoric techniques.

In addition to gathering data on the performance of simple, CPA-free, single-solution equilibrium isochoric freezing on a wider variety of complex organ and tissue constructs, advancement of the broader field of isochoric cryopreservation requires a fundamental reckoning with hydrostatic pressure toxicity. Based on our observations thus far, exploration of this pressure toxicity may seek information on two related phenomena: a discrete threshold in pressure after which human biologics undergo precipitous morphological damage and the long-term development of time-dependent injurious effects.

In our initial heart preservation studies, we observed that pressures above approximately 40 MPa yielded near-immediate morphological damage, manifesting as contraction bands, sarcomere disruption, and vacuolization. While the body of previous work investigating whole organs under enhanced hydrostatic pressure is relatively thin, a series of studies by Takahashi et al.[34] on high-

pressure preservation and subsequent transplantation of rat livers also probed various pressures between 30 and 70 MPa and found that only those exposed to pressures less than 40 MPa yielded viable transplants. Interestingly, we have also observed a similar pressure cutoff in our study of sweet cherries[8], the quality of which deteriorated precipitously at pressures greater than roughly 40 MPa and in preliminary explorations (unpublished) of our islet preservation protocol[7] (which we ended up conducting at -3°C / 30 MPa for this reason). This consistency across biological systems may potentially point to materials-scale pressure dependences common to many biologics, and must be probed further to gain a fundamental understanding of the mechanisms of disruption at play, which may then also elucidate the time-dependent effects of lower pressure discussed in section 4.2.

However, while understanding the effects of pressure on complex biologics is of paramount fundamental interest and may enable more effective single-solution equilibrium isochoric freezing, any diversion from the central task of developing effective preservation protocols for clinical use is a diversion that comes at the cost of savable lives. Thus, we must concurrently acknowledge that, in light of our certain knowledge that as-of-yet poorly understood mechanisms induce substantial pressure toxicity, avenues that avoid or minimize enhanced pressures should be pursued.

To that end, isochoric supercooling represents a promising alternative. This approach enjoys all of the benefits of equilibrium isochoric freezing without the drawback of pressure toxicity—but comes at the cost of global thermodynamic stability. Our faith in the use of this technique must be a function of our faith in the stability of the metastable supercooled state. Based on the results of section 3.1, isochoric supercooling proves extremely stable, including in the face of all manner of perturbations that might be encountered during clinical use and transportation, at modest low temperatures (down to -3°C). While in theory the low temperature limit of cryopreservation should be pushed as far as possible, mounting evidence within the field and within this thesis indeed suggests that preservation in the high-subzero centigrade regime may prove sufficient to be transformative in the current preservation/transplantation space, and I will argue that isochoric supercooling should be promptly investigated with whole-organ constructs, even at these mild degrees of cooling.

Furthermore, while an overarching goal of isochoric techniques is to avoid high concentrations of cytotoxic cryoprotectants, low doses of physiological freeze modulators such as non-metabolizable glucose (3-O-methyl-d-glucose or 3-OMG), trehalose, mannitol, sodium chloride, etc. may enable further reduction of the storage temperature. Fundamental study is needed on the relationship between isochoric preservation in all of its thermodynamic varieties and the introduction of various classes of physiological solutes. For supercooling in particular, very little is known about the material properties that enhance *metastability* independent of stable freezing point depression, and the extension of the isochoric theory developed herein with to aqueous solutions may illuminate a path towards lower temperature, high-stability isochoric supercooling.

Finally, it should be noted that continued exploration of isochoric preservation of living matter should not stop at human biology—the world currently faces a wave of mass extinction and biodiversity reduction, especially in the marine domain, and a model-agnostic technique such as isochoric preservation may enable long-term preservation of otherwise disappearing groups of

flora and fauna, such as the hundreds of species of coral inhabiting the shrinking Great Barrier Reef or delicate seeds from the vanishing Amazon rain forest.

Applications in the food domain

As increasing hunger accompanies population expansion across the globe, the need to reduce global food waste has never been more urgent. Isochoric preservation presents a method of cold storage that protects sensitive foodstuffs from damaging ice crystallization and maintains high nutritional quality without the requirement of replacing the world's global refrigeration infrastructure or introducing chemical preservatives.

The studies relayed and referenced herein suggest that in at least certain classes of waste-prone food products (in our case tough-skinned whole fruits), isochoric preservation is extremely effective at industrially relevant time scales (4 weeks) and at exceptionally modest subzero temperatures (-2.5°C). These modest temperature requirements are encouraging for two reasons: Firstly, higher-temperature long-term storage is less energy intensive than lower-temperature alternatives, and thus less expensive. Secondly, the pressures for which isochoric chambers must be designed increase as a function of decreasing storage temperature, and thus milder temperatures enable use of thinner-walled chambers with more mobility, which, at the pressure employed in our tomato study for example (25.7 MPa), may even be constructed from a hard plastic.

Continued study is required to better understand the food groups for which isochoric preservation is most suited, and the mechanisms of damage-avoidance driving superior performance in those groups. As mentioned previously, an essential aspect of this line of research is the fundamental dependence of material-level behaviors on pressure, which may well yield insight that proves translatable to the medical domain. Combined studies demonstrating long-term sterilization effects in pre-infected whole food products should also be conducted, in order to determine whether anti-bacterial results may be obtained in a purely passive manner. Furthermore, in order to reduce isochoric preservation to practice in the food industry, rigorous mechanical and thermal optimization of the unit chambers is required, accompanied by analysis of the chamber volume scales that would prove most economical for combined long-term storage and cold-transportation purposes.

Finally, considerations of energy consumption are essential to the argument for isochoric food preservation. Isochoric systems serve not only to prevent energy-intensive ice formation, but also to augment temperature stability of both the contained food system and the surrounding refrigerator. Systems-level analysis of the effects of incorporating isochoric freezing into large scale cold storage facilities should be investigated, and ultimately, an economic model which incorporates the combined value of increased food quality / reduced waste, passive bacterial sterilization, and reduced energy consumption should be developed.

Final Remarks

In this thesis, I have presented several variations on the theme of constant-volume freezing. I have had the unique opportunity to traverse the rich and unexplored terrain of isochoric aqueous thermodynamics and kinetics and isochoric preservation of complex biological matter, and I

cannot envision a more stimulating subject on which to have expended the past three years of furious experimenting and confounded head-scratching. I hope sincerely that the ideas articulated herein may tickle, vex, or otherwise inspire the reader, and that this thesis may serve as an effective invitation to work in this wonderful field.

6. Bibliography

1. Powell-Palm, M. J., Rubinsky, B. & Sun, W. Freezing water at constant volume and under confinement. *Commun. Phys.* **3**, (2019).
2. Powell-Palm, M. J., Koh-Bell, A. & Rubinsky, B. Isochoric conditions enhance stability of metastable supercooled water. *Appl. Phys. Lett.* (2020) doi:10.1063/1.5145334.
3. Zhang, Y. *et al.* Isochoric vitrification: An experimental study to establish proof of concept. *Cryobiology* (2018) doi:10.1016/j.cryobiol.2018.06.005.
4. Powell-Palm, M. J., Aruda, J. & Rubinsky, B. Thermodynamic Theory and Experimental Validation of a Multiphase Isochoric Freezing Process. *J. Biomech. Eng.* (2019) doi:10.1115/1.4043521.
5. Wan, L. *et al.* Preservation of rat hearts in subfreezing temperature isochoric conditions to – 8 °C and 78 MPa. *Biochem. Biophys. Res. Commun.* (2018) doi:10.1016/j.bbrc.2018.01.140.
6. Wan, L., Powell-Palm, M. J., Clemens, M. G. & Rubinsky, B. Time-dependent Effects of Pressure during Preservation of Rat Hearts in an Isochoric System at Subfreezing Temperatures. *Cryo Letters* (2019).
7. Powell-Palm, M. J., Zhang, Y., Aruda, J. & Rubinsky, B. Isochoric conditions enable high subfreezing temperature pancreatic islet preservation without osmotic cryoprotective agents. *Cryobiology* (2019) doi:10.1016/j.cryobiol.2019.01.003.
8. Bilbao-Sainz, C. *et al.* Preservation of sweet cherry by isochoric (constant volume) freezing. *Innov. Food Sci. Emerg. Technol.* (2019) doi:10.1016/j.ifset.2018.10.016.
9. Powell-Palm, M. J. & Rubinsky, B. A shift from the isobaric to the isochoric thermodynamic state can reduce energy consumption and augment temperature stability in frozen food storage. *J. Food Eng.* (2019) doi:10.1016/j.jfoodeng.2019.02.001.
10. Polge, C., Smith, A. U. & Parkes, A. S. Revival of spermatozoa after vitrification and dehydration at low temperatures. *Nature* (1948) doi:10.1038/164666a0.
11. Mazur, P. Cryobiology: The Freezing of Biological Systems. *Science (80-.).* **168**, 939–949 (1970).
12. Mazur, P. Freezing of living cells: mechanisms and implications. *Am. J. Physiol. Physiol.* (1984) doi:10.1152/ajpcell.1984.247.3.C125.
13. Belzer, F. O. & Southard, J. H. Principles of solid organ preservation by cold storage. *Transplantation* **45**, 673–676 (1988).
14. Elliot, D. G., Wang, S. & Fuller J., B. Cryoprotectants: A review of the actions and applications of cryoprotective solutes that modulate cell recovery from ultra-low temperatures. *Cryobiology* **76**, 74–91 (2017).
15. Fahy, G. M. The relevance of cryoprotectant 'toxicity' to cryobiology. *Cryobiology* (1986) doi:10.1016/0011-2240(86)90013-1.
16. Giwa, S. *et al.* The promise of organ and tissue preservation to transform medicine. *Nat. Biotechnol.* **35**, 530–542 (2017).
17. Guibert, E. E. *et al.* Organ preservation: Current concepts and new strategies for the next decade. *Transfusion Medicine and Hemotherapy* (2011) doi:10.1159/000327033.
18. Ward, A., Klassen, D. K., Franz, K. M., Giwa, S. & Lewis, J. K. Social, economic, and policy implications of organ preservation advances. *Current Opinion in Organ Transplantation* (2018) doi:10.1097/MOT.0000000000000532.
19. Jang, T. H. *et al.* Cryopreservation and its clinical applications | Elsevier Enhanced Reader. *Integrative Medicine Research* (2017) doi:10.1016/J.IMR.2016.12.001.
20. Taylor, M. J., Weegman, B. P., Baicu, S. C. & Giwa, S. E. New Approaches to Cryopreservation of Cells, Tissues, and Organs. *Transfus. Med. Hemotherapy* **46**, 197–215 (2019).
21. John Morris, G. & Acton, E. Controlled ice nucleation in cryopreservation - A review. *Cryobiology* (2013) doi:10.1016/j.cryobiol.2012.11.007.
22. Farrant, J. Mechanism of cell damage during freezing and thawing and its prevention. *Nature* (1965) doi:10.1038/2051284a0.
23. Pegg, D. E., Wang, L. & Vaughan, D. Cryopreservation of articular cartilage. Part 3: the liquidus-tracking method. *Cryobiology* (2006) doi:10.1016/j.cryobiol.2006.01.004.
24. Kay, A. G., Hoyland, J. A., Rooney, P., Kearney, J. N. & Pegg, D. E. A liquidus tracking approach to the cryopreservation of human cartilage allografts. *Cryobiology* (2015) doi:10.1016/j.cryobiol.2015.05.005.
25. Tessier, S. N. *et al.* Partial freezing: A nature-inspired strategy for organ banking. *Cryobiology* (2018)

doi:10.1016/j.cryobiol.2017.12.036.
26. Tessier, S. N. *et al.* Effect of Ice Nucleation and Cryoprotectants during High Subzero-Preservation in Endothelialized Microchannels. *ACS Biomater. Sci. Eng.* (2018) doi:10.1021/acsbiomaterials.8b00648.
27. do Amaral, M. C. F., Lee, R. E. & Costanzo, J. P. Hepatocyte responses to in vitro freezing and β-adrenergic stimulation: Insights into the extreme freeze tolerance of subarctic Rana sylvatica. *J. Exp. Zool. Part A Ecol. Genet. Physiol.* (2015) doi:10.1002/jez.1905.
28. Huang, H., Yarmush, M. L. & Usta, O. B. Long-term deep-supercooling of large-volume water and red cell suspensions via surface sealing with immiscible liquids. *Nat. Commun.* (2018) doi:10.1038/s41467-018-05636-0.
29. Berendsen, T. A. *et al.* Supercooling enables long-term transplantation survival following 4 days of liver preservation. *Nat. Med.* **20**, 790–793 (2014).
30. de Vries, R. J. *et al.* Supercooling extends preservation time of human livers. *Nature Biotechnology* (2019) doi:10.1038/s41587-019-0223-y.
31. Amir, G. *et al.* Subzero nonfreezing cryopresevation of rat hearts using antifreeze protein I and antifreeze protein III. *Cryobiology* (2004) doi:10.1016/j.cryobiol.2004.02.009.
32. Amir, G. *et al.* Prolonged 24-hour subzero preservation of heterotopically transplanted rat hearts using antifreeze proteins derived from arctic fish. *Ann. Thorac. Surg.* (2004) doi:10.1016/j.athoracsur.2003.04.004.
33. Fuller, B. J., Petrenko, A. & Guibert, E. Human organs come out of the deep cold. *Nat. Biotechnol.* (2019) doi:10.1038/s41587-019-0264-2.
34. Takahashi, T. *et al.* Functional integrity of the rat liver after subzero preservation under high pressure. *Transplant. Proc.* (2000) doi:10.1016/S0041-1345(00)01440-8.
35. Rubinsky, B., Perez, P. A. & Carlson, M. E. The thermodynamic principles of isochoric cryopreservation. *Cryobiology* **50**, 121–138 (2005).
36. Preciado, J. A. & Rubinsky, B. Isochoric preservation: A novel characterization method. *Cryobiology* (2010) doi:10.1016/j.cryobiol.2009.06.010.
37. Ukpai, G., Năstase, G., Şerban, A. & Rubinsky, B. Pressure in isochoric systems containing aqueous solutions at subzero Centigrade temperatures. *PLoS One* **12**, (2017).
38. Perez, P. A., Preciado, J., Carlson, G., DeLonzor, R. & Rubinsky, B. The effect of undissolved air on isochoric freezing. *Cryobiology* **72**, 225–231 (2016).
39. Szobota, S. A. & Rubinsky, B. Analysis of isochoric subcooling. *Cryobiology* **53**, 139–142 (2006).
40. Tulk, C. A., Molaison, J. J., Makhluf, A. R., Manning, C. E. & Klug, D. D. Absence of amorphous forms when ice is compressed at low temperature. *Nature* (2019) doi:10.1038/s41586-019-1204-5.
41. Fitzner, M., Sosso, G. C., Cox, S. J. & Michaelides, A. Ice is born in low-mobility regions of supercooled liquid water. *Proc. Natl. Acad. Sci.* (2019) doi:10.1073/pnas.1817135116.
42. Stern, J. N., Seidl-Nigsch, M. & Loerting, T. Evidence for high-density liquid water between 0.1 and 0.3 GPa near 150 K. *Proc. Natl. Acad. Sci.* (2019) doi:10.1073/pnas.1819832116.
43. Zhu, W. *et al.* Room temperature electrofreezing of water yields a missing dense ice phase in the phase diagram. *Nat. Commun.* (2019) doi:10.1038/s41467-019-09950-z.
44. Kim, Y.-J., Lee, Y.-H., Lee, S., Nada, H. & Lee, G. W. Shock growth of ice crystal near equilibrium melting pressure under dynamic compression. *Proc. Natl. Acad. Sci.* (2019) doi:10.1073/pnas.1818122116.
45. Cheng, B., Engel, E. A., Behler, J., Dellago, C. & Ceriotti, M. Ab initio thermodynamics of liquid and solid water. *Proc. Natl. Acad. Sci. U. S. A.* (2019) doi:10.1073/pnas.1815117116.
46. Taylor, M. J., Weegman, B. P., Baicu, S. C. & Giwa, S. E. New Approaches to Cryopreservation of Cells, Tissues, and Organs. *Transfusion Medicine and Hemotherapy* (2019) doi:10.1159/000499453.
47. Powell-Palm, M. J., Zhang, Y., Aruda, J. & Rubinsky, B. Isochoric conditions enable high subfreezing temperature pancreatic islet preservation without osmotic cryoprotective agents. *Cryobiology* (2019) doi:10.1016/j.cryobiol.2019.01.003.
48. Wan, L. *et al.* Preservation of rat hearts in subfreezing temperature isochoric conditions to – 8 °C and 78 MPa. *Biochem. Biophys. Res. Commun.* (2018) doi:10.1016/j.bbrc.2018.01.140.
49. Mikus, H. *et al.* The nematode Caenorhabditis elegans survives subfreezing temperatures in an isochoric system. *Biochem. Biophys. Res. Commun.* **477**, 401–405 (2016).
50. David, R. O. *et al.* Pore condensation and freezing is responsible for ice formation below water saturation for porous particles. *Proc. Natl. Acad. Sci.* (2019) doi:10.1073/pnas.1813647116.
51. Salvati Manni, L. *et al.* Soft biomimetic nanoconfinement promotes amorphous water over ice. *Nat. Nanotechnol.* (2019) doi:10.1038/s41565-019-0415-0.

52. Levinger, N. E. Water in confinement. *Science (80-.).* (2002) doi:10.1126/science.1079322.
53. Mashl, R. J., Joseph, S., Aluru, N. R. & Jakobsson, E. Anomalously immobilized water: A new water phase induced by confinement in nanotubes. *Nano Lett.* (2003) doi:10.1021/nl0340226.
54. Rasaiah, J. C., Garde, S. & Hummer, G. Water in Nonpolar Confinement: From Nanotubes to Proteins and Beyond. *Annu. Rev. Phys. Chem.* (2007) doi:10.1146/annurev.physchem.59.032607.093815.
55. Alba-Simionesco, C. *et al.* Effects of confinement on freezing and melting. *Journal of Physics Condensed Matter* (2006) doi:10.1088/0953-8984/18/6/R01.
56. Schmidt, R., Walther Hansen, E., Stacker, M., Akporiaye, D. & Henrik Ellestad, O. *Pore Size Determination of MCM-41 Mesoporous Materials by means of NMR Spectroscopy, N2 adsorption A Preliminary Study*. *J. Am. Chem. Soc* (1995).
57. Zuber, B. & Marchand, J. Predicting the volume instability of hydrated cement systems upon freezing using poro-mechanics and local phase equilibria. *Mater. Struct. Constr.* (2004) doi:10.1617/14165.
58. De Luca, S. *et al.* Effects of Confinement on the Dielectric Response of Water Extends up to Mesoscale Dimensions. *Langmuir* (2016) doi:10.1021/acs.langmuir.6b00791.
59. Rubinsky, B., Perez, P. A. & Carlson, M. E. The thermodynamic principles of isochoric cryopreservation. *Cryobiology* (2005) doi:10.1016/j.cryobiol.2004.12.002.
60. Alberty, R. A. Use of Legendre Transforms in Chemiccal Thermodynamics. *Pure Appl. Chem.* (2001) doi:10.1351/pac200173081349.
61. Zia, R. K. P., Redish, E. F. & McKay, S. R. Making sense of the Legendre transform. *Am. J. Phys.* (2009) doi:10.1119/1.3119512.
62. Callen, H. B. Thermodynamics and an Introduction to Thermostatistics, 2nd ed. *Am. J. Phys.* (1998) doi:10.1119/1.19071.
63. *Guideline on Thermodynamic Properties of Supercooled Water*. (2015).
64. *Revised Release on the Equation of State 2006 for H2O Ice Ih*. (2009).
65. Gibbs, J. W. On the equilibrium of heterogeneous substances. *Am. J. Sci.* **96**, 441–458 (1878).
66. Gordon, P. *Principles of Phase Diagrams in Materials Systems*. (McGraw-Hill, Inc., 1968).
67. Clouet, E. Modeling of Nucleation Processes. in *ASM Handbook Vol. 22A, Fundamentals of Modeling for Metals Processing* (eds. Furrer, D. U. & Semiatin, S. L.) 203–219 (2009).
68. Pruppacher, H. R. & Klett, J. D. *Microphysics of Clouds and Precipitation*. (Kluwer Academic Publishers, 1997).
69. Sun, W. *et al.* The thermodynamic scale of inorganic crystalline metastability. *Sci. Adv.* (2016) doi:10.1126/sciadv.1600225.
70. Navrotsky, A. Nanoscale effects on thermodynamics and phase equilibria in oxide systems. *ChemPhysChem* (2011) doi:10.1002/cphc.201100129.
71. Sun, W., Kitchaev, D. A., Kramer, D. & Ceder, G. Non-equilibrium crystallization pathways of manganese oxides in aqueous solution. *Nat. Commun.* (2019) doi:10.1038/s41467-019-08494-6.
72. Shi, T. *et al.* Shear-Assisted Formation of Cation-Disordered Rocksalt NaMO2 (M = Fe or Mn). *Chem. Mater.* (2018) doi:10.1021/acs.chemmater.8b03490.
73. Ding, H. *et al.* Computational Approach for Epitaxial Polymorph Stabilization through Substrate Selection. *ACS Appl. Mater. Interfaces* (2016) doi:10.1021/acsami.6b01630.
74. Potticary, J. *et al.* An unforeseen polymorph of coronene by the application of magnetic fields during crystal growth. *Nat. Commun.* (2016) doi:10.1038/ncomms11555.
75. Aber, J. E., Arnold, S., Garetz, B. A. & Myerson, A. S. Strong dc electric field applied to supersaturated aqueous glycine solution induces nucleation of the γ polymorph. *Phys. Rev. Lett.* (2005) doi:10.1103/PhysRevLett.94.145503.
76. Kitchaev, D. A., Dacek, S. T., Sun, W. & Ceder, G. Thermodynamics of Phase Selection in MnO2 Framework Structures through Alkali Intercalation and Hydration. *J. Am. Chem. Soc.* (2017) doi:10.1021/jacs.6b11301.
77. Sun, W. *et al.* Thermodynamic Routes to Novel Metastable Nitrogen-Rich Nitrides. *Chem. Mater.* (2017) doi:10.1021/acs.chemmater.7b02399.
78. Hudait, A., Qiu, S., Lupi, L. & Molinero, V. Free energy contributions and structural characterization of stacking disordered ices. *Phys. Chem. Chem. Phys.* (2016) doi:10.1039/c6cp00915h.
79. Lavernia, E. J. & Srivatsan, T. S. The rapid solidification processing of materials: Science, principles, technology, advances, and applications. *Journal of Materials Science* vol. 45 287–325 (2010).
80. Stonehouse, G. G. & Evans, J. A. The use of supercooling for fresh foods: A review. *Journal of Food Engineering* (2015) doi:10.1016/j.jfoodeng.2014.08.007.

81. Berendsen, T. A. *et al.* Supercooling enables long-term transplantation survival following 4 days of liver preservation. *Nat. Med.* (2014) doi:10.1038/nm.3588.
82. Hickling, R. Nucleation of freezing by cavity collapse and its relation to cavitation damage. *Nature* (1965) doi:10.1038/206915a0.
83. Hickling, R. Transient, high-pressure solidification associated with cavitation in water. *Phys. Rev. Lett.* **73**, 2853–2856 (1994).
84. Luque de Castro, M. D. & Priego-Capote, F. Ultrasound-assisted crystallization (sonocrystallization). *Ultrason. Sonochem.* (2007) doi:10.1016/j.ultsonch.2006.12.004.
85. Young, S. W. & Van Sicklen, W. J. The mechanical stimulus to crystallization. *J. Am. Chem. Soc.* (1913) doi:10.1021/ja02198a002.
86. Myint, P. C. & Belof, J. L. Rapid freezing of water under dynamic compression. *J. Phys. Condens. Matter* **30**, 233002 (2018).
87. Myint, P. C. *et al.* Nanosecond Freezing of Water at High Pressures: Nucleation and Growth near the Metastability Limit. *Phys. Rev. Lett.* **121**, 155701 (2018).
88. Powell-Palm, M. J., Koh-Bell, A. & Rubinsky, B. Isochoric conditions enhance stability of metastable supercooled water. *Appl. Phys. Lett.* (2020).
89. Gilmore, F. R. *The growth or collapse of a spherical bubble in a viscous compressible liquid*. *Hydrodynamics Laboratory, California Institute of Technology* (1952).
90. Flynn, H. G. Cavitation dynamics. I. A mathematical formulation. *Cit. J. Acoust. Soc. Am.* **57**, 1379 (1975).
91. Hicking, R. & Plesset, M. S. Collapse and rebound of a spherical bubble in water. *Phys. Fluids* **7**, 7–14 (1964).
92. *Revised Release on the IAPWS Formulation 1995 for the Thermodynamic Properties of Ordinary Water Substance for General and Scientific Use*. (2018).
93. *Revised Release on the Pressure along the Melting and Sublimation Curves of Ordinary Water Substance*. (2011).
94. Lee, G. W., Evans, W. J. & Yoo, C.-S. Crystallization of water in a dynamic diamond-anvil cell: Evidence for ice VII-like local order in supercompressed water. *Phys. Rev. B* **74**, 134112 (2006).
95. Gleason, A. E. *et al.* Compression Freezing Kinetics of Water to Ice VII. *Phys. Rev. Lett.* **119**, 025701 (2017).
96. Sterbentz, D. M., Myint, P. C., Delplanque, J. P. & Belof, J. L. Numerical modeling of solid-cluster evolution applied to the nanosecond solidification of water near the metastable limit. *J. Chem. Phys.* **151**, 164501 (2019).
97. Myint, P. C., Benedict, L. X. & Belof, J. L. Free energy models for ice VII and liquid water derived from pressure, entropy, and heat capacity relations. *J. Chem. Phys.* **147**, 084505 (2017).
98. Kashchiev, D. Solution of the non-steady state problem in nucleation kinetics. *Surf. Sci.* **14**, 209–220 (1969).
99. Kerboua, K. & Hamdaoui, O. Void fraction, number density of acoustic cavitation bubbles, and acoustic frequency: A numerical investigation. *J. Acoust. Soc. Am.* (2019) doi:10.1121/1.5126865.
100. Powell-Palm, M. J., Rubinsky, B. & Sun, W. Freezing water at constant volume and under confinement. *Commun. Phys.* **3**, (2020).
101. Rubinsky, B., Perez, P. A. & Carlson, M. E. The thermodynamic principles of isochoric cryopreservation. *Cryobiology* (2005) doi:10.1016/j.cryobiol.2004.12.002.
102. Huang, H., Yarmush, M. L. & Usta, O. B. Long-term deep-supercooling of large-volume water and red cell suspensions via surface sealing with immiscible liquids. *Nat. Commun.* **9**, 3201 (2018).
103. Clouet, E. Modeling of Nucleation Processes. in *Fundamentals of Modeling for Metals Processing, ASM Handbook* 203–219 (2009).
104. Akio, S., Seiji, O., Akira, T., Hiroshi, U. & Ken'ichi, T. Fundamental research on external factors affecting the freezing of supercooled water. *Int. J. Heat Mass Transf.* (1992) doi:10.1016/0017-9310(92)90094-9.
105. Callen, H. B. & Griffiths, R. B. Thermodynamics and an Introduction to Thermostatistics. *Am. J. Phys.* **55**, 860 (1987).
106. Hickling, R. Nucleation of freezing by cavity collapse and its relation to cavitation damage. *Nature* **206**, 915–917 (1965).
107. Mathur, A. *et al.* Human iPSC-based cardiac microphysiological system for drug screening applications. *Sci. Rep.* (2015) doi:10.1038/srep08883.
108. Zhang, Z., Sun, D. W., Zhu, Z. & Cheng, L. Enhancement of Crystallization Processes by Power Ultrasound: Current State-of-the-Art and Research Advances. *Compr. Rev. Food Sci. Food Saf.* (2015) doi:10.1111/1541-4337.12132.

109. Chow, R., Blindt, R., Chivers, R. & Povey, M. A study on the primary and secondary nucleation of ice by power ultrasound. *Ultrasonics* (2005) doi:10.1016/j.ultras.2004.06.006.
110. Pototsky, A. & Bestehorn, M. Faraday instability of a two-layer liquid film with a free upper surface. *Phys. Rev. Fluids* (2016) doi:10.1103/physrevfluids.1.023901.
111. Ward, K., Zoueshtiagh, F. & Narayanan, R. Faraday instability in double-interface fluid layers. *Phys. Rev. Fluids* (2019) doi:10.1103/PhysRevFluids.4.043903.
112. Bazilevskii, A. V., Kalinichenko, V. A. & Rozhkov, A. N. Effect of Fluid Viscosity on the Faraday Surface Waves. *Fluid Dyn.* (2018) doi:10.1134/S0015462818060150.
113. Talib, E. & Juel, A. Instability of a viscous interface under horizontal oscillation. *Phys. Fluids* (2007) doi:10.1063/1.2762255.
114. Ohsaka, K. & Trinh, E. H. Dynamic nucleation of ice induced by a single stable cavitation bubble. *Appl. Phys. Lett.* (1998) doi:10.1063/1.121706.
115. Saclier, M., Peczalski, R. & Andrieu, J. A theoretical model for ice primary nucleation induced by acoustic cavitation. *Ultrason. Sonochem.* (2010) doi:10.1016/j.ultsonch.2009.04.008.
116. Goyer, G. G., Bhadra, T. C. & Gitlin, S. Shock Induced Freezing of Supercooled Water. *J. Appl. Meteorol.* (1965) doi:10.1175/1520-0450(1965)004<0156:sifosw>2.0.co;2.
117. Luyet, B. J. & Gehenio, P. M. The survival of Moss vitrified in liquid air and its relation to water content. *Biodynamica* **42**, 1–7 (1938).
118. Luyet, B. J. & Hodapp, E. L. Revival of Frog's Spermatozoa Vitrified in Liquid Air. *Proc. Soc. Exp. Biol. Med.* **39**, 433–434 (1938).
119. Gonzales, F. & J., L. B. Resumption of heart beat in chick embryo frozen in liquid nitrogen. *Biodynamica* **7**, 1–5 (1950).
120. Luyet, B. J. & Gehenio, P. M. Survival of vinegar eels after congelation in liquid nitrogen. *Anat. Rec.* **108**, 544–544 (1950).
121. Luyet, B. J. On the mechanism of cellular death by high pressure cytological modifications accompanying death in yeast. *Comptes Rendus Hebd. Des Seances L Acad. Des Sci.* **204**, 1506–1508 (1937).
122. Luyet, B. J. & Hodapp, E. L. Mechanism of cellular death by high pressure, compression of yeast in sodium chloride solutions. *Proc. Soc. Exp. Biol. Med.* **36**, 615–617 (1937).
123. Luyet, R. & Guilliermond, A. The mechanism of the death of cells by high pressures the intensity and the duration of pressures lethal for yeast. *Comptes Rendus Hebd. Des Seances L Acad. Des Sci.* **204**, 1214–1215 (1937).
124. Hodapp, E. L. & Luyet, B. J. On the mechanism of death by hydrostatic pressure in para-mecia. *Biodynamica* **6**, 101–109 (1947).
125. Rall, W. F. & Fahy, G. M. Ice-free cryopreservation of mouse embryos at− 196 C by vitrification. (1985).
126. Fahy, G. M., MacFarlane, D. R., Angell, C. A. & Meryman, H. T. Vitrification as an approach to cryopreservation. *Cryobiology* **20**, 699 (1983).
127. Fahy, G. M., MacFarlane, D. R., Angell, C. A. & Meryman, H. T. Vitrification as an approach to cryopreservation. *Cryobiology* **21**, 407–26 (1984).
128. Fahy, G. M. *et al.* Physical and biological aspects of renal vitrification. *Organogenesis* **5**, 167–75 (2009).
129. Taylor, M. J. Biology of cell survival in the cold: the basis for biopreservation of tissues and organs. in *Advances in Biopreservation* (ed. Baust J.M. (eds.), J. G. and B.) 15–62 (CRC - Taylor and Francis, 2006).
130. Taylor, M. J., Song, Y. C., Chen, Z. Z., Lee, F. & Brockbank, K. G. M. Interactive Determinants for Optimized Stabilization of Autologous Vascular Grafts During Surgery. *Cell Preserv. Technol.* **2**, 198–208 (2004).
131. Brockbank, K. G. M. & Taylor, M. J. Tissue Preservation. in *Advances in Biopreservation* (eds. Baust, J. G. & Baust, J. M.) 157–196 (Taylor & Francis, 2006).
132. Taylor, M. J. Hypothermic Blood Substitution: Special Considerations for Protection of Cells during ex vivo and in vivo Preservation. *Transfus. Med. Hemotherapy* **34**, 226–244 (2007).
133. Iwanaga et al., Y. Comparison of Unisol and UW Solution in combination with perfluorodecalin in the two layer method(TLM) for pancreas preservation prior to islet isolation. *Transplantation.* **Supplement**, 386 (2002).
134. Taylor, M. J., Rhee, P., Chen, Z. & Alam, H. B. Design of preservation solutions for universal tissue preservation in vivo: demonstration of efficacy in preclinical models of profound hypothermic cardiac arrest. *Transplant. Proc.* **37**, 303–7 (2005).
135. Baicu, S. C. & Taylor, M. J. Acid-base buffering in organ preservation solutions as a function of temperature: new parameters for comparing buffer capacity and efficiency. *Cryobiology* **45**, 33–48 (2002).

136. Taylor, M. J. Patent US6492103 B1, System for Organ and Tissue Preservation and Hypothermic Blood Substitution. (2002).
137. Taylor, M. J., Campbell, L. H., Rutledge, R. N. & Brockbank, K. G. Comparison of Unisol with Euro-Collins solution as a vehicle solution for cryoprotectants. *Transplant. Proc.* **33**, 677–9 (2001).
138. Perez, P. A., Preciado, J., Carlson, G., DeLonzor, R. & Rubinsky, B. The effect of undissolved air on isochoric freezing. *Cryobiology* (2016) doi:10.1016/j.cryobiol.2016.04.002.
139. Berejnov, V., Husseini, N. S., Alsaied, O. A. & Thorne, R. E. Effects of cryoprotectant concentration and cooling rate on vitrification of aqueous solutions. *J. Appl. Crystallogr.* (2006) doi:10.1107/S0021889806004717.
140. Szobota, S. A. & Rubinsky, B. Analysis of isochoric subcooling. *Cryobiology* (2006) doi:10.1016/j.cryobiol.2006.04.001.
141. Lovelock, J. E. The haemolysis of human red blood-cells by freezing and thawing. *BBA - Biochim. Biophys. Acta* (1953) doi:10.1016/0006-3002(53)90273-X.
142. Rubinsky, B., Perez, P. A. & Carlson, M. E. The thermodynamic principles of isochoric cryopreservation. *Cryobiology* **50**, 121–138 (2005).
143. Rubinsky, B., Perez, P. A. & Carlson, M. E. The thermodynamic principles of isochoric cryopreservation. *Cryobiology* **50**, 121–138 (2005).
144. Rubinsky, B. & Pegg, D. E. A mathematical model for the freezing process in biological tissue. *Proc. R. Soc. B Biol. Sci.* (1988) doi:10.1098/rspb.1988.0053.
145. Pegg, D. E. Principles of Cryopreservation BT - Cryopreservation and freeze-drying protocols. in *Cryopreservation and freeze-drying protocols* vol. 368 39–57 (2007).
146. Pegg, D. E. Principles of Cryopreservation. *Cryopreserv. Free. Dry. Protoc. 3rd Ed.* **1257**, 3–19 (2015).
147. Pegg, D. E. & Diaper, M. P. ON THE MECHANISM OF INJURY TO SLOWLY FROZEN ERYTHROCYTES. *Biophys. J.* **54**, 471–488 (1988).
148. Karlsson, J. O. M. & Toner, M. Long-term storage of tissues by cryopreservation: Critical issues. *Biomaterials* **17**, 243–256 (1996).
149. Ye, B. Heart Transplantation: What are the Alternatives? *J. Clin. Exp. Cardiolog.* (2013) doi:10.4172/2155-9880.s9-e001.
150. Belzer, F. O. & Southard, J. H. Principles of solid-organ preservation by cold storage. *Transplantation* **45**, 673–6 (1988).
151. Lopukhin, S. Y., Peek, D. F. M., Southard, J. H. & Belzer, F. O. Cold storage of the heart with University of Wisconsin solution and 2,3-butanedione monoxime: Langendorff vs isolated working rabbit heart model. *Cryobiology* (1996) doi:10.1006/cryo.1996.0018.
152. Rubinsky, B., Arav, A., Hong, J. S. & Lee, C. Y. Freezing of mammalian livers with glycerol and antifreeze proteins. *Biochem. Biophys. Res. Commun.* (1994) doi:10.1006/bbrc.1994.1512.
153. Masson, P., Tonello, C. & Balny, C. High-pressure biotechnology in medicine and pharmaceutical science. *Journal of Biomedicine and Biotechnology* (2001) doi:10.1155/S1110724301000158.
154. Ueno, T. *et al.* Liver transplantation using liver grafts preserved under high pressure. *Artif. Organs* (2005) doi:10.1111/j.1525-1594.2005.00139.x.
155. Takahashi, T. *et al.* Preservation of rat livers by supercooling under high pressure. in *Transplantation Proceedings* (2001). doi:10.1016/S0041-1345(00)02268-5.
156. Southard, J. H. & Belzer, F. O. Organ preservation. *Annu. Rev. Med.* **46**, 235–247 (1995).
157. Ueno, T. *et al.* Liver transplantation using liver grafts preserved under high pressure. *Artif. Organs* **29**, 849–855 (2005).
158. Frey, B. *et al.* Cells Under Pressure – Treatment of Eukaryotic Cells with High Hydro- static Pressure, from Physiologic Aspects to Pressure Induced Cell Death. *Curr. Med. Chem.* (2008) doi:10.2174/092986708785909166.
159. Liu, F. *et al.* Optimal method for short-term or long-term islet preservation: comparison of islet culture, cold preservation and cryopreservation. *J. Artif. Organs* **17**, 337–343 (2014).
160. Kojayan, G. G., Alexander, M., Imagawa, D. K. & Lakey, J. R. T. Systematic review of islet cryopreservation. *Islets* (2018) doi:10.1080/19382014.2017.1405202.
161. Ichii, H. *et al.* Shipment of Human Islets for Transplantation. *Am. J. Transplant.* **7**, 1010–1020 (2007).
162. Ikemoto, T. *et al.* Assessment of Islet Quality following International Shipping of more than 10,000 km. *Cell Transplant.* **19**, 731–741 (2010).
163. Ikemoto, T. *et al.* New Stepwise Cooling System for Short-Term Porcine Islet Preservation. *Pancreas* **39**, 960–963 (2010).

164. Terai, S. *et al.* Effect of Oxygenated Perfluorocarbon on Isolated Islets During Transportation. *J. Surg. Res.* **162**, 284–289 (2010).
165. BROWN, M. S. TEXTURE OF FROZEN FRUITS AND VEGETABLES. *J. Texture Stud.* (1977) doi:10.1111/j.1745-4603.1977.tb01147.x.
166. Dermesonlouoglou, E. K., Giannakourou, M. C. & Taoukis, P. Stability of dehydrofrozen tomatoes pretreated with alternative osmotic solutes. *J. Food Eng.* (2007) doi:10.1016/j.jfoodeng.2005.09.026.
167. Mulabagal, V., Lang, G. A., Dewitt, D. L., Dalavoy, S. S. & Nair, M. G. Anthocyanin content, lipid peroxidation and cyclooxygenase enzyme inhibitory activities of sweet and sour Cherries. *J. Agric. Food Chem.* (2009) doi:10.1021/jf8032039.
168. Chaovanalikit, A. & Wrolstad, R. E. Total Anthocyanins and Total Phenolics of Fresh and Processed Cherries and Their Antioxidant Properties. *J. Food Sci.* (2004) doi:10.1111/j.1365-2621.2004.tb17858.x.
169. Ferretti, G., Bacchetti, T., Belleggia, A. & Neri, D. Cherry antioxidants: From farm to table. *Molecules* (2010) doi:10.3390/molecules15106993.
170. Kris-Etherton, P. M. *et al.* Bioactive compounds in foods: Their role in the prevention of cardiovascular disease and cancer. in *American Journal of Medicine* (2002). doi:10.1016/s0002-9343(01)00995-0.
171. Préstamo, G. & Arroyo, G. High hydrostatic pressure effects on vegetable structure. *J. Food Sci.* (1998) doi:10.1111/j.1365-2621.1998.tb17918.x.
172. Barrett, D. M., Beaulieu, J. C. & Shewfelt, R. Color, flavor, texture, and nutritional quality of fresh-cut fruits and vegetables: Desirable levels, instrumental and sensory measurement, and the effects of processing. *Crit. Rev. Food Sci. Nutr.* (2010) doi:10.1080/10408391003626322.
173. McInerney, J. K., Seccafien, C. A., Stewart, C. M. & Bird, A. R. Effects of high pressure processing on antioxidant activity, and total carotenoid content and availability, in vegetables. *Innov. Food Sci. Emerg. Technol.* (2007) doi:10.1016/j.ifset.2007.04.005.
174. Khan, M. K. *et al.* Effect of novel technologies on polyphenols during food processing. *Innovative Food Science and Emerging Technologies* (2018) doi:10.1016/j.ifset.2017.12.006.
175. Pénicaud, C., Achir, N., Dhuique-Mayer, C., Dornier, M. & Bohuon, P. Degradation of β-carotene during fruit and vegetable processing or storage: Reaction mechanisms and kinetic aspects: A review. *Fruits* (2011) doi:10.1051/fruits/2011058.
176. Tian, S. P., Jiang, A. L., Xu, Y. & Wang, Y. S. Responses of physiology and quality of sweet cherry fruit to different atmospheres in storage. *Food Chem.* (2004) doi:10.1016/j.foodchem.2003.10.014.
177. Molina-García, A. D. The effect of hydrostatic pressure on biological systems. *Biotechnol. Genet. Eng. Rev.* (2002) doi:10.1080/02648725.2002.10648021.
178. Kong, C. H. Z. *et al.* Antifreeze peptide pretreatment minimizes freeze-thaw damage to cherries: An in-depth investigation. *LWT - Food Sci. Technol.* (2017) doi:10.1016/j.lwt.2017.06.002.
179. Alonso, J., Rodriguez, T. & Canet, W. Effect of Calcium Pretreatments on the Texture of Frozen Cherries. Role of Pectinesterase in the Changes in the Pectic Materials. *J. Agric. Food Chem.* (1995) doi:10.1021/jf00052a031.
180. Alonso, J., Tortosa, M. E., Canet, W. & Rodríguez, M. T. Ultrastructural and Changes in Pectin Composition of Sweet Cherry from the Application of Prefreezing Treatments. *J. Food Sci.* (2006) doi:10.1111/j.1365-2621.2005.tb08314.x.
181. Patras, A., Brunton, N. P., Da Pieve, S. & Butler, F. Impact of high pressure processing on total antioxidant activity, phenolic, ascorbic acid, anthocyanin content and colour of strawberry and blackberry purées. *Innov. Food Sci. Emerg. Technol.* (2009) doi:10.1016/j.ifset.2008.12.004.
182. Pifferi, P. G. & Cultrera, R. ENZYMATIC DEGRADATION OF ANTHOCYANINS: THE ROLE OF SWEET CHERRY POLYPHENOL OXIDASE. *J. Food Sci.* (1974) doi:10.1111/j.1365-2621.1974.tb17980.x.
183. Poiana, M. A., Moigradean, D. & Alexa, E. Influence of home-scale freezing and storage on antioxidant properties and color quality of different garden fruits. *Bulg. J. Agric. Sci.* (2010).
184. Piccolella, S. *et al.* Antioxidant properties of sour cherries (Prunus cerasus L): Role of colorless phytochemicals from the methanolic extract of ripe fruits. *J. Agric. Food Chem.* (2008) doi:10.1021/jf0734727.
185. Omoni, A. O. & Aluko, R. E. The anti-carcinogenic and anti-atherogenic effects of lycopene: A review. *Trends Food Sci. Technol.* (2005) doi:10.1016/j.tifs.2005.02.002.
186. Cantwell, M., Nie, X. & Hong, G. Impact of Storage Conditions on Grape Tomato Quality. *Symp. A Q. J. Mod. Foreign Lit.* (2009).
187. Abushita, A. A., Hebshi, E. A., Daood, H. G. & Biacs, P. A. Determination of antioxidant vitamins in

tomatoes. *Food Chem.* (1997) doi:10.1016/S0308-8146(96)00321-4.
188. Singleton, V. L. & Jr., R. J. A. Colorimetry of Total Phenolics with Phosphomolybdic-Phosphotungstic Ac1. Singleton VL, Jr. RJA (1965) Colorimetry of Total Phenolics with Phosphomolybdic-Phosphotungstic Acid Reagents. Am J Enol Vitic 16:144–158. https://doi.org/10.12691/ijebb-2-1-5id Rea. *Am. J. Enol. Vitic.* (1965) doi:10.12691/ijebb-2-1-5.
189. Brand-Williams, W., Cuvelier, M. E. & Berset, C. Use of a free radical method to evaluate antioxidant activity. *LWT - Food Science and Technology* (1995) doi:10.1016/S0023-6438(95)80008-5.
190. Lisiewska, Z. & Kmiecik, W. Effect of storage period and temperature on the chemical composition and organoleptic quality of frozen tomato cubes. *Food Chem.* (2000) doi:10.1016/S0956-7135(99)00110-3.
191. URBANYI, G. & HORTI, K. Colour and carotenoid content of quick-frozen tomato cubes during frozen storage. *Acta Aliment.* (1989).
192. Tangwongchai, R., Ledward, D. A. & Ames, J. M. Effect of high-pressure treatment on the texture of cherry tomato. *J. Agric. Food Chem.* (2000) doi:10.1021/jf990796p.
193. Chylińska, M., Szymańska-Chargot, M., Deryło, K., Tchórzewska, D. & Zdunek, A. Changing of biochemical parameters and cell wall polysaccharides distribution during physiological development of tomato fruit. *Plant Physiol. Biochem.* (2017) doi:10.1016/j.plaphy.2017.09.010.
194. FUCHIGAMI, M., HYAKUMOTO, N. & MIYAZAKI, K. Programmed Freezing Affects Texture, Pectic Composition and Electron Microscopic Structures of Carrots. *J. Food Sci.* (1995) doi:10.1111/j.1365-2621.1995.tb05623.x.
195. Anthon, G. E. & Barrett, D. M. Characterization of the temperature activation of pectin methylesterase in green beans and tomatoes. *J. Agric. Food Chem.* (2006) doi:10.1021/jf051877q.
196. Favell, D. J. A comparison of the vitamin C content of fresh and frozen vegetables. *Food Chem.* (1998) doi:10.1016/S0308-8146(97)00165-9.
197. Giovanelli, G., Lavelli, V., Peri, C. & Nobili, S. Variation in antioxidant components of tomato during vine and post-harvest ripening. *J. Sci. Food Agric.* (1999) doi:10.1002/(SICI)1097-0010(199909)79:12<1583::AID-JSFA405>3.0.CO;2-J.
198. Farneti, B., Schouten, R. E. & Woltering, E. J. Low temperature-induced lycopene degradation in red ripe tomato evaluated by remittance spectroscopy. *Postharvest Biol. Technol.* (2012) doi:10.1016/j.postharvbio.2012.05.008.
199. Biacs, P. & Wissgott, U. Investigation of colour changes of some tomato products during frozen storage. *Nahrung - Food* (1997) doi:10.1002/food.19970410512.
200. BEGLIOMINI, A. L., MONTEDORO, G., SERVILI, M., PETRUCCIOLI, M. & FEDERICI, F. OXIDOREDUCTASES FROM TOMATO FRUIT: INHIBITORY EFFECT OF A FUNGAL GLUCOSE OXIDASE. *J. Food Biochem.* (1995) doi:10.1111/j.1745-4514.1995.tb00529.x.
201. Gümüşay, Ö. A., Borazan, A. A., Ercal, N. & Demirkol, O. Drying effects on the antioxidant properties of tomatoes and ginger. *Food Chem.* (2015) doi:10.1016/j.foodchem.2014.09.162.
202. Toor, R. K. & Savage, G. P. Antioxidant activity in different fractions of tomatoes. *Food Res. Int.* (2005) doi:10.1016/j.foodres.2004.10.016.
203. Bernard, H. *et al.* Large multistate outbreak of norovirus gastroenteritis associated with frozen strawberries, Germany, 2012. *Eurosurveillance* **19**, 20719 (2014).
204. SARVIKIVI, E. *et al.* Multiple norovirus outbreaks linked to imported frozen raspberries. *Epidemiol. Infect.* **140**, 260–267 (2012).
205. CALDER, L. *et al.* An outbreak of hepatitis A associated with consumption of raw blueberries. *Epidemiol. Infect.* **131**, 745–751 (2003).
206. Scavia, G. *et al.* A large prolonged outbreak of hepatitis A associated with consumption of frozen berries, Italy, 2013–14. *J. Med. Microbiol.* **66**, 342–349 (2017).
207. Niu, M. T. *et al.* Multistate Outbreak of Hepatitis A Associated with Frozen Strawberries. *J. Infect. Dis.* **166**, 518–524 (1992).
208. Harmonie brand, IGA brand, Co-op brand, Western Family brand and unbranded frozen vegetable products recalled due to Listeria monocytogenes - Food Recall Warning - Canadian Food Inspection Agency. http://www.inspection.gc.ca/about-the-cfia/newsroom/food-recall-warnings/complete-listing/2016-05-07/eng/1462667105675/1462667109404.
209. Affairs, O. of R. Recalls, Market Withdrawals, & Safety Alerts - Updated: CRF Frozen Foods Expands Voluntary Recall to Include All Frozen Vegetable and Fruit Products Due To Possible Health Risk.
210. FDA Investigated Listeria Outbreak Linked to Frozen Vegetables | FDA. https://www.fda.gov/food/outbreaks-foodborne-illness/fda-investigated-listeria-outbreak-linked-frozen-

vegetables.
211. Catford, A., Ganz, K. & Tamber, S. Enumerative Analysis of *Salmonella* in Outbreak-Associated Breaded and Frozen Comminuted Raw Chicken Products. *J. Food Prot.* **80**, 814–818 (2017).
212. Hassan, R. *et al.* Multistate outbreak of *Salmonella* Paratyphi B variant L(+) tartrate(+) and *Salmonella* Weltevreden infections linked to imported frozen raw tuna: USA, March–July 2015. *Epidemiol. Infect.* **146**, 1461–1467 (2018).
213. Bilbao-Sainz, C. *et al.* Preservation of sweet cherry by isochoric (constant volume) freezing. *Innov. Food Sci. Emerg. Technol.* **52**, (2019).
214. Mújica-Paz, H., Valdez-Fragoso, A., Samson, C. T., Welti-Chanes, J. & Torres, J. A. High-Pressure Processing Technologies for the Pasteurization and Sterilization of Foods. *Food Bioprocess Technol.* **4**, 969–985 (2011).
215. Mukhopadhyay, S. *et al.* Inactivation of Salmonella enterica and Listeria monocytogenes in cantaloupe puree by high hydrostatic pressure with/without added ascorbic acid. *Int. J. Food Microbiol.* **235**, 77–84 (2016).
216. Gänzle, M. & Liu, Y. Mechanisms of pressure-mediated cell death and injury in Escherichia coli: from fundamentals to food applications. *Front. Microbiol.* **6**, 599 (2015).
217. Storz, G. & Hengge, R. *Bacterial Stress Responses*. (ASM Press, 2011). doi:10.1128/9781555816841.
218. Wu, V. C. H. A review of microbial injury and recovery methods in food. *Food Microbiol.* **25**, 735–744 (2008).
219. Bilbao-Sainz, C. *et al.* Preservation of sweet cherry by isochoric (constant volume) freezing. *Innov. Food Sci. Emerg. Technol.* **52**, 108–115 (2019).
220. Coulomb, D., Dupon, J. L. & Pichard, A. The Role of Refrigeration in the Global Economy. *29th Inf. Note Refrig. Technol.* (2015).
221. Coulomb, D. Refrigeration and cold chain serving the global food industry and creating a better future: two key IIR challenges for improved health and environment. *Trends Food Sci. Technol.* (2008) doi:10.1016/j.tifs.2008.03.006.
222. James, S. J. & James, C. The food cold-chain and climate change. *Food Res. Int.* (2010) doi:10.1016/j.foodres.2010.02.001.
223. IIR. *The role of refrigeration in worldwide nutrition, 5th informatory note on refrigeration on food*. (2009).
224. Hasanuzzaman, M., Saidur, R. & Masjuki, H. H. Effects of operating variables on heat transfer and energy consumption of a household refrigerator-freezer during closed door operation. *Energy* (2009) doi:10.1016/j.energy.2008.11.003.
225. Geppert, J. & Stamminger, R. Analysis of effecting factors on domestic refrigerators' energy consumption in use. *Energy Convers. Manag.* (2013) doi:10.1016/j.enconman.2013.08.027.
226. Gigiel, A. & Collett, P. Energy consumption, rate of cooling and weight loss in beef chilling in UK slaughter houses. *J. Food Eng.* (1989) doi:10.1016/0260-8774(89)90002-2.
227. Bustabad, O. M. Weight loss during freezing and the storage of frozen meat. *J. Food Eng.* (1999) doi:10.1016/S0260-8774(99)00065-5.
228. Ullah, J., Takhar, P. S. & Sablani, S. S. Effect of temperature fluctuations on ice-crystal growth in frozen potatoes during storage. *LWT - Food Sci. Technol.* (2014) doi:10.1016/j.lwt.2014.06.018.
229. Martins, R. C., Almeida, M. G. & Silva, C. L. M. The effect of home storage conditions and packaging materials on the quality of frozen green beans. *Int. J. Refrig.* (2004) doi:10.1016/j.ijrefrig.2004.04.008.
230. Năstase, G., Lyu, C., Ukpai, G., Şerban, A. & Rubinsky, B. Isochoric and isobaric freezing of fish muscle. *Biochem. Biophys. Res. Commun.* **485**, 279–283 (2017).
231. Lyu, C., Nastase, G., Ukpai, G., Serban, A. & Rubinsky, B. A comparison of freezing-damage during isochoric and isobaric freezing of the potato. *PeerJ* (2017) doi:10.7717/peerj.3322.
232. Tassou, S. A., Lewis, J. S., Ge, Y. T., Hadawey, A. & Chaer, I. A review of emerging technologies for food refrigeration applications. *Applied Thermal Engineering* (2010) doi:10.1016/j.applthermaleng.2009.09.001.
233. Tušek, J. *et al.* A regenerative elastocaloric heat pump. *Nat. Energy* (2016) doi:10.1038/nenergy.2016.134.
234. Powell-Palm, M. J., Preciado, J., Lyu, C. & Rubinsky, B. Escherichia coli viability in an isochoric system at subfreezing temperatures. *Cryobiology* (2018) doi:https://doi.org/10.1016/j.cryobiol.2018.10.262.
235. Reid, D. S. Basic physical phenomena in freezing and thawing of plant and animal tissues. in *Frozen Food Technology* (ed. Mollett, C. P.) 1–18 (Chapman and Hall, 1996).
236. Lide, D. R. CRC Handbook of Chemistry and Physics, 84th Edition, 2003-2004. *Handb. Chem. Phys.* (2003) doi:10.1136/oem.53.7.504.
237. Zhang, J., Liu, L., Mu, W., Moga, L. M. & Zhang, X. Development of temperature-managed traceability

system for frozen and chilled food during storage and transportation. *J. Food, Agric. Environ.* (2009).
238. Ndraha, N., Hsiao, H. I., Vlajic, J., Yang, M. F. & Lin, H. T. V. Time-temperature abuse in the food cold chain: Review of issues, challenges, and recommendations. *Food Control* (2018) doi:10.1016/j.foodcont.2018.01.027.
239. Birdseye, C. Method of preserving piscatorial products. (1924).
240. Mastani Joybari, M., Haghighat, F., Moffat, J. & Sra, P. Heat and cold storage using phase change materials in domestic refrigeration systems: The state-of-the-art review. *Energy Build.* (2015) doi:10.1016/j.enbuild.2015.06.016.
241. Azzouz, K., Leducq, D. & Gobin, D. Enhancing the performance of household refrigerators with latent heat storage: An experimental investigation. *Int. J. Refrig.* (2009) doi:10.1016/j.ijrefrig.2009.03.012.
242. Sonnenrein, G. *et al.* Reducing the power consumption of household refrigerators through the integration of latent heat storage elements in wire-and-tube condensers. *Int. J. Refrig.* (2015) doi:10.1016/j.ijrefrig.2014.12.011.
243. Cheng, W.-L., Mei, B.-J., Liu, Y.-N., Huang, Y.-H. & Yuan, X.-D. A novel household refrigerator with shape-stabilized PCM (Phase Change Material) heat storage condensers: An experimental investigation. *Energy* (2011) doi:10.1016/j.energy.2011.08.050.
244. Elarem, R., Mellouli, S., Abhilash, E. & Jemni, A. Performance analysis of a household refrigerator integrating a PCM heat exchanger. *Appl. Therm. Eng.* (2017) doi:10.1016/j.applthermaleng.2017.07.113.
245. Savović, S. & Caldwell, J. Finite difference solution of one-dimensional Stefan problem with periodic boundary conditions. *Int. J. Heat Mass Transf.* (2003) doi:10.1016/S0017-9310(03)00050-4.
246. Rizwan-uddin. One-dimensional phase change with periodic boundary conditions. *Numer. Heat Transf. Part A Appl.* **35**, 361–372 (1999).
247. Rizwan-uddin. A Nodal Method for Phase Change Moving Boundary Problems. *Int. J. Comut. Fluid Dyn.* **11**, 211–221 (1999).
248. Bilbao-Sainz, C. *et al.* Preservation of spinach by isochoric (constant volume) freezing. *Int. J. Food Sci. Technol.* (2020) doi:10.1111/ijfs.14463.
249. Bolz, R. E. & Tuve, G. L. *CRC Handbook of Tables for Applied Engineering Science.* (The Chemical Rubber Co., 1920).
250. Sanz, P. D., Otero, L., De Elvira, C. & Carrasco, J. A. Freezing processes in high-pressure domains. *Int. J. Refrig.* (1997) doi:10.1016/S0140-7007(97)00027-3.
251. Nagornov, O. V & Chizhov, V. E. Thermodynamic properties of ice, water, and a mixture of the two at high pressures. *J. Appl. Mech. Tech. Phys.* **31**, 378–385 (1990).
252. Ter Minassian, L., Pruzan, P. & Soulard, A. Thermodynamic properties of water under pressure up to 5 kbar and between 28 and 120 °C. Estimations in the supercooled region down to -40 °C. *J. Chem. Phys.* (1981) doi:10.1063/1.442402.

7. Appendix

A1: Supplementary formulations for derivation of isochoric nucleation barrier

A1.1 Derivation of specific volumes of water and ice-1h as a function of absolute ice nucleus volume. The goal of this derivation is to enable determination of the specific volume of each phase as function of ice nucleus growth, which in turn enables calculation of the specific Helmholtz free energies of each phase as a function of ice nucleus growth, $F_{\mathrm{water}}(v_{\mathrm{water}}(V_{\mathrm{ice}}))$ and $F_{\mathrm{ice}}(v_{\mathrm{ice}}(V_{\mathrm{ice}}))$. These parameters are employed in the main text in the derivation of the isochoric nucleation barrier.

In the following text, subscripts function as follows:

$X_{\mathrm{s}} = property\ of\ whole\ system$
$X_{\mathrm{w}} = property\ of\ water\ phase$
$X_{\mathrm{i}} = property\ of\ ice\ phase$

As described in the main text section entitled “Mathematical formulation of the system”, the four constraints that govern an isochoric system comprised of supercooled water and an emergent ice nucleus are:

Conservation of mass, absolute system volume, and specific system volume:

$$V_{\mathrm{s}} = V_{\mathrm{i}} + V_{\mathrm{w}} \tag{1}$$

$$m_{\mathrm{s}} = m_{\mathrm{i}} + m_{\mathrm{w}} \tag{2}$$

$$v_{\mathrm{s}} = \frac{V_{\mathrm{s}}}{m_{\mathrm{s}}} = \frac{V_{\mathrm{i}}+V_{\mathrm{w}}}{m_{\mathrm{i}}+m_{\mathrm{w}}} \tag{3}$$

Continuity of pressure between phases:

$$-\left(\frac{dF_{\mathrm{w}}}{dv}\right)|_{v_{\mathrm{w}}} = -\left(\frac{dF_{\mathrm{i}}}{dv}\right)|_{v_{\mathrm{i}}} \tag{4}$$

Using the continuity of pressure, the specific volumes of the water and ice phases may be related. For the purposes of this analysis, we assume a parabolic form for each of the *F(v)* curves relating specific free energy to specific volume:

$$F_{\mathrm{i}}(v) = Av^2 + Bv + C \tag{5}$$

$$F_{\mathrm{w}}(v) = Dv^2 + Ev + F \tag{6}$$

and thus

$$\left(\frac{dF_{\mathrm{i}}}{dv}\right) = 2Av + B \tag{7}$$

$$\left(\frac{dF_{\mathrm{w}}}{dv}\right) = 2Dv + E \tag{8}$$

Now substituting into Eq. 4, an expression for v_{w} in terms of v_{i} is achieved:

$$-\left(\frac{dF_{\mathrm{w}}}{dv}\right)|_{v_{\mathrm{w}}} = -\left(\frac{dF_{\mathrm{i}}}{dv}\right)|_{v_{\mathrm{i}}} \tag{4}$$

$$-(2Av_{\mathrm{i}} + B) = -(2Dv_{\mathrm{w}} + E) \tag{9}$$

$$v_{\mathrm{w}} = \frac{A}{D}\, v_{\mathrm{i}} + \left(\frac{B-E}{2C}\right) \tag{10}$$

$$C_1 = \left(\frac{B-E}{2C}\right) \tag{11}$$

$$v_{\mathrm{w}} = \frac{A}{D}\, v_{\mathrm{i}} + C_1 \tag{12}$$

This relatability of the specific volumes is an essential product of the pressure continuity requirement, and a unique fundamental feature of isochoric systems.

Now, using eqs. 1-3 and eq. 12, we may derive the functions $v_{\mathrm{w}}(V_{\mathrm{i}})$ and $v_{\mathrm{i}}(V_{\mathrm{i}})$ (eqs. 22 and 23), which give the specific volume of each phase as a function of the absolute volume of the ice nucleus:

$$V_{\mathrm{i}} = V_{\mathrm{s}} - V_{\mathrm{w}} \tag{13}$$

$$V_{\mathrm{i}} = v_{\mathrm{s}}m_{\mathrm{s}} - v_{\mathrm{w}}m_{\mathrm{w}} \tag{14}$$

$$V_{\mathrm{i}} = v_{\mathrm{s}}m_{\mathrm{s}} - \left(\frac{A}{D}\, v_{\mathrm{i}} + C_1\right)(m_{\mathrm{s}} - m_{\mathrm{i}}) \tag{15}$$

$$V_{\mathrm{i}} = v_{\mathrm{s}}m_{\mathrm{s}} - \frac{A}{D}v_{\mathrm{i}}m_{\mathrm{s}} + \frac{A}{D}v_{\mathrm{i}}m_{\mathrm{i}} - C_1m_{\mathrm{s}} + C_1m_{\mathrm{i}} \tag{16}$$

$$V_{\mathrm{i}} = v_{\mathrm{s}}m_{\mathrm{s}} - \frac{A}{D}v_{\mathrm{i}}m_{\mathrm{s}} + \frac{A}{D}V_{\mathrm{i}} - C_1m_{\mathrm{s}} + C_1\frac{V_{\mathrm{i}}}{v_{\mathrm{i}}} \tag{17}$$

$$\frac{V_{\mathrm{i}}\left(1-\frac{A}{D}\right)}{m_{\mathrm{s}}} = \frac{V_{\mathrm{s}}}{m_{\mathrm{s}}} - \frac{A}{D}v_{\mathrm{i}} - C_1 + \frac{C_1}{m_{\mathrm{s}}}\frac{V_{\mathrm{i}}}{v_{\mathrm{i}}} \tag{18}$$

$$\frac{V_{\mathrm{i}}\left(1-\frac{A}{D}\right)-V_{\mathrm{s}}}{m_{\mathrm{s}}} + C_1 = -\frac{A}{D}v_{\mathrm{i}} + \frac{C_1}{m_{\mathrm{s}}}\frac{V_{\mathrm{i}}}{v_{\mathrm{i}}} \tag{19}$$

$$\left(\frac{V_{\mathrm{i}}\left(1-\frac{A}{D}\right)-V_{\mathrm{s}}}{m_{\mathrm{s}}} + C_1\right)v_{\mathrm{i}} = -\frac{A}{D}v_{\mathrm{i}}^2 + \frac{C_1V_{\mathrm{i}}}{m_{\mathrm{s}}} \tag{20}$$

$$\frac{A}{D}v_{\mathrm{i}}^2 + \left(\frac{V_{\mathrm{i}}\left(1-\frac{A}{D}\right)-V_{\mathrm{s}}}{m_{\mathrm{s}}} + C_1\right)v_{\mathrm{i}} - \frac{C_1V_{\mathrm{i}}}{m_{\mathrm{s}}} = 0 \tag{21}$$

$$v_{\mathrm{i}} = -\frac{\left(\frac{V_{\mathrm{i}}\left(1-\frac{A}{D}\right)-V_{\mathrm{s}}}{m_{\mathrm{s}}}+C_1\right) \pm \sqrt{\left(\frac{V_{\mathrm{i}}\left(1-\frac{A}{D}\right)-V_{\mathrm{s}}}{m_{\mathrm{s}}}+C_1\right)^2 - 4\left(\frac{A}{D}\right)\left(-\frac{C_1V_{\mathrm{i}}}{m_{\mathrm{s}}}\right)}}{2\left(\frac{A}{D}\right)} \tag{22}$$

$$v_{\mathrm{w}} = \frac{A}{D}\, v_{\mathrm{i}} + C_1 \tag{23}$$

These expressions may now be used to determine the specific free energy of each phase as a function of the absolute ice nucleus volume, $F_{\mathrm{w}}(v_{\mathrm{w}}(V_{\mathrm{i}}))\ and\ F_{\mathrm{i}}(v_{\mathrm{i}}(V_{\mathrm{i}}))$, in the derivation of the isochoric nucleation barrier in the main text.

A1.2 Parameters used in the calculation of the free energy curve in main text Figure 2.3A:

System absolute volume $V_{\mathrm{s}} = 2\,x\,10^{-22}\,m^3$

System specific volume $v_{\mathrm{s}} = 0.001\,m^3\,kg^{-1}$

System mass $m_{\mathrm{s}} = 2\,x\,10^{-19}\,kg$

Temperature $T = -4.15\,°C$

For all calculations plotted in Figure 3, the same system specific volume was retained, and the interfacial free energy gamma was calculated using the following relation from Pruppacher and Klett[68]:

$$\gamma = (28.0 + 0.25T)\ mJ\,m^{-2}$$

in which the units of temperature are degrees Celsius.

For the purposes of relating the radius of the ice nucleus to its volume and surface area, the nucleus was assumed spherical.

A2. Thermodynamic modeling of multicomponent isochoric freezing

Herein is provided a more rigorous walkthrough of the algorithm used to predict the equilibrium states of single- and multiphase isochoric systems. Please note that the information provided here does not deal in conceptual interpretation of multiphase isochoric phenomena, and the reader should refer back to the main text if conceptual clarification is needed.

A2.1 Isochoric Freezing: Concept and Thermodynamic Model

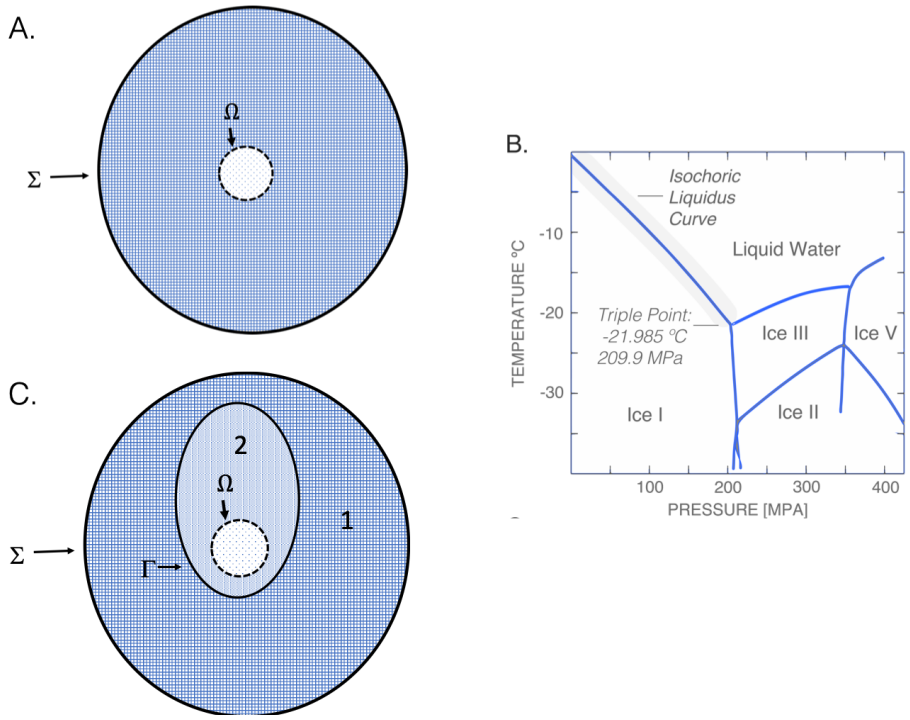

Figure A1. Thermodynamic information for use in isochoric model. A. Thermodynamic schematic for a single-phase isochoric system. B. Phase diagram of pure water. C. Thermodynamic schematic for a multiphase isochoric system.

The state of a system comprised of an aqueous solution in thermodynamic equilibrium is uniquely defined by two independent thermodynamic properties, e.g. pressure P, and temperature, T, and the solution composition, c, of all the species in the solution. In a thermodynamic system in which ice and water co-exist in thermodynamic equilibrium, the pressure and temperature are not independent properties and the liquidus curve on the phase diagram defines the correlation between them. Therefore, the thermodynamic state of a system is defined by either pressure, P, or temperature T, and the thermodynamic property of quality, Z, which gives the percentage weight of the liquid phase relative to the total weight of the two-phase mixture of solid and liquid phase. In the thermodynamic analysis of a process of freezing of biological matter, it is assumed that the system goes through a series of states of thermodynamic equilibrium. In most of the studies on freezing/thawing of biological matter, it is assumed that the system is at constant pressure, isobaric – and usually atmospheric. The thermodynamic states of equilibrium in an isobaric process are defined by the Gibbs free energy. By contrast, we study the process of freezing/thawing of biological matter in a constant volume, isochoric system whose state of equilibrium is defined by the Helmholtz free energy. As mentioned earlier, our approach in analyzing the isochoric freezing/thawing process deals with processes that go through continuous series of states of thermodynamic equilibrium. Therefore, to understand the process it is sufficient to follow the path of states of thermodynamic equilibrium. Here we will show how to develop the mathematic model for those states, first in a single-phase system and then in a multiphase system. Since thermodynamics deals with states of thermodynamic equilibrium this model cannot apply to rapid transients in thermodynamic properties, such as the phenomenon of supercooling. The mathematical model is based on the following concepts:

a) The analyzed thermodynamic system contains a mixture of ice and water, in which the ice and liquid co-exist and are in thermodynamic equilibrium.
b) In an ice/water system in thermodynamic equilibrium, the temperature and pressure are dependent properties
c) In an isochoric system the volume is constant and mass in conserved.
d) In an isochoric system containing ice and water in thermodynamic equilibrium, at a prescribed temperature or pressure, the only possible variable that adjusts itself to fulfill the requirement of thermodynamic equilibrium and constant volume is the "quality" of the system, i.e. the relative percentage of ice and liquid in the system.
e) Either temperature or pressure; the quality at that temperature or pressure; and the composition, completely specify the process of freezing in isochoric cryopreservation.

To study the process of isochoric freezing we developed a mathematical model of all the thermodynamic states of equilibrium in an aqueous solution of initial volume V and mass, m, and composition, C, in which the water in the solution is in thermodynamic equilibrium with ice. Our mathematical approach is to use an iterative method of solution, that generates the value of the quality Z, for any temperature T or pressure P, along the path of thermodynamic equilibrium in an isochoric system in which ice and water are in thermodynamic equilibrium. We will describe first the model for a single phase aqueous system and then for a multiphase system. A schematic of the single-phase system is shown in Figure S1A. The figure shows a closed system surrounded by a boundary Σ , that is rigid and can transfer heat but no mass. Ice has formed in the system. The ice is separated from the liquid phase by the boundary Ω. The boundary Ω , separates between ice and an aqueous solution at thermodynamic equilibrium, in contact with each other. Therefore, the temperature and pressure are dependent thermodynamic properties whose correlation is prescribed by the liquidus line, between ice and water (Figure S1B). At thermodynamic equilibrium, the temperature and pressure are constant throughout the system. Ice has a tight crystallographic structure and therefore, it is assumed that the domain of ice is made of pure ice, without solutes.

A2.2 Thermodynamic model of a single-composition isochoric system at subfreezing temperatures

The algorithm for defining the thermodynamic state of an isochoric ice/solution system is as follows:

1) Completely specify the analyzed isochoric system. In such a system the volume is constant and given, the mass of each species in the volume is given. Assume closed rigid walls of the system and conservation of mass in the system. Assume that the pressure and temperature are uniform throughout the system at equilibrium.

2) The goal of the analysis is to completely define the thermodynamic state of the system when it is in a thermodynamic state in which there is a mixture of ice and water in contact with each other in thermodynamic equilibrium, for the given volume and composition.

3) The algorithm attempts to define the thermodynamic state of the given system (volume and composition) when the analyzed system is at a certain pressure P. Al the other thermodynamic properties are unknown and are determined through the iterative algorithm. The thermodynamic state is found through an iterative process

4) In a first step we calculate the equilibrium temperature from the equations given below.

   For example, if the solution is pure water, the correlation between temperature and pressure is given by the liquidus line on the phase diagram (Figure S1B). The pressure temperature phase diagram for pure water is well known, e.g. [1]. A regression correlation between temperature T_l [ºC] and pressure P_l [MPa] on the liquidus line for pure water was developed in [2]:

   $$T_l(P_l) = -4E\text{-}10\ P_l^3 - 3E\text{-}7\ P_l^2 - 0.0081\ P_l + 0.0081 \qquad (1)$$

   This correlation is valid from 0 ºC to the triple point between water, ice I and ice III; at -21.985°C and 209.9 MPa. Therefore, for a given P, equation (1) gives the corresponding, temperature, T.

   However, the problem is more complicated in biological materials which are made of aqueous solutions. Furthermore, during cryopreservation, cryoprotectants are often added, thereby further increasing the complexity of the problem. In this study, we use as a first order approximation the following correlation between temperature, pressure and composition:

   $$T(P, C) = -4E\text{-}10\ P^3 - 3E\text{-}7\ P^2 - 0.0081\ P + 0.008 + \Sigma\Delta T\ (Cn) \qquad (2)$$

   The approximation assumes that the temperature at thermodynamic equilibrium is a linear combination of the effect of pressure and the freezing point depression, $\Sigma\Delta T(c)$, due to the osmotic effect of the various solutes. This is a well-known approximation commonly used in research in cryobiology, e.g. [3]. In this first order approximation we assume that the effect of pressure and solute concentration on the water freezing temperature are independent of each other and that each chemical species effect is also independent on each other. We anticipate that this assumption is correct at lower concentrations and that at concentrations the effects may not be linearly additive.

   Non-linear correlations should probably be obtained later, when more research is done in this field and new experimental data becomes available. Appendix A1.A gives various correlations between freezing point depression and concentration in various chemical species of interest to cryobiology. It should be noticed that the concentration of the various species is known before freezing, but is not known at any subfreezing temperature. Because ice cannot contain solutes (it has a tight crystallographic structure) the solutes are all found

in the unfrozen solution. However, the volume of the unfrozen solution depends on the fraction of ice which in turn depends on the concentration of solutes. This is where the need for an iterative solution arises. For the first iteration we recommend using the initial concentration of solutes in the unfrozen solution, although any initial guess will eventually converge to the final composition.

5) From the temperature and pressure calculated in 4) we use principles on conservation of mass, experimental data on specific volume of ice and water as a function of temperature, coefficients of thermal expansion and compressibility, to calculate the quality of the system. The derivation and the mode of calculation are given in Appendix A1.B.

6) From the quality and principles of conservation of mass of solutes we can calculate the concentration in the unfrozen volume. We evaluate the new concentration due to the formation of ice and from the assumption that ice does not incorporate solutes and conservation of mass using the following equation:

$$c_1 = \frac{c_0}{Z} \qquad (3)$$

where, c_1 is the new calculated concentration, c_0 is the initial concentration at atmospheric pressure in the unfrozen solution and Z is the quality, calculated as described in appendix A1.B.

7) Replace the concentration assumed in step 4 with the newly calculated concentration from eq. (3).

8) Repeat step 4 to calculate the temperature due to the newly calculated concentration.

9) Evaluate the percent difference of freezing temperature with the temperature of the previous iteration.

$$\%diff = \frac{\left|T_{ph}^{i} - T_{ph}^{i-1}\right|}{T_{ph}^{i}} \qquad (4)$$

In which T_{ph}^{i} is the temperature obtained in the present iteration and T_{ph}^{i-1} is the temperature of the previous iteration.

10) If the percent of difference is less than a specified tolerance terminate the loop and record the freezing temperature and the quality at the analyzed pressure.

11) If not repeat the loop from step 4 until convergence to the specific tolerance.

A2.3 Thermodynamic model of a multiphase (multicomposition) isochoric system at subfreezing temperatures

In this part of the study we seek to develop the fundamental thermodynamic model for analysis of multiphasic aqueous systems at subfreezing temperature. In order fix ideas we will use the multiphase system in Figure S1C. The system in Fig 1C consists of two different aqueous phases, 1 and 2, with a different initial composition and a different osmolality. In this example, without loss of generality, let us assume that phase 2, is completely encased by phase 1. They are separated by a boundary, Γ , that is impermeable to matter, is completely malleable and can transfers heat and pressure. Phase A is surrounded by a boundary Σ , that is rigid, and can transfer heat, but does not transfer mass. The composite, phases 1 and 2 are therefore, isochoric and at thermodynamic equilibrium. There is a uniform temperature and pressure throughout the entire domain bounded by the rigid boundary Σ. As mentioned earlier, our approach in analyzing the isochoric freezing/thawing process deals with processes that go through continuous series of states of thermodynamic equilibrium. Therefore, to understand the process it is sufficient to follow the path of states of thermodynamic equilibrium. Here we will show how to develop the mathematic model for the multiphase system. Since thermodynamics deals with states of thermodynamic equilibrium this model cannot apply to rapid transients in thermodynamic properties, such as the phenomenon of supercooling. The mathematical model is based on the assumptions a) to e) listed for the single phase system.

As with the single phase freezing model, for the multiphase case we developed a mathematical model of all the thermodynamic states of equilibrium in aqueous solutions in which at least in one of the phases, 1 or 2, the solution is in thermodynamic equilibrium with ice. In contrast to the single phase model, here we deal with two phases, 1 and 2 that have a known initial mass and composition which can be different between the two and are both constrained in a rigid volume, V. The two phases, 1 and 2, are separated by a boundary Γ, that does not allow any mass transfer between the phases. Assuming, for the purpose of this example, that the initial osmolality of the material in system 1 is higher than that in system 2, when the uniform temperature of the composite systems 1 and 2 drops below the phase transition temperature of material 2, at the pressure of the systems, freezing will begin in system 2. This will generate a new phase, ice, in system 2, separated from the liquid phase in system 2 by the boundary Ω (see Fig 1C). The boundary Ω , separates between ice and an aqueous solution at thermodynamic equilibrium in phase 2, in contact with each other. Therefore, the temperature and pressure are dependent thermodynamic properties and the thermodynamic state of the interface will be prescribed by the liquidus line, between ice and water (Figure S1B). Because the entire system is in thermodynamic equilibrium this will be also the temperature and pressure of the phase 1, from the second law of thermodynamics across boundary, Γ . As with the previous algorithm, it is assumed that ice cannot contain solutes.

The algorithm for defining the thermodynamic state of a multiphase isochoric ice/ solution system is similar to the algorithm for the single phase freezing system with the following differences: in steps 1) to 6):

1) Completely specify the analyzed isochoric system. In multiphase system the volume of the composite system is constant and given. The mass of water and solutes in each of the

phases are given. Assume closed rigid walls of the composite system and conservation of mass in the all phases of the system, e.g. 1 and 2 in Figure S1C. Assume that the pressure and temperature are uniform throughout all the phases in the composite system at equilibrium.

2) The goal of the analysis is to completely define the thermodynamic state of the multiphase system when one of the phases is in a thermodynamic state of equilibrium. in which there is a mixture of ice and water in contact with each other. temperature and pressure of the other phases in which there is no thermodynamic equilibrium between ice and water is prescribed by the temperature and pressure by the system in which there is thermodynamic equilibrium between ice and a solution, again from the second law of thermodynamics.

3) The algorithm begins with an iteration to define the thermodynamic state of the multiphase system (volume and composition) when the entire multiphase system is at a certain pressure P. All the other thermodynamic properties are unknown.

4) Step 4 is identical to that in the single-phase system, i.e. the temperature at the ice/solution interface is calculated from the pressure and composition. Since there is no mass transfer between the various phases, the only relevant composition is the one in the phase in which ice and water are in equilibrium. The composition of the other phases is irrelevant to the state of thermodynamic equilibrium of the multiphase system. As in the single-phase system, the concentration of the various species in the system that freezes is known before freezing, but is not known at any subfreezing temperature. Because ice cannot contain solutes (it has a tight crystallographic structure) the solutes are all found in the unfrozen solution. However, the volume of the unfrozen solution depends on the fraction of ice which in turn depends on the concentration of solutes, which makes the model non-linear and the solution is found iteratively. Again, the composition of the phases in which there is no ice – remain unchanged throughout the freezing in the phase that experiences freezing.

5) From the temperature and pressure calculated in 4) we use principles on conservation of mass, experimental data on specific volume of ice and water as a function of temperature, coefficients of thermal expansion and compressibility, to calculate the quality of the system. Because the phase in which there is no ice is at the same temperature and pressure as the phase in which there is ice, and because we assume that all the solutions behave as pure water, all the phases contribute to the calculation of the quality of the composite system, in terms of their compressibility and thermal expansion. Therefore the expression for the quality is the same as in the single phase system, Equation B5.

6) This step is where there is a substantial difference between single and multiphase freezing systems. Because we have a multiphase system, there are several possible situations. To fix ideas, we will use the example in Figure S1C, in which there are two possibilities.

A) If the mass of ice calculated from Equation B13 is smaller than the mass in phase 2, than freezing is confined only to phase 2. Since the boundary between phase 1 and 2 is impermeable, the conservation of mass used to calculate the solute concentration in phase 2 is affected only by the original amount of solutes in phase 2, and phase 1, has no effect on the concentration. Therefore, the concentration of any species in phase 2 is given by

$$c_2 = c_{20} \frac{m_2}{(Z(m_1 + m_2) - m_1)} \quad (5)$$

B) If the entire mass of ice in phase 2 is frozen, and freezing extends into phase 1, then the concentration of the chemical species in phase 1 is affected only by the initial concentration in phase 1 and the portion of ice that has formed in phase 1 and is given by:

$$c_1 = c_{10} \frac{m_1}{Z(m_1 + m_2)} \quad (6)$$

7) Steps 7 - 11 are identical in function to those in the single-phase algorithm. Note however that at points between cases A) and B) above, which is to say in the temperature span between the point at which Phase 2 has frozen completely and the pressure-adjusted freezing point of Phase 1, only the temperature will change, and this algorithm is not applicable. This "transition zone" is discussed with greater conceptual rigor and visual aid in the main text.

Sub-Appendix A2.A

Data on the freezing point depression of NaCl and other additives of interest to cryopreservation can be found in reference [4]. An analytical correlation was obtained from the data in [4], of the form:

$$\Delta T_{NaCl}(c) = -294.15\ c^3 - 80.193\ c^2 - 54.402\ c \quad (A1)$$

The freezing point depression, due to ethylene glycol and due to glycerol in water, is also found in that reference. The correlation for freezing point depression of ethylene glycol as a function of temperature is given by,

$$\Delta T_{e\text{- glycol}}(c) = 231.48c^4 - 354.94c^3 + 76.389c^2 - 49.559c + 0.0132 \quad (A2)$$

In the case of glycerol the relation between freezing temperature and concentration was so irregular that different correlations where produced for segments of the temperature in different ranges of concentration.

$0 \leq c < 0.2895$

$$\Delta T_{glycerol}(c) = 92.743\ c^3 - 75.17\ c^2 - 16.408\ c$$

$0.2895 \leq c < 0.3378$

$$\Delta T_{glycerol}(c) = -1006.1\ c^3 + 561.08\ c^2 - 128.97\ c + 5.9249 \qquad \text{(A3)}$$

$0.3378 \leq c < 0.4825$

$$\Delta T_{glycerol}(c) = -9811.1\ c^3 + 12223\ c^2 - 5085.7\ c + 689.01$$

$0.4825 \leq c < 0.6755$

$$\Delta T_{glycerol}(c) = 394.85\ c^2 - 573.06\ c + 165.43$$

The concentrations c, used in these equation are in terms of mass ratio, i.e. mass of substance per volume of solution. The following equation can be used to correlate the concentration (mass ratio) with molarity.

$$c = MW \times M \times v \qquad \text{(A4)}$$

Where MW is the molecular weight, M molarity, and υ is the solution specific volume.

Sub-Appendix A2.B – Derivation of the expression for quality in an isochoric system

Following is a general derivation for the quality or phase fraction, *Z*, which is the ratio between the mass of the liquid solution to the total mass of the mixture of liquid and ice in an isochoric, constant volume system. In the derivation given below, V, m, v, are absolute volume, mass, and specific volume respectively. The subscripts, 0, 1, 2, are for the original conditions, ice and liquid, respectively. The original conditions in our isochoric analysis are a pressure of one atmosphere, the change of phase temperature of the liquid solution at that pressure and the assumption that the original specific volume is that of the pure liquid solution at that pressure and temperature. The expression for *Z*, is obtained from conservation of mass in a constant volume.

At all times,

$$m_0 = m_1 + m_2 \qquad \text{(B1)}$$

$$V_0 = V_1 + V_2 \qquad \text{(B2)}$$

The quality *Z* is,

$$Z = \frac{m_2}{m_0} = \frac{m_2}{m_1 + m_2} \tag{B3}$$

Conservation of mass in a constant volume and from the definition of specific volume yields,

$$\upsilon_0 = \frac{V_0}{m_0} = \frac{V_1 + V_2}{m_0} = \frac{m_1 V_1}{m_0 m_1} + \frac{m_2 V_2}{m_0 m_2} = \frac{(m_0 - m_2)}{m_0}\upsilon_1 + Z\upsilon_2 = (1 - Z)\upsilon_1 + Z\upsilon_2 \tag{B4}$$

Reorganization of the terms in equation A4, produces a general expression for the quality of the mixture during isochoric freezing in terms of the specific volumes of the ice and unfrozen solution at each state of thermodynamic equilibrium

$$Z = \frac{\upsilon_0 - \upsilon_1}{\upsilon_2 - \upsilon_1} \tag{B5}$$

To calculate quality we need values for specific volume as a function of temperature and pressure, compressibility and coefficients of thermal expansion. We have found data for water and ice in [250]. The specific volumes for ice and water as a function of temperature and pressure will be given in the following set of equations.

For ice:

$$v_1 = v_{10} \exp\left[-\int_{P_o}^{P} \beta_{T1}(P', T)dP' + \int_{T_0}^{T} \alpha_{T1}(P_o, T')dT' \right] \tag{B6}$$

Here β and α are the compressibility coefficient and the coefficient of thermal expansion respectively. The subscript 0 represents the properties at the freezing point of pure water at 1 atmosphere.

$$\alpha_{T1}(P_o, T) = A_1 + A_2 T + A_3 T^2 + A_4 T^3 \tag{B7}$$

$$\beta_{T1}(P, T) = \frac{\beta_{T1}^0}{1 + m_1 \beta_{T1}^0 P}; \qquad \beta_{T1}^0 = \frac{\beta_1}{1 - \beta_2 T} \tag{B8}$$

Where $A_1 = 1.5756\ 10^{-4}$, $A_2 = 5.556\ 10^{-7}$, $A_3 = 2.655\ 10^{-8}$, $A_4 = 7.11\ 10^{-10}$,
$\beta_1 = 1.827\ 10^{-5}$, $\beta_2 = 1.418\ 10^{-3}$, $m_1 = 5$. The units in equations (6) to (8) are degrees Celsius for temperature and bars for pressure.

The correlations and constants for ice are from reference [5].

For water:

$$v_2 = v_{10} \exp\left[-\int_{P_o}^{P} \beta_{T2}(P',T)dP' + \int_{T_{k0}}^{T_k} \alpha_{T2}(P_o,T')dT' \right] \tag{B9}$$

The compressibility and thermal expansion coefficients are:

$$\beta_{T2}(P,T) = \left(\sum_{i=0}^{4} b_i P^i \right) \times 10^{-4} \tag{B10}$$

$$\alpha_{T2} = \left(A + \frac{B}{C + \Gamma} \right) \times 10^{-4} \tag{B11}$$

In equation (8) A, B, C and Γ are functions of temperature and pressure expressed as follows.

$$\begin{aligned} A &= a_1 + a_2 T_K + a_3 T_K^2 \\ B &= a_4 + a_5 T_K + a_6 T_K^2 + a_7 T_K \Gamma + a_8 \Gamma \\ C &= a_8 + a_9 T_K + a_{10} T_K^2 + a_{11} T_K^3 \\ \Gamma &= P + a_{13} P^2 + a_{14} P^3 \end{aligned} \tag{B12}$$

where

$a_1 = 4.78506\ 10^1$	$a_8 = -2.76522\ 10^1$
$a_2 = -8.12847\ 10^{-2}$	$a_9 = -4.28067\ 10^3$
$a_3 = 8.49849\ 10^{-5}$	$a_{10} = -3.39150\ 10^1$
$a_4 = 5.56047\ 10^5$	$a_{11} = 3.65873\ 10^{-1}$
$a_5 = -3.76355\ 10^3$	$a_{12} = -5.89617\ 10^{-4}$
$a_6 = 5.56395$	$a_{13} = 3.28892\ 10^{-4}$
$a_7 = 5.59682\ 10^{-3}$	$a_{14} = 2.65933\ 10^{-8}$

and

$b_0 = 4.41753\ 10^{-1}$	$b_3 = -2.08128\ 10^{-12}$
$b_1 = -1.09205\ 10^{-4}$	$b_4 = 8.86050\ 10^{-17}$
$b_2 = 1.99785\ 10^{-8}$	

The specific volume of water can be calculated numerically using the constants given above. The units are degrees Kelvin for temperature and bars for pressure. The expressions and the constants for water are from reference [5].

From equations (1), (2) and (B7) to (B12) it is possible to obtain, through numerical integration the specific volumes of ice and water in a two phase, equilibrium, ice-water system, at each temperature and its corresponding pressure. From knowledge of the original specific volume of the water, and the specific volumes of water and of ice at the new thermodynamic equilibrium conditions, we can obtain from equation (B6) the percentage weight of water relative to the

percentage weight of the mixture in an isochoric system, at each temperature and pressure. The percent of ice in the mixture is given by:

$$Ice\_\% = (1 - Z) \times 100 \quad \text{(B13)}$$

It should be noticed here that we have taken, as a first order assumption, saline, glycerol and ethylene glycol as water, because there is no readily available data.

$$Z = \frac{m_2}{m_B + m_A} \quad \text{(B14)}$$

Because we have a multiphase system, there are two situations. If $m_2 < m_B$ than the freezing will be confined only to phase B. Since there is no transfer of mass between phase A and phase B, and the solute is confined to the unfrozen volume in phase B, the concentration in phase B is given from conservation of mass. If, $Z < \frac{m_2}{m_B + m_A}$, than the new concentration in the liquid part of phase, c_{Bn} is given by:

$$c_{Bn} = c_{B0} \frac{m_B}{(Z(m_A + m_B) - m_A)} \quad \text{(B15a)}$$

If, $Z > \frac{m_2}{m_B + m_A}$, , then the entire fluid in phase B is frozen and now freezing begins in phase A. For this case the new concentration in phase A, c_{An} is given by:

$$c_{An} = c_{A0} \frac{m_A}{Z(m_A + m_B)} \quad \text{(B15b)}$$

In this case evaluate the new concentration in the phase that is in contact with the ice.